Titre: Title:	Experimental and numerical evaluation of the effects of concrete lift joints on static and seismic response of gravity dams
Auteur: Author:	Luciano Fronteddu
Date:	1997
Type:	Mémoire ou thèse / Dissertation or Thesis
Référence: Citation:	Fronteddu, L. (1997). Experimental and numerical evaluation of the effects of concrete lift joints on static and seismic response of gravity dams [Ph.D. thesis, École Polytechnique de Montréal]. PolyPublie. https://publications.polymtl.ca/6810/

UNIVERSITÉ DE MONTRÉAL

EXPERIMENTAL AND NUMERICAL EVALUATION OF THE EFFECTS OF CONCRETE LIFT JOINTS ON STATIC AND SEISMIC RESPONSE OF GRAVITY DAMS

LUCIANO FRONTEDDU

DÉPARTEMENT DES GÉNIES CIVIL, GÉOLOGIQUE ET DES MINES

ÉCOLE POLYTECHNIQUE DE MONTRÉAL

THÈSE PRÉSENTÉE EN VUE DE L'OBTENTION

DU DIPLÔME DE PHILOSOPHIAE DOCTOR (Ph.D.)

(GÉNIE CIVIL)

NOVEMBRE 1997

National Library of Canada
Acquisitions and Bibliographic Services
395 Wellington Street
Ottawa ON K1A 0N4
Canada

Bibliothèque nationale du Canada
Acquisitions et services bibliographiques
395, rue Wellington
Ottawa ON K1A 0N4
Canada

Your file Votre référence

Our file Notre référence

0-612-33002-8

Canada

UNIVERSITÉ DE MONTRÉAL

ÉCOLE POLYTECHNIQUE DE MONTRÉAL

Cette thèse intitulée

EXPERIMENTAL AND NUMERICAL EVALUATION

OF THE EFFECTS OF CONCRETE LIFT JOINTS

ON STATIC AND SEISMIC RESPONSE OF GRAVITY DAMS

présentée par: FRONTEDDU Luciano

en vue de l'obtention du diplôme de : Philosophiae Doctor

a été dûment acceptée par le jury d'examen constitué de:

M. SOULIÉ Michel, Ph.D., président

M. TINAWI René, Ph.D., membre et directeur de recherche

M. LÉGER Pierre, Ph.D., membre et co-directeur de recherche

M. FILIATRAULT André, Ph.D., membre

M. VENTURA Carlos, Ph.D., membre

Un giovane sogna

per altri fu preso
da scuola, dal sogno

partito lontano
lavorato per altri

sogno rotto
e mai ritrovato.

al mio padre

Young man wished

for others taken
out of school, out of dream

travelled far
worked for others

broken dream
never rejoined.

to my father

ACKNOWLEDGMENTS

I would like to thank Professor René Tinawi for allowing me the opportunity to work on this great research topic, for his thorough support and precious guidance. I would like to thank Professor Pierre Léger for his true involvement in the research, for his numerous and thorough comments, and for his always appropriate advice. The financial support through graduate scholarships from the Natural Sciences and Engineering Research Council of Canada (NSERC) and the Fonds pour la formation de chercheurs et l'aide à la recherche (FCAR) are gratefully acknowledged. The financial support from Hydro-Québec, Alcan, NSERC and the Canadian Electrical Association (CEA) is also gratefully acknowledged.

Special thanks are due to the staff of the Structures Laboratory at École Polytechnique, Mr. Gérard Degrange, Mr. Denis Fortier, and Mr. Patrice Bélanger, for making the passage in the lab a successful and pleaseful experience. A very special word of gratitude is due Mr. Martin Leclerc who assisted me in the laboratory, and who created the INTRFACE postprocessor program GAPLOT. I also wish to thank Marie-Claude Janelle for her assistance in preparing and testing the specimen.

I wish to thank Dr. Faouzi Ghrib for very valuable discussions. Thanks are due to Dr. Albert Nessim for his encouragements and for providing me with some consulting work in the course of my studies.

Final thanks are due to my family, specially my father Pietro Fronteddu, for his help, encouragement, and never ending faith. I also wish to thank my two sons, Pierre Georges, and Jean-Christophe, for making home such a joyful and lively place. Last but not least I would like to thank my wife Natalie for her love, patience and faith.

RÉSUMÉ

Les barrages en béton au Canada, avec une moyenne d'âge de 50 ans, présentent des signes évidents de détérioration, particulièrement aux joints de construction. La fissuration et la rupture le long de ces joints mobilisent les propriétés de résistance au frottement qui, sous chargement cyclique tels les séismes, peuvent entraîner une dissipation d'énergie par mécanisme de frottement.

Dans ce projet, dix-huit spécimens de surface de béton de 250mm×500mm ont été soumis à des essais de frottement statiques et dynamiques. Il a été observé que le coefficient de friction diminue lorsque la contrainte normale à l'interface est augmentée. Les courbes hystérétiques sont stables; il n'y a aucune dégradation significative de la résistance au frottement. Le concept d'angle de frottement résultant de la somme d'un angle de friction de base et d'un angle de rugosité suffit pour capter les différents phénomènes observés sur les variables expérimentales. Ainsi, le coefficient de friction de rugosité d'un joint préparé au jet d'eau à haute pression est égal à 80% de celui d'une fissure naturelle dans le béton. Le coefficient de friction de rugosité d'un joint sans préparation est égal à 15% de celui d'une fissure naturelle dans le béton. Le coefficient de friction de base dynamique est égal à 85% de sa valeur statique.

Avec ces résultats expérimentaux, un modèle constitutif hystérétique des joints de construction a été développé. Ce modèle inclut l'initiation et la propagation de la fissure ainsi que le comportement du joint entièrement fissuré. Un logiciel d'éléments finis a été développé (INTRFACE) pour ce modèle, en utilisant l'élément fini "gap-friction" pour la simulation numérique du joint. Un barrage type de 90m avec joints a été analysé sous trois configurations différentes: (i) un joint à la base du barrage, (ii) un joint à la base ainsi qu'un joint près de la crête et (iii) huit joints également espacés sur la hauteur du barrage. Les analyses dynamiques nonlinéaires révèlent que l'énergie de frottement et le glissement résiduel maximal peuvent servir de critères pour l'évaluation de la sécurité d'un barrage sous l'effet d'un séisme majeur.

ABSTRACT

Concrete gravity dams in Canada are ageing. With an average of 50 years of service, there are definite signs of deterioration, particularly along lift joints, sometimes due to inadequate construction techniques. The safety assessment of dams, including the response of lift joints under extreme loads, has not been addressed adequately in the context of advanced numerical analysis using relevant load-displacement constitutive models.

Cracking and failure along lift joints in dams involve frictional strength characteristics which, under transient loadings such as earthquakes, may lead to energy dissipation by friction sliding. Eighteen specimens with concrete-concrete joint surface area of 500mm× 250mm were subjected to sliding friction tests. The friction coefficient was found to decrease with increasing applied normal stress. Hysteresis loops are very stable; there is no significant degradation in response. The friction angle characterizing the shear strength is the sum of a basic angle and a roughness angle. Roughness of waterblasted joints is equal to 80% of monolithic cracked specimens roughness, while roughness of untreated joints is equal to 15% of monolithic cracked concrete roughness. The dynamic sliding hysteresis loops are enhanced by reducing the basic friction coefficient to 85% of the static value.

Based on the experiments, a hysteretic concrete-concrete lift joint constitutive model was developed. The initial linear elastic response of the joint interface, the crack initiation and propagation, and the fully cracked sliding friction response, were combined in a three-state constitutive model. The model was implemented into the newly developed finite element program INTRFACE that uses nonlinear gap-friction interface element as numerical support. A typical 90 m concrete gravity dam with lift joints was analysed for three possible situations: (i) a base joint at the foundation, (ii) a base joint and a lift joint near the crest, and (iii) eight lift joints evenly distributed along the dam height. Nonlinear transient dynamic analyses indicate that the total energy dissipated by friction, and the maximum residual sliding displacements could be adopted as a basis for assessing the potential damage under a severe earthquake.

CONDENSÉ

Les joints de construction introduisent des zones de faiblesse dans les barrages qui les rendent particulièrement vulnérables à la fissuration. Les barrages en béton au Canada, avec une moyenne d'âge de 50 ans, présentent des signes évidents de détérioration aux joints de construction. Une étude exhaustive de la stabilité d'un barrage se fait en considérant ces joints comme des plans de rupture potentielle. Or, les études classiques de stabilité au tremblement de terre requièrent l'utilisation d'une force statique équivalente pour représenter le séisme. Ce type d'analyse ne tient pas compte de la nature oscillatoire et transitoire du séisme, ni des possibilités de dissipation d'énergie le long des joints de construction. Cette thèse de doctorat étudie donc l'effet des joints sur le comportement sismique des barrages par: a) une revue exhaustive de la littérature, b) un programme expérimental afin de caractériser le comportement dynamique des joints, c) le développement d'un modèle constitutif de joint basé sur les essais expérimentaux, d) l'utilisation du modèle dans le cadre de l'analyse par éléments finis et e) l'application du modèle à un barrage type avec joints.

Revue de la littérature

Une revue exhaustive de la littérature sur les joints a été effectuée. La littérature portant directement sur les joints de construction est plutôt limitée. Afin de couvrir toutes les facettes de cette problématique, il faut parcourir la littérature de plusieurs champs différents tel qu'illustré à la figure 1. Les problèmes de contact (figure 1[1]) permettent de poser les équations de base du problème à résoudre. Les joints de roc (figure 1[2]) font l'objet d'études particulièrement pour la stabilité des massifs rocheux où se posent les problèmes d'échelle et d'adéquation des essais de laboratoire versus les conditions du terrain. En fissuration du béton jaillit toujours la question de la résistance au cisaillement qui se trouve caractérisée dans les modèles de friction intergranulaire (figure 1[3]). L'étude sismique des barrages couvre le terrain d'application de la problématique

(figure 1[4]). Enfin, tous ces domaines se trouvent intégrés dans l'étude de la stabilité des barrages en considérant de façon explicite la présence des joints.

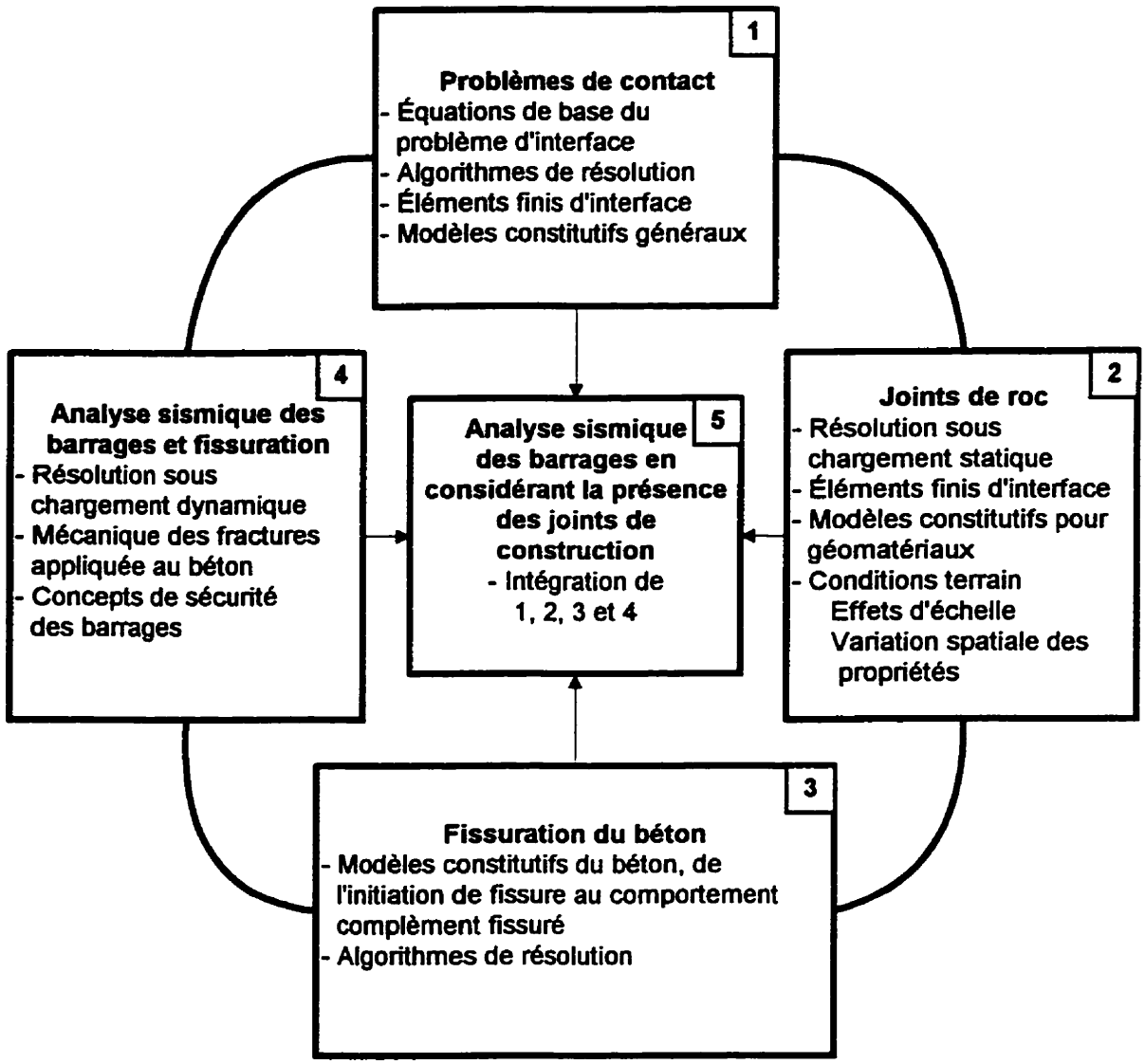

Figure 1 *Revue de la littérature.*

Essais expérimentaux et résultats

Dans ce projet, dix-huit spécimens de surface de béton de 250mm×500mm ont été soumis à des essais de frottement statiques et dynamiques. Quatre types de surface ont été considérés: a) des surfaces obtenues de la fissuration de béton initialement monolithique, b) des surfaces préparées au jet d'eau à haute pression, c) des surface sans préparation et

d) des surfaces planes de fond de coffrage. Chaque spécimen était en premier lieu fissuré en flexion. Par la suite, le spécimen était reconstitué sur le montage pour essais de glissement. Les essais de glissement se déroulaient en 3 grandes étapes: a) l'enveloppe de rupture prédynamique (ou initiale) obtenue en imposant des cycles de déplacement à six niveaux de charge normale; b) le comportement dynamique obtenu en soumettant le spécimen à 10 cycles de déplacement à 2 Hz, 10 cycles à 7 Hz et 2 cycles à 2 Hz, ce à 4 niveaux de charge normale; enfin c) l'enveloppe de rupture postdynamique en répétant l'étape (a).

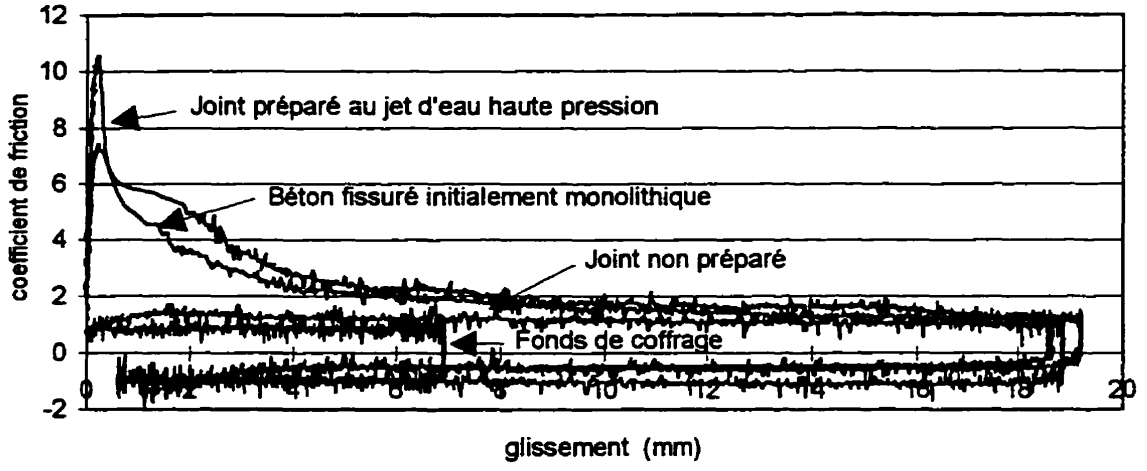

Figure 2 *Coefficient de friction statique expérimental à 100 kPa.*

Des courbes expérimentales typiques sont illustrées à la figure 2. Le coefficient de friction est le ratio de la force de cisaillement appliquée à la force normale appliquée. Les fonds de coffrage ont un comportement rigide plastique alors que les autres types de spécimens présentent un pic suivi d'une perte rapide de résistance et d'un plateau. Les joints non préparés atteignent graduellement la résistance maximale alors que les spécimens à joint préparé et les spécimens de béton fissuré ont un pic très bien défini.

Le tableau 1 indique les coefficients de friction mesurés moyens pour chaque type de spécimen. Au-delà de 500 kPa, tous les spécimens se comportent de façon rigide plastique par conséquent, aucun pic n'est donné pour la contrainte de 2000 kPa. Les coefficients de friction des surfaces planes de fonds de coffrage sont beaucoup plus faible que les autres

types de surfaces. La rugosité de l'interface accroît la résistance au glissement. Cette rugosité est reliée à la géométrie de la surface alors que le coefficient de friction de base est relié à la nature des matériaux qui interagissent à l'interface.

Tableau 1 *Coefficient de friction moyen mesuré sous chargement prédynamique.*

Type de spécimen	Charge normale σ_n=100kPa				Charge normale σ_n=2000kPa	
	μ mesuré moyen		$\bar{\mu}_I$ mesuré moyen (rugosité)		μ mesuré moyen	$\bar{\mu}_I$ mesuré moyen (rugosité)
	Pic	Résiduel	Pic	Résiduel	Résiduel	Résiduel
Surfaces "fond de coffrage"	0.87	0.75	0.00	0.00	0.75	0.00
Non préparé	1.44	1.11	0.15	0.04	0.79	0.04
Préparé	7.90	1.49	0.80	0.12	1.06	0.13
Béton fissuré	7.80	1.59	0.80	0.29	1.15	0.18

Il ressort de ces résultats que la préparation au jet d'eau à haute pression accroît de beaucoup la résistance au glissement des joints. À σ_n=100 kPa, le coefficient de friction d'une surface préparée atteint 550% du coefficient de friction d'une surface non préparée. À σ_n=100 kPa, la résistance résiduelle d'une surface préparée est 134% de la résistance d'une surface non préparée.

Des résultats types des essais dynamiques sont présentés à la figure 3. La caractéristique principale de ces boucles d'hystérésis est l'absence de dégradation de la réponse. Avec la préparation de surface, la réponse évolue de purement rigide plastique c'est-à-dire en forme de rectangle pour les fonds de coffrage, à élasto-plastique avec écrouissage (forme de parallélogramme). Cette transition est provoquée par la rugosité. L'aire des boucles d'hystérésis indique la capacité du béton à dissiper de l'énergie.

Le tableau 2 dresse un sommaire des coefficients de friction dynamiques moyens. De ces résultats, deux groupes distincts émergent: a) les surfaces de fond de coffrage et joints non préparés d'un côté et de l'autre, b) les joints préparés et le béton fissuré. Le contenu en fréquences de la charge dynamique appliquée ne semblent avoir aucun effet sur la résistance du joint. Cependant, sous chargement dynamique, le coefficient de friction de base décroît à 85% de sa valeur statique.

Tableau 2 *Coefficient de friction moyen mesuré sous chargement dynamique.*

Type de spécimen	Charge normale σ_n=100kPa		Charge normale σ_n=1500kPa	
	μ moyen mesuré 2 Hz	μ moyen mesuré 7 Hz	μ moyen mesuré 2 Hz	μ moyen mesuré 7 Hz
Surfaces "fond de coffrage"	0.85	0.83	0.55	0.50
Non préparé	1.00	0.95	0.66	0.60
Préparé	1.13	1.07	0.89	0.85
Béton fissuré	1.18	1..12	0.95	0.92

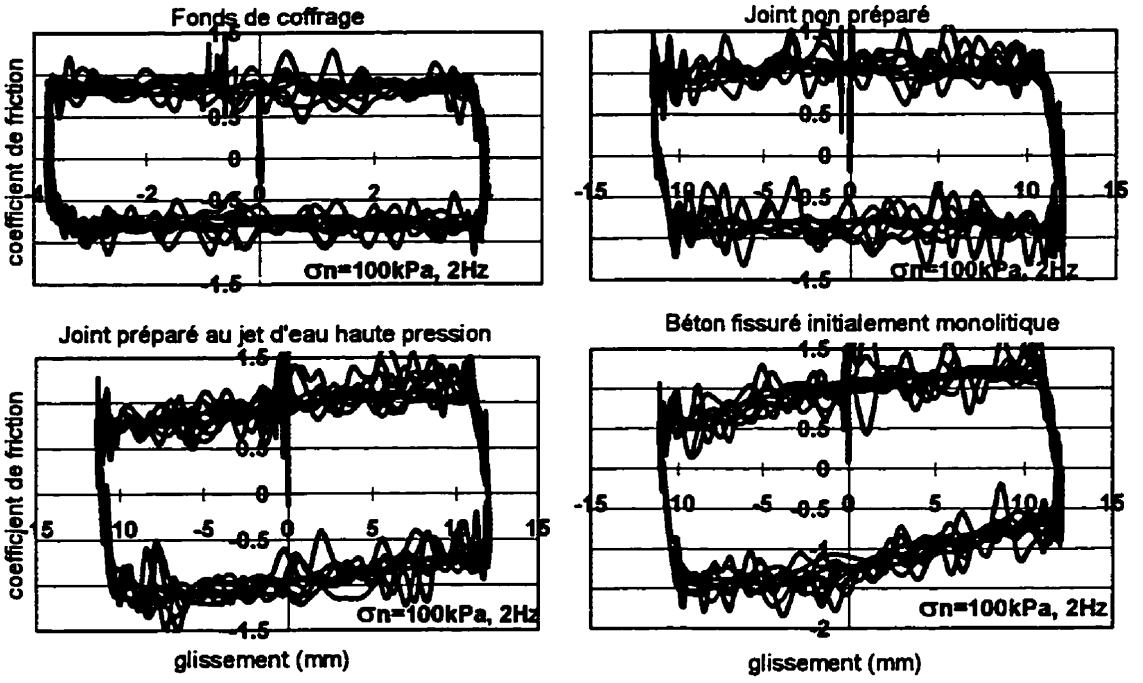

Figure 3 *Coefficients de friction dynamiques à 100 kPa, 2 Hz.*

Modèle constitutif de glissement des joints

Un modèle constitutif a été développé à partir des résultats expérimentaux. Il est basé sur le concept du coefficient de friction de base, μ_b, et du coefficient de rugosité, $\overline{\mu}_i$, lequel est dépendant de la préparation de la surface. Le coefficient de friction effectif doit être calculé tel:

$$\mu = \frac{\lambda_d \mu_b + \chi_i \bar{\mu}_i}{1 - \lambda_d \chi_i \mu_b \bar{\mu}_i} \qquad (1)$$

où

μ = coefficient de friction pour le type d'interface et le niveau de charge normale, σ_n,
μ_b = coefficient de friction de base
$\bar{\mu}_i$ = coefficient de friction de rugosité ($\bar{\mu}_{ip}$ ou $\bar{\mu}_{ir}$ tel que prescrit),
λ_d = facteur de réduction dynamique, λ_d = 1.00 cisaillement statique,
λ_d = 0.85 cisaillement dynamique.
χ_i = facteur d'interface, χ_i = 1.00 béton fissuré,
χ_i = 0.80 joint préparé au jet d'eau,
χ_i = 0.15 joint non préparé
χ_i = 0.00 surface planes type fond de coffrage.

Sur la base de tous les résultats expérimentaux, (928 valeurs), un modèle à deux pentes pour le coefficient de friction de base, μ_b, est défini tel:

$$\begin{aligned} \mu_b &= 0.950 - 0.00022\sigma_n \quad pour \quad \sigma_n \le 500kPa \\ \mu_b &= 0.865 - 0.00005\sigma_n \quad pour \quad 500kPa \le \sigma_n \le 2000kPa \end{aligned} \qquad (2)$$

où σ_n est en kPa.

Le coefficient de friction de rugosité maximal (au pic), $\bar{\mu}_i$, est défini tel:

$$\begin{aligned} \bar{\mu}_{ip} &= 0.90 - 0.001367\sigma_n \quad pour \quad \sigma_n \le 250kPa \\ \bar{\mu}_{ip} &= 0.40 - 0.0001167\sigma_n \quad pour \quad 250kPa \le \sigma_n \le 1500kPa \\ \bar{\mu}_{ip} &= 0.30 - 0.000050\sigma_n \quad pour \quad 1500kPa \le \sigma_n \le 2000kPa \end{aligned} \qquad (3)$$

et le coefficient de friction de rugosité résiduel est obtenu de:

$$\bar{\mu}_{ir} = 0.30 - 0.000050\sigma_n \qquad (4)$$

pour tous niveaux de contrainte normale, σ_n.

Ce modèle constitutif original a été intégré dans un modèle constitutif à trois phases des joints de béton soit: a) phase élastique, b) phase d'initiation et de propagation de fissure et c) phase de fissuration complète du béton. Le modèle ci-haut représente le comportement complètement fissuré d'un joint de béton.

Outil numérique

Un logiciel d'éléments finis a été développé (INTRFACE) pour ce modèle, en utilisant l'élément fini "gap-friction" pour la simulation numérique du joint. Cet élément consiste en 2 ressorts translationnels et 2 amortisseurs visqueux insérés entre 2 noeuds. Deux algorithmes de résolution par contrôle indirect des déplacements ont été implantés dans le logiciel afin de favoriser la validation sous chargement statique de l'élément d'interface. La méthode α a été choisie pour résoudre les équations de mouvement.

Application

Un barrage type de 90m avec joints est analysé sous trois configurations différentes: (i) un joint à la base du barrage, (ii) un joint à la base ainsi qu'un joint près de la crête et (iii) huit joints également espacés sur la hauteur du barrage. L'objectif est de comparer la philosophie de calcul des recommendations du CDSA (1995) pour les barrages versus des analyses par éléments finis nonlinéaires qui permettent la simulation du glissement le long de l'interface. Le modèle du barrage analysé est illustré à la figure 4.

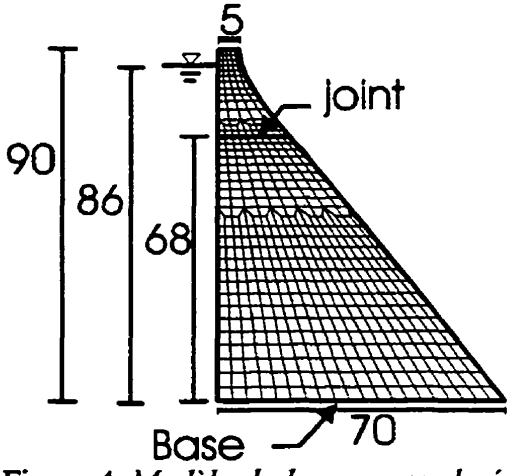

Figure 4 *Modèle du barrage analysé*

Les analyses suivant l'approche CDSA (1995) ne fournissent qu'une seule information c'est-à-dire l'accélération requise pour induire le glissement. Les analyses nonlinéaires par éléments finis fournissent non seulement l'accélération qui induit tout glissement initial mais également le déplacement résiduel du barrage après le séisme ainsi que l'énergie dissipée dans le barrage par friction et par amortissement visqueux. La figure 5 illustre les résultats tirés de l'analyse par éléments finis.

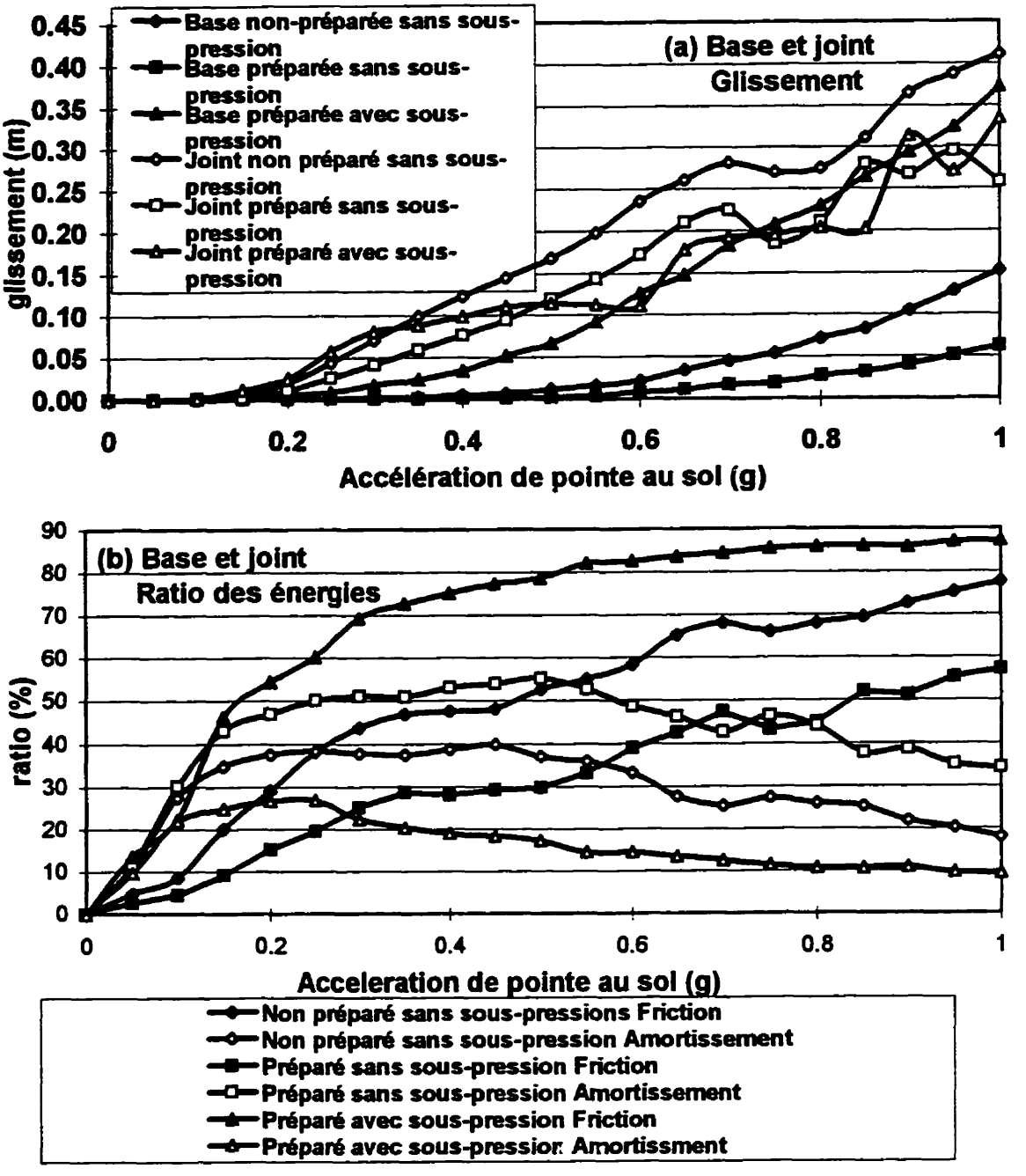

Figure 5 *Résultats des analyses nonlinéaires pour modèle à deux joints.*

Les résultats tel qu'énumérés au tableau 3 indiquent d'une part que l'accélération nécessaire pour entraîner un premier glissement, calculée par éléments finis, est similaire à celle obtenue des analyses classiques. Par contre, les valeurs de glissement résiduel

correspondantes sont plutôt faibles. Ces faibles glissements conjugués au fait qu'ils puissent constituer un mécanisme de dissipation d'énergie non-négligeable pour un barrage (voir figure 5(b)) remettent en question la notion de sécurité basée strictement sur un critère d'équilibre de forces statiques équivalentes. Un tel critère ne permet pas d'évaluer la portée des conséquences d'une transgression du critère en termes de dommages à la structure.

Tableau 3 *Résultats des analyses par éléments finis nonlinéaires.*

	Base seule		Base et joint			
Condition du joint	APS au glis. initial	glis. résiduel	APS au glis. initial à la base	glis. résiduel à la base	APS au glis. initial	glis. résiduel au joint
Non préparé, sans S-P	0.20g	2.3mm	0.25g	1.4mm	0.10g	0.3mm
Préparé sans S-P	0.30g	1.6mm	0.45g	2.0mm	0.15g	2.6mm
Préparé avec S-P	0.10g	1.8mm	0.15g	3.4mm	0.10g	1.0mm

S-P= sous pression, APS=accélération de pointe au sol

Conclusions

Les conclusions principales de cette thèse de doctorat sont les suivantes.

Comportement général des joints:

Le coefficient de friction diminue lorsque la charge normale est augmentée. La préparation de la surface détermine les propriété de résistance des joints. Ainsi, les joints préparés ont un comportement similaire au béton fissuré initialement monolithique alors que les joints non préparés se comportent comme des surfaces planes type "de fond de coffrage".

Comportement dynamique des joints:

Les boucles d'hystérésis sont très stables, la résistance ne se dégrade pas avec les cycles de glissement. Le contenu en fréquences du glissement imposé n'a pas d'effet sur le

comportement du joint. Une certaine dépendance du coefficient de friction à la vitesse de glissement a pu être observée. Enfin, aucune relation ne peut être établie entre l'accélération et le coefficient de friction.

Modèle constitutif des joints:

Un modèle constitutif pour joints a été développé. Il inclut les caractéristiques fondamentales des joints soit: la préparation de l'interface, la grosseur de l'agrégat utilisé, la contrainte normale appliquée, σ_n, et la nature de la charge appliquée, statique ou dynamique.

Concernant la sécurité des barrages:

Les analyses classiques de stabilité au glissement sous charge sismique sont dépendantes de la distribution de la charge sismique équivalente appliquée sur le modèle de calcul ainsi que de la position des joints considérés.

L'analyse par éléments finis nonlinéaires avec simulation explicite du glissement le long du joint permet d'obtenir non seulement l'intensité du tremblement de terre requis pour entraîner un glissement mais également le déplacement résiduel qui en résulte.

Un critère de sécurité des barrages basé sur le glissement admissible

Un tel critère met à profit les propriétés mécaniques des joints. Ce critère doit être déterminé de façon à maintenir à tout moment l'intégrité du système barrage-réservoir-fondation. Ainsi, suite au glissement admissible ce dernier ne doit pas rendre inopérant le système de drainage et tout équipement important ne devra pas être endommagé.

TABLE OF CONTENTS

LIST OF TABLES

LIST OF FIGURES

NOTATION

The following is a list of the symbols used in the text:

LATIN SYMBOLS:

a_0, a_1	:	damping proportionality factors
A_n	:	tributary area
b	:	out-of-plane thickness of joint element
b_c	:	cracked Biot coefficient
b_u	:	uncracked Biot coefficient
B	:	base contact of lift joint width
B_{ij}, $i,j=n,t$	:	stiffness terms
c_n	:	normal joint element damper constant
c_t	:	tangential joint element damper constant
c_{pn}	:	normal compliance
c_{pt}	:	tangential compliance
$[C]$	:	damping matrix
$[C_o]$	:	elasticity matrix
d	:	damage variable
ds	:	surface differential element
dx	:	volume differential element
D^{II}	:	shear softening modulus
D_{max}	:	maximum aggregate size
DI	:	damage index
DI_n	:	damage index in normal direction
DI_t	:	damage index in tangential direction
$[D_{LE}]$	:	linear elasticity state matrix
$[D_{ID}]$	:	initiation and development state matrix
$[D_{AI}]$	:	opened crack state matrix
e	:	eccentricity of the applied loads resultant on the base
E_c	:	modulus of elasticity of concrete
E_{ijkl}	:	elasticities of material
E^K	:	kinetic energy
E^D	:	damping energy
E^R	:	restoring forces energy
E^P	:	work done by static forces
E^Q	:	seismic input energy
EEI	:	energy error indicator
$f()$	:	work done by external loads
f'_c	:	concrete compressive strength
f_i	:	body forces
$f_n(), f_t()$	:	normal and tangential stress functions

f_r	:	flexural tensile strength of concrete (modulus of rupture)
$f_{r\,avg}$	:	average measured modulus of rupture for a given type of specimen
$f_{r\,avg\,H}$	:	average measured modulus of rupture for the monolithic specimens
f_{sp}	:	splitting tensile strength of concrete
f_t	:	concrete tensile strength
f_{Tj}	:	concrete tensile strength
F_P	:	prestressing force
$\{\Delta f_{unb}\}$	:	vector of unbalanced forces
$\{f\}$	:	vector of applied forces
$\{F\}$	:	vector of applied forces
g	:	initial gap opening
G	:	shear modulus
$G(w)$	:	shear modulus function
G_f	:	concrete fracture energy
G_f^I	:	mode I concrete fracture energy
G_f^{II}	:	mode II concrete fracture energy
$\{G\}$	:	constraint
h	:	finite element characteristic length
h_{if}	:	thin layer finite element thickness
h_r	:	reservoir water head
H	:	hydrostatic thrust
i	:	roughness angle
i_{obs}	:	experimentally measured roughness angle
$j()$	:	work done by friction forces
k_{ij}, i,j=n,t	:	stiffness terms
k_{in}	:	minimum tensile normal stiffness
K_{IC}	:	fracture toughness
$[K]$	:	stiffness matrix
l	:	joint element length
N	:	applied or measured normal load
m_n	:	exponent of normal compliance
m_t	:	exponent of tangential compliance
$[M]$	:	mass matrix
p	:	initial normal stress
p_{eff}	:	effective uplift pressure
p_{ini}	:	initial applied uplift pressure
p_{res}	:	water pressure at the upstream joint tip
$\{p\}$	:	vector of external forces
P	:	measured three-point bending test force
PGA	:	peak ground acceleration
q	:	best fit coefficient
Q_H	:	concrete horizontal inertia force
Q_{RH}	:	added inertia force to represent dam-reservoir hydrodynamic

		interaction
Q_V	:	concrete vertical inertia force
$\{r\}$	:	vector of restoring forces
R	:	applied loads resultant
$\{\Delta S\}$	:	target displacement increment
S_A °	:	geometric or failure angle component
S_i	:	target total displacement
S_ρ	:	nonlocal normal stress distribution function
SSF	:	sliding safety factor
Δt	:	time step
t_i	:	external forces
T	:	applied or measured shear load (tangential load)
T_1	:	first natural vibration period
$\{u\}$	:	vector of displacements
$\{\dot{u}\}$	:	vector of velocities
$\{\ddot{u}\}$	:	vector of relative accelerations
$\{\ddot{u}_g\}$	:	vector of ground accelerations
$\{\ddot{u}_t\}$	:	vector of total accelerations
$u(dof_m)$	:	displacement at degree of freedom m
U	:	uplift thrust
$\tilde{u}_i$	:	displacements predictions for time step i
$\{u\}$	:	vector of displacements
$\tilde{v}_i$	:	velocities predictions for time step i
w	:	crack opening
W	:	dam weight
W_k	:	potential of contact forces

GREEK SYMBOLS:

α	:	time integration factor
α_p	:	penalty factors
Δ	:	increment of quantities
β	:	time integration factor
β_s	:	shear retention factor
δ_n	:	normal displacement to the sliding plane
δ_{nfc}	:	opening at full consumption of fracture energy
δ_{nm}	:	maximum closure
δ_{nmax}	:	overall maximum opening reached in the time history
δ_r	:	shear displacement at beginning of residual friction coefficient plateau
δ_t	:	shear displacement

δ_{tfc}	:	shear displacement at full consumption of fracture energy
δ_{tmax}	:	overall maximum shear displacement reached in the time history
$\{\varepsilon\}$	:	strain tensor
ξ	:	damping ratio
γ	:	time integration factor
γ_{nt}	:	shear strain
γ_h	:	water weight per volume
Γ_C	:	candidate contact surface
Γ_F	:	portion of boundary where forces are prescribed
λ	:	total load factor (indirect displacement control method)
$\overline{\lambda}_i$	:	computed total displacement (indirect displacement control method)
λ_L	:	Lagrange multiplier
λ_d	:	dynamic reduction factor
η	:	ratio between secant modulus and initial isotropic elastic modulus
μ	:	coefficient of friction
μ_b	:	basic friction coefficient or friction coefficient along the asperities
μ_{mes}	:	measured friction coefficient
$\overline{\mu}_i$	:	roughness coefficient of friction
$\overline{\mu}_i^p$	:	peak roughness coefficient of friction
$\overline{\mu}_i^r$	:	residual roughness coefficient of friction
ϕ	:	angle of friction
ϕ_b	:	basic angle of friction
ϕ_f	:	angle of friction at shearing though of the asperities
ϕ_{mes} or ϕ_{obs}	:	measured angle of friction
ϕ_n	:	static friction angle
ϕ_r	:	residual friction angle
$\phi_\varepsilon(\,)$	:	nonlinear stress function
Ω	:	elastic body domain (volume)
Π	:	total potential energy expression
ψ_o	:	dilatation angle
$\overline{\sigma}$	:	average relative normal stress ratio
σ_f	:	normal stress at failure of asperities
σ_i	:	initial normal stress at zero normal deformation
σ_n	:	normal stress on sliding plane
τ_{app}	:	apparent shear strength
τ_c	:	mass concrete cohesion
τ_i	:	joint cohesion
τ_n	:	nominal joint shear strength

τ_o	:	joint threshold shear strength
τ_p	:	joint peak shear strength
τ_r	:	joint residual shear strength
χ_i	:	interface roughness factor
ν	:	Poison's ratio
ν_i i=n,t	:	displacements

CHAPTER 1
Introduction

1.1 Overview

More than 50% of all dams in Canada have been in service for over 40 years. In concrete dams, ageing effects are becoming more and more visible at lift joint locations. Many old concrete dams are now showing clear evidence of debonding at joint locations. Construction practice at the beginning of the century was not as stringent as it is today. Little was known about the importance of concrete surface preparation prior to pouring the next lift. As a result, joint surfaces were often left with laitance, and inadequate concrete mixes were used. Dams were designed considering joints as planes of weakness. Sliding and overturning stability at the joint location was usually checked for a "no-tension" condition considering triangular uplift pressure distribution in most severe cases where no drainage provisions existed. Shear keys or a wavy joint profile were also sometimes provided.

With increasing knowledge of hydrology and seismicity, the "probable maximum flood" and the "maximum design earthquake" magnitudes have often been increased. These revised loading criteria, when considered on ageing structures, stimulated many owners to reevaluate their dams for stability under extreme conditions. The Canadian Electrical Association (CEA, 1990) and CDSA (1995) published guidelines for the seismic safety assessment of dams. The seismic safety philosophy adopted in most dam safety guidelines is twofold: (i) under a moderate intensity earthquake, operating basis earthquake, OBE, the dam should remain essentially elastic, while (ii) under the maximum design earthquake the dam can suffer structural damage, however the reservoir should be contained.

Increased earthquake loading criterion required expenditure of 48M$US for the retrofit of Stewart Mountain dam in Arizona (Rosenbaum, 1991). This arch dam (65 m)

exhibited debonding across horizontal lift joints. The structural continuity of the dam lift joints was restored using post-tensioned cables. Seven Sisters gravity dam (18 m) in Manitoba (Ferguson et al. 1994), as illustrated in Fig.1.1a, and Big Eddy buttress dam (49 m) in Ontario (Gore and Bickley, 1987) were rehabilitated with post-tension cables due to deterioration and leaching of horizontal construction joints that allowed water seepage through the structure. Alcan resorted to a similar retrofit technique at the Isle-Maligne complex in the province of Quebec (Dufresne et al. 1992), as shown in Fig.1.1b.

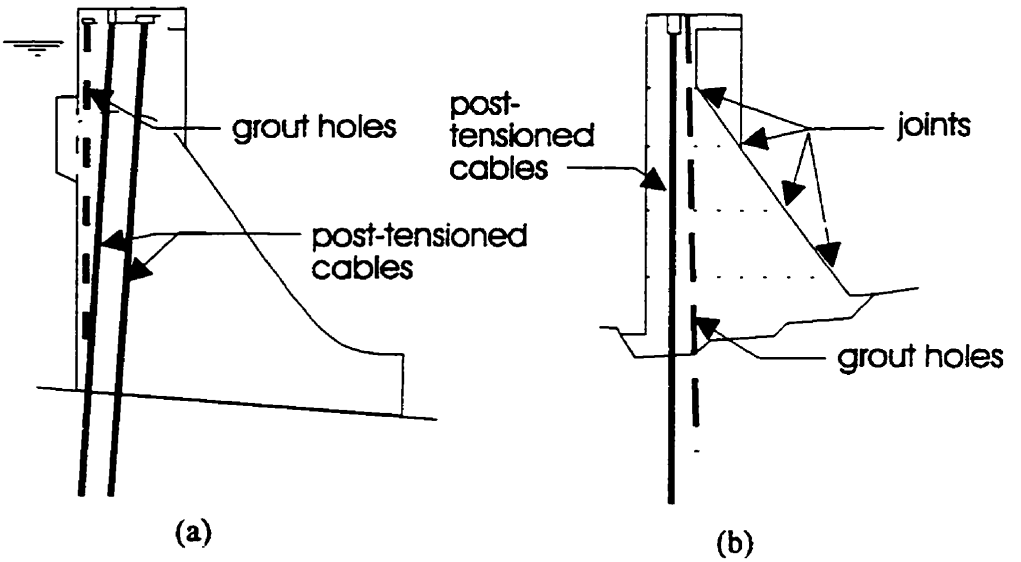

Fig. 1.1 *Post-tensioned cables provided at (a) Seven Sisters (adapted from Ferguson et al. 1994), and (b) Isle-Maligne (adapted from Turcotte et al. 1994)*

The deterioration of lift and construction joints favors the development of a significant anisotropic structural behaviour with a reduced load carrying capability. Detrimental consequences resulting from water penetration in joints are: (i) the increase in uplift pressure, (ii) the opening and loss of bond, (iii) the leaching out of cementing compounds, (iv) the increase in risk of a deleterious alkali-aggregate reaction (AAR), and (v) the penetration by cold water that favors damage from freeze-thaw cycles (Pacelli et al., 1993).

The Electric Power Research Institute in the U.S. published a thorough report on the tensile and frictional properties to be assigned to concrete and lift joints, while analyzing

existing dams for static loads (EPRI, 1992). However, no results were reported in terms of load-deformation response of the joint material. A knowledge of load-deformation response of concrete joints is essential to perform finite element analysis of jointed dams.

The load-deformation behaviour of concrete-concrete lift joints under static and earthquake loading, and the related structural response of "jointed" dams, have not been assessed properly to date. A "realistic" modelling of the effect of lift joints on the hydrological safety and earthquake safety of concrete dams is required to support, with confidence, the safety assessment and the design of effective and economical defensive measures, if need be. The National Research Council in the U.S. (NRC, 1990) stressed on the urgent need for research on joints in concrete dams.

1.2 Definition of the research problem

Seismic safety assessment of gravity dams has generally been limited to classical stability studies where the earthquake load is applied as an equivalent static load. Very little studies have been conducted on the dynamic response of gravity dams with explicit modelling of lift joints because of the complexity of the problem and because classical methods of analysis, based on beam theory or strength of materials, are still being preferred to finite element methods by most consultants in the dam industry. However, the higher level of trust in the classical methods has been challenged by fracture mechanics studies applied to dams (Bažant, 1990).

The finite element method has been initially developed for solving elasticity problems in small deformations where equilibrium is always somehow recovered. Stability problems require the determination of failure mechanisms. The linear elastic finite element method does not enable direct stability check as recommended in dam safety guidelines. Furthermore, at geometrical discontinuities such as corners, notches, and crack tip, stress singularities arise. Using the linear elastic finite element analysis, the stress singularity converges to infinity as the mesh is refined. Linear elastic fracture mechanics LEFM accounts for these singularities for predicting crack penetration and propagation.

Unfortunately, LEFM is mainly based on closed form solutions not applicable to dams in the context of earthquake analysis.

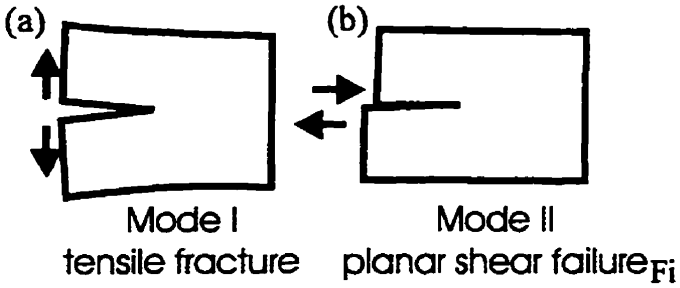

g. 1.2 *Modes of failure*

Nonlinear fracture mechanics NLFM has been applied successfully to the seismic response of gravity dams using both the discrete crack approach (Ayari and Saouma, 1990) and the smeared crack approach (Bhattacharjee and Léger, 1994; Ghrib and Tinawi, 1994). Both approaches did not consider lift joints, and they only dealt with tensile mode I type of failure (see Fig. 1.2). Even more, they require tensile softening for shear damage to occur. Also in these studies, mass concrete and lift joint limit strengths under a combination of compression and shear have not been considered.

Combined compression and shear state requires special attention first because this condition occurs over uncracked ligaments (see Fig. 1.3) between a crack tip and the downstream face and at the dam base contact joint, and second because it requires special numerical techniques for simulation. In addition, in the smeared crack approach, under earthquake loads, fracture energy is dissipated by a softening and eventually a cracking mechanism. Any frictional dissipation of energy at joints has been ignored in the past.

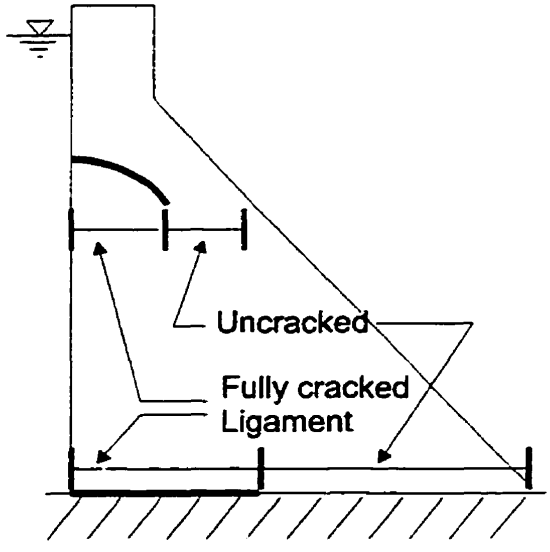

Fig. 1.3 *Locations for combined compression and shear to occur in dams*

Thus, it is very important to develop structural analysis tools, well suited to dam stability assessment, that enable a rational modelling of potential failure mechanisms such as lift joints and the base contact joint recognizing their particular load-displacement

responses. This formulation of the problem is complex but essential since any pseudo-static method is based on a sustained load rather than a cyclic loading. The cycling nature of the response, if considered in the seismic safety assessment, can therefore capture frictional dissipative mechanisms on a rational basis.

Agreement between the adopted material constitutive models and material strength parameters on one hand, and the real material and joint behaviour on the other hand, is the Achille's heel of numerical simulation methods. Getting sound static and dynamic material strength, stiffness and damping parameters for massive structures, such as dams, is an expensive and difficult task. Of course, in situ testing is the most valuable method because the measurements are performed with the actual dam material and load conditions. But this technique, which can be destructive on a very limited scale for obvious reasons, is complicated and expensive. Laboratory testing on scaled models enables to study the behaviour of the structure under extreme load conditions impossible to simulate on the site. However, uncertainties arise from scaling laws. Laboratory testing on material samples taken from the dam site gathers the advantages of the two above mentioned techniques. Laboratory testing on material samples is simple, not as expensive as in situ testing, but generally as reliable. Accordingly, dam owners resort to samples to get material strength data from simple tests such as compression tests (compressive strength, modulus of elasticity, Poisson's ratio) and direct shear tests (cohesion, angle of friction).

It is possible to get the most from a data collection program if the relevant parameters, that have a distinct effect on the structural response, are known beforehand. Thus, these relevant parameters are first to be identified. Only then, simple tests results may will be used to support the definition of transient dynamic material properties required to perform comprehensive nonlinear earthquake analysis.

1.3 Research methodology and objectives

To study the effect of concrete-concrete lift joints on the static and dynamic stability of concrete gravity dams, the following methodology was adopted (Fig. 1.4).

1- Review of literature,

2- Experimental dynamic sliding shear tests on 18 specimens 250mm×500mm concrete-concrete lift joint specimens, with different surface preparation: monolithic, waterblasted, untreated, flat independent, Fig. 1.4(a),

3- Development of a hysteretic lift joint constitutive model using experimental data, Fig. 1.4(b).

4- Finite element implementation of the lift joint constitutive model and of a gap-friction element, in a newly developed specialized computer program INTRFACE, and validation on simple structural systems, Fig. 1.4(c),

5- Parametric analyses on the static and earthquake response analysis of a 90m gravity dam using nonlinear finite element computer program INTRFACE with an explicit modelling of lift joints using gap-friction elements, Fig. 1.4(d).

The following objectives have been considered in this research program:

General objectives:

(i) the gathering of relevant information from the literature on joints for stating the pros and cons of the various numerical methods,

(ii) the development of a new concrete-concrete interface constitutive model, considering the particularities of lift joint surface preparations and dynamic loading,

(iii) the implemention of the model in a finite element analysis computer program to simulate dynamic sliding of gravity dams,

(iv) the validation of numerical models from original experimental results,

(v) the determination of the most significant parameters and safety indices to interpret the nonlinear analysis of jointed concrete gravity dams.

(vi) the establishment of practical conclusions and general guidelines for the seismic safety of ageing dams.

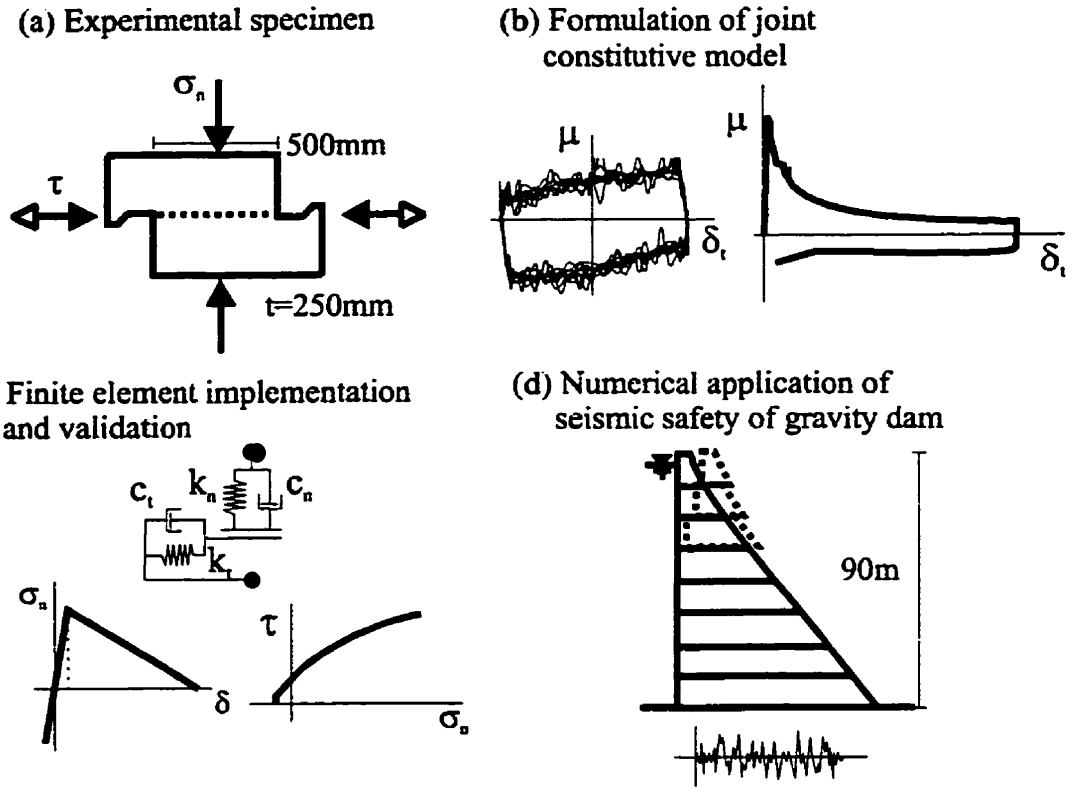

Fig. 1.4 *Overview of the methodology developed to address the research problem.*

Objectives of the experimental work reported in the thesis

(i) to simulate dynamic sliding that could occur along a lift joint in a concrete dam as a function of applied normal stress,

(ii) to determine the effect of lift joint surface preparation on its cyclic load-displacement response,

(iii) to relate dynamic direct shear response to static shear strength material properties (friction, cohesion),

(iv) to study the effect of the frequency content of the imposed shear displacement on the shear response.

Objectives of the numerical developments reported in the thesis

(i) to simulate the complete tensile mode I and shear mode II behaviour of lift joint, including crack initiation, crack propagation and fully cracked behaviour,

(ii) to study and to compare the various mechanisms of energy dissipation, viscous damping energy dissipation and frictional energy dissipation.

1.4 Original contributions of the thesis

To the best of the author's knowledge, the following items can be considered as original contributions of the thesis:

- A comprehensive literature review of measured dam lift joint strength parameters, joint models, and previous analytical studies on jointed dams has been presented.

- A realistic static and dynamic behaviour of lift joints with different surface preparation has been observed under laboratory conditions.

- A new concrete-concrete static and dynamic interface constitutive model has been developed based on original experimental data, to apply in static and dynamic sliding analysis of structures.

- A new nonlinear concrete-concrete interface model has been applied to predict the seismic response of concrete gravity dams with various lift joint conditions within the framework of the finite element method. The effect of uplift pressure in the joints has been considered.

- A novel approach to assess the seismic safety of jointed concrete dams has been undertaken and a safety index based on allowable displacements has been proposed.

1.5 Organization of the thesis

The thesis is organized in eight chapters as shown in Fig. 1.5. Following the introduction, Chapter 2 presents a review of the literature relevant to the objectives of the thesis. The definition of concrete lift joints according to construction codes and joint material properties defined from empirical relations as well as experimentally measured properties are reviewed. The various aspects of finite element simulations of jointed structures are presented. Past investigations on the static and dynamic stability of jointed dams are also described.

Chapter 3 and Chapter 4 cover the whole experimental programme that led to the development of the proposed concrete-concrete interface constitutive model. In Chapter 3 the experimental program is presented. The test specimens, the test setup, and the instrumentation, are described. The testing procedures used for the various types of tests that were conducted are discussed: static shear strength tests, bending tests, and static and dynamic sliding friction tests.

The measured strengths for the various types of tests are presented in Chapter 4. The specimens behaviour under the various tests is thoroughly described. The effects of various parameters such as surface roughness, velocity and acceleration, and degradation of the joint surfaces, are discussed. Static predynamic, dynamic, and static postdynamic responses are compared.

From the experiments described in Chapter 3 and Chapter 4 a hysteretic lift joint sliding friction constitutive model was developed in Chapter 5. It reproduces the measured experimental behaviour. The complete constitutive model covers the behaviour of an uncracked joint, up to a fully cracked joint, by coupling a nonlinear fracture mechanics based cracking model to the sliding friction constitutive model.

Chapter 6 covers the finite element implementation and validation of the joint constitutive model. The nonlinear solution algorithm for static tensile fracture, static shear

failure, and dynamic analysis are described. Simple validation problems are presented to highlight the advantages and deficiencies of the joint constitutive model.

Applications of the nonlinear constitutive model to the static and seismic analysis of a jointed gravity dams (90m high) is presented in Chapter 7. The number of modelled lift joints has been varied. The surface preparation was considered to be "good" in a first series (water blasted interface) and "bad" (untreated) in a second series. The uplift pressure effect was investigated. Comparisons between pseudo-static and pseudo-dynamic seismic analyses, generally used in practice, and nonlinear finite element dynamic stability analyses, have been discussed.

Finally, the conclusions of this research program, and the recommendations for industrial application of the experimental results and the proposed nonlinear constitutive model are presented in Chapter 8. Recommendations for future research are also discussed in this chapter.

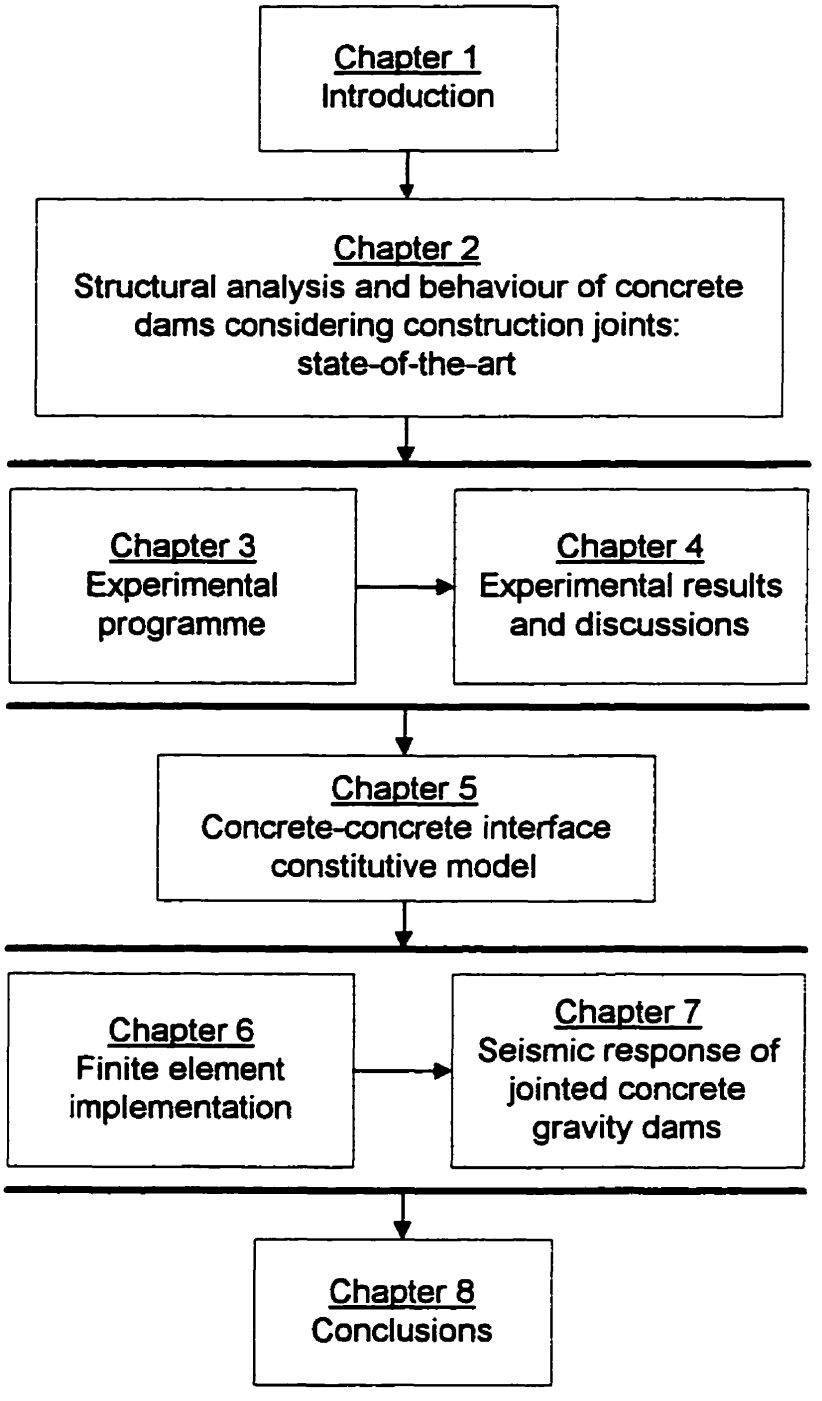

Fig. 1.5 *Organization of the thesis.*

CHAPTER 2

Structural analysis and behaviour of concrete dams considering construction joints: state-of-the-art

2.1 Introduction

This chapter covers in the first section, the available concrete joints material data gathered from the literature together with the values suggested by dam safety guidelines. Various constitutive models applicable to joints are presented in the second section. The implementation of joint models into a finite element analysis is discussed in the third section. A review of past investigations and case studies concludes the chapter. A more detailed literature review is available in Fronteddu (1994).

2.2 Joints in dams

In this section, the purpose of providing joints in a dam structure is explained. The various requirements on joint preparation are described. The material properties, as suggested in the literature, are presented.

2.2.1 Definition and purpose

Pacelli et al. (1993) defined construction joints as locations where the existing concrete has become so rigid that newly placed concrete cannot be integrally incorporated with it. ICOLD (1986) defines seven types of joints: (i) contraction or monolithic joint, (ii) expansion joint, (iii) isolation joint, (iv) control joint, (v) horizontal lift joint, (vi) construction joint, and (vii) cold joint. The first four types of joints are introduced on purpose by the dam designer to accommodate geometrical changes or movements. These are non-adhesive joints.

Horizontal lift joints, construction joints and cold joints are adhesive type of joints where bonding between surfaces is to be maximized in order not to affect the monolithic

action of the dam. These adhesive joints result from the construction techniques used, mainly the limited capacity of pouring concrete, and the requirements to be met on temperature control and shrinkage control (Xia et al. 1979, Garkun et al. 1989). Time elapsed between the first and second pour is of key importance for bonding. Joints are normally introduced in concrete structures to control cracking. The designer aims at having the least possible number of these joints. Different types of joints are illustrated in Fig. 2.1.

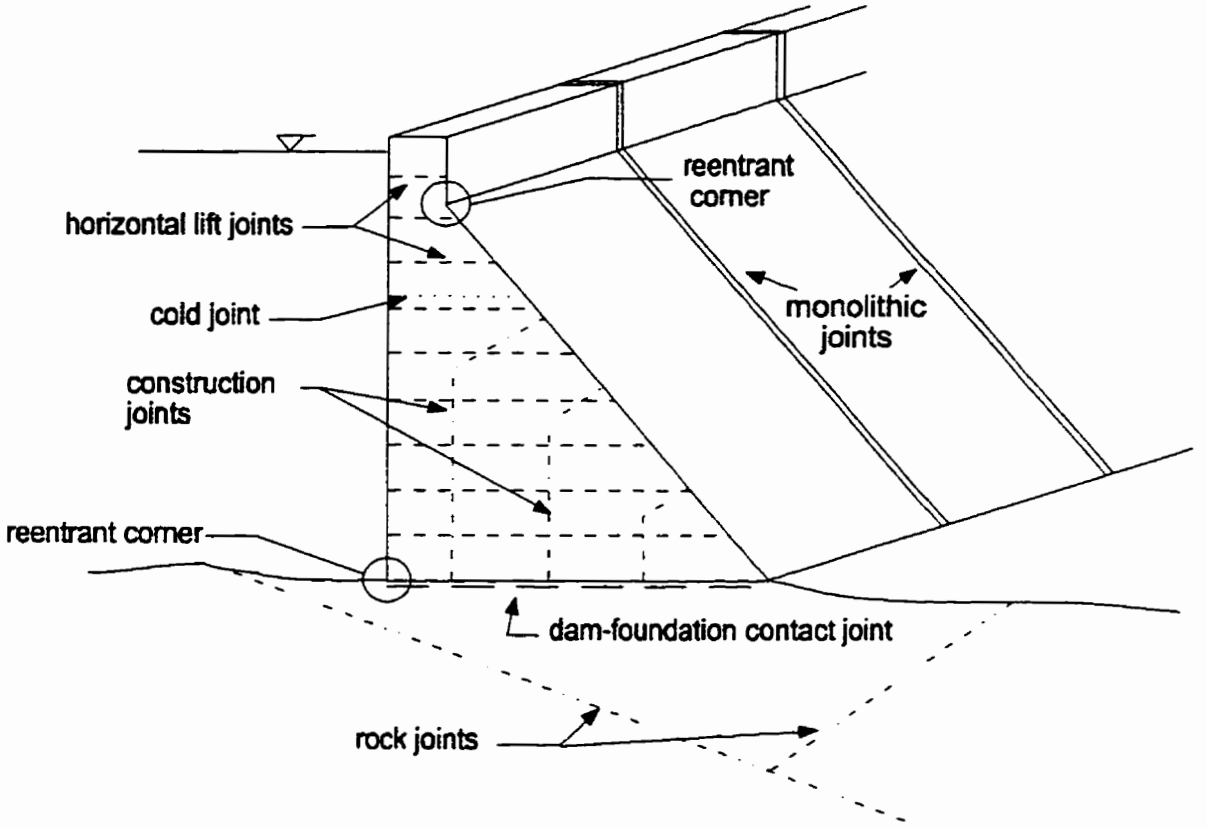

Fig. 2.1 *Planes of weakness in concrete dams.*

The surface preparation determines the bonding conditions thus the resistance of the joint. In samples taken from concrete dams, lift joints may be easily identified because of a layer of mortar or laitance. However, when the joints were cleaned before placing the next lift, they are difficult to see in samples (EPRI, 1992).

2.2.2 Joints and codes

In concrete codes in general, construction joints are considered as weak planes in an otherwise monolithic member (Suprenant, 1988). Tests on reinforced concrete beams indicated that construction joints reduce the shear strength by 40% but do not affect the shear strength of roughened members (in these tests, a roughened member had 1.6 mm (1/16 in) texture; Suprenant, 1988). Bending strength of reinforced concrete is not affected by construction joints (Suprenant, 1988). Most codes give provisions on how to prepare the surfaces and where to position the joints. The CSA CAN3.A23.1 code requires the cleaning of joint surfaces, the removing of the laitance, and the partial exposure of aggregates. Just before pouring the concrete, the surface should be wetted and the standing water should be removed. The use of stiffwire brushes, scabblers, waterblasters or sandblasters is suggested for cleaning and removing the laitance. Similar provisions may be found in the ACI 318-89 code.

For mass concrete, ACI Committee 207 (ACI 207, 1980) recommended wet sandblasting for cleanup of horizontal joint surfaces preparatory to placement of the next lift. Height of lifts is dependent on the specified means to limit temperature rise due to cement hydration. ACI 207 does not give any limitation on lift height. Typical lift heights range from 75 cm at the foundation for several lifts, through 1.5 m, and 2.3 m in gravity dams, and 3 m or more for semi-mass concrete structures. In cold weather, continuous lifts up to 15 m have been used.

ICOLD bulletin on dam construction (ICOLD, 1990) recommends two procedures for cleaning lift surfaces. Combined jet of water and compressed air at a minimum of 400 kPa is recommended on surfaces that have not completely hardened, while wet sandblasting is recommended on hardened surfaces. Joints on formed faces should be avoided, if not sand blasting and epoxy resin coating should be used. Roughening old concrete with hand tools or pneumatic hammers is to be avoided. According to ICOLD (1990) lift height is to be determined by (i) dissipation of the heat of hydration, and (ii)

formwork handling and cost. ICOLD gives no method for determining a lift height. Based on experience a lift height of 1.5 m with no artificial cooling of the concrete is generally adequate for heat dissipation.

Public utilities adopt their own technical guidelines based on codes, standards, current state-of-the-practice and experience. SEBJ (1992) recommends the use of grout on wide horizontal lift surfaces and concrete mixes with 20 mm maximum aggregate size. If deep narrow forms are used, reinforcement is provided at the bottom or if the bottom surface is irregular.

2.2.3 Plain concrete properties

Usually, lift joint properties are related to the intact dam concrete properties, it is thus advisable to briefly review intact concrete properties. However, important issues such as rate effects which have been investigated for homogeneous concrete specimens have not been quite studied for joints.

The assumed tensile strength, f_t, in analyses of concrete dams is often based on studies by Raphaël (1984). He suggested $f_t=0.324(f'_c)^{2/3}$ (MPa), which is usually replaced by the following simple expression $f_t=0.1f'_c$. Raphaël (1984) also suggested to increase the tensile strength by 50% for earthquake loading to account for rate effects on strength. The tangent modulus combined with the actual tensile strength does not result in the proper cracking strain because the stress-strain diagram before reaching the peak tensile stress is nonlinear. Therefore f_t may be further increased by 33% (Raphaël, 1984) while USBR (1976) suggests 20%. This increase is valid only for linear elastic analyses. The tangent modulus as suggested by CEA (1990) should be increased by 25% to account for rate effects (Bhattacharjee and Léger, 1992) .

Fracture mechanics (FM) properties of dam concrete are fairly different than structural concrete FM properties. Brühwiler and Wittmann (1990) measured specific fracture energy values, G_f, ranging between 175 N/m and 257 N/m for dam concrete, while Reinhardt et al. (1986) measured values between 60 N/m and 130 N/m for structural

concrete. Brühwiler and Wittmann (1990) observed that the dam concrete failure surface is characterized by aggregate cracking henceforth dam concrete G_f is affected by the nature and material properties of aggregates rather than by aggregate size. This would explain why G_f for dam concrete is greater than the corresponding value for structural concrete. They found no dependence of fracture properties on rate effects. However they observed a reduction in fracture energy with increasing precompressive loading, but unfortunately they did not quantify this decrease. Saouma et al. (1991b) observed a reverse effect on the fracture toughness. They measured the fracture toughness, K_{Ic}, in situ and observed that due to confining effects the in situ K_{Ic} would be approximately three times the one measured in laboratory.

How may the knowledge acquired on rate effects and confinement effects on intact concrete be extended to construction joints? In practice, joint tensile strength has been magnified due to dynamic loading as it is the usual practice for intact concrete. It makes sense to believe that cohesion increases as tensile strength does increase. Dependency of angles of friction, ϕ, on the sliding velocity is still an open question for debate (Oden and Martins, 1985). However, NRC (1990) states that in seismic safety evaluation of dams, the static values of the cohesion and friction angle are usually not increased for rapid loading rate effects due to a lack of experimental evidence to justify a magnification factor.

2.2.4 Strength of material properties

Attention given to surface preparation may vary from site to site, thus an in situ testing program is mandatory to assess reliable joint properties (EPRI, 1992). Field data, tests on cores or in situ testing, serve two purposes. First, the strengths measured for a given site are usually greater than the ones obtained from empirical estimates meant to be lower bounds in the design process. Second, site investigations reduce the uncertainty, thus lower factors of safety may be adopted (EPRI, 1992).

If no field data is available, empirical estimates are required. Dowling and Hall (1989) suggested to use a tensile strength of $0.5\sqrt{f_c'}$ (in MPa) which may be increased by

15% to account for rate effects. Ahmadi and Khoshrang (1992) suggested a tensile strength equal to 60% of the flexural tensile strength of plain concrete f_r, as given by ACI (1990):

$$f_{Tj} = 0.6 f_r = 0.36\sqrt{f'_c} \tag{2.1}$$

where f_{Tj} is the joint tensile strength. For cold joints, Reich (1993) adopted a tensile strength of 55% the splitting strength (from split cylinder tests) of plain concrete or 66% of the direct tensile strength of plain concrete.

EPRI (1992) observed a great scatter of experimental results on the tensile strength and observed a poor correlation between f_{Tj} and f'_c. However, they suggested to use f_{Tj} =175 psi (1.207 MPa) as an average. For the shear strength, they recommended the following values for a bonded joint: τ_j=310 psi (2.14 MPa), ϕ=57°; and for an unbonded joint: τ_j=70 psi (0.48 MPa) and ϕ=49° and τ_j=0 and ϕ=48° as a lower bound. The guidelines proposed by the Canadian Dam Safety Association (CDSA, 1995) recommend to use the following joint tensile strength: f_{Tj} =0.05f'_c. The shear strength in mass concrete (cohesion) should be taken as $\tau_c = 0.17\sqrt{f'_c}$. The cohesion at lift joints could be taken as half that of mass concrete unless joints are deteriorated. The angle of static friction ϕ_n may be taken as 55° and the angle of residual sliding friction ϕ_r may be taken as 45°. CDSA (1995) states two Mohr-Coulomb formulas for computing peak and residual shear strengths:

$$\begin{aligned} \tau_p &= \sigma_n \tan\phi_n + \tau_o \\ \tau_r &= \sigma_n \tan\phi_r + \tau_n \end{aligned} \tag{2.2}$$

where τ_p is the joint peak shear strength, τ_o is the threshold shear strength (cohesion), τ_r is the residual shear strength, τ_n is the nominal residual shear strength value up to 100 kPa (if supported by tests, if not it should be considered as zero), σ_n is the normal stress acting on the joint. The shear stress-displacement response and the Mohr-Coulomb envelope are

illustrated in Fig. 2.2. The apparent cohesion, τ_{app}, corresponds to the cohesion assuming a linear failure envelope tangent to ϕ_n. It should be noted that different safety factors correspond to peak and residual shear strengths.

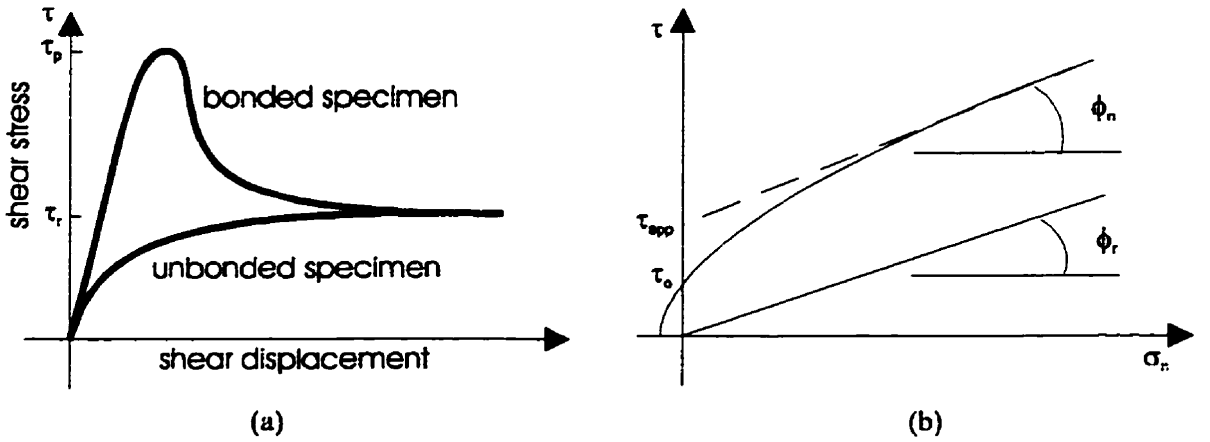

Fig. 2.2 *(a) Shear stress-displacement response and (b) failure envelope.*

2.2.5 Experimental evidence

Few experimental studies have been conducted on construction joints. The data gathered in the literature is site specific. Link (1969) considers that, for a quality built concrete dam, cohesion values between 2.5 MPa and 3.5 MPa, and friction angles between 45° and 54.5° (μ=1.0 and μ=1.4) could be adopted. He reported tests performed by French engineers on construction joints which showed little less shear strength than general mass concrete.

Pacelli et al. (1993) reviewed the effectiveness of joint treatment at several dam sites in Brazil. These treatments were wet sandblasting, greencutting, and high pressure waterblasting. Mechanical properties are governed by joint treatment. Untreated joints had average tensile strength and shear strength of 40% monolithic, while treated joints reached 85% monolithic on average. The authors consider treated joints as being as good as monolithic concrete. The best treatments are high pressure waterblasting and wet sandblasting, but properly controlled greencutting at early age (i.e. less than 5 days) is

almost as good. Providing a mortar layer on treated joints increased the strength properties by at least 10% monolithic. Surface roughness had little effect.

McLean and Pierce (1988) gathered test data taken from the U.S. Bureau of Reclamation. The data distinguished between bonded and unbonded joints. A single friction angle value is used for peak and residual conditions. The friction angle, ϕ, for bonded joints varied between 25° and 78° with an average value of 55°, the cohesion varied between 205 psi and 527 psi (1.4 MPa and 3.6 MPa) with an average of 350 psi (2.4 MPa). The friction angle for unbonded joints varied between 35° and 51° with an average of 47°, the apparent cohesion varied between 18 psi and 216 psi (0.1 MPa and 1.5 MPa) with an average of 86 psi (0.6 MPa). The concept of apparent cohesion for unbonded joints is related to the shear failure envelope (see Fig. 2.2(b)). The authors could achieve a better fit on their experimental results by using a bilinear model. The parent material properties are as follows: $40° < \phi < 76°$ with an average of 58°, cohesion varied between 269 psi and 573 psi (1.9 MPa and 4.0 MPa) with an average of 364 psi (2.5 MPa). Unbonded joints apparent cohesion values are much lower than bonded joint cohesion values while angles of friction are similar. Shear strength values of bonded joints, whether treated or untreated, are comparable to parent material properties.

Lo et al. (1991a) defined three states to characterise core samples: (i) bonded: the contact is intact; (ii) weakly bonded: the contact is broken when received but the fracture surface is fresh and matching; and (iii) unbonded: the contact is broken when received, the fracture surface is weathered, and matching is very poor. Bonded contacts can resist tension and possess cohesion, while unbonded contacts exhibit only frictional resistance. Weakly bonded contacts are bonded contacts that were broken during drilling. Since the contact was not strong enough to resist the coring operations, Lo et al. (1991a) recommend to use the minimum values for strength and cohesion.

Lo et al. (1991b) proposed guidelines for determining joint friction angle from core samples. The friction angle, ϕ, is considered as being the sum of two components: the basic friction angle, ϕ_b, which corresponds to the sliding of two smooth surfaces, and the

roughness angle ,*i*, which accounts for the interlocking of asperities. Roughness is affected by scale effects thus samples a few orders of magnitude smaller than the real structure can only provide the basic friction angle. Lo et al. (1991b) suggested to calculate the basic friction angle as the difference between the friction angle measured in the laboratory and the roughness of the sample surface:

$$\begin{aligned} \phi_b &= \phi_{obs} - i_{obs} \\ \phi_{obs} &= \tan^{-1}(T/N) \;\; ; \;\; i_{obs} = \tan^{-1}(\delta_n/\delta_t) \end{aligned} \tag{2.3}$$

where ϕ_{obs} and i_{obs} are the friction angle and the roughness measured in the laboratory, N and T are the normal and tangential forces applied on the sample, δ_n and δ_t are the measured normal and tangential displacements. It is implicit in Eq.(2.3) that the normal and tangential displacements should be monitored during the tests. The real friction angle is the sum of the basic friction angle and the in situ roughness which should be evaluated on site. Lo et al. (1990) reported basic friction angles for concrete to concrete sliding between 29° and 36° with an average of 32°. They also measured cohesion values close to twice the tensile strength.

Besides strength of material properties, joint permeability is an important property. High permeability has several detrimental consequences as described earlier. For a joint without treatment and without mortar, Pacelli et al. (1993) measured coefficients of permeability in the order of 10^{-10}m/s or 90% of that of monolithic concrete. With treatment, the joints were as impervious as concrete.

2.2.6 Fracture mechanics properties

Tschegg et al. (1993) have studied the effect of construction joints on crack profiles. They conducted wedge splitting tests on specimens cast in two stages. The first half of the specimen (called old concrete in the following) was cast and left to cure for 28 days before the second half (called new concrete) was poured. In a series of specimens, the inner surface of the old concrete was smoothed with a hand brush, while in the second

series, the inner surface was sand blasted and moistened afterwards. The distance between the joint and the specimen center line (aligned with the notch) was also varied. A typical test specimen is shown in Fig. 2.3. Rough interface specimens fracture energy, G_f, was 50% greater than the smooth interface fracture energy: 15.2 N/m against 10 N/m, while the parent material fracture energy was 125 N/m. The fracture energy of an interface is roughly 10% that of the parent material. The observed crack profiles showed: (i) that the crack is deflected in the interface, and (ii) that cracks initiate in the interface and at the notch at the same time.

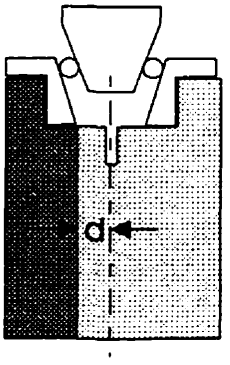

Fig. 2.3 *Wedge splitting test specimen with joint.*

Saouma et al. (1991a) conducted wedge splitting test on dam concrete on specimens similar to Tschegg et al. (1993). Three days after the first lift was poured, the inner surface of the old concrete was sandblasted to remove laitance, kept saturated dried and the second lift was poured. After 28 days the specimens were tested. They observed that the peak load for cold joint (CJ) specimens reached 50% of the monolithic specimens peak load. The fracture toughness, K_{Ic}, for CJ specimens was 40% to 70% that of monolithic specimens (0.52 $MN/m^{3/2}$ to 0.72 $MN/m^{3/2}$ vs 0.86 $MN/m^{3/2}$ to 1.34 $MN/m^{3/2}$), and the fracture energy, G_f, was 30% to 60% that of monolithic specimens (80.6 N/m to 138.4 N/m vs 223 N/m to 240 N/m). The higher G_f values correlated with rougher surfaces. Interestingly, Saouma and his colleagues observed that the residual crack opening displacement after each loading cycle was smaller for CJ specimens. In general, the CJ specimens exhibited higher variations and lower crack resistance results than monolithic specimens.

There is a great difference between Tschegg et al. (1993) and Saouma et al. (1991a) measured G_f values. In the first case, only 10% of the monolithic G_f value was reached, while in the second case 55% on average was reached. In addition, the specimens had different dimensions, Tschegg's specimens fracture area was twice that of Saouma's

specimens. More importantly, the old concrete surface in the Saouma et al. (1991a) study was only three days old when the new concrete was poured; while the old concrete surface was 28 days old when the second lift was poured by Tschegg et al. (1993).

2.3 Constitutive models for joints

Joints in dams are usually characterized by standard Mohr-Coulomb failure envelope e.g. tensile strength, cohesion, and angle of friction. Coulomb's model is a simple average representation of the crack shear resistance known as a friction type model. Sophisticated models, aggregate interlock models, may be devised to characterize shear on irregular surfaces. Figure 2.4 shows the different types of discontinuity constitutive models.

2.3.1 Shear friction models

In Coulomb's model, joint closure is assumed to occur suddenly and sliding is assumed to be rigid, as shown in Fig. 2.5. However there is a discrepancy between experimental observations and Coulomb's model, as shown in Fig. 2.6 and Fig. 2.7 for rock joints for example. For jointed materials such as rock, the normal stiffness at closing increases with the applied normal load to reach a constant value. Five factors have been identified by Bandis et al. (1983) to influence the normal stiffness k_{nn}: (i) the wall roughness, (ii) the initial contact area, (iii) the strength and deformability of the asperities, (iv) the thickness, type and physical properties of the infilling material, and (v) the interlocking state. The normal stiffness is found to be greater for an interlocked joint than for a dislocated joint but this difference decreases when the joint is submitted to load cycles (Bandis,1990). Unlike other joint properties, normal stiffness is not subjected to scale effects (Barton et al. 1985) because normal closure is dominated by small scale roughness. Issues such as closing and scale effects have not been studied for concrete lift joints. However, due to the similar nature of rock and concrete it is reasonable to assume a similar behaviour at a cracked lift joint.

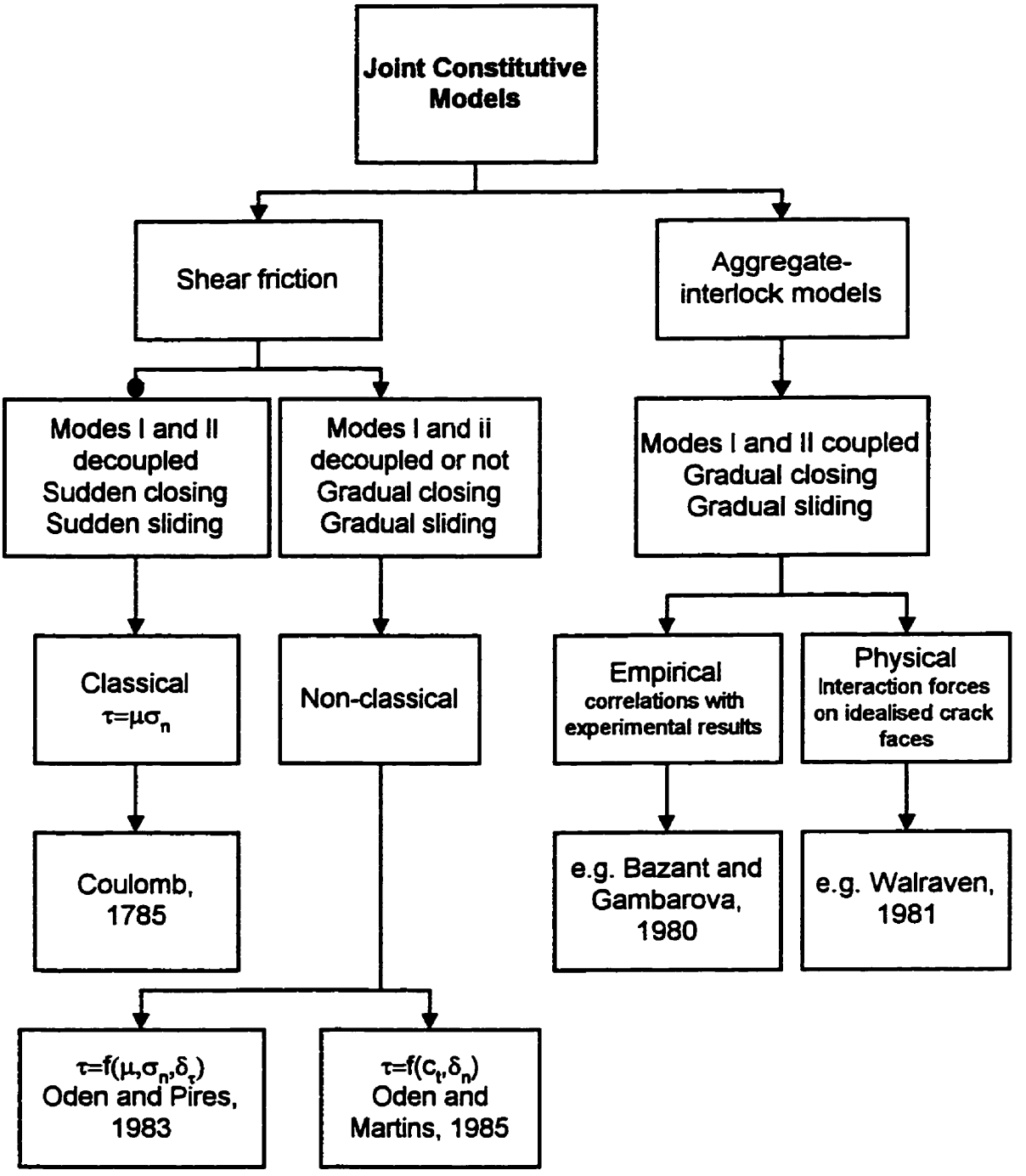

Fig. 2.4 *Constitutive models for discontinuities.*

To describe the behaviour of rock joints, two slopes linear model was first proposed by Goodman and Dubois (1972) assuming the joint could resist some tension, σ_t, before complete separation.

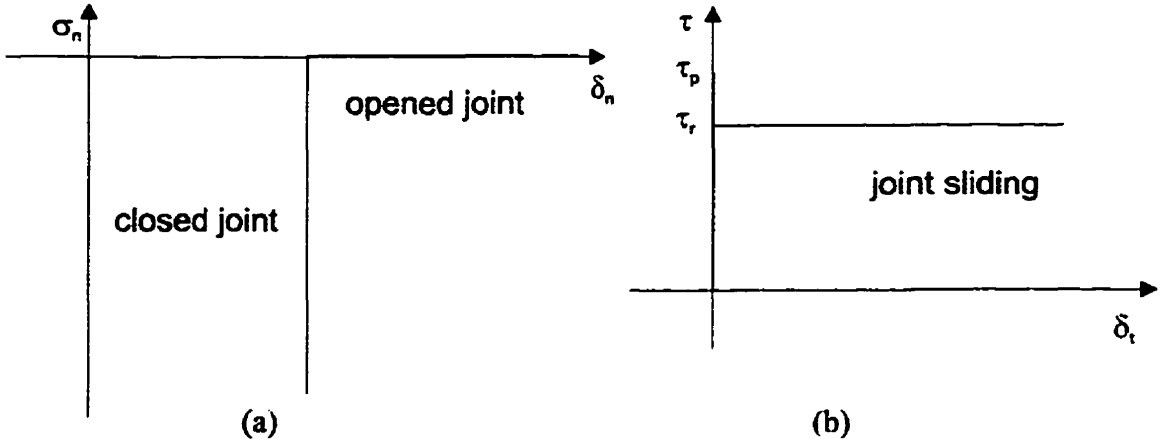

Fig. 2.5 *Stress-displacement relationships in Coulomb model: a) normal, b) tangent.*

Hyperbolic function were also proposed (Goodman, 1974) :

$$\sigma_n = \left(\frac{\delta_n}{\delta_{nm} - \delta_n}\right)\sigma_i + \sigma_i \qquad (2.4)$$

where δ_n is the closure, δ_{nm} is the maximum closure, σ_i is the initial stress level at zero deformation which would result in a vertical offset from the origin (Fig. 2.6).

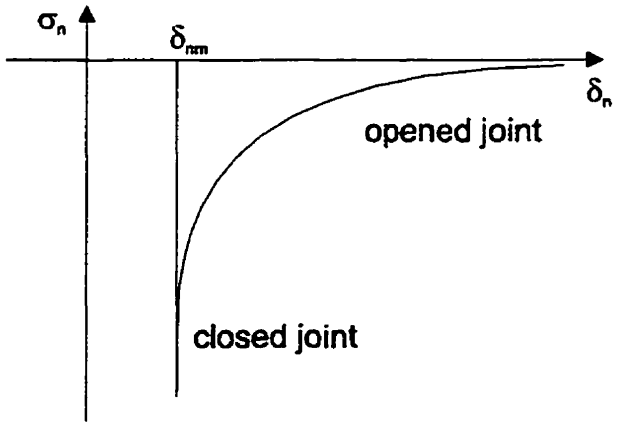

Fig. 2.6 *Typical rock joint behaviour as modelled by Goodman (1974).*

For dislocated joints, hyperbolic function does not fit very well the experimental data, hence semi-log expressions were proposed (Bandis et al. 1983):

$$\log\sigma_n = p + q\log\delta_n \tag{2.5}$$

where p is the initial normal stress and q is a best fit coefficient. Very often, the load-displacement relationship is assumed to be nonlinear elastic in cyclic compression of the joint, i.e. the cycles are nonhysteretic.

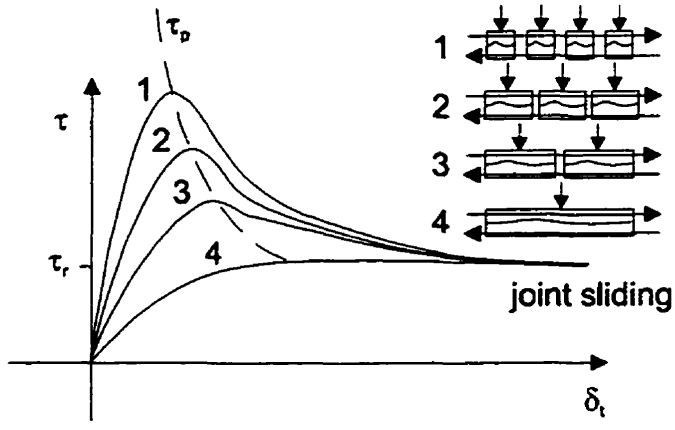

Fig. 2.7 *Typical rock joint behaviour in shear (adapted from Bandis, 1990).*

Joint shear stress-displacement relationship (Fig. 2.7) may be divided into three zones (Sun et al. 1985): (i) a stiff zone until τ reaches a high proportion of the peak shear stress (τ_p), (ii) a transition zone from the elastic to the plastic state, and (iii) a sliding zone. This relationship is scale dependent: the peak shear stress (τ_p) decreases with an increasing joint area (Bandis et al. 1981). For different joint lengths, the joint shear behaviour is controlled by irregularities of different sizes hence, among joint properties, shear stiffness is the most affected by scale effects (Barton et al. 1985). Bandis et al. (1981) also realized that nonlinear pre-peak behaviour is more pronounced for weathered joints than for fresh joints. Similarly, Saeb and Amadei (1992) observed that the structural behaviour is a function of the mated state of the joint: unmated joints are more flexible than mated joints.

Elasto-plastic shear stress-displacement relationships are often adopted (Goodman and Dubois, 1972, and Xiurun, 1981). The transition from the peak shear stress to the residual stress may be modelled by a sudden drop (Xiurun, 1981) or with softening

(Goodman, 1976). Nonlinear equations have also been used as shear stress-displacement relationships (Kulhaway, 1975).

Dilatancy may or may not be considered according to the effect it may have on the solution. As defined by Plesha (1987), the dilatancy is the tendency of two bodies to separate during relative tangential motion because the asperity surfaces of one body slide on those of the other. If the dilatancy is constrained, compressive normal stresses will be induced on the joint surfaces. Dilatancy requires a finite tangential displacement to be mobilized (Barton et al., 1985). It increases while reaching the peak shear stress and decreases in the post-peak range. Dilatancy decreases with increasing normal stress (Gerrard, 1986) and also decreases with increasing shear displacement in the post-peak range (Bandis, 1990). As the joint dilates, the local bearing stress on the asperity increases and so does the local friction stress. At once, the energy required to shear through the asperity will be smaller than the energy spent to slide over the asperity (Bro, 1992).

Dilatancy is hard to measure experimentally. Very often it is simply neglected. However, dilatation plays an important role in water conductivity of joints. Barton et al. (1985) used the concept of dilatation angle, ψ_o, to predict the joint opening δ_n:

$$\delta_n = \delta_t \tan \psi_o \tag{2.6}$$

The dilatation angle is a function of the mobilized joint roughness coefficient (JRC).

In the above models, the peak shear stresses or residual shear stresses are defined in relation with the applied normal load using the classical Mohr-Coulomb formula, as in Eq.(2.2). The most recognized definition of the friction angle was proposed by Bandis et al. (1981) as:

$$\phi = \phi_b + \psi_o + S_A^o \tag{2.7}$$

where ϕ_b is the basic friction angle (measured on a smooth undamaged surface), ψ_o is the dilatation angle, and $S_A{}^\circ$ is a geometric or failure component which Sun et al. (1985) considered as being the frictional resistance produced by wear. The friction angle may be evaluated using the joint roughness coefficient JRC and joint wall compressive strength JCS. Jaeger and Cook (1979) proposed to evaluate ϕ as:

$$\phi = \phi_b + \psi_o \tag{2.8}$$

Gerrard (1986) proposed the following equation for ϕ:

$$\phi = \left(\phi_b + \psi_o - \phi_f\right)\left(1 - \bar{\sigma}\right) + \phi_f \tag{2.9}$$

where ϕ_f is the angle at shearing through the asperities, and $\bar{\sigma}$ is the average relative normal stress i.e. the ratio (σ_n/σ_f) between the applied normal stress (σ_n) and the normal stress (σ_f) at which failure occurs through the asperities. Simple linear failure envelopes could be enhanced at lower σ_n by using a nonlinear equation to be in better agreement with test results (Ladanyi and Archambault, 1969, and Gerrard, 1986). Similarly, EPRI (1992) suggested the use a of bilinear envelope at low σ_n for concrete lift joints.

The shear strength of rock joints is strongly anisotropic (Handanyan et al., 1990). The basic friction angle ϕ_b is independent of the sliding direction because it is a material property, but the sum (ψ_o+$S_A{}^\circ$) is direction dependent because it is a surface property. In addition, the sum (ψ_o+$S_A{}^\circ$) is scale dependent and decreases with increasing joint length (Bandis et al., 1981). The shear strength is also scale dependent (Huang and Doong, 1990). Therefore laboratory test data may not warrant a conservative design, and a method requiring a mapping of the site into weaker and stronger zones and a statistical assessment of the measured properties should be adopted (Volpe et al., 1991). The formula proposed by Lo et al. (1991b), Eq.(2.3), for calculating the joints friction angle is very similar to Bandis et al. (1981) expression where the sum (ψ_o+$S_A{}^\circ$) would be substituted by the roughness angle *i*.

Alternatives to the Mohr-Coulomb sliding model may be found in the literature. Oden and Pires (1983) suggested to consider the nonlocal and nonlinear character of friction. The nonlocal attribute implies that motion at a point of contact (say an asperity) will occur when the shear stress at that point reaches a value proportional to a weighted measure of the normal stresses in the neighbourhood of the point. The nonlinear attribute is a correction to the rigid plastic assumption of Coulomb friction. As a result, Oden and Pires (1983) proposed the following expression for the tangential stress, $\tau(\delta)$:

$$\tau(\delta) = -\mu\, S_\rho(\sigma_n(\delta))\, \phi_\epsilon(|\delta_t|)\frac{\delta_t}{|\delta_t|} \tag{2.10}$$

where δ is the vector of displacements, δ_t is the tangential displacement, μ is the coefficient of friction, $S_\rho(\sigma_n(\delta))$ is nonlocal normal stress distribution function, $\phi_\epsilon(|\delta_t|)$ is the nonlinear stress function.

Oden and Martins (1985) enhanced the previous model by defining the normal and tangential stresses in terms of compliance:

$$\begin{aligned} \sigma_n(\delta) &= -c_{pn}\langle \delta_n - g \rangle_+^{m_n} \\ |\tau(\delta)| &\le c_{pt}\langle \delta_n - g \rangle_+^{m_t} \end{aligned} \tag{2.11}$$

where c_{pn}, c_{pt}, m_n and m_t are material properties, δ_n is the normal displacement, g is the initial gap opening, and $\langle\,\rangle_+$ is the Macaulay bracket. Based on Tolstoi's (1967) work, they considered a single coefficient of friction independent of velocity. Ibrahimbegovic and Wilson (1989) adopted a similar approach in seismic analysis of gravity dams with nonlinear behaviour at the dam foundation contact joint.

2.3.2 Aggregate interlock models

The approach adopted in dam engineering up to now has been to extend what was known for rock joints to concrete joints and cracks. Joint surfaces are not perfectly flat due to surface preparation and cracks may not be necessarily confined in the joint but rather run in the surrounding concrete. Therefore, it is worthwhile to inquire if what is known for fully cracked concrete behaviour may be extended to joints.

Cracked concrete behaviour in shear is dictated by the interaction of aggregates bearing against a mortar paste. Cracks run along aggregates unless these are weaker than the cement paste. When the crack is subjected to shear loading, the two faces move relative to each other in opposite directions constraining aggregates to bear against mortar. Stresses applied on mortar by an aggregate are a combination of radial stresses and frictional stresses. The resultant force is not parallel to the crack put rather at an angle and this causes the crack to open even more. This dilatation coupled with friction makes tangent crack behaviour dependent on applied load and external restraints. Reinhardt and Walraven (1982) defined aggregate interlock as the result of an interaction between shear displacements and normal displacements on the one hand, and shear stresses and normal stresses on the other hand.

Frictional stresses cannot exist without compressive stresses (Bažant and Gambarova, 1980). There is not a single characteristic stress-displacement (stress-slip) relationship for aggregate interlock (Divakar et al., 1987). The stress-slip relationship depends on the normal loading situations at the crack i.e. whether or not there is some kind of normal stiffness which restrains dilatation, thus increasing the normal stress, thus increasing the shear resistance.

The traditional approach is to express stresses in terms of displacements as $\sigma_n = f_n(\delta_n, \delta_t)$, and $\tau = f_t(\delta_n, \delta_t)$ where f_n and f_t are normal and tangential function, respectively. The stiffness formulation may be written as:

$$\begin{Bmatrix} d\sigma_n \\ d\tau \end{Bmatrix} = \begin{bmatrix} B_{nn} & B_{nt} \\ B_{tn} & B_{tt} \end{bmatrix} \begin{Bmatrix} d\delta_n \\ d\delta_t \end{Bmatrix} \tag{2.12}$$

where σ_n is the stress normal to the crack, τ is the shear stress along the crack, δ_n and δ_t are the normal and tangential displacements. The stiffness coefficients are derived from the *f* functions:

$$B_{nn} = \frac{\partial f_n}{\partial \delta_n} \quad , \quad B_{nt} = \frac{\partial f_n}{\partial \delta_t} \quad , \quad B_{tn} = \frac{\partial f_t}{\partial \delta_n} \quad , \quad B_{tt} = \frac{\partial f_t}{\partial \delta_t} \tag{2.13}$$

This stiffness formulation can be used with any model. The stiffness matrix generated by the derivatives of Eq.(2.13) is in most cases not symmetrical. This causes the principal strains and stresses directions not to remain parallel.

Aggregate interlock models may be divided in two groups (Feenstra et al., 1991a): (i) the empirical models, directly based on experimental data, and (ii) the physical models, resulting from conceptual work.

2.3.2.1 Empirical models

They are the result of a correlational work on experimental variables chosen by the authors. Fenwick and Paulay (1968) were the first to conduct a detailed experimental study on aggregate interlock and to suggest an empirical set of equations. Since then, others, e.g. Taylor (1974), Houde and Mirza (1974), Mattock (1974), Paulay and Loeber (1974), Laible et al. (1977), have also proposed their own models. Bažant and Gambarova (1980) gathered some of the available experimental data at the time to devise the rough cracks model (later improved by Gambarova and Karacoç, 1983).

Other empirical models have been proposed in the literature: Chen and Schnobrich (1981); Reinhardt and Walraven (1982); Divakar et al., (1987); Yoshikawa et al., (1989). Among these models, only Bažant and Gambarova (1980) involve the maximum aggregate

size, D_{max}, as a parameter. Reinhardt and Walraven (1982) did not find that D_{max} had any definite effect on the response. Tassios and Vintzéleou (1987) attempted to model the full response of a crack under cyclic loading.

Empirical formulations may become quite complex. The equations do not have any physical sense and the important parameters are usually hidden behind regression coefficients. For example, Yoshikawa et al. (1989) involves 20 material constants obtained from numerical regression.

2.3.2.2 *Physical models*

Physical models are based on solving for the interaction forces, which may be identified easily between two idealized crack surfaces, as shown in Fig. 2.8. Some researchers assimilate the crack surface to a flat surface disrupted by protruding spherical aggregates, others to a crenellated surface, a serrated surface, or a sinusoidal surface. The idealization ends up in formulations gathering relevant surface properties.

Walraven (1981) proposed a model (the two-phase model) that became a benchmark. Concrete is considered as being a collection of spherical aggregate particles embedded in a mortar matrix (Fig. 2.8a). Bond between aggregate and mortar is the weakest link. In addition, aggregates are much stronger than mortar in structural concrete. The overall crack roughness (the tortuous crack path in mortar) is excluded because it is considered to have a minor effect on the response compared to the roughness caused by aggregates. The aggregate size plays a subordinate role in the shear response compared to the grading curve. The distance between aggregates causes the resistance mechanism in aggregate interlock to be dominated by plastic deformations in mortar resulting from the bearing action of aggregates. This explains the proportionality between the shear resistance and the mortar strength. Walraven's two-phase model has been extended to reverse cyclic loading first by Pruijssers (1988) and then by Walraven (1994). Other physical models were proposed in the literature: Riggs and Powell (1986); Skrikerud and Bachmann (1986); Divakar and Fafitis (1992).

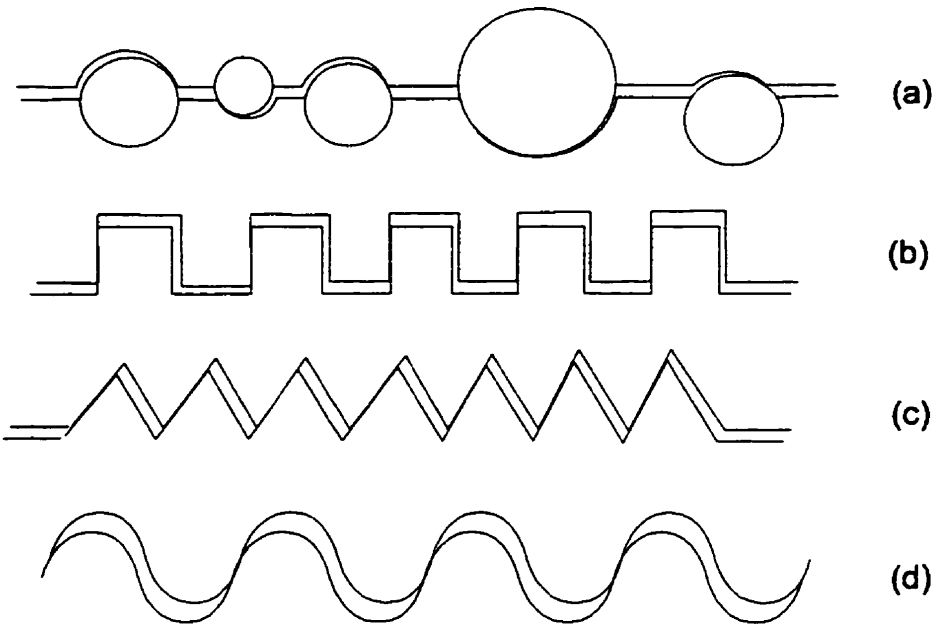

Fig. 2.8 *Idealized crack profiles: a) flat surface with protruding aggregates, b) crenellated, c) serrated, d) sinusoidal*

This study of different aggregate interlock models shows that the general understanding of shear transfer across cracked concrete surface has evolved significantly in the past twenty years. But even in so called physical models, a great level of empiricism is required to match the observed phenomena with numerical tools.

2.4 Structural models for discontinuities

There are two approaches for modelling discontinuities: (i) the continuum approach, and (ii) the discrete approach, as shown in Fig. 2.9. In continuum approaches, the discontinuity is not modelled as such but rather its effects on the behaviour of the continuum are captured somehow. In discrete approaches, the discontinuity is explicitly included in the finite element mesh.

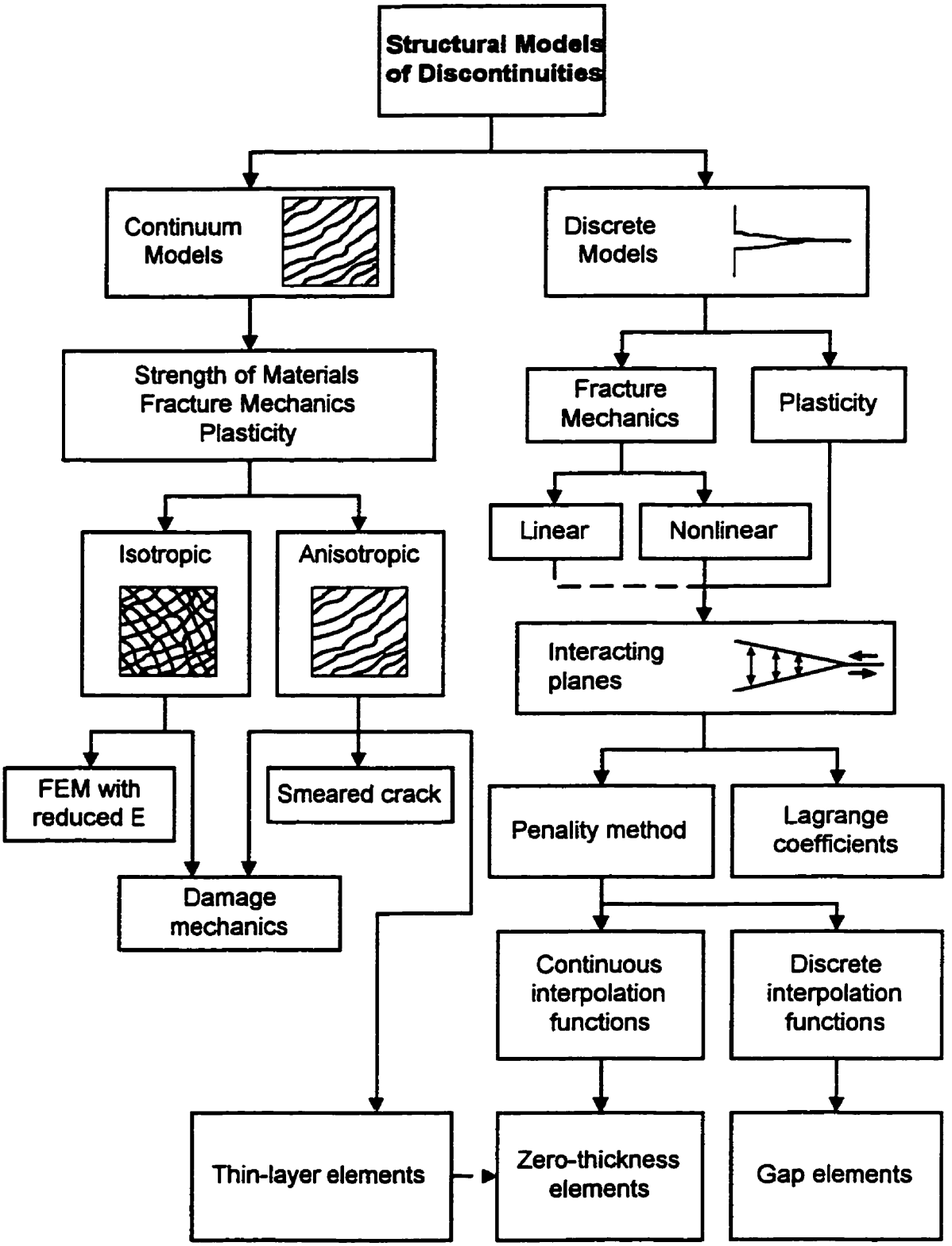

Fig. 2.9 *Structural models of discontinuities.*

2.4.1 Continuum models - isotropic formulation

The traditional way of treating cracks or closely spaced joints in a finite element analysis is to use a reduced stiffness (Fardis and Buyukozturk, 1979). Isotropic damage mechanics formalizes this simple approach. The stress tensor (σ) is uniformly reduced by multiplying the linear elastic response by a reduction factor namely a damage variable. It may be expressed as:

$$1.\sigma = (1-d)[C_0]\{\varepsilon\} \tag{2.14}$$

where d is the damage variable, $[C_0]$ is the elasticity matrix of uncracked concrete, $\{\varepsilon\}$ is the strain tensor (Ghrib and Tinawi, 1994). The damage variable is computed according to the initial state and deformation history.

2.4.2 Continuum models - anisotropic formulation

Anisotropic models take into account the crack orientation in the determination of the constitutive matrices. The following will focus on the definition of the shear rigidity, for more details the reader is referred to Bhattacharjee and Léger (1992) for a thorough literature review on this topic.

The basic orthotropic constitutive matrix may be expressed as:

$$\begin{bmatrix} \sigma_n \\ \sigma_t \\ \tau_{nt} \end{bmatrix} = \begin{bmatrix} H_n & \nu_{tn} H_n & 0 \\ \nu_{nt} H_t & H_t & 0 \\ 0 & 0 & G_{nt} \end{bmatrix} \begin{bmatrix} \varepsilon_n \\ \varepsilon_t \\ \gamma_{nt} \end{bmatrix} \tag{2.15}$$

where directions n and t are the orthotropic directions, ν_{ij} are the Poisson's ratio, and G_{nt} is the shear modulus. Parameters H_n and H_t correspond to:

$$H_n = \frac{E_n}{1 - \nu_{nt}\nu_{tn}} \quad , \quad H_t = \frac{E_t}{1 - \nu_{nt}\nu_{tn}} \tag{2.16}$$

In recent years, research efforts have been mainly focused on defining the moduli E_n and E_t to reproduce crack propagation. Shear response did not receive as much attention. Typically, the shear modulus is defined as $G_{nt}=\beta_s G$ where β_s is a shear retention factor which accounts for the degradation of the shear modulus due to crack development (Suidan and Schnobrich, 1973).

Bhattacharjee and Léger, (1994) studied crack propagation in concrete dams using a smeared crack model where the shear retention factor was evaluated as:

$$\beta_s = \frac{1+\nu}{1-\eta\nu^2}\left(\frac{\eta\varepsilon_n - \varepsilon_t}{\varepsilon_n - \varepsilon_t} - \eta\nu\right) \tag{2.17}$$

where η is the ratio between the damaged secant modulus and the initial isotropic elastic modulus, and ν is the Poisson's ratio. The choice of ϵ_n and ϵ_t dictates the type of model: if they are the principal strains at all times, the model is said to be coaxial rotating, if they are always chosen along the initial orientation of cracking it is said to be fixed.

Ghrib and Tinawi (1994) proposed an anisotropic damage mechanics model that allows cracking in 2 directions. Damage is captured through the d_i variables which correspond to two perpendicular directions (i=1,2). The authors introduced a damage limit, δd_R, which controls rotation. If a stress-state yields an increase in damage greater than δd_R, the damage direction will be rotated towards the principal stress direction. Fixed crack models tend to be biased by the mesh and do not succeed to reproduce mixed mode loading situations that cause crack rotation such as in concrete dams (Ghrib and Tinawi, 1994). Rotating crack models are much more efficient in these situations.

Gajer and Dux (1990, 1991) evaluate the softened shear modulus, $G(w)$, explicitly as a function of the crack opening, w, using an aggregate interlock formula based on Divakar et al. (1987) instead of using a shear retention factor.

In their crack band model, Bažant and Oh (1983) introduced the concept of fracture energy in a smeared crack model which enhanced the evaluation of the normal stiffness. The concept of fracture energy has also been applied to the shear response by defining a shear softening curve similar to the tensile softening curve (Rots and de Borst, 1987). The mode II shear softening modulus, D^{II}, is related to the ultimate shear stress, τ_u, and the mode II fracture energy, G_f^{II}. The stress-free crack shear strain, γ_u, is calculated as the stress-free normal strain, ϵ_u: $\gamma_u=2\times G_f^{II}/(\tau_u\times h)$ where h is the finite element characteristic length. The elastic shear modulus is assumed to hold until cracking. At onset of cracking, the cracked shear stress is assumed to start at zero with a D_o^{II} shear stiffness. Shear stresses will develop upon rotation of the principal stress axes. However, this approach has not been developed any further because of the difficulty to define the mode II fracture energy.

Models that gather in a compact fashion the elastic, the crack tensile softening response, and the fully cracked response were proposed by Dahlblom and Ottosen (1990) and Gambarova and Valente (1990).

The great advantage of continuum models is to enable the prediction of the crack propagation with a single finite element mesh. However, at closing, in most models the material is assumed to recover its initial elastic properties except in El-Aidi and Hall (1989a,b) who studied the seismic response of jointed gravity dams. This shortcoming discourages the use of a continuum formulation for studying joints specially in dams where the objective is not only to study crack propagation in the joint but also to assess global sliding/overturning stability.

2.4.3 Discrete models

2.4.3.1 Interface elements

In discrete models, the crack or the discontinuity is modelled explicitly instead of being smeared in a given volume. Discrete models may be used in different contexts:

(i) directly through special joint finite elements i.e. interface elements (gap-elements, zero-thickness elements, thin-layer elements), (ii) based on theoretical solutions given from fracture mechanics, or (iii) in a combination of the previous two.

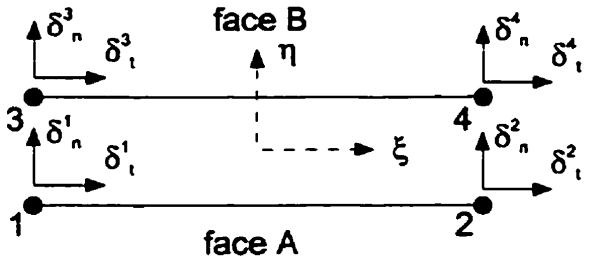

Fig. 2.10 *Joint interface element*

The mathematical derivation of interface elements is similar to standard finite elements derivation. An interface element is shown in Fig. 2.10. The vector of nodal displacements is $\{a\}=\{\delta^1_n \ldots \delta^4_n\ \delta^1_t \ldots \delta^4_t\}$. If the following constitutive matrix $[C]$, where the coupling terms are set to zero just like in Goodman et al. (1968), is adopted:

$$[C] = \begin{bmatrix} k_n & 0 \\ 0 & k_t \end{bmatrix} \tag{2.18}$$

the stiffness matrix of the whole element, assuming linear interpolation functions, yields:

$$[K] = \frac{1}{6}bl\begin{bmatrix} 2k_n & k_n & -2k_n & -k_n & 0 & 0 & 0 & 0 \\ k_n & 2k_n & -k_n & -2k_n & 0 & 0 & 0 & 0 \\ -2k_n & -k_n & 2k_n & k_n & 0 & 0 & 0 & 0 \\ -k_n & -2k_n & k_n & 2k_n & 0 & 0 & 0 & 0 \\ 0 & 0 & 0 & 0 & 2k_t & k_t & -2k_t & -k_t \\ 0 & 0 & 0 & 0 & k_t & 2k_t & -k_t & -2k_t \\ 0 & 0 & 0 & 0 & -2k_t & -k_t & 2k_t & k_t \\ 0 & 0 & 0 & 0 & -k_t & -2k_t & k_t & 2k_t \end{bmatrix} \tag{2.19}$$

where b is the out of plane thickness, l is the element length. Now, if instead of considering the displacement fields along the element length, the nodal displacements were considered to represent a certain tributary area, A. The stiffness matrix would be:

$$[K] = \frac{1}{2}bl\begin{bmatrix} k_n & 0 & -k_n & 0 & 0 & 0 & 0 & 0 \\ 0 & k_n & 0 & -k_n & 0 & 0 & 0 & 0 \\ -k_n & 0 & k_n & 0 & 0 & 0 & 0 & 0 \\ 0 & -k_n & 0 & k_n & 0 & 0 & 0 & 0 \\ 0 & 0 & 0 & 0 & k_t & 0 & -k_t & 0 \\ 0 & 0 & 0 & 0 & 0 & k_t & 0 & -k_t \\ 0 & 0 & 0 & 0 & -k_t & 0 & k_t & 0 \\ 0 & 0 & 0 & 0 & 0 & -k_t & 0 & k_t \end{bmatrix} \tag{2.20}$$

It is obvious in Eq.(2.20), that forces at nodes 2 and 4 are independent from the displacements at nodes 1 and 3. Thus there is no coupling between nodal pairs along the interface element. This derivation is equivalent to using gap elements. Therefore a single derivation gathers both types of elements which are devised according to the interpolation function adopted.

If a thickness is assigned to the joint element, a strain vector can be defined by simply dividing the relative displacements by the thickness. That is the thin-layer element (Ghaboussi et al. 1973). A thin-layer element is a standard element with a reduced thickness. The constitutive matrix is the isotropic plane stress or plane strain elasticity matrix where the following joint properties would be substituted for the elastic modulus, E, and the shear modulus, G:

$$\begin{aligned} E &= h_{if}\,k_n \\ G &= h_{if}\,k_t \end{aligned} \qquad \nu = \frac{E}{2G} - 1 = \frac{k_n}{2k_t} - 1 \tag{2.21}$$

where h_{if} is the element thickness, and ν is Poisson's ratio. The local stiffness matrix of the interface, $[C]$, connecting local stresses to local strains is:

$$[C]\{\varepsilon\} = \begin{bmatrix} h_{if}\,k_n & 0 \\ 0 & h_{if}\,k_t \end{bmatrix} \begin{Bmatrix} \varepsilon_n \\ \gamma_{nt} \end{Bmatrix} \; ; \quad \varepsilon_n = \frac{\Delta\delta_n}{h_{if}} \; , \; \gamma_{nt} = \frac{\Delta\delta_t}{h_{if}} \qquad (2.22)$$

The material properties presented in Eq. (2.21) used in the constitutive matrix of a 4-node isoparametric element enable the element to behave as an interface element. As the thickness to length ratio, h_{if}/l, is reduced, the thin-layer element behaviour converges to the zero-thickness element behaviour. The zero-thickness element may be considered as a limit state of the thin-layer element.

To enhance the prediction of the thin-layer element, the elastic modulus in the direction which is parallel to the interface, E_t, was set to zero by Sharma and Desai (1992). This process reduces the effect of the element thickness on the convergence of the element (Hohberg, 1992).

Using a thin-layer element is closer to the physics of a problem where a certain layer of material is mobilized by sliding.

2.4.3.2 Fracture mechanics

Fracture mechanics theory applies to crack propagation and not to crack initiation; it requires a crack to exist a priori. It is now common practice in concrete dams to assume debonding at a construction joint for justifying the existence of the crack used to start fracture mechanics calculations (Linsbauer, 1985).

Classical linear elastic fracture mechanics (LEFM) requires theoretical solutions for the stress intensity factors of the section. Tabulated solutions do exist for typical dam cross sections (Linsbauer, 1985). However, these solutions, available for static loadings, may not be useful for generalized loadings such as earthquakes. Nevertheless, combining the finite elements method with fracture mechanics theory enables one to analyze different cross sections under different loadings. The crack or joint is modelled explicitly, and stress intensity factors are calculated at the crack tip using the contour integral for

instance. The finite element mesh may be modified in the course of the analysis to capture the changes occurring in the material, an approach known as the adaptative mesh technique. Among adaptive mesh techniques, one approach would be to halve the next cracked element by introducing an interface element (Gerstle et Xie, 1992). A more complicated technique to follow crack propagation with singular elements, as used in LEFM, was presented by Tasdemir et al. (1990).

Shear stresses along the crack may be captured by concentrated forces at the nodes along the crack profile. Considering shear stresses Tasdemir et al. (1990), could enhance predictions on crack profiles in mixed modes. However, great numerical difficulties are associated with this adaptative remeshing technique which may be time consuming specially under seismic loading. In certain situations, the crack profile and its position may be known in advance from test results or field observations or even approximated easily from test results, experience, or intuition. An interesting alternative would be to position interface elements along the expected crack profile, and to activate these elements as the crack propagates.

This idea has been used by Feenstra et al. (1991a,b). They defined three states (similar to Gambarova and Valente, 1990): (i) the linear elastic state $[D_{LE}]$, (ii) the development state (initiation and development of the discrete crack) $[D_{ID}]$, and (iii) the open crack state $[D_{AI}]$. The constitutive matrices for the different states may be written as:

$$[D_{LE}] = \begin{bmatrix} \frac{E}{h_{if}} & 0 \\ 0 & \frac{G}{h_{if}} \end{bmatrix}, \quad [D_{ID}] = \begin{bmatrix} \frac{f_{t'}}{2G_f} & 0 \\ 0 & 0 \end{bmatrix}, \quad [D_{AI}] = \begin{bmatrix} D_{nn} & D_{nt} \\ D_{tn} & D_{tt} \end{bmatrix} \qquad (2.23)$$

where h_{if} is the interface height, n and t are the normal and tangential directions (along the crack). Feenstra et al. (1991a,b) used this approach to study the stability of different aggregate interlock models.

It is thus possible to combine nonlinear fracture mechanics, which is already very efficient in concrete, with interface elements. This seems to be the most promising approach to model joint problems and planes of weakness in concrete dams.

2.5 Past investigations of the structural response of jointed dam-foundation systems

Situations that involve adhesive joints or similar weak planes arise quite often in dam engineering besides the explicit study of lift joints and construction joints. Retrofitting a cracked dam requires a stability analysis of the cracked plane. Raising of an existing dam requires a study of the stress state at the interface between old and new concrete to assess or not the monolithic behaviour of the new structure. Even stress transfer between vertical construction joints may be a concern. Different structural analysis methods, with the required input parameters and computed output responses, are illustrated in Fig. 2.11.

2.5.1 Classical method

The classical way of investigating threat to safety at a plane of weakness is to perform a stability analysis. The sliding safety factor (*SSF*) is computed as:

$$SSF = \frac{(W - Q_V - U + F_P)\mu + \tau_0 A}{Q_H + Q_{RH} + H} \tag{2.24}$$

where W is the dam weight, Q_V is the concrete vertical inertia force, U is the uplift thrust at the plane being investigated, F_P is the prestressing force, if any, μ is the coefficient of friction, τ_o is the cohesion, A is the cohesive area, Q_H is the concrete horizontal inertia force, Q_{RH} is the added inertia force to represent dam-reservoir

hydrodynamic interaction, and H is the hydrostatic thrust. CDSA (1995) for instance requires a sliding safety factor SSF=1.0 for residual sliding conditions (τ_o=0), and SSF=1.1 for peak sliding conditions for the earthquake safety evaluation of dam i.e. non-zero cohesion if τ_o and μ are supported by experimental results, and SSF=1.3, if not.

Equation (2.24) is usually applied sequentially over the dam's height along potential failure planes assumed to be horizontal. However, the historical failure of the Bouzey masonry dam in France has indicated that even though the rupture surface was horizontal near the upstream side, it curved downwards near the downstream side. Therefore the possibility of diagonal shear cracks propagating from the end of horizontal cracks should be considered in assessing the stability of concrete dams (ANCOLD, 1991). Moreover, it can be expected that more than one crack (joint) might be competing simultaneously to propagate within the dam. Curvilinear failure surfaces and simultaneous crack propagation are usually not considered in simplified analysis using Eq.(2.24).

The Val de la Mare Dam (UK., 30m), illustrated in Fig. 2.12a, is an example of a dam suffering from AAR with numerous damaged lift joints analysed using the classical approach (Horswill et al. 1994). Assuming zero cohesion and a friction angle of 35°, under the "Maximum Credible Earthquake MCE" with accelerations of 0.2g horizontal and 0.1g vertical, and assuming a linear uplift pressure distribution between the upstream face and the downstream face, the safety factors were found to be slightly below unity if drainage was not operational. Safety factors were raised by using the uplift pressure values measured on site along lift joints.

For static load cases, the computation of joints sliding safety factors is straightforward but for earthquake loading, the determination of inertia forces is not that simple. Singhal and Nuss (1991) employed two different methods for the stability assessment of a retrofit scheme to improve debonded lift joints at Stewart Mountain arch dam (USA, 65 m). First, they performed a linear elastic finite element analysis of the dam by a modal-superposition time-history method considering any weak plane as being bonded.

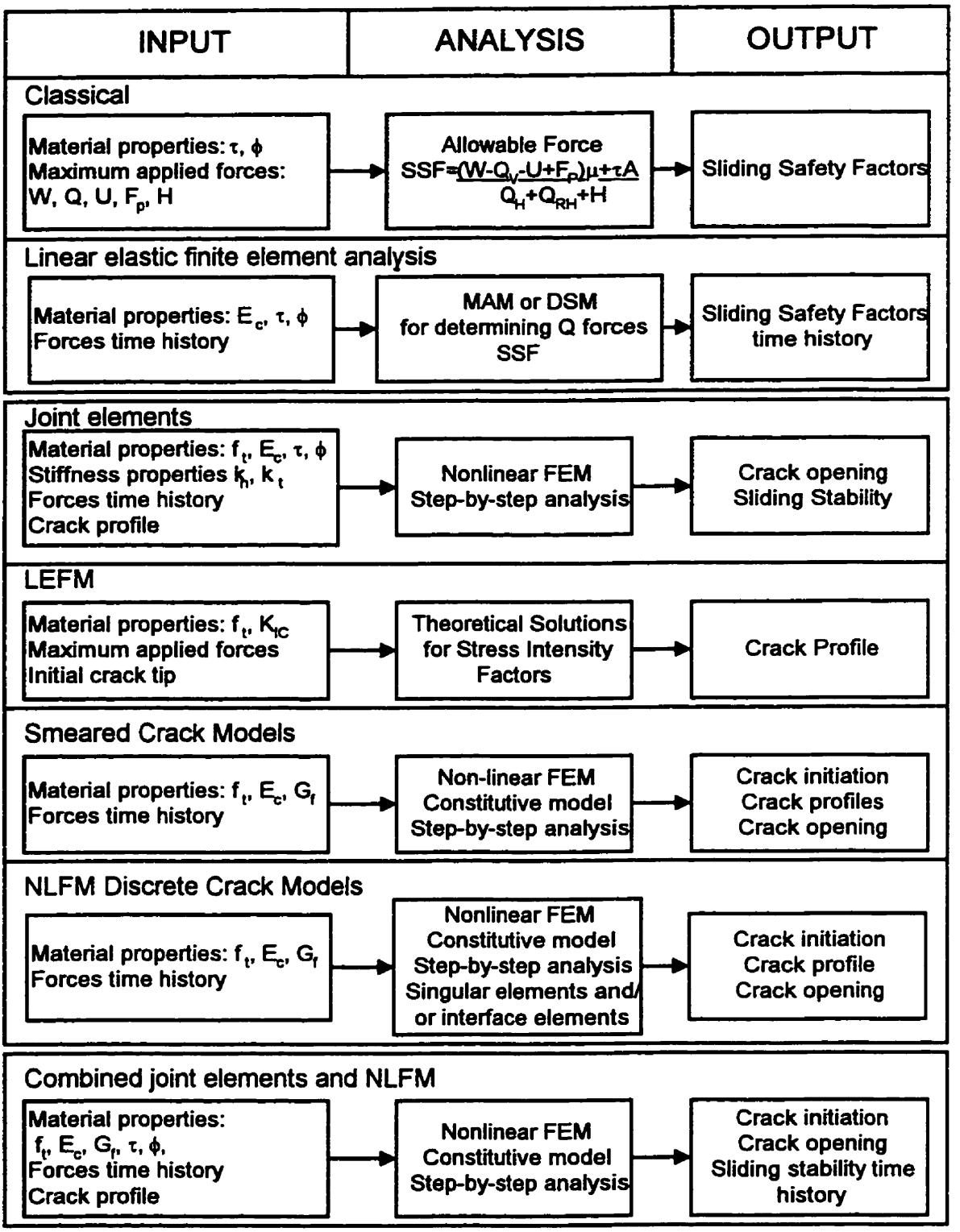

Fig. 2.11 *Concrete joints investigation methods.*

Then, they extracted the inertia forces of concrete using two different methods: (i) the displacement × stiffness method (DSM), and (ii) the mass × acceleration method (MAM). For the DSM, they simply took the displacements at the end of selected time steps and multiplied by the stiffness matrix to get the forces. For the MAM, the nodal accelerations at predetermined locations (say between two weak planes) are multiplied by the masses above that location. MAM is considered as an approximate check of the DSM.

Ahmadi and Khoshrang (1992) adopted a similar approach to verify the adequacy of the retrofitted top section of the Sefidrud buttress dam (Iran, 106m) illustrated in Fig. 2.12b. This dam suffered severe cracking at the top lift joint locations due to a magnitude 7.6 earthquake (Indermaur et al. 1991). Ahmadi and Khoshrang (1992) first conducted a linear time-history analysis of the retrofitted dam including the prestressing tendons. They made sure that the tensile stresses were not greater than the tensile strength of both the tendons and the concrete. Then, they performed a local stability analysis on the retrofitted section (top part). The concrete inertia force at the centroid of the top block was computed from the maximum absolute horizontal acceleration obtained at that location during the global analysis. In the procedure adopted by Singhal and Nuss (1991) and by Ahmadi and Khoshrang (1992) it is assumed that the joint will never be subjected to tension.

Fan and Sled (1992) in the seismic safety evaluation of Cleveland gravity dam (Canada, 100 m), where 3D restraints provided by canyon walls are important, considered the equivalent tensile strength at lift joints to be ½ those in main concrete. They used the results of 3D and 2D linear elastic finite element analyses to estimate the depth of crack penetration from the upstream face. The uncracked portion is assumed to resist the post-earthquake loads. They adopted a Mohr-Coulomb model with a friction angle of 45°, and a cohesion of 0.35 MPa. This approach does provide a rational assessment of the post-earthquake resistance of the dam, but the earthquake resistance assessment relies on the judgement of the analyst who will determine if the stress levels reached in the linear dynamic analysis are acceptable or not.

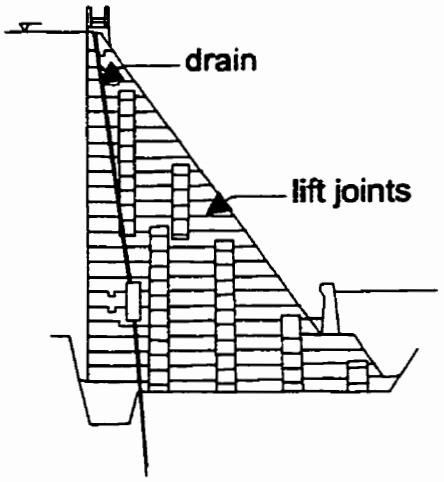

(a) Val de la Mare Dam
(adapted from Horswill et al. 1994)

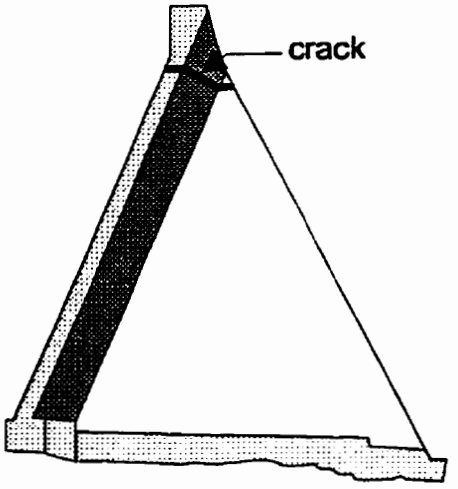

(b) Cracking at Sefidrud dam after 1990 Manjil earthquake
(adapted from Indermaur et al. 1991)

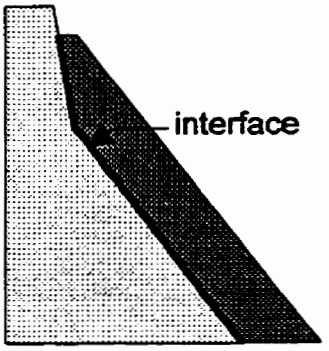

(c) Retrofiting of the Koyna dam, interface between old and new concrete
(adapted from Pande et al. 1979)

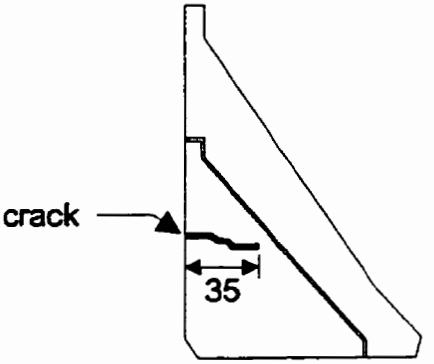

(d) Crack stepping from lift joint to lift joint
(adapted from Orekhov et al. 1989)

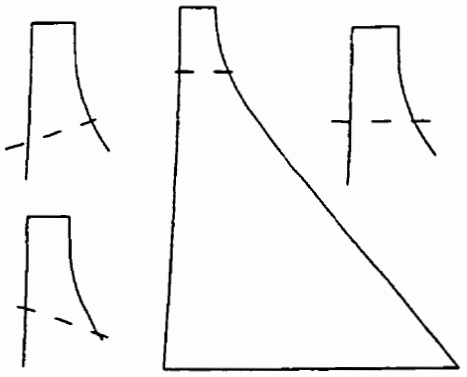

(e) Effect of joints on dam response
(adapted from El-Aidi and Hall, 1989b)

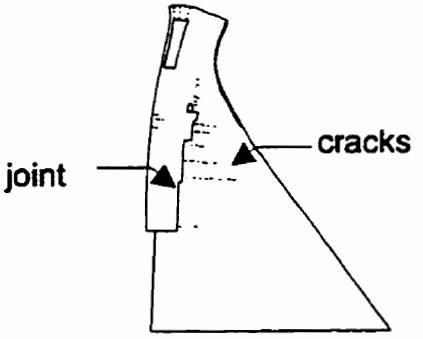

(f) Smeared crack analysis combined with discrete interface elements
(adapted from Oliver et al. 1988)

Fig. 2.12 *Dams analysed or retrofitted at lift joints.*

Stress transfer between old and new concrete in a raised dam is always investigated with attention. There was a question on that particular topic at the 1979 ICOLD Congress in New Delhi (Question 48). The interface joint is usually parallel to the downstream face. In this case, it is usual practice to conduct a linear elastic finite element analysis and then to check if tensile stresses occur in the normal direction to the interface (Chavarri et al. 1979, Hollingworth and Druyts, 1979, Uchida and Higashigawa, 1979).

2.5.2 Joint elements

The obvious approach to extend a simple linear elastic finite element analysis to consider structural planes of weaknesses is to use joint elements. Surprisingly, gap-friction elements have not been used very often for modelling lift joints in concrete dams. Bhatti et al. (1994) have used spring elements to model the lift joints of a deteriorated arch dam. Pande et al. (1979) adopted thin-layer interface elements to model the construction joint between the Koyna Dam original concrete and the buttresses built to reinforce the dam after the 1967 earthquake (see Fig. 2.12c). The buttresses were built leaving a gap between the old and the new concrete to be grouted later. Pande and his colleagues (1979) modelled the gap material as an elasto-plastic material with cohesion. The parameters adopted for the dynamic analysis were: τ_o=2.8 MPa, ϕ=45°, E_{gap}=2800 MPa (so low to account for shrinkage and creep effects), E_{conc}=28000 MPa, and ζ=20% of critical damping. This damping coefficient is extremely high compared to similar studies and no arguments were given to justify such a high value. They concluded that it is extremely important to have the buttress fully bonded to the original dam for the effectiveness of the retrofit and to avoid out of phase vibrations of the dam and buttress.

Léger and Katsouli (1989) adopted gap-friction elements for conducting a parametric study with nonlinear behaviour at the concrete/rock interface for a 90 m dam. They investigated the dynamic sliding safety factors and residual sliding displacements, they suggested the percentage of base not in contact at one instant in time during the design earthquake, as an important limit state.

Ahmadi and Khoshrang (1992) and Ahmadi et al. (1992) adopted 8-node interface elements to model the discrete crack formed in the Sefidrud buttress dam (Fig. 2.12b). They adopted 5% damping, tensile strength of 1.1 MPa at discrete crack location and base joint, a normal and shear stiffness of 200 GPa/m and 16 GPa/m, respectively. Their simulations predicted cracking would occur at the base not at the actual location that occurred during the earthquake.

Dowling and Hall (1989) in seismic analyses of arch dams positioned their own special joint element between the vertical planes of shell elements to reproduce the contraction joints and also between horizontal planes. These horizontal planes represented locations where cantilever cracking was constrained to occur as first suggested by the vertical orientation of contraction joints and secondly by possible weakness along lift joints. No slip was allowed to occur. The cracking predicted in their numerical analyses is such that they expect the no-slip assumption to be violated.

Xia et al. (1979) studied the advantages and inconvenience of vertical and diagonal construction joints in concrete gravity dams. They observed that above 40% of contact along the vertical of diagonal joint, the dam behaviour approaches the fully grouted behaviour. They noted that a dam with a diagonal joint under the dead load and water load, will have a stress distribution along the base very close to that of a monolithic section. The dead load acting along the diagonal joint will prevent it to open, thus grouting is not necessary for diagonal joints. In conclusion, they consider diagonal joints to be preferable to vertical joints.

Khrapkov et al. (1989) investigated the effects of construction joints in a similar fashion but using the Lagrange multipliers method. They observed that considering (i) joint opening, (ii) loading and construction stages, as well as (iii) temperature effects during construction, results in a stress state which is totally different than the one of a dam calculated as a monolith and loaded at once. They noted that very often the construction joints do not need to be grouted.

Orekhov et al. (1989) studied the effect of diagonal construction joints on the stress distribution using the Goodman et al. (1968) joint element. In a previous study, Orekhov et al. (1986) built plaster models of a buttress dam with a powerhouse on its downstream face. They were separated by a vertical joint. The authors could measure tensile stresses on the upstream side and on the downstream side of ungrouted joints in the buttresses. The stress distributions were enhanced by providing good quality grout, and by making these joints inclined toward downstream face. Grouting of the vertical joint had very little effects on the stress distribution but grouting increased the global bearing capacity at failure.

2.5.3 Linear elastic fracture mechanics (LEFM)

Orekhov et al. (1989) also used linear elastic fracture mechanics to study crack propagation through a concrete dam with weakened horizontal joints. The fracture toughness of concrete was taken as K_{Ic}=800 kN/m$^{3/2}$, while the fracture toughness of weakened horizontal joints was set at K_{Ic}=500 kN/m$^{3/2}$. They predicted that a crack initiated in a joint would eventually be deflected in the mass concrete. If the crack was to meet another joint on its way to the foundation it would be trapped in the joint for a certain length and then would be deflected out again as illustrated in Fig. 2.12d.

2.5.4 Discrete crack models

It is quite surprising to realize that discrete crack models have not been used to model lift joints or construction joints. Skrikerud and Bachmann (1986), developed a model using 4-node interface elements which are introduced within cracked elements to model the crack. They considered the frictional resistance at the crack during opening using a reverse cyclic aggregate interlock model and studied the Koyna Dam. Upon crack closing, elastic properties are recovered. They found that aggregate interlock has little effect on the response. Feltrin et al. (1990) enhanced Skrikerud and Bachmann (1986) model by introducing the concept of fracture energy. They observed that smoother

aggregate interlock properties lead to further cracking, in other words crack roughness restrains cracking.

Ayari and Saouma (1990) developed the discrete crack approach using linear elastic fracture mechanics. The crack propagates according to an empirical crack propagation function. However, upon closing, concrete elastic properties are recovered at the crack.

2.5.5 Smeared crack models

Explicit modelling of deteriorated lift joints has been attempted by Ghrib and Tinawi (1994). Lift joints were considered as zones of reduced elastic properties. This study provides information on the dam response due to an earlier crack opening at joint locations but it does not assess the stability because the elastic properties are recovered upon joint closing.

El-Aidi and Hall (1989a,b) have modelled the effect of pre-existing cracks or lift joints using a smeared crack approach (see Fig. 2.12e). They considered the crack to be acting in compression by using a Mohr-Coulomb yield criterion to limit the shear stresses transmitted at the crack. The initial shear modulus being used in the tangent constitutive matrix, iterations are required during sliding. They analyzed Pine Flat gravity dam (USA, 122 m) with the following properties for plain concrete: μ=0.75 (ϕ=36.9°), f_t=600 psi (4.14 MPa), K_{Ic}=2000 lb/in$^{3/2}$ (2200 kN/m$^{3/2}$). The lift joint properties were assumed to be half those of plain concrete: f_t=300 psi (2.07 MPa), K_{Ic}=1000 lb/in$^{3/2}$ (1100 kN/m$^{3/2}$). Cracking was only allowed at the joint. They observed that the crack wanted to deviate downwards in mass concrete once it reached the interior of the dam. This indicates that lift joints should be much weaker than the surrounding concrete to fully contain the crack.

The approach of combining the smeared crack method with interface elements has been applied to masonry walls by Lotfi and Shing (1994), and to concrete gravity dams by Oliver et al. (1988). The constitutive models used were as proposed by Carol and Alonso (1983). Oliver et al. (1988) analyzed a 79 m high gravity dam where a vertical construction joint was provided, extending from a drainage gallery located at a third of the

total height from the top, to an horizontal joint at a third of the total height from the bottom (see Fig. 2.12f). They managed to get a very good agreement with displacements measured at the site.

Obviously, a jointed dam does not behave as a monolith. An analysis where joints are modelled explicitly can reveal very useful information particularly in relation to structural behaviour and failure mechanism under severe loading. This may reduce the cost of construction by an optimization of the grouting operation (grout would be provided only where need be) and optimization of strengthening/rehabilitation measures.

2.6 Conclusions

A review of the structural analysis of jointed concrete dams has been presented in this chapter. The emphasis was put on lift joints. Concrete joints are planes of weakness in an otherwise monolithic structure because joints have about half the resistance of monolithic concrete. Mohr-Coulomb failure criterion is generally adopted to represent joint behaviour even though other constitutive models could be well suited for the joint problem. As a result, Mohr-Coulomb parameters (τ, ϕ) measured for existing dams have been widely reported in the literature.

It appears that very little has been done on the seismic response of jointed dams with thorough assessment of sliding. Hence promising approaches could be identified for solving joint problems in dams. Non-classical friction models enable one to reproduce various nonlinear stress-displacement relationships as well as the simple Mohr-Coulomb relationship. Interface elements such as the zero-thickness element can be coupled with fracture mechanics principles to simulate crack propagation along a predefined joint while retaining the capability to follow crack trajectory deflecting within the concrete mass. However, these approaches should be validated for their reliability and efficiency in the context of structural analysis of jointed dams.

There is a pressing need for experimental results to validate numerical models. The use of simple static shear test results in dynamics studies is debatable. Friction properties could be affected by the frequency content, the acceleration, velocity, or joint degradation due to loading cycles. However, the global response of the dam will not be affected in the same way as a single joint segment by variations of these joint parameters. A valuable contribution would be to identify which joint modelling parameters are worth studying thoroughly.

CHAPTER 3
Experimental programme

3.1 Introduction

The first objective of the experimental programme was to provide experimental results to validate the numerical models of concrete to concrete and concrete lift joints dynamic sliding. The second objective was to establish a relationship between static shear strength test results and dynamic shear strength responses. The third one was to study the effect of the frequency content on the dynamic sliding characteristics.

In this chapter, the test specimens are described and the material properties are given. Also, the test setup, which was used to load the specimens, and the instrumentation used during testing, are described. Finally, the experimental procedure is explained.

3.2 Test specimens

The following experimental variables were investigated: (i) the joint surface preparation, (ii) the frequency content of the imposed sliding displacements, and (iii) the normal load acting on the joint surfaces. The specimens (Fig. 3.1) and the experimental setup (Fig. 3.2) were designed for applying a direct shear load along the joint plane for a given normal load.

3.2.1 Description

The specimens were divided in four series according to the surface preparation. Four specimens without any joint were cast monolithically (Series H). The lift joint specimens (Series R and Series F) were cast in two pours, the second half of the specimen being poured three days after the first half. Among the lift joint specimens, five had their lift surfaces waterblasted six hours after the pour (Series R). The other five specimens had their lift surfaces left untreated except being kept wet (Series F). In the last series, four

specimens with joints formed by two independent plane surfaces were tested (Series D). No reinforcement was provided across the joints.

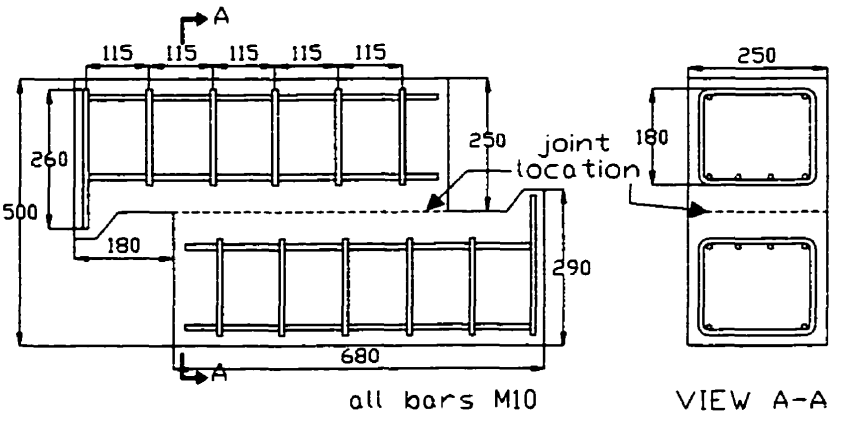

Fig. 3.1 *Specimen geometry.*

A total of 18 specimens with joint surfaces of 0.250 m x 0.500 m were tested. Figure 3.1 shows the specimen geometry. The contact surface will vary during the test due to the displacement of the top half on the bottom half. As a result, the maximum variation of the confinement pressure, ±4%, is considered as negligible.

3.2.2 Material properties

The concrete mix had a water to cement ratio of 0.70. Type III cement was used. The aggregates were crushed limestone with a maximum aggregate size of 20 mm. The specimens were kept 100% humid until testing (ref. Table 3.1).

Standard cylinder tests, 150mm in diameter and 300 mm in height, indicated an average compressive strength, f'_c, of 27.9 MPa, the average modulus of elasticity, E_c, reached 31484 MPa, and Poisson's ratio, ν, was found to be 0.2. Split cylinder tests on standard cylinders (diameter of 150 mm, length of 300 mm) indicated a splitting tensile strength, f_{sp}, of 2.7 MPa. Four-point bending tests on 75×100×400 mm long standard prisms showed a modulus of rupture, f_r, of 3.98 MPa (ref. Table 3.2).

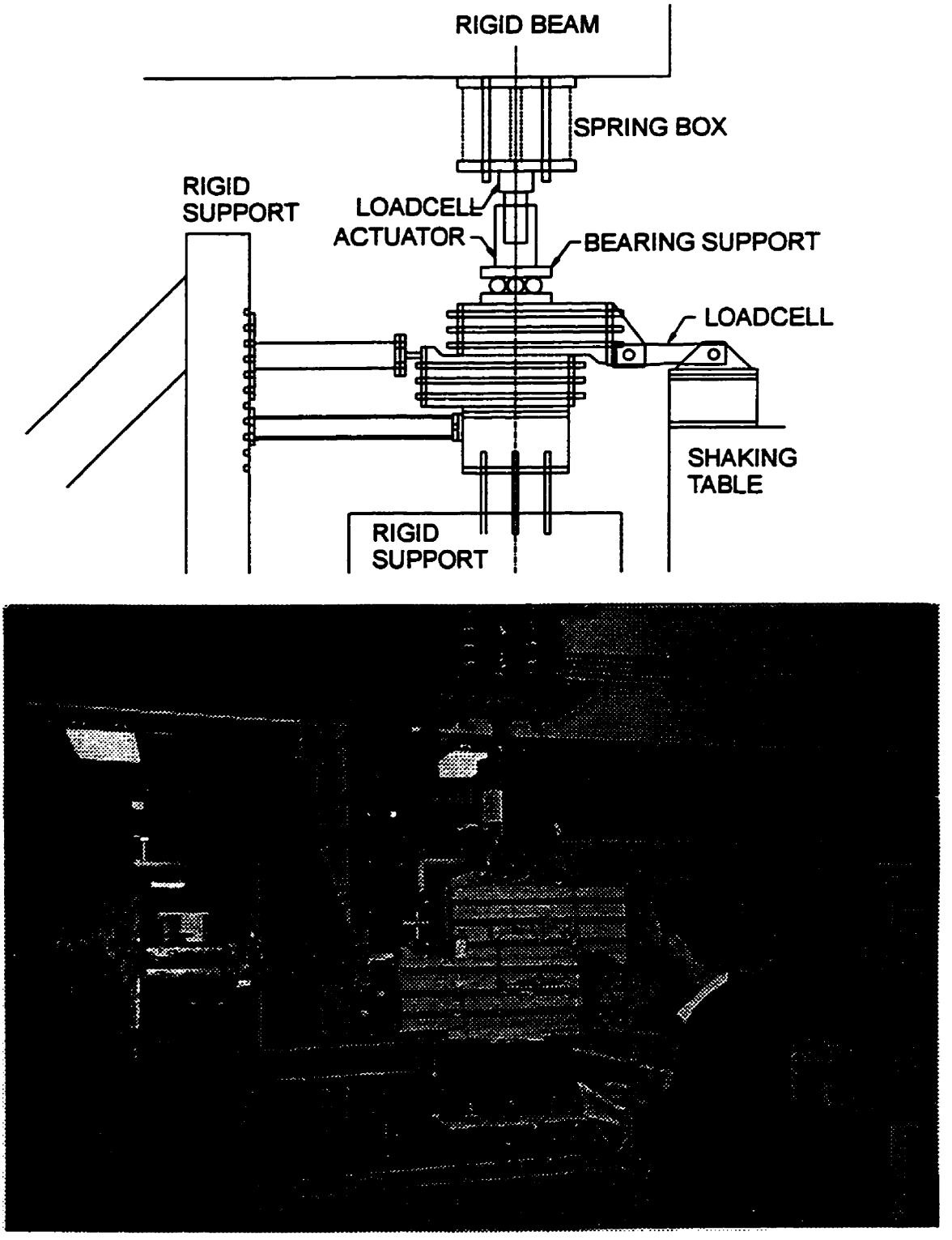

Fig. 3.2 *Test setup.*

Table 3.1 *Concrete mix.*

Fine Aggregate	Sand from Joliette (Canada)
Coarse Aggregate (D_{max}=20mm)	Limestone (Canada)
Type III Cement	230 kg/m^3
Water to cement ratio	0.70
Storage conditions • Humidity • Temperature	 100 % 24°C

Table 3.2 *Measured material properties.*

Properties	Minimum	Maximum	Average	No. of samples
f'_c (MPa)	19.4	32.6	27.9	21
E_c (MPa)	29014	34049	31484	7
f_{sp} (MPa)	1.89	3.49	2.72	20
f_{cr} (MPa)	1.23	2.27	1.77	20
f_r (MPa)	3.15	4.67	3.98	19
ν	0.17	0.22	0.20	7

3.2.3 Surface preparation

Five specimens had the lift surface waterblasted. A 2000 psi waterjet machine was used for the surface preparation as shown in Fig. 3.3. A series of waterblasting tests indicated that, for the concrete mix used here, six hours of cure were sufficient to get an efficient waterblasting, which is achieved when laitance is removed, and aggregates are sitting firmly in the paste.

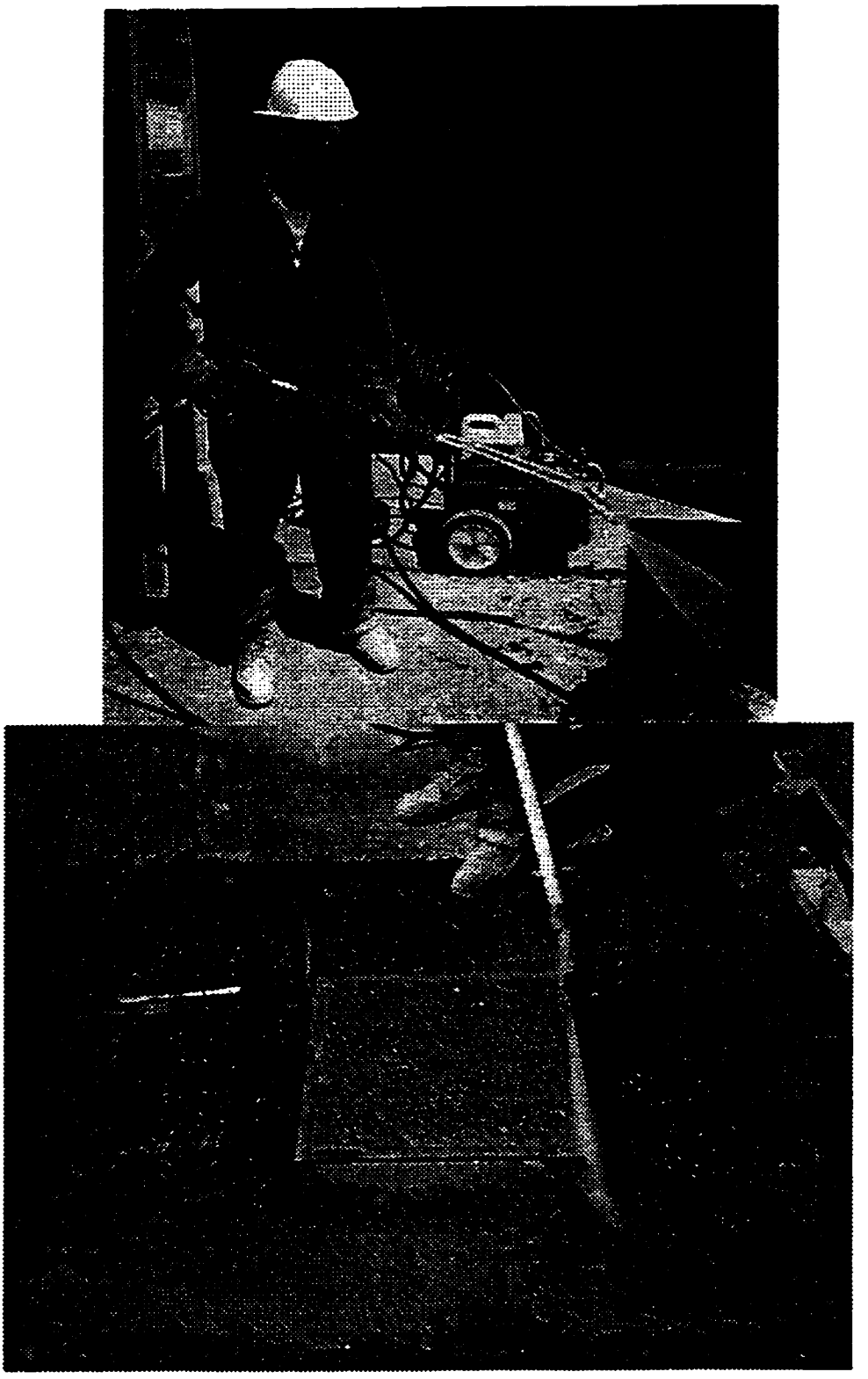

Fig. 3.3 *Surface preparation: equipment and procedure.*

Figure 3.4 shows the difference between the waterblasted surface and the untreated surface after three days of cure just before the second pour.

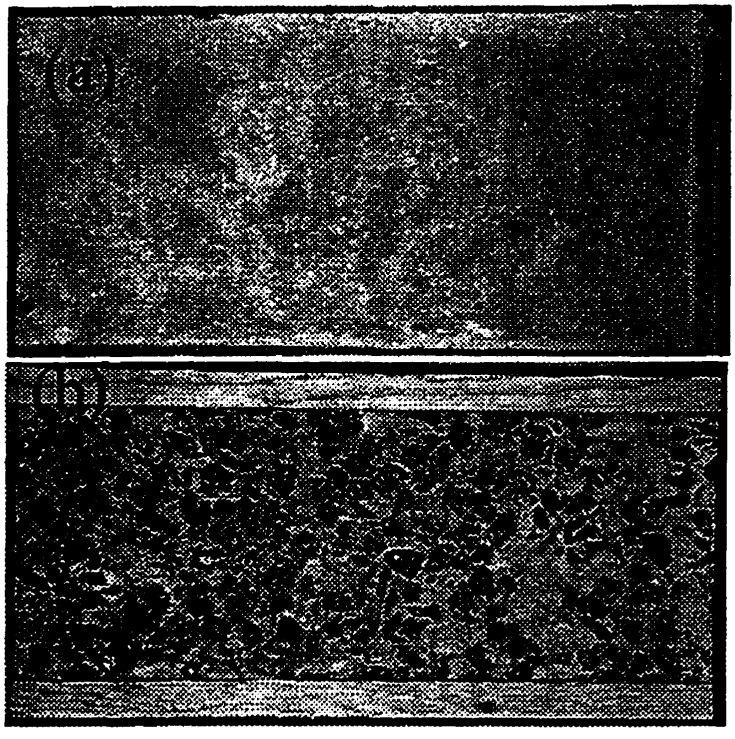

Fig. 3.4 *Surface preparation: (a) untreated surface, (b) waterblasted surface*

3.3 Test setup

3.3.1 Loading frame

The test setup is shown in Fig.3.2. The objective was to have the upper half of the specimen sliding on the bottom half. The applied shear force is aligned with the sliding plane to avoid any moment to be induced in the setup. Due to specimen roughness, the upper half specimen will move upwards however, since that displacement is very small, the resulting eccentricity is considered to be negligible. This shear force is applied through the controlled actuator of the adjacent shaking table. The normal load is applied by an actuator sitting on rollers to allow the upper block to move freely with respect to the upper part of the actuator. A spring box was of (stiffness=2.5 N/m) inserted between the

actuator and the rigid beam to allow upward movements of the upper block.

3.3.2 Instrumentation

Instrumentation is illustrated in Fig. 3.5. Data was not filtered. Normal and tangential relative displacements were measured between the upper and lower blocks using linear variable differential transformers (LVDT). Normal and tangential accelerations were monitored by accelerometers. The applied shear force was measured on the rigid link between the shaking table and the upper block. A pressure transducer on the vertical actuator was used to monitor the applied normal load. The instruments were read at a sample rate of 20 Hz for the static tests. For the dynamic tests, it was 200 Hz which is a compromise between the volume of data and storage..

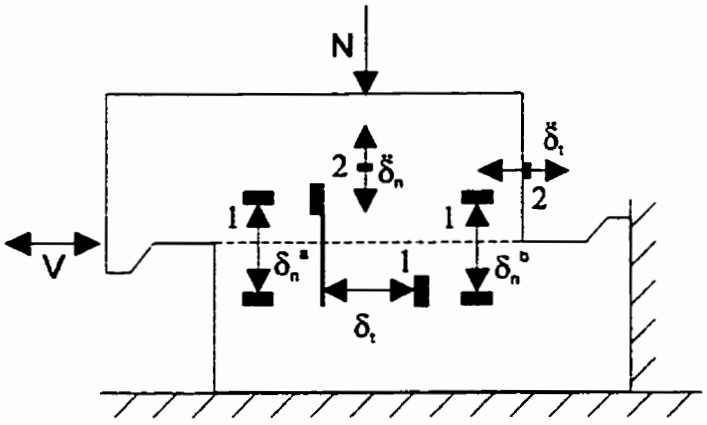

Fig. 3.5 *Instrumentation: (1) LVDT. (2) accelerometer, (N) loadcell to measure normal load, (V) loadcell to measure shear load.*

3.4 Procedure

3.4.1 Static shear strength tests

The test procedure is illustrated in Fig. 3.6. At first, five specimens (two monolithic (H), one waterblasted joint (R), and two untreated joints (F)) were subjected to static shear tests by applying a shear load but no normal load using the setup shown in Fig. 3.2. These tests were intended for measuring the joint cohesion. From these five specimens, only the two untreated joints could be subjected to sliding friction tests since these shear tests resulted in curved crack profiles for the other three specimens.

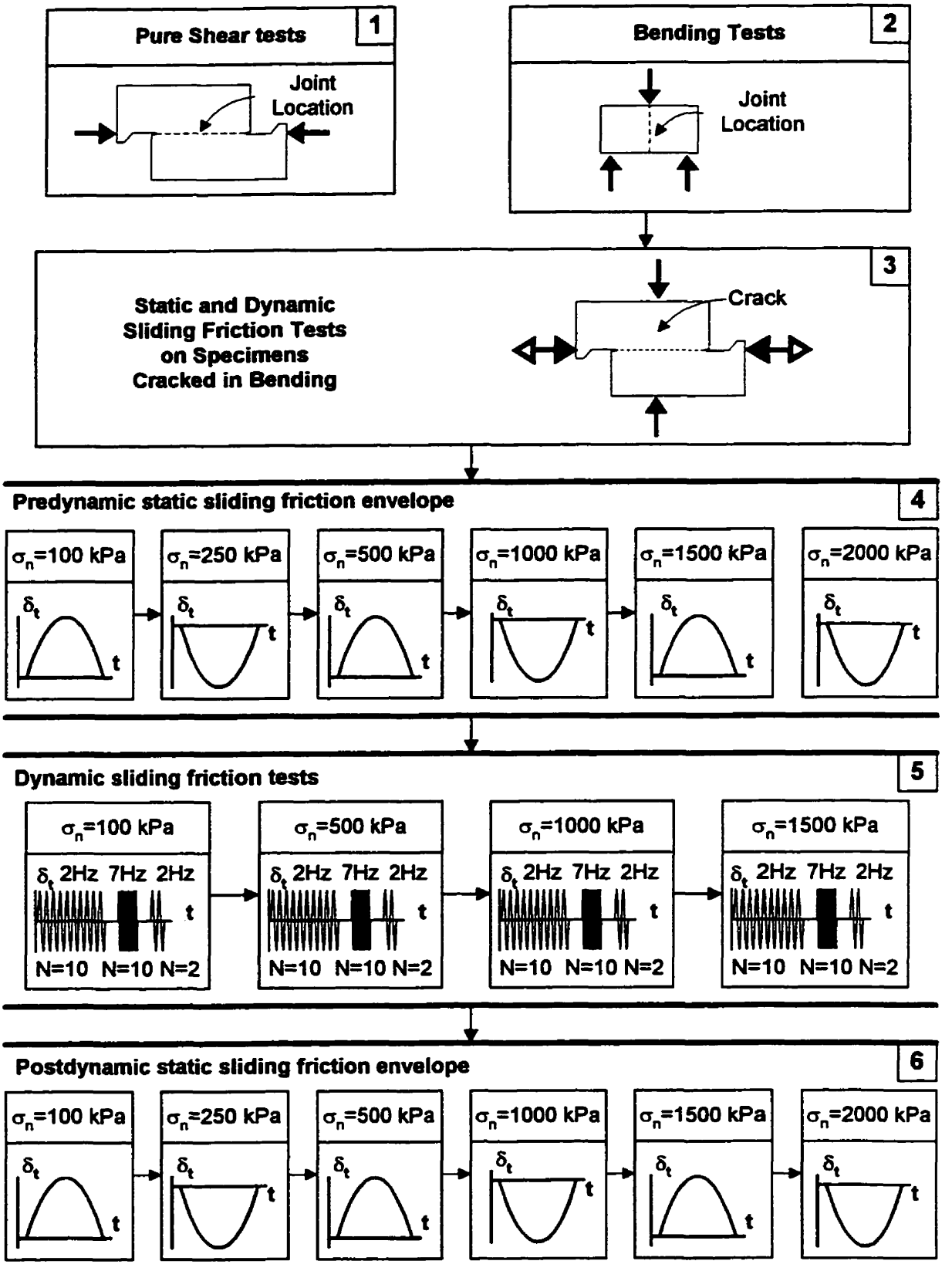

Fig. 3.6 *Test procedure*

3.4.2 Bending tests

To create a sliding plane, nine specimens were subjected to three-point bending tests: two monolithic specimens, four waterblasted joints, and three untreated joints. The specimens were laid on the side to induce cracking in the joints (see Fig. 3.7). The monolithic and waterblasted joints specimens were notched before testing with a 25 mm notch at the beginning and a 25 mm notch at the end of the expected cracking plane. All these cracked specimens were then tested in sliding friction.

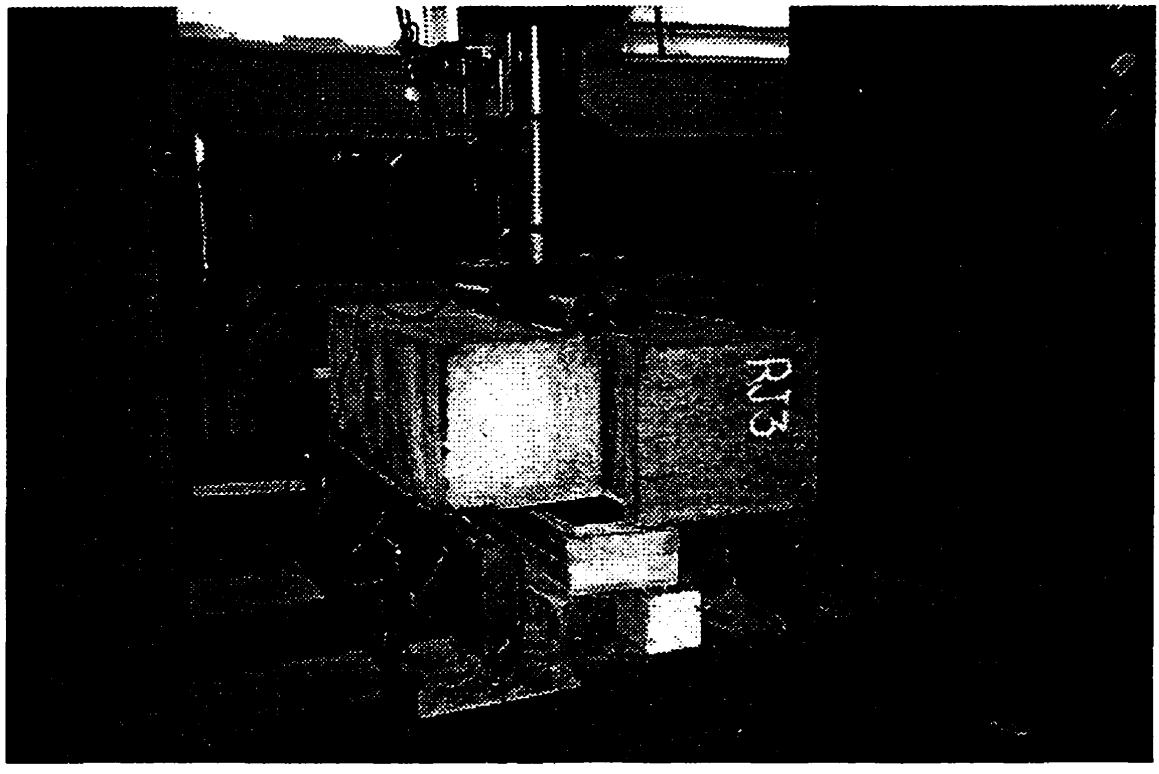

Fig. 3.7 *Bending tests setup*

Bending tests generate cracks in mode I. Cracks appear in dams because of a build up of tensile stsresses that ought to be released. These tensile stresses might be caused by foundation movements, temperature gradients, geometrical irregularities, and restraints. In general, cracks in dams are mode I cracks.

3.4.3 Static and dynamic sliding friction tests

Sliding friction tests were performed in three steps. First, the predynamic static sliding friction envelope was obtained by subjecting the upper block to a complete forward-backward displacement cycle at a prescribed normal load level. This process was repeated for 6 normal load levels (see Fig. 3.6[4]): 100 kPa, 250 kPa, 500 kPa, 1000 kPa, 1500 kPa, and 2000 kPa. Dynamic displacement cycles were then imposed to the specimen. At a prescribed normal load level, 10 cycles at 2 Hz were imposed, a pause, then 10 cycles at 7 Hz, another pause, and finally 2 cycles at 2 Hz. Dynamic tests were repeated at 4 normal load levels (see Fig. 3.6[5]): 100 kPa, 500 kPa, 1000 kPa, and 1500 kPa. The experiments on a specimen were concluded by repeating the static sliding friction envelope sequence to get the postdynamic static sliding friction envelope (see Fig. 3.6[6]).

The excitation frequencies were chosen to represent the frequency content of earthquakes according to the location in Canada. In eastern Canada, earthquakes have higher frequencies (assumed here to be 7 Hz) than earthquakes in western Canada,.(2Hz).

3.5 Summary

Eighteen specimens were tested. Four specimens were monolithic, five had a waterblasted joint surface, five had untreated joint surfaces, and four were flat independent plane concrete surfaces. Cohesion and bending resistance were measured. The static sliding friction predynamic, dynamic and postdynamic envelopes were obtained by subjecting the specimens to complete displacement cycles at given normal load levels, that were incremented.

CHAPTER 4

Experimental results and discussions

4.1 Introduction

In this chapter, static shear strength results are first presented. Bending tests that served to generate crack profiles for the sliding friction tests are also presented. The bulk of this chapter covers the friction tests that were the primary object of the test programme. Thorough description is given and key concepts raised by the tests are discussed.

4.2 Static shear strength

4.2.1 Experimental response

Five specimens were subjected to static shear tests. The results are given in Table 4.1. Untreated joints broke while being put in place. This indicates a very low cohesion, in the order of 25 kPa. The waterblasted joint specimens and the monolithic specimens resisted to the maximum capacity of the shaking table, an applied shear force of 250 kN that corresponds to a cohesion of 2000 kPa. An additional shear force coupled with the shaking table was applied through an actuator at a 125 mm vertical offset from the joint plane. The combined forces induced a sudden brittle failure. The crack did not propagate along the waterblasted joint. It penetrated the parent material at about 45° to the horizontal.

4.2.2 Discussion

The effect of surface preparation on cohesion is indubitable. Waterblasted joint specimens behaved like monolithic specimens while untreated joint specimens barely showed any cohesive resistance. The CDSA guidelines (1995) suggests to use 50% of $0.17\sqrt{f'_c}$ for the cohesion at a lift joint location. The tests show that joint preparation has

an effect on cohesion such that waterblasted joint cohesion is comparable to that of monolithic concrete.

Table 4.1 *Pure shear test results*

Specimens	Shear force (kN)	Cohesion (kPa)
Untreated FJ1	≈3	≈25
Untreated FJ2	≈3	≈25
Waterblasted RJ1	250	>2000
Monolithic cracked PRH	250	>2000
Monolithic cracked H1	250	>2000

4.3 Bending tests

4.3.1 Experimental response

Table 4.2 shows the three-point bending tests that were used to produce nearly horizontal cracks along the joint interfaces. The moduli of rupture of the specimens are quite high compared to the measured f_r values of 3.98 MPa obtained from standard tests. This is due to the span to depth ratio that was less than 2 (450 mm-span and 200 mm or 250 mm-depth). However, series results can be compared to each other. The waterblasted joints reached 82% of the average monolithic specimens modulus of rupture while the untreated joints reached 45% of the monolithic modulus of rupture.

The waterblasted specimens and monolithic specimens had a notch to initiate the crack and a notch to end the crack. The notches were effective because the flexural cracks ran flat from notch to notch. The untreated joint specimens had no notch. Nonetheless, the flexural cracks initiated and propagated along the untreated joint.

4.3.2 Discussion

These results are in agreement with results on wedge splitting tensile strength tests (see Fig. 2.3) that were carried in similar studies on concrete joint specimens (Saouma et al. 1991; Tschegg et al. 1993). Even the CDSA guidelines (1995) suggest to use 50% of monolithic concrete bending strength for any type of joint. The waterblasted joint specimens are rather on the higher side of resistance.

Table 4.2 *Bending test results.*

Specimens	P (kN)	h (mm)	f_r (MPa)	$f_{r\,avg}$ (MPa)	$f_{r\,avg}/f_r$ %
Untreated FJ3	136	250	5.03	3.91	45
Untreated FJ4	111	250	4.10		
Untreated FJ5	71	250	2.62		
Waterblasted RJ3	169	200	9.76	7.21	82
Waterblasted RJ4	101	200	5.83		
Waterblasted RJ5	105	200	6.06		
Monolithic cracked H2	142	200	8.20	8.80	100
Monolithic cracked H3	163	200	9.41		

where P is the applied normal load, h is the depth, and f_r is the modulus of rupture.

4.4 Friction tests

4.4.1 Experimental static sliding friction responses

Figure 4.1 illustrates the static sliding friction behaviour of the different types of specimens subjected to normal stress, σ_n, of 100 kPa and 1500 kPa. The coefficient of friction was calculated as:

$$\mu_{mes} = \frac{T}{N} = \tan\phi_{mes} \tag{4.1}$$

where

N = the measured normal force,
T = the measured shear force,
μ_{mes} = friction coefficient (ratio of measured normal force to measured shear force),
ϕ_{mes} = corresponding friction angle of the ratio of measured normal to shear forces.

Figure 4.1(a) shows the typical responses of two flat independent concrete surfaces. The friction coefficient varies from a positive value to a negative value as the applied shear force is reversed; a convention adopted instead of using the absolute values of T and N to illustrate the hysteresis loops. The response was rigid-plastic up to a normal stress of 500 kPa. At 1000 kPa, the specimens turned to a stick-slip type of response. This stick-slip is not believed to be a material attribute but rather caused by the brutal decrease in resistance to movement, when large shear stresses are applied, which is so sudden that the displacement control system of the shaking table has no time to stabilise the sliding response.

At low normal stress (σ_n < 500 kPa), untreated joint specimens generally exhibited a peak strength, followed by a slight decrease in strength and a residual plateau. As illustrated in Fig. 4.1(b), some specimens required a certain shear displacement to mobilize the peak strength. At high normal stress (σ_n > 500 kPa), the response was rigid-plastic.

Waterblasted joint specimens and cracked monolithic specimens behaved similarly (see Fig. 4.1(c,d)). Under low normal stress (σ_n < 500 kPa), the specimen reached the peak strength with a linear stiffness. It was followed by an exponential unloading that ends up on a residual strength plateau. The difference between the peak and the residual strength is decreasing with increasing normal stress. At high normal stress (σ_n > 500 kPa), the response was rather rigid plastic. At any stress level, the half cycle backward displacement to the initial position required a lower applied shear force than the initial half cycle forward displacement. This was also observed for the untreated joint specimens. However, the difference between the forward applied shear stress and the backward applied shear stress was smaller for untreated joint specimens than for waterblasted and cracked monolithic specimens.

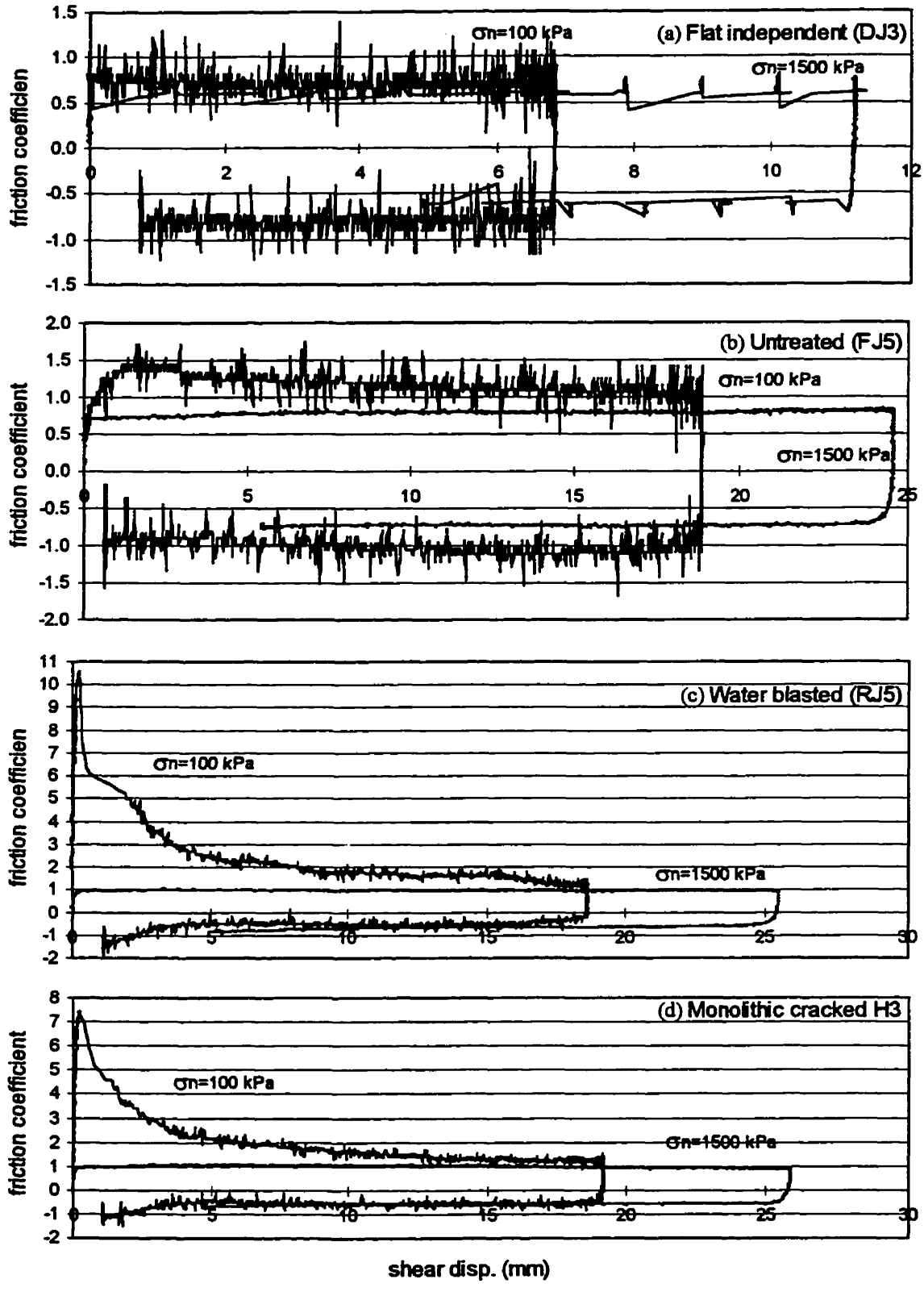

Fig. 4.1 *Experimental static sliding friction response*

4.4.2 Experimental dynamic sliding friction responses

Figure 4.2 shows typical hysteresis loops at 2 Hz of the various types of specimens. The displacements evolve in a clockwise manner on the loops. That is, for positive friction coefficients the displacements varied from negative values to positive values, and for negative friction coefficients the displacements varied from positive values to negative values. The responses at low normal stress level appears to be oscillating because the electronic noise on the instrumentation was significant at low stress level. The coefficient of friction being the ratio of two measured values, the noise was thus amplified. Post-digital filtering was not performed for a single reason: the filtering of all channels and tests was not worth the effort since only the average measured friction coefficient was considered in the discussions and derivations of the dynamic test results.

The striking feature of the measured hysteresis loops is their stability. The responses do not degrade with the number of cycles even, after 20 cycles at a given stress level. With the introduction of surface preparation, the dynamic responses appear to evolve from pure rigid plastic behaviour i.e. rectangular loops for flat independent surfaces [Fig. 4.2 (a) and (b)] to rigid hardening behaviour i.e. parallelogram loops for monolithic cracked specimens [Fig. 4.2 (g) and (h)]. The area enclosed by the loops also indicate the ability of concrete-concrete joints to dissipate a significant amount of energy by friction.

Among the other interesting features of the hysteresis loops is the decrease of the dynamic friction coefficient with the increase in normal stress that occurs for any type of surface. The loops are not sharp at the four corners, two corners are rounded. This softening of the response occurs when the sliding velocity decreases for stopping the specimen and reversing the applied shear stress. These observations are also valid for cycles at 7 Hz.

The inertia force due to the sliding block have not been considered in the analysis. It is evaluated to reach 0.5 kN at the most, thus it reaches about 5% of the applied shear force at a normal stress of 100kPa, 1% at 500 kPa, 0.5% at 1000 kPa, 0.33% at 1500 kPa.

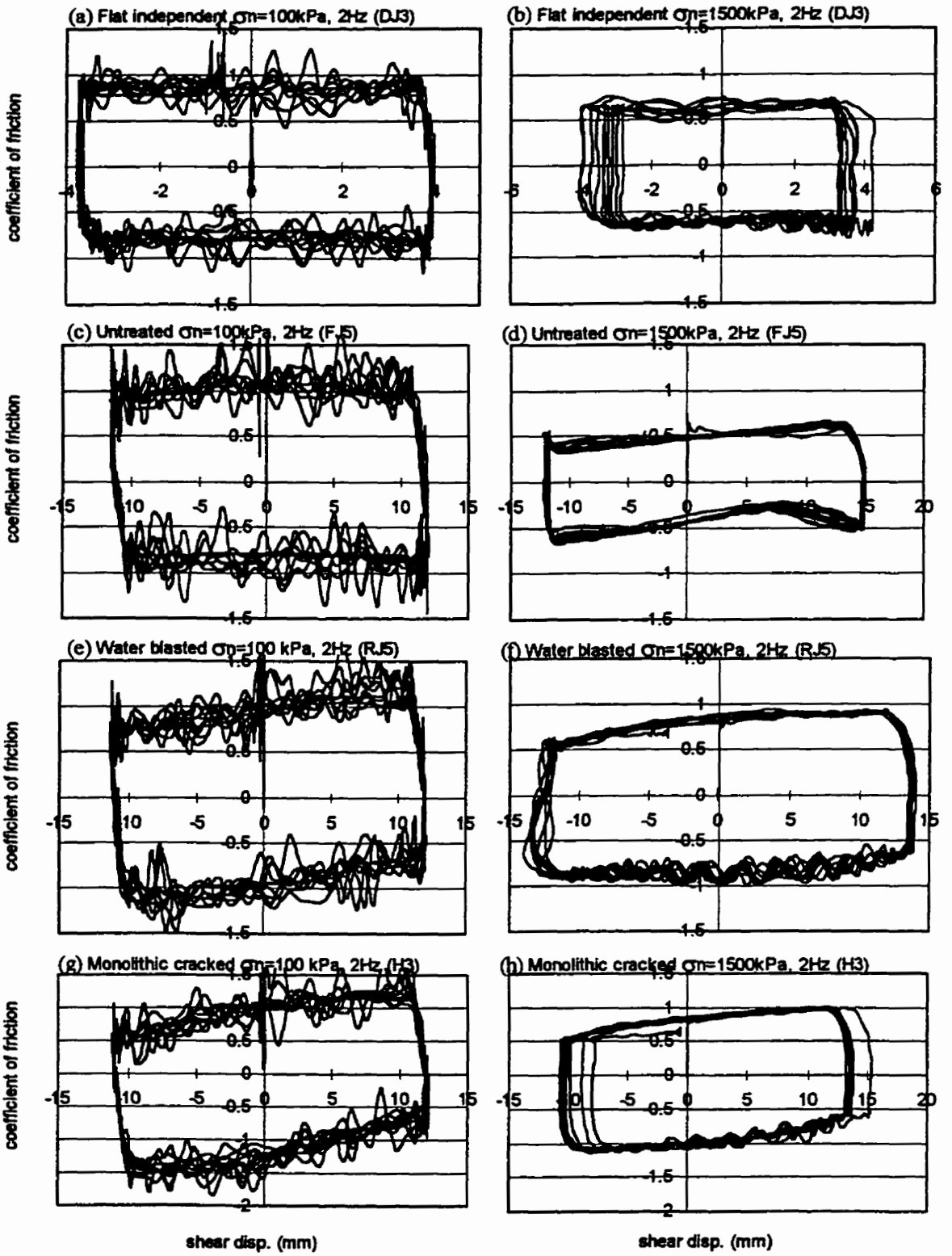

Fig. 4.2 *Experimental dynamic hysteretic response at 2 Hz.*

It might be observed in Fig. 4.2 that there is a bias toward higher displacements in certain plots. That is related to the control system of the shaking table.

Figure 4.3 presents comparison between the average dynamic coefficient of friction by specimen type and by imposed shear displacement frequency. The coefficient of friction is not affected by the vibration frequency. Comparison between Fig. 4.3 (a) and (c) indicate that 10 cycles at 7 Hz (ref. Fig. 4.3 b) did not affect the shear strength (refer to Fig. 3.4[5] for the test procedure). Two sets of results are distinct on the graphs, there is the cracked monolithic specimens and waterblasted joints on one side, and the untreated and flat independent concrete surfaces on the other.

The average measured dynamic friction coefficients show no dependency on the frequency content of the applied shear stress. The friction coefficients on flat independent surfaces reached 0.85 at 100 kPa and 0.55 at 1500 kPa at 2Hz; and μ=0.83 at 100 kPa and 0.5 at 1500 kPa at 7 Hz. The untreated joint surfaces had a μ of 1.0 at 100 kPa and 0.66 at 1500 kPa at 2 Hz; μ=0.95 at 100 kPa and 0.60 at 1500 kPa at 7 Hz. The waterblasted surfaces showed friction coefficients of 1.13 at 100 kPa and 0.89 at 1500 kPa at 2 Hz: μ==1.07 at 100 kPa and 0.85 at 1500 kPa at 7 Hz. The monolithic cracked μ reached 1.18 at 100 kPa and 0.95 at 1500 kPa at 2 Hz; μ=1.12 at 100 kPa and 0.92 at 1500 kPa at 7 Hz.

The decreases of dynamic friction coefficients with increase in normal stress from 100 kPa to 1500 kPa are 37.5 % for the flat independent surfaces, 46 % for the untreated joints, 21 % for the waterblasted specimens, and 17 % for the monolithic specimens. Water blasting the surfaces increased the dynamic friction coefficients by 13% and 38 % on average compared to the untreated surfaces. The increases of monolithic cracked friction coefficients compared to the flat independent surfaces are 34 % at 100 kPa and 78 % at 1500 kPa.

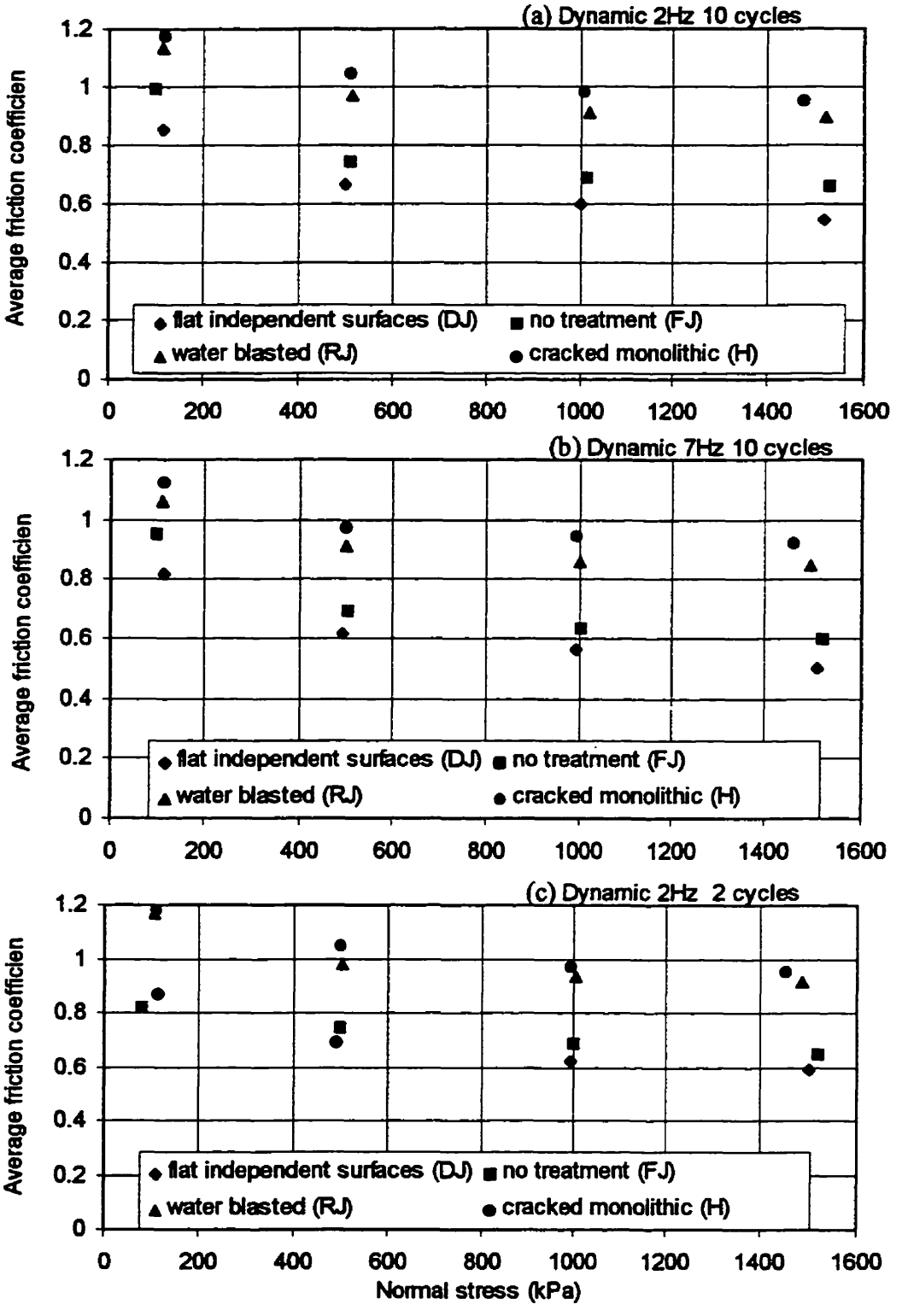

Fig. 4.3 *Measured average dynamic sliding friction coefficients.*

4.5 Discussion

4.5.1 Effect of roughness on interface behaviour

A striking feature in the static sliding test results is the important difference between the applied shear force in the forward half cycle to reach the target displacement and the half cycle backward displacement to the initial position. The explanation is in the upward joint responses, or the dilatancy, of the specimens displacement (normal to the shear displacement). Figure 4.4 shows typical normal displacements for the different types of specimens.

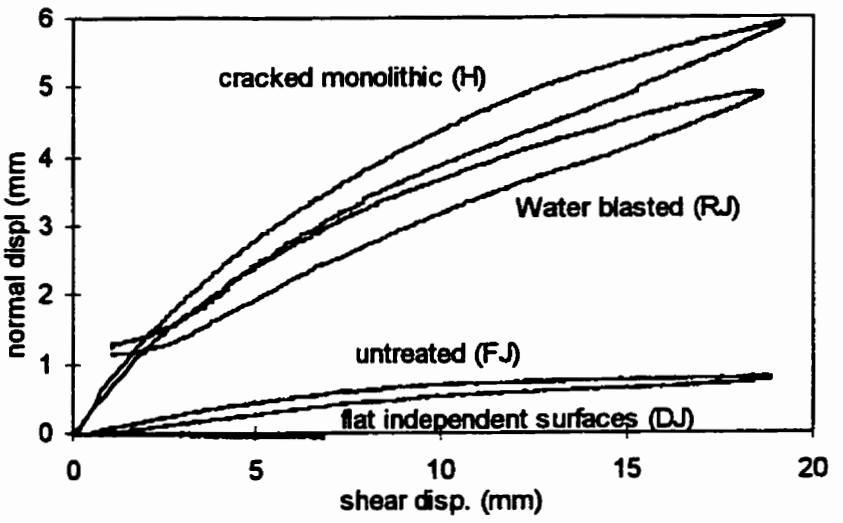

Fig. 4.4 *Normal displacement during predynamic static sliding friction tests.*

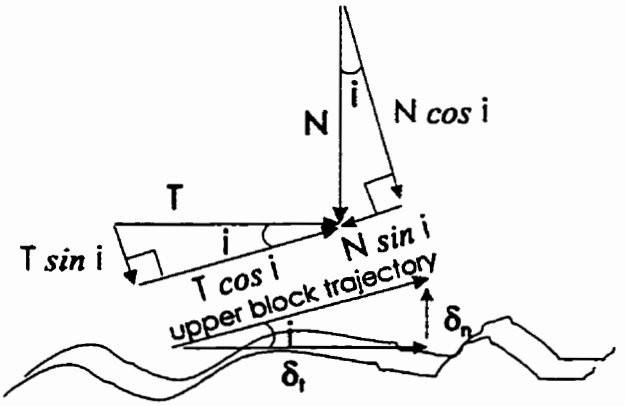

Fig. 4.5 *Applied forces at the interface.*

Due to the riding up of the asperities, the normal displacement on rougher interfaces is much higher than the normal displacement on flatter interfaces. As a result, the true trajectory of the upper block is not parallel to the interface but at an angle *i* to the interface as illustrated in Fig. 4.5. Considering the coefficient of friction acting along the upper block trajectory, or along the asperities, the following relationship is obtained:

$$T\cos i - N\sin i = \mu_b\left[N\cos i + T\sin i\right] \tag{4.2}$$

where
i = the upper trajectory angle or roughness angle,
μ_b = the coefficient of friction along the asperities or basic friction angle

Dividing the right and the left hand sides of Eq.(4.2) by $N\cos i$ yields:

$$\frac{T}{N} - \tan i = \mu_b\left[1 + \frac{T}{N}\tan i\right] \tag{4.3}$$

$$\tan i = \bar{\mu}_i = \frac{\Delta\delta_n}{\Delta\delta_t} \tag{4.4}$$

where
$\Delta\delta_t$ = the shear displacement increment,
$\Delta\delta_n$ = the normal displacement increment corresponding to $\Delta\delta_t$.
$\bar{\mu}_i$= roughness friction coefficient

From Eq.(4.1) and Eq.(4.4), and by isolating μ_b in Eq.(4.3), the following expression is obtained:

$$\mu_b = \frac{\mu_{mes} - \bar{\mu}_i}{1 + \mu_{mes}\bar{\mu}_i} \tag{4.5}$$

In terms of friction angles, μ_b is obtained as follows:

$$\mu_b = \frac{\tan\phi_{mes} - \tan i}{1 + \tan\phi_{mes}\tan i} = \tan(\phi_{mes} - i) = \tan\phi_b \tag{4.6}$$

The above derivation illustrates that the friction coefficient involves an interface geometrical component (i), and a material basic characteristic, the basic friction angle (ϕ_b). This approach was first adopted in rock mechanics by Patton (1966). Lo et al. (1991) used this formulation to interpret sliding friction tests of concrete-rock gravity dam contact joint samples, and dam concrete lift joint samples.

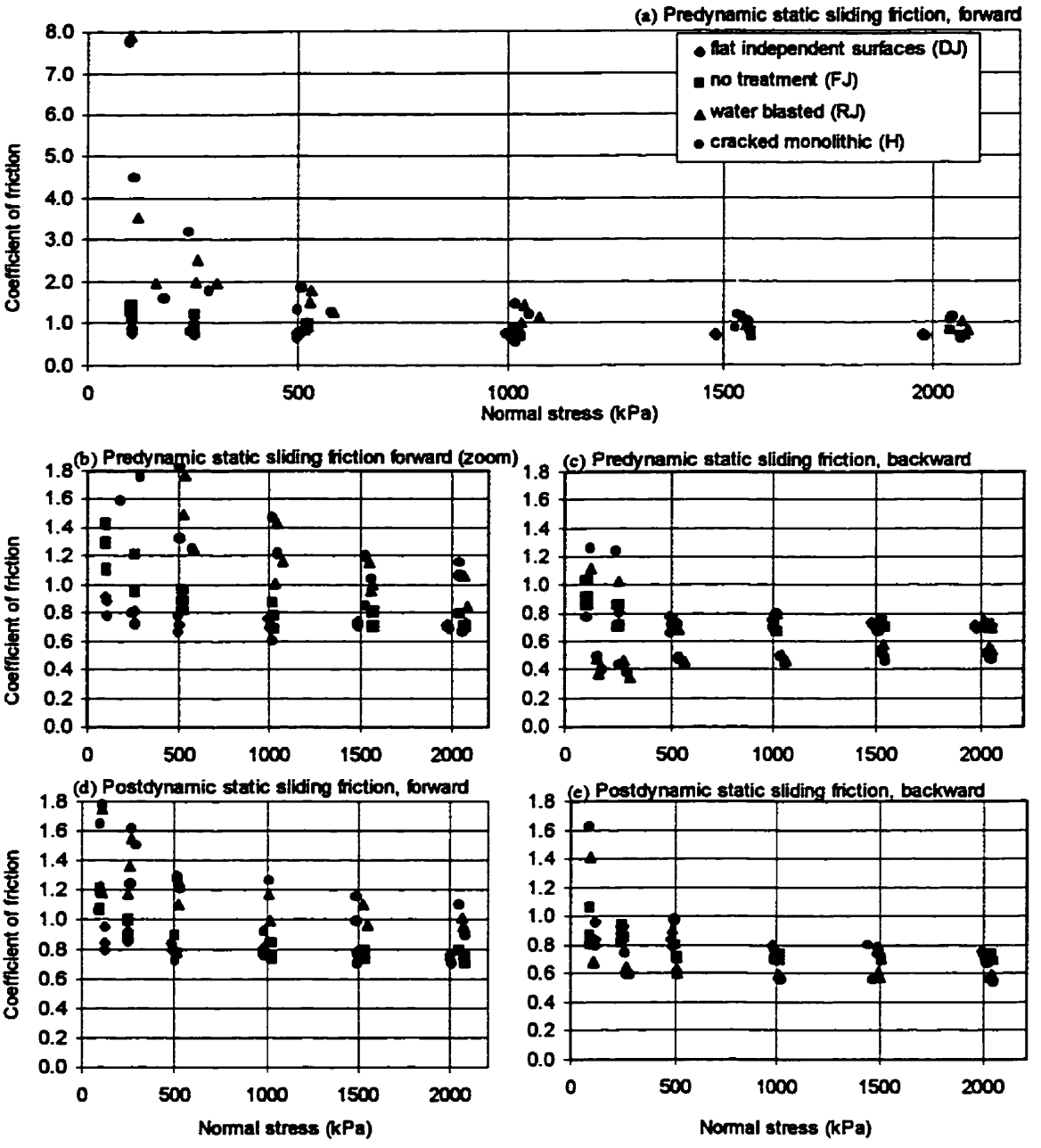

Fig. 4.6 *Measured friction coefficient.*

Comparisons between the average measured friction coefficients (see Fig.4.6 (a,b)) and the average basic friction coefficients (see Fig. 4.7 (a)) for the various types of specimens demonstrate that the basic friction coefficient is indeed independent from the type of interface and thus may be considered as a fundamental concrete material property. This assertion holds true for the concrete mix that was tested.

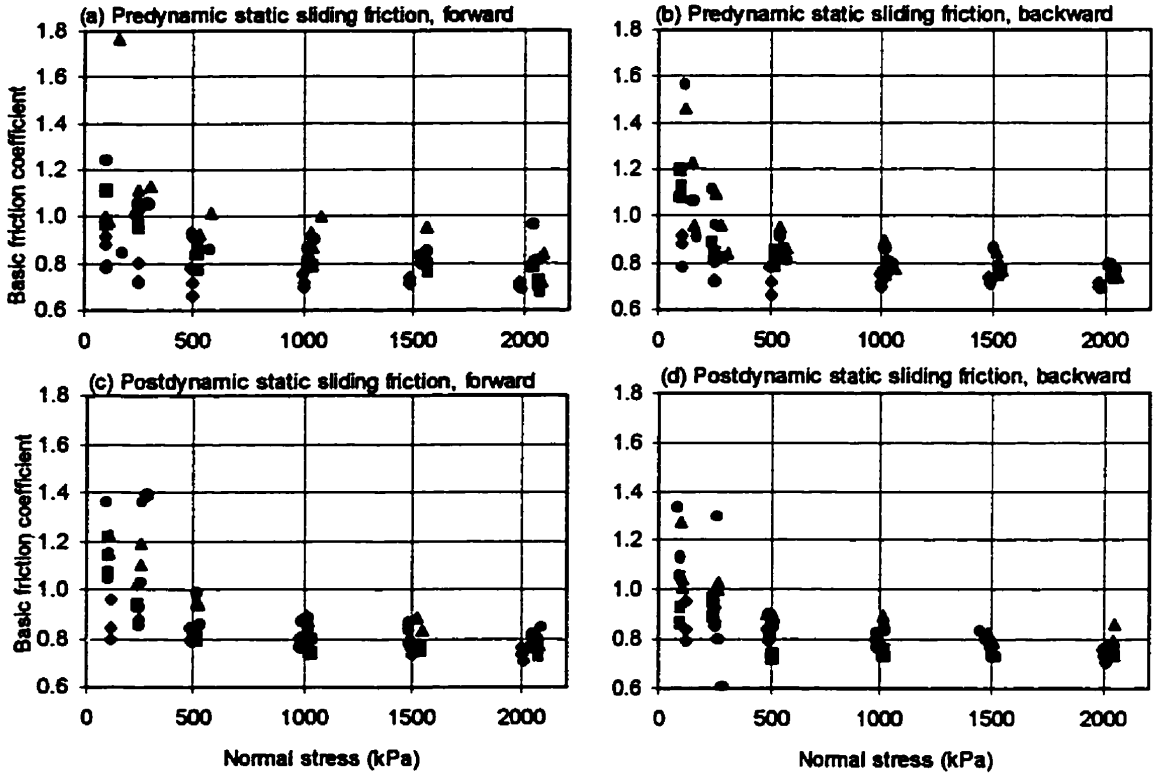

Fig. 4.7 *Basic friction coefficient.*

Figure 4.8 shows the basic friction (μ_b) hysteretic response. The loops have about the same characteristics as the experimental measured friction coefficient (μ_{mcs}) hysteretic response (see Fig. 4.2). The loops are stable, and the frictional resistance decreases with the increase in normal stresses. However, unlike the measured friction coefficient, the type of interface does not have any effect on the loops since the loops more or less stay in a rectangular shape.

Figure 4.7 and Fig. 4.8 confirm that the concept of combining basic (μ_b) and roughness ($\overline{\mu}_i$) friction coefficient is adequate to describe the static and dynamic behaviour of concrete interfaces. The spikes at the end of the cycles in Fig. 4.8 correspond to locations were the shear and normal displacements are zero thus leading to a calculated roughness friction coefficient equal to infinity.

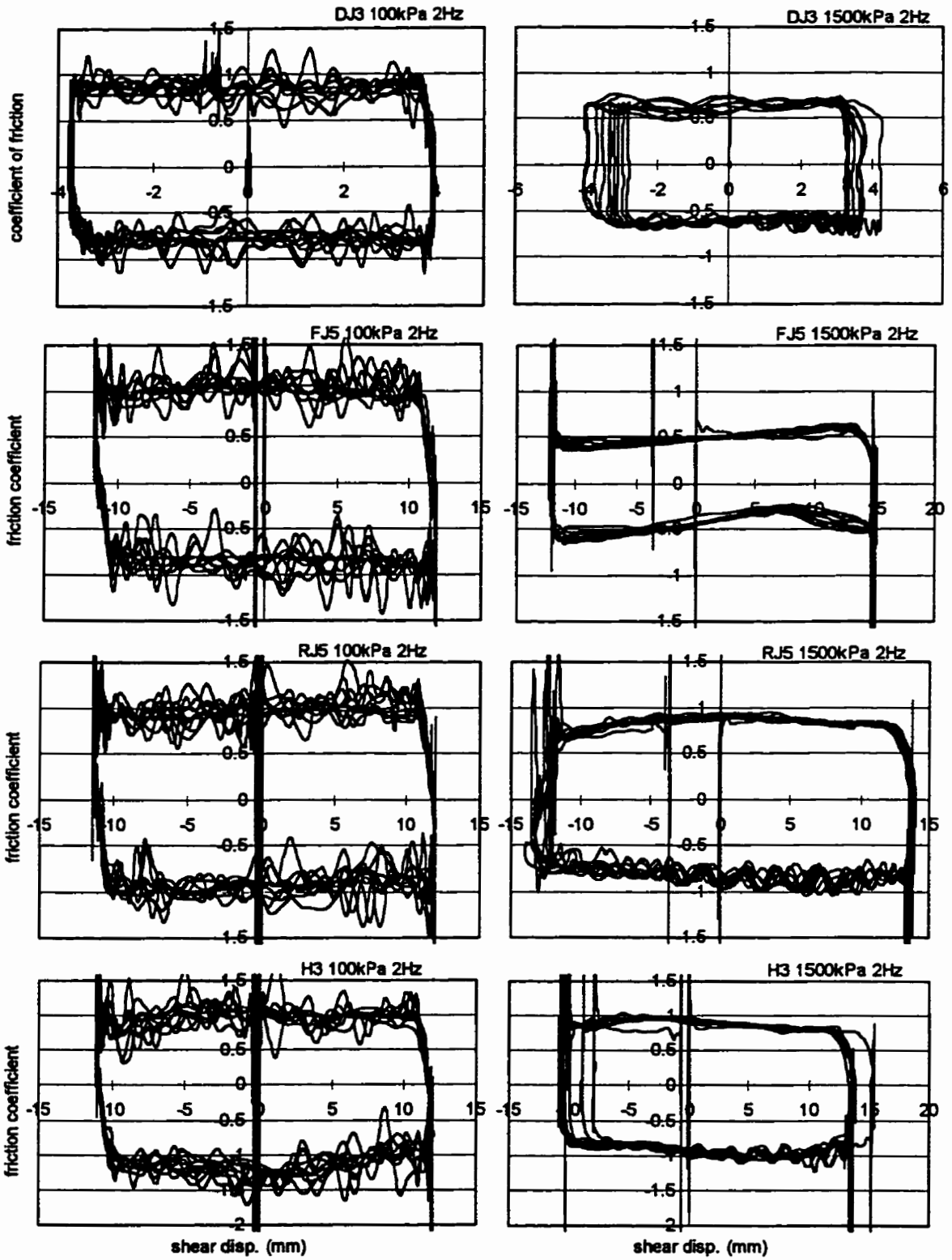

Fig. 4.8 *Basic friction hysteretic response; DJ=flat independent plane surfaces, FJ=untreated, RJ=waterblasted, H=monolithic cracked.*

4.5.4 Comparison between static predynamic, dynamic and static postdynamic responses

The average extreme values (maximum and minimum) and the average friction coefficient per displacement half cycle (forward to the target and backwards to the initial position) are plotted per specimen types in Fig. 4.6. The peak μ_{mcs} values (above μ_{mcs}=2.0) reached in the predynamic forward cycles were not attained in the postdynamic tests at low normal stress levels (σ_n < 500 kPa). Similarly, the low μ_{mcs} values (below μ_{mcs}=0.6) reached in the predynamic tests were not attained in the postdynamic tests. Figure 4.9 shows how the roughness friction coefficients, $\bar{\mu}_i$, decreased by 300% at σ_n = 100 kPa between predynamic and postdynamic loading. The residual roughness and the basic friction coefficients (Fig. 4.7) were not substantially affected by the severe dynamic reversed cyclic loading events.

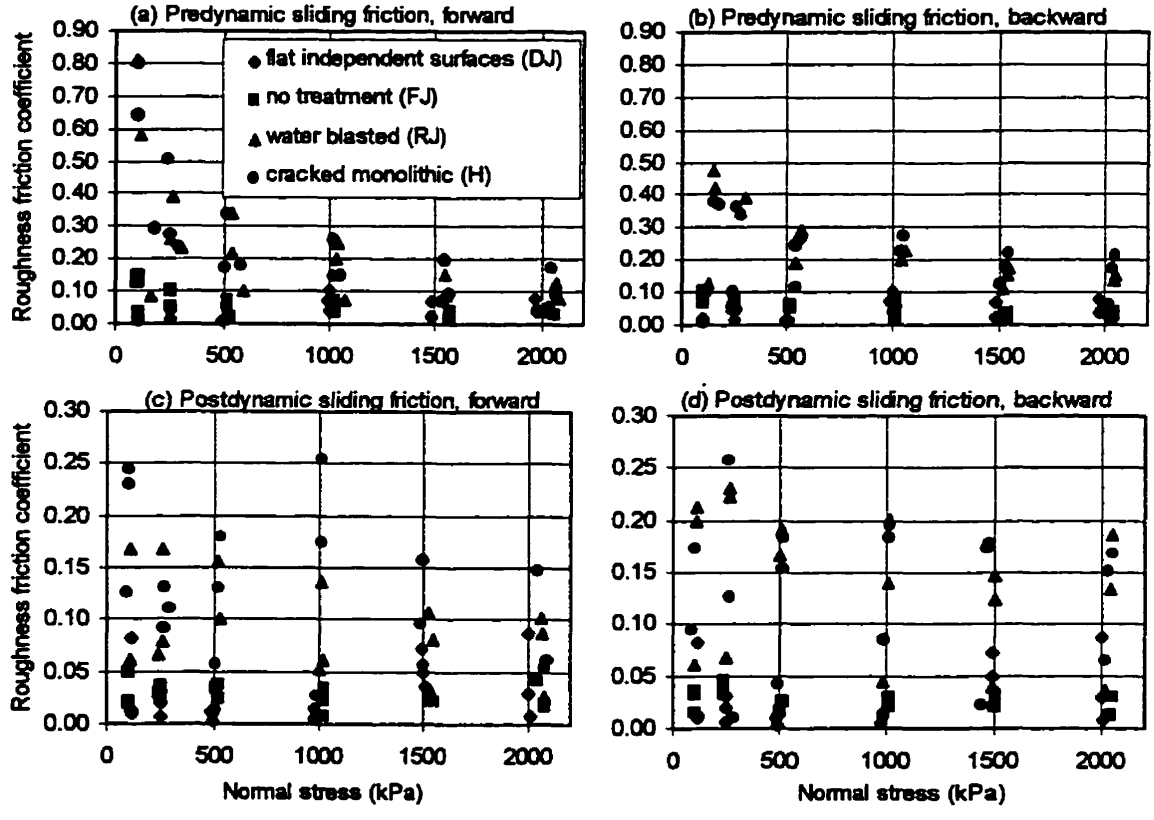

Fig. 4.9 *Roughness friction coefficient.*

The monolithic specimens reached an average predynamic peak friction coefficient of 1.5 that is greater than 1.4 (ACI code,1990) up to σ_n = 1000 kPa, after that, a value of 1.2 would be more adequate. A friction coefficient of 1.2 for the residual shear strength at any normal stress level would also be adequate. For the waterblasted joints, a peak value for μ of 1.4 could be adopted up to σ_n = 1000 kPa, but μ=1.1 would be adequate for all stress levels which is close to μ=1.0 as suggested in the ACI code. A residual μ of 1.0 is in fair agreement with the experimental results. Untreated joints exhibited a peak μ of 0.9 up to σ_n = 1000 kPa, and 0.8 up to σ_n = 2000 kPa. A residual μ of 0.8 would be in agreement with the experimental results. ACI code suggests a μ value of 0.6 for this type of joints.

4.5.5 The concept of degradation of the response

The stability of the hysteresis loops is an important finding of this study. This unexpected behaviour may be explained by looking at the normal displacements (see Fig. 4.10).

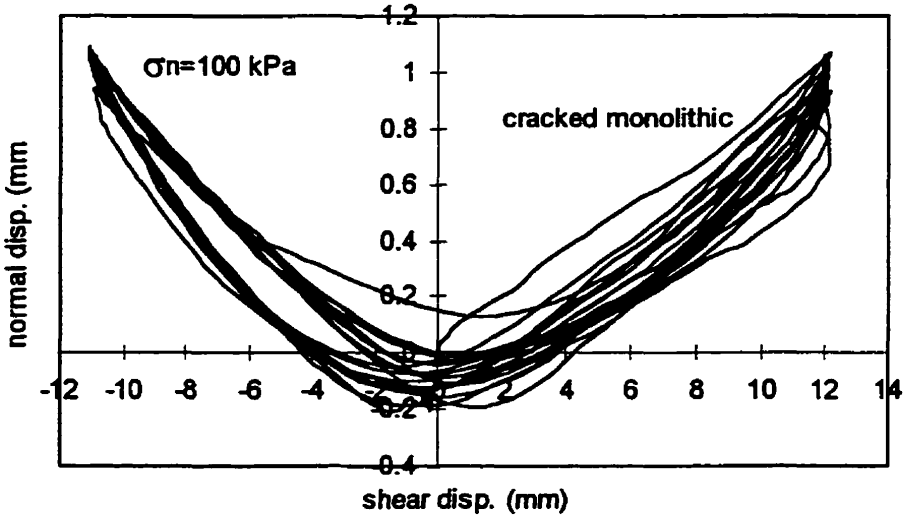

Fig. 4.10 *Normal displacement for a cracked monolithic specimen under dynamic reversed cyclic sliding friction test, 10 cycles at 2 Hz.*

The normal displacements become more and more negative at the initial horizontal position of the specimen as the number of cycles increases. The upper and lower faces of

the crack basically grind into each other. In the tests, since the displacement bounds were fixed, the asperities of one face were always rubbing off the cement paste of the other face at the same location. Therefore the nature of the materials being grinded against each other stayed the same and response degradation never occurred. This behaviour involves aggregate versus cement paste. The relative strength of one to the other is expected to be a significant parameter in the process.

4.5.6 Friction coefficient dependency on sliding velocity and acceleration

Figure 4.11 shows for a cracked monolithic specimen, the friction coefficient plotted against the corresponding sliding velocity during a dynamic test at 2 Hz. The loops in the 2nd and 4th quadrant of Fig. 4.11 (a) shrink to lines in Fig. 4.11 (b). This confirms the adequacy of using the concept of the basic friction angle. Figure 4.11 (b) could be replaced by the superposition of two curves: two plateaus and one reversed S.

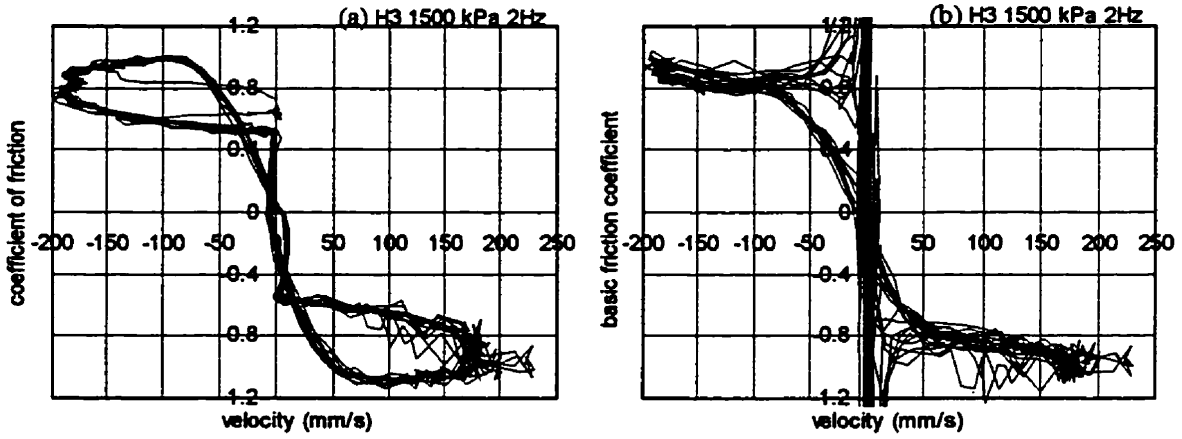

Fig. 4.11 *Sliding friction velocity dependency for a cracked monolithic specimen: (a) friction coefficient* μ_{mes}, *(b) basic friction coefficient* μ_b.

The plateaus at low sliding velocity occur when the upper block begins sliding. The S portion occurs when the upper block slows down for the shear load reversal. On that portion, the basic friction coefficient decreases with decreasing sliding velocity. In Fig. 4.2 this phenomenon corresponds to the rounded corners of the hysteresis loops.

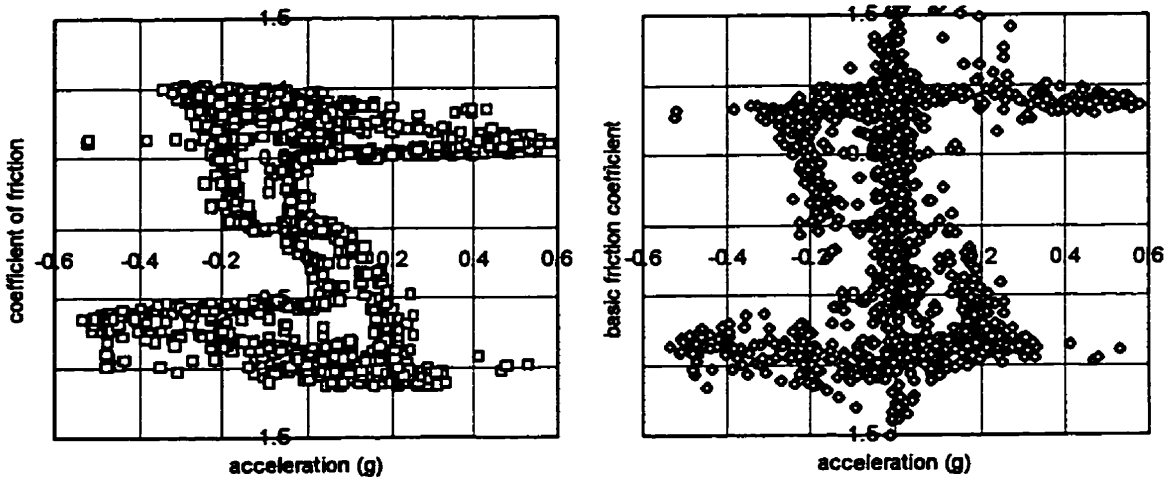

Fig. 4.12 *Friction coefficient dependency on acceleration.*

As illustrated in Fig. 4.12, a similar dependency between the basic friction coefficient and the sliding acceleration was not observed.

4.6 Summary and conclusions

The main findings of the experimental programme may be summarized as follows.

4.6.1 General behaviour

The coefficient of friction decreases with increasing applied normal stress. The specimen behaviour in sliding friction depends on surface preparation. Cracks induced along waterblasted joint surfaces are rough, while cracks induced along unprepared joint surfaces are flat. As a result, waterblasted joints behave like cracked monolithic concrete. Unprepared joint surfaces behave like flat independent concrete surfaces.

4.6.2 Behaviour under dynamic shear

Hysteresis loops are very stable; there is no significant degradation in response. The frequency content of the imposed sliding displacements has no effect on the measured response. The coefficient of friction is somehow dependent on sliding velocity. There is no relation between the coefficient of friction and the acceleration.

CHAPTER 5

Concrete-concrete interface constitutive model

5.1 Introduction

This chapter presents the concrete-concrete interface constitutive model that was implemented into the finite element program INTRFACE to represent lift joints. Crack initiation and propagation at the interface is reproduced using a fracture energy based model. It is coupled to an hysteretic sliding friction model derived from the experimental results presented in Chapter 4. In this chapter, first the empirical concrete joint sliding friction constitutive model is presented. Then, a three-state constitutive model for simulation of the complete concrete joint interface behaviour, involving crack initiation, propagation, and shear sliding, is presented. The chapter ends with a description of the procedure adopted for the simulation of water pressure inside the joints.

5.2 Concrete-concrete joint sliding friction constitutive model

5.2.1 Data reduction

The experimental results presented in Chapter 4 are used to devise a new empirical concrete-concrete interface constitutive model using the concept of basic friction coefficient, μ_b, and roughness friction coefficient, $\bar{\mu}_i$.

$$\mu = \frac{\mu_b + \bar{\mu}_i}{1 - \mu_b \bar{\mu}_i} \tag{5.1}$$

The effect of surface preparation on the friction coefficient and any wear effects are introduced through the roughness friction coefficient, $\bar{\mu}_i$. The basic friction coefficient is independent of the surface preparation. For a displacement cycle, μ_b is calculated once according to the applied normal load, while $\bar{\mu}_i$ is computed for each characteristic point of the displacement cycle (Fig. 5.1).

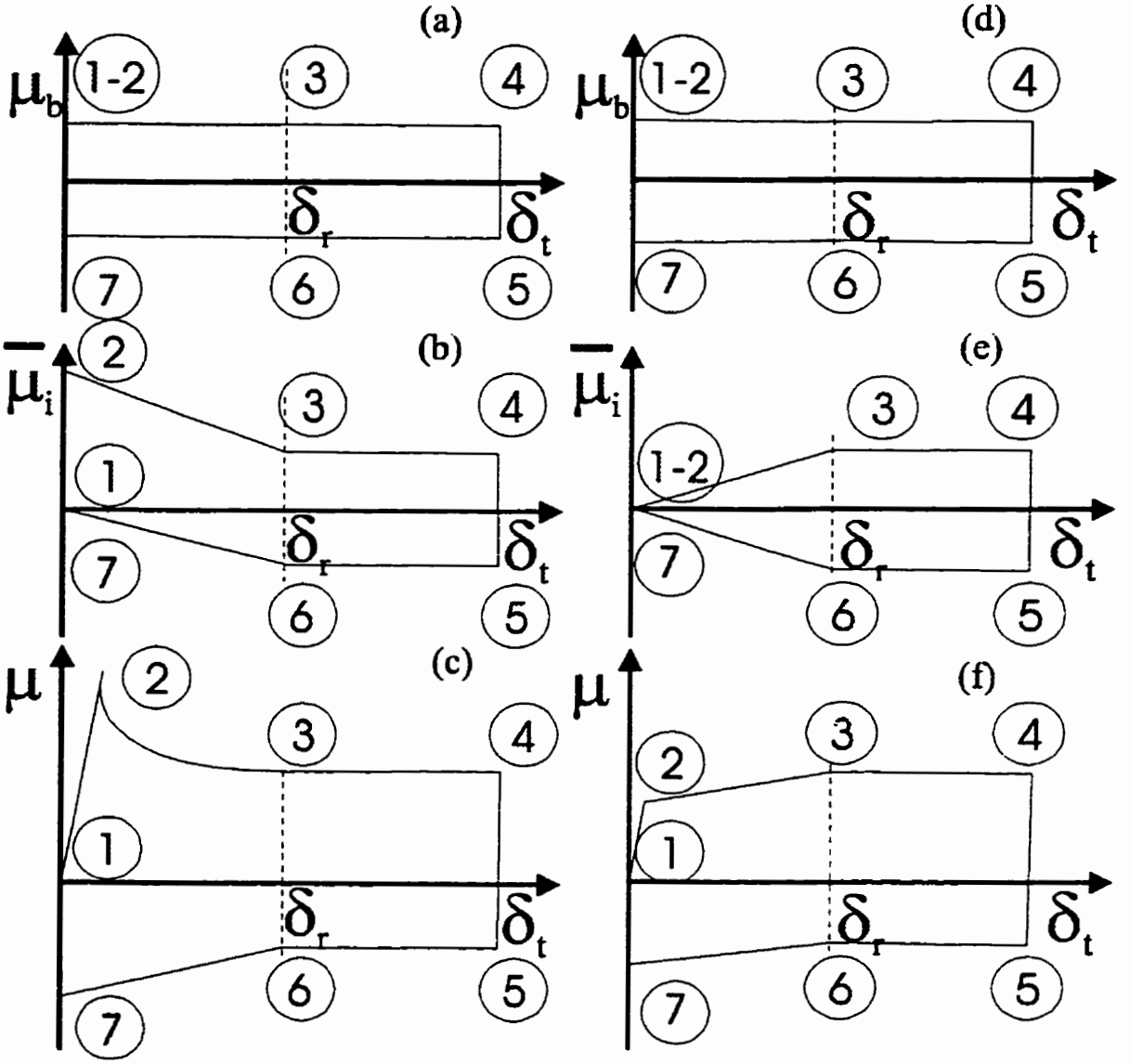

Fig. 5.1 *Sliding friction coefficient - hysteretic responses: (a,b,c) predynamic loops, (d,e,f) dynamic and postdynamic loops.*

As illustrated in Fig. 5.1(c) and (f), a complete forward-backward sliding displacement cycle for predynamic, dynamic and postdynamic interface conditions is defined by seven segments. The predynamic cycle, (Fig. 5.1(c)) begins by segment (1-2), the initial elastic response to the peak, to reach point (2), which is obtained using the peak roughness coefficient, $\bar{\mu}_i^p$ (Fig. 5.1(b)). It is followed by segment (2-3), the transition to the residual sliding friction plateau. Point (3) is determined using the residual roughness

coefficient, $\bar{\mu}_i^r$ (Fig. 5.1(b)), at a sliding displacement, δ_r, equal to half the maximum aggregate size, D_{max}. Segment (3-4) is the residual sliding friction plateau. The sliding displacement reversal, (4-5), occurs at a constant sliding displacement thus the reversal is a rigid process. Point (5), the residual sliding friction strength backward, is determined from the negative value of the residual roughness coefficient, $\bar{\mu}_i^r$, used for points (3) and (4). Segment (5-6) is the residual friction plateau in the backward direction. The roughness coefficient, $\bar{\mu}_i^r$, decreases linearly to zero (6-7), between point (6), at a sliding displacement, δ_r, equal to $\frac{1}{2}D_{max}$, and point (7), the initial perfect match position.

The dynamic and postdynamic sliding displacement cycles have as many segments as the predynamic cycle, however only three parameters are to be computed: (1) the basic friction coefficient, μ_b (Fig. 5.1(d)), (2) the residual roughness coefficient, $\bar{\mu}_i^r$ (Fig. 5.1(e)), and (3) the displacement at the beginning of the residual plateau. The cycle begins by segment (1-2), the initial nearly rigid response to the initial sliding displacement, to reach point (2), which involves no roughness. Thus, the initial sliding occurs at an applied stress equal to the basic frictional strength, ($\mu_b\sigma_n A_n$) where A_n is the area upon which σ_n is applied. It is followed by (2-3), the transition to the residual sliding friction plateau. Point (3) is determined by the residual roughness coefficient, $\bar{\mu}_i^r$, at a sliding displacement, δ_r, equal $\frac{1}{2}D_{max}$. Displacement δ_r may be considered as the displacement required to fully mobilize the residual roughness. In segment (2-3), the transition is assumed to be a straight line. Segment (3-4) is the residual sliding friction plateau. The sliding displacement reversal, (4-5), occurs at a constant sliding displacement thus, just like the predynamic displacement cycle, the reversal is a rigid process. Point (5), the backward residual sliding friction strength is determined from the negative value of the residual roughness coefficient, $\bar{\mu}_i^r$, used for points (3) and (4). Segment (5-6) is the residual friction plateau in the backward direction. The roughness coefficient decreases

linearly to zero (6-7), between point (6), at a sliding displacement, δ_r, equal to $\frac{1}{2}D_{max}$, and point (7), at zero or initial perfect match position.

Based on all test measurements (928 data points), a dual-slope model for the basic friction coefficient is proposed:

$$\begin{aligned} \mu_b &= 0.950 - 0.00022\sigma_n \quad && for \quad \sigma_n \le 500kPa \\ \mu_b &= 0.865 - 0.00005\sigma_n \quad && for \ 500kPa \le \sigma_n \le 2000kPa \end{aligned} \tag{5.2}$$

where σ_n is in kPa. Equation (5.2) is illustrated in Fig. 5.2.

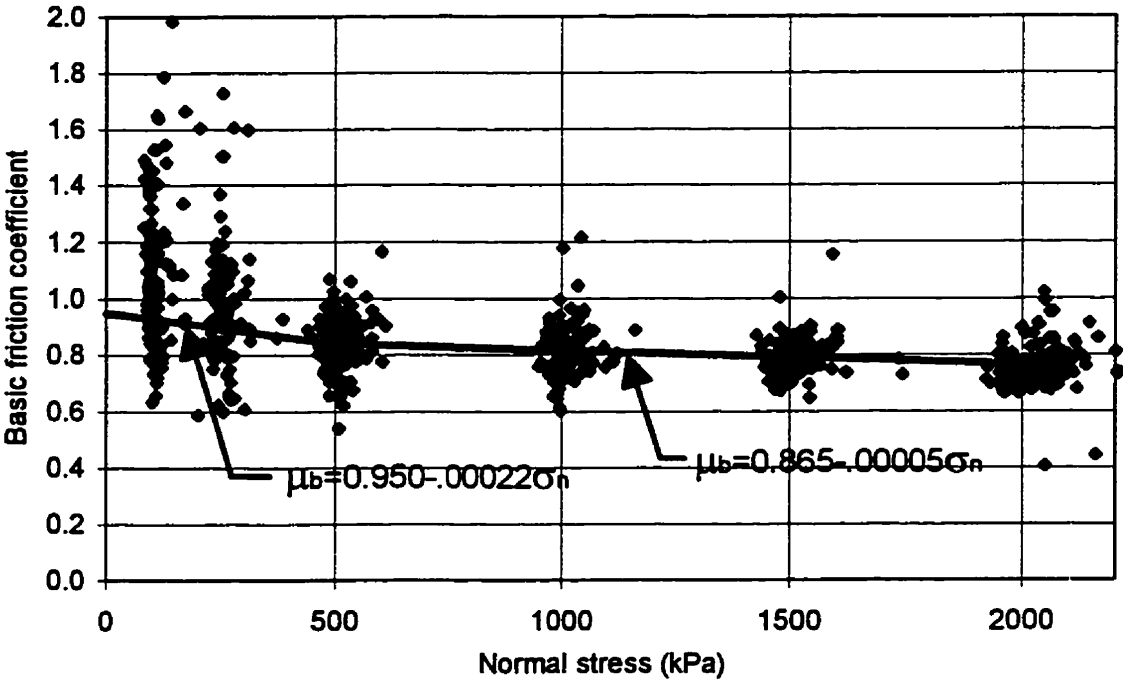

Fig. 5.2 *Basic friction coefficient dual-slope model.*

The lower bound μ in Eq. (5.1) is given by the flat independent plane surfaces model. No roughness is involved; the model is basically rigid-plastic. For that type of surface, sliding occurs when the applied loading reaches the basic frictional strength, with μ_b given by Eq.(5.2).

The model equations for different types of joints are summarized in Table 5.1. The upper bound μ derived from Eq.(5.1), using μ_b and $\bar{\mu}_i^p$ or $\bar{\mu}_i^r$, is given by the monolithic cracked surfaces model. The typical predynamic shear-displacement response loop is similar to the one illustrated in Fig. 5.1(a), while the dynamic and postdynamic loops are described by the loop of Fig. 5.1(b).

5.2.2 Model equations

The behaviour of water blasted interfaces is very similar to monolithic cracked concrete as discussed earlier. The postdynamic roughness friction coefficient is modeled using a single equation corresponding to the predynamic residual roughness friction coefficient, $\bar{\mu}_i^r$. The equations given in Table 5.1 are the best fit equations. A good approximation for water blasted interfaces would be achieved using 80% of the roughness coefficients ($\bar{\mu}_i^p$ and $\bar{\mu}_i^r$)obtained from the monolithic equations for predynamic, dynamic, and postdynamic behaviour.

Table 5.1 *Concrete interface model basic and roughness coefficients.*

Interface type	σ_n	Predynamic roughness coefficient		Postdynamic roughness coefficient
		Peak $\bar{\mu}_i^p$	Residual $\bar{\mu}_i^r$	$\bar{\mu}_i^r$
Monolithic	$\sigma_n \le 400$	$0.90 - 0.001367\sigma_n$	$0.30 - 0.000050\sigma_n$	$0.30 - 0.000050\sigma_n$
	$400 < \sigma_n \le 1500$	$0.40 - 0.0001167\sigma_n$	$0.30 - 0.000050\sigma_n$	$0.30 - 0.000050\sigma_n$
	$1500 < \sigma_n \le 2000$	$0.30 - 0.000050\sigma_n$	$0.30 - 0.000050\sigma_n$	$0.30 - 0.000050\sigma_n$
Water blasted	$\sigma_n \le 275$	$0.875 - 0.00175\sigma_n$	$0.25 - 0.0000375\sigma_n$	$0.25 - 0.0000375\sigma_n$
	$275 < \sigma_n \le 1200$	$0.44 - 0.000185\sigma_n$	$0.25 - 0.0000375\sigma_n$	$0.25 - 0.0000375\sigma_n$
	$1200 < \sigma_n \le 2000$	$0.25 - 0.0000375\sigma_n$	$0.25 - 0.0000375\sigma_n$	$0.25 - 0.0000375\sigma_n$
Untreated	$\sigma_n \le 1000$	$0.15 - 0.00015\sigma_n$	$0.05 - 0.000005\sigma_n$	$0.05 - 0.000005\sigma_n$
	$1000 < \sigma_n \le 2000$	$0.05 - 0.000005\sigma_n$	$0.05 - 0.000005\sigma_n$	$0.05 - 0.000005\sigma_n$
Flat independent*	$\sigma_n \le 500$	$\mu_b = 0.950 - 0.00022\sigma_n$		
	$500 < \sigma_n \le 2000$	$\mu_b = 0.865 - 0.00005\sigma_n$		

*basic friction coefficient

Even though untreated joint surfaces are close to flat independent surfaces in behaviour, little roughness is sufficient to alter the shape of the loop. The predynamic loop is similar to Fig. 5.1(a) with a much lower peak strength as compared to monolithic concrete. Untreated joint surfaces roughness coefficients may be approximated using 15% of the monolithic concrete roughness equations.

For all types of interfaces, the postdynamic loop model is to be used for the dynamic hysteresis loops. However, a better fit to the experimental results was obtained by reducing the basic friction coefficient to 85% of the static value. This reduction of the basic friction coefficient also enhances the model predictions on the other types of specimens. However, the roughness is not affected by the rapid loading rate.

A simple constitutive model may thus be summarized in the following equation:

$$\mu = \frac{\lambda_d \mu_b + \chi_i \bar{\mu}_i}{1 - \lambda_d \chi_i \mu_b \bar{\mu}_i} \tag{5.3}$$

where $\bar{\mu}_i$ is defined by the equations for the monolithic specimen given in Table 5.1. Two correction factors are introduced: λ_d, the dynamic reduction factor equal to 1.00 for static loading and 0.85 for dynamic loading; and χ_i, the interface roughness factor equal to 1.00 for cracked monolithic concrete, 0.80 for water blasted joints, 0.15 for untreated joints, and 0.00 for flat independent concrete surfaces. Typical model predictions are compared with experimental results in Fig. 5.3(a) and Fig. 5.3(b).

Dilatancy may be computed from the model equations using the roughness coefficient:

$$\Delta\delta_n = \bar{\mu}_i \Delta\delta_t \tag{5.4}$$

where δ_n and δ_t are the normal and tangential displacements respectively. The integration of normal displacement increments, $\Delta\delta_n$, will lead to the dilatancy; $\bar{\mu}_i$ should be considered to vary with the shear displacement and normal stresses as described in the previous section.

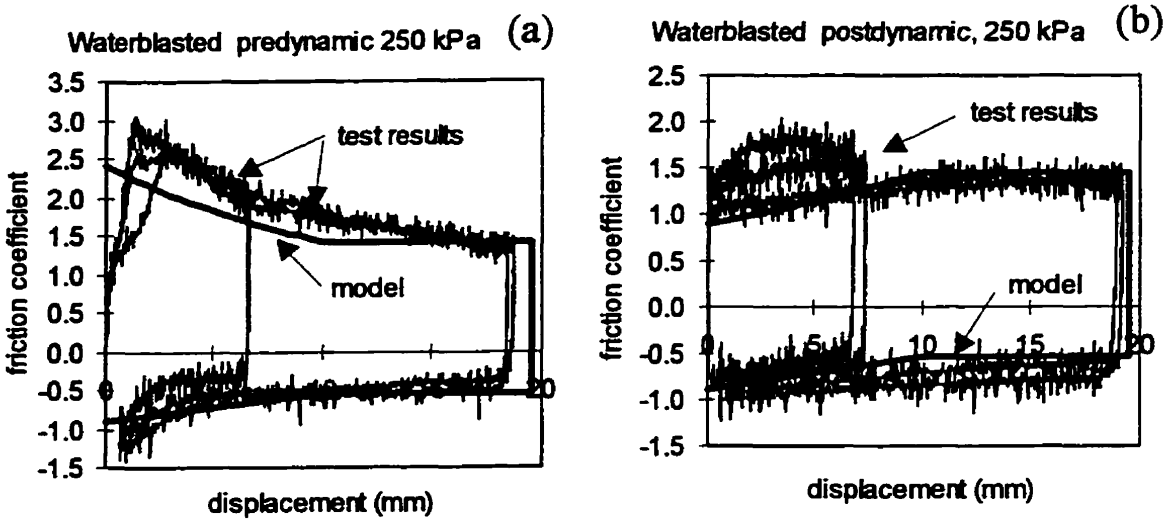

Fig. 5.3 *Comparisons between constitutive model and experimental results.*

5.3 Concrete-concrete joint three-state constitutive model

The constitutive model covers the three possible states of the interface: (i) linear elastic response prior to tensile and/or shear cracking, (ii) crack initiation, tensile and/or shear crack propagation, and (iii) fully cracked response. The key elements in the model are the failure envelopes, and the stress-displacement relationships described by the normal stress versus opening-closing displacements (mode I) and shear stress versus shear displacements or sliding (mode II). The failure envelope and the stress-displacement relationships evolve according to the loads and displacements history. Furthermore, the failure envelope and the stress-displacement curve interact with each other. This interaction is illustrated in Fig. 5.4. The transition from one state to another occurs when the state of stress reaches the failure envelope. The following sections describe each state, and how to evolve from one to another.

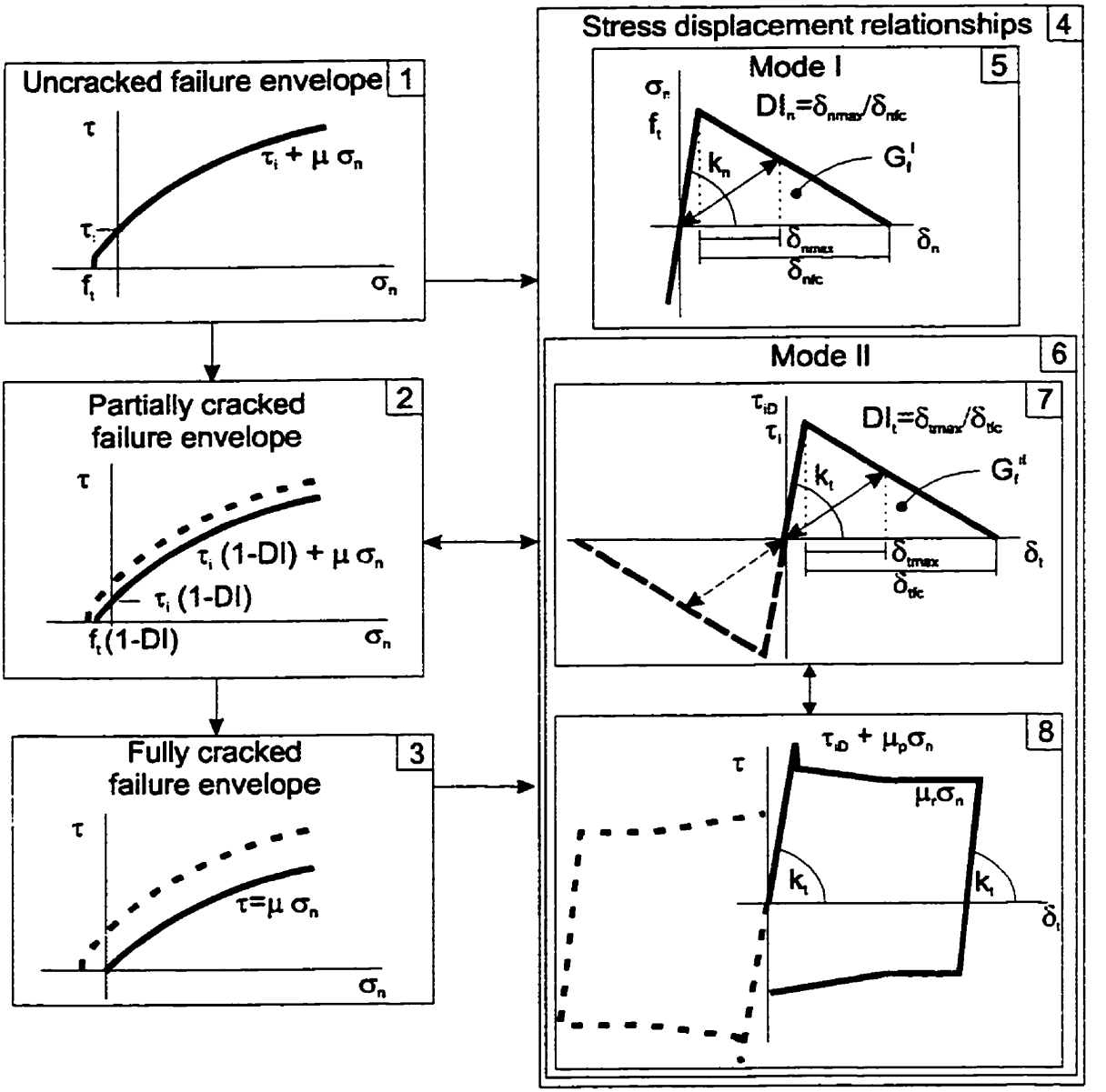

Fig. 5.4 *Three-state concrete interface constitutive model.*

5.3.1 Uncracked response

The uncracked response is linear elastic in tension, compression, and shear. The capacity is bounded by the uncracked failure envelope as illustrated in Fig. 5.4[1]. Three material parameters are required to draw the failure envelope: the concrete tensile strength, f_t, the cohesion, τ_i, and the friction coefficient, μ. The concrete tensile strength,

f_t, is the uniaxial tensile limit of the failure envelope. No limit was considered in compression since the expected compressive stresses in concrete gravity dams are usually well below the compressive strength of concrete. The cohesion is the pure shear limit strength.

In a state of combined compression and shear the classical Mohr-Coulomb equation (Eq. 2.2) defines the failure envelope.

$$\tau = \tau_i + \mu\sigma_n \tag{5.5}$$

The coefficient of friction, μ, is determined according to the concrete-concrete joint sliding friction constitutive model described in Section 5.2.

In a state of combined tension and shear, since the normal stress is in the positive range, the shear strength will be lower than the cohesion:

$$\tau = \tau_i - \mu\sigma_n \tag{5.6}$$

The coefficient of friction used in the tensile range is defined from the sliding friction constitutive model with σ_n =0MPa.

5.3.2 Partially cracked response

Once the state of stress reaches the failure envelope, a crack is assumed to be initiated. No biaxial effect is considered since the joint is assumed to be a discrete seem in the material. Once cracked, the response follows a classical G_f fracture energy based model (see Fig. 5.4[5] and Fig. 5.4[7]). In tension, the fracture model requires the tensile strength, f_t, the mode I fracture energy, G_f^I , and the initial normal stiffness, k_n, of the interface. In shear, the fracture model requires the initial cohesion, τ_i, the mode II fracture energy, G_f^{II}, and the shear stiffness, k_t. The opening and shear displacement at full consumption of fracture energy are computed from:

$$\delta_{nfc} = \frac{2G_f^I}{f_t} - \frac{f_t A_n}{k_n} \quad and \quad \delta_{tfc} = \frac{2G_f^{II}}{\tau_i} - \frac{\tau_i A_n}{k_t} \tag{5.7}$$

where A_n is the tributary area of the gap-friction element. The accumulated damage, DI, is computed by the damage index as the maximum between DI_n and DI_t:

$$DI_n = \frac{\delta_{n\max}}{\delta_{nfc}} \quad and \quad DI_t = \frac{\delta_{t\max}}{\delta_{tfc}} \tag{5.8}$$

where δ_{nmax} is the overall maximum opening reached in the load history, while δ_{tmax} is the absolute value of the maximum shear displacement reached in the load history. The tensile normal stiffness decreases as damage increases as:

$$k_{ni} = k_n\,(1 - DI) \tag{5.9}$$

Unloading and reloading in tension follows the overall minimum tensile normal stiffness, k_{ni}. The cohesion also decreases with increasing damage as:

$$\tau = \tau_i\,(1 - DI) \tag{5.10}$$

The effect of reducing both the cohesion and the tensile strength is to shrink the failure envelope as illustrated in Fig. 5.4[2].

Under any state of damage, the normal response in compression is considered to be linear elastic. The cohesive strength in compression follows the mode II fracture energy model. Thus the shear strength is the sum of the cohesion which decreases with increasing shear displacement, and a frictional component function of the normal stress and the friction coefficient.

5.3.3 Fully cracked response

The fully cracked failure envelope is illustrated in Fig. 5.4[3]. The shear strength is a sole function of the applied normal stress and shear displacement. The shear stress-displacement relationship follows the concrete-concrete joint sliding friction constitutive model of Section 5.2.

The uniaxial response is rather simple. There is no resistance in tension, thus there are zero tensile and zero shear stresses for any crack opening. In compression, the

response stays linear elastic and follows the initial normal stiffness. Crack closing occurs when the normal displacement reaches the zero value regardless to the sliding displacement.

5.4 Water penetration in joints

Since the aim of this study is the behaviour of concrete gravity dams subjected to earthquakes, the interaction between joints and water is to be considered somehow to establish the initial conditions prior to the earthquake. During the earthquake, the initial uplift pressure is assumed to remain unchanged.

It is assumed that water has no effect on the material properties of the interface. This assumption is debatable. Recent research on rock joints, Katani et al. (1997), indicated that water reduces the friction coefficient with increasing sliding velocity. Since the experimental programme involved no water, no information on the behaviour of "wet" joints was obtained. Consequently water in joints or uplift pressure was considered as an external load only. As a result, if the interface is in tension, the uplift water pressure will increase the tension. On the other hand, if the interface is in compression, the uplift water pressure shares the load thus reducing the compression on the interface.

The water pressure is assumed to evolve according to the state of damage. Biot coefficients are used to determine the effective water pressure at the interface. Two limit states are considered for Biot coefficients: (i) the uncracked Biot coefficient, $0 \le b_u \le 1$, and (ii) the fully cracked Biot coefficient, $0 \le b_c \le 1$. The effective uplift pressure, p_{eff}, at a given location along a joint is calculated as follows:

$$\begin{aligned} p_{eff} &= H\left(DI, p_{res}, p_{ini}\right) \times B\left(DI, b_u, b_c\right) \\ p_{eff} &= \left\{\left(p_{res} - p_{ini}\right) DI + p_{ini}\right\} \times \left\{\left(b_c - b_u\right) DI + b_u\right\} \end{aligned} \tag{5.11}$$

where p_{res} is the water pressure at the upstream joint tip, p_{ini} is the initial applied uplift water pressure. The evolution of the Biot coefficient and the applied water head at the joint according to the state of damage [$B(DI, b_u, b_c)$] are illustrated in Fig. 5.5(b).

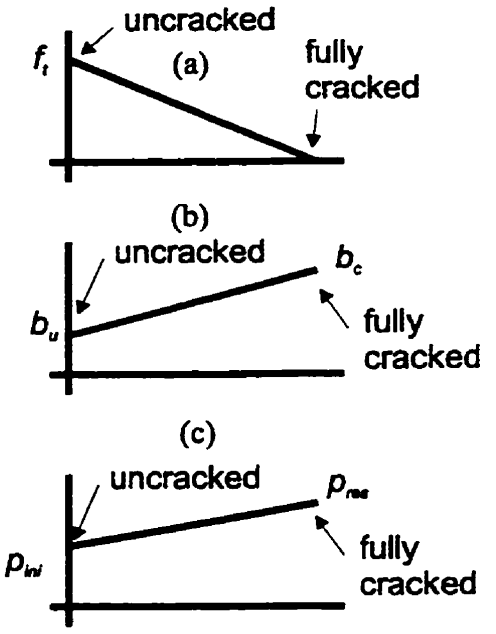

Fig. 5.5 *Variation with respect to (a) the state of damage, (b) Biot coefficient, and (c) the applied water head.*

The initial water pressure distribution, p_{ini}, is usually assumed to vary linearly from the upstream joint tip water head to the downstream joint tip water head (if the downstream end of the joint is in contact with water; if not, zero water head is assumed at the downstream end). The applied uplift water head is assumed to evolve with increasing damage [$H(DI, p_{res}, p_{ini})$] as illustrated in Fig. 5.5(c). Thus, as the fully crack ligament elongates along the joint, the applied water head at the crack tip is kept equal to the upstream joint tip water head level. In partially cracked elements the water head increases in proportion to damage.

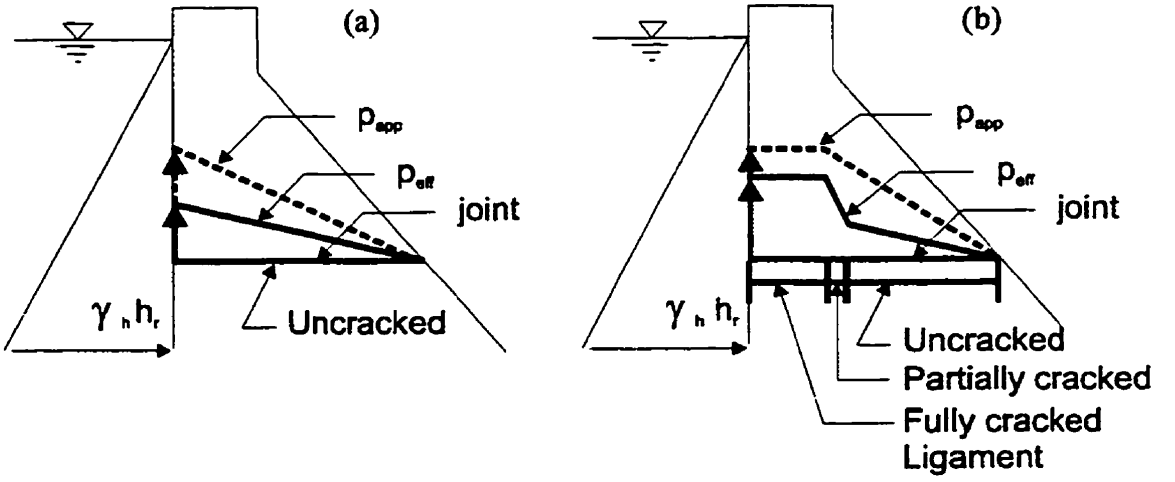

Fig. 5.6 *Uplift water pressure along a joint*

Typical uplift water pressure distribution is illustrated in Fig.5.6 (USBR, 1979).

5.5 Summary and conclusions

An original empirical concrete-concrete joint sliding friction constitutive model is proposed. The friction angle characterising the shear strength is calculated as the sum of a basic angle and a roughness angle. The concept of peak and residual friction values are adequate to describe the basic frictional behaviour. The roughness of water blasted joints is equal to 80% of the roughness of monolithic specimens, while the roughness of untreated joints is equal to 15% of the roughness of monolithic cracked concrete. The dynamic sliding hysteresis loops are enhanced by reducing the basic friction coefficient to 85% of the static value.

A three-state constitutive joint model was presented. It covers: (i) the linear elastic response prior to cracking, (ii) crack initiation and crack propagation in tension or shear, and (iii) the fully cracked response. The key elements in the model are the failure envelope and the stress-displacement relationships. Water penetration is considered as an external load that evolves according to the state of damage of the interface.

CHAPTER 6

Finite element implementation of a nonlinear concrete lift joint constitutive model

6.1 Introduction

This chapter presents the implementation of the nonlinear three-state concrete lift joint constitutive model, as described in Chapter 5. At first, the nonlinear gap-friction element adopted herein is presented in the context of contact problem theory. The solution strategies for the static and dynamic equilibrium equations are then described with the tensile and shear state determination of the gap-friction element. To conclude the chapter, some validation problems on simple beams and structural systems are analysed.

6.2 Finite element simulation of interfaces

6.2.1 Theoretical strategies for simulation of interfaces

Discontinuities such as construction joints in dams are a special case of a more general problem called the contact problem. As defined by Lee (1993), a contact problem is a situation where there are changes in the boundary constraints during loading. What distinguishes the contact problem from other equilibrium problems are the conditions to be satisfied on the contact surface. In classical contact problem theory, these conditions are: (i) impenetrability of the contacting bodies, (ii) tensile tractions not allowed, and (iii) the development of tangential and normal components of the contact force, related through an appropriate friction law. The first condition, from a numerical analysis point of view, is the most difficult to satisfy and the tolerance upon violation will determine the most appropriate numerical scheme to be used. The second condition will be satisfied within the context of a fracture energy based tensile softening model as described in Chapter 5.

There are two possible variational formulations for the contact problem (Zhong and Mackerle, 1992). The first form, also called direction method (Chen and Tsai, 1986), is a constrained minimization problem involving a variational inequality such as formulated by Duvaut and Lions (1972) or Campos et al. (1982). It may be stated as follows:

$$\begin{aligned} \Pi(v) &= \tfrac{1}{2}a(v,v) - f(v) - j(v) \\ a(v,v) &= \int_{\Omega} E_{ijkl}\, v_{k,l}\, v_{i,j}\, dx \\ f(v) &= \int_{\Omega} f_i\, v_i\, dx + \int_{\Gamma_F} t_i\, v_i\, ds \\ j(v) &= \int_{\Gamma_C} \mu |\sigma_n(x)|\, |v_t|\, ds \end{aligned} \tag{6.1}$$

where v is an acceptable displacement field, Ω is the elastic body domain (volume), E_{ijkl} are the elasticities of the material, dx is a volume differential element, Γ_F is the portion of the boundary where forces are prescribed, Γ_C is the candidate contact surface, ds is a surface differential element, f_i are body forces, t_i are external forces, μ is the coefficient of friction, $\sigma_n(x)$ is the normal stress on the contact surface and v_t is the tangential component of the displacement along the contact surface. The first term in the $\Pi(v)$ expression is the strain energy of the body, $f(v)$ is the work done by external loads, and $j(v)$ is the work done by friction forces. The solution to the problem is the displacement field v that minimizes the potential energy $\Pi(v)$. The main advantages of this approach are: the possibility to prove uniqueness of the solution, the geometrical or material inconsistencies are avoided, different laws for boundary conditions may be used, material nonlinearities are covered using the same principles, and an error criteria may be obtained (Böhm, 1987).

The second variational formulation of the contact problem, also called iterative method (Chen and Tsai, 1986), is a direct application of the principle of virtual work. It follows the approach usually adopted for typical problems of structural engineering. It may be formulated as follows:

$$\Pi_l = \Pi - \sum_k W_k \tag{6.2}$$

where Π_l is the total potential energy, Π is the usual form of the potential energy leading to the equilibrium equations, and ΣW_k is the potential of the contact forces (Bathe and Chaudhary, 1985).

In the second variational formulation, the contact conditions are addressed as constraints. There are several methods available to formulate a constraint problem. The most widely used are the Lagrange multipliers method, and the penalty method (see Fig. 2.9).

Lagrange multipliers enable to introduce the constraint in the expression of the potential energy. As described by Cook et al. (1989), let a given system be subjected to the constraint $\{G\}$ where λ_L represent the Lagrange multipliers

$$\Pi_l = \Pi + \lambda_L \{G\} \tag{6.3}$$

Let Π be a structural mechanics system subjected to the constraint $\{G\} = [C]\{\delta\} - \{Q\}$:

$$\Pi_l = \tfrac{1}{2}\{\delta\}^T[K]\{\delta\} - \{F\}\{\delta\} + \{\lambda_L\}\{[C]\{\delta\} - \{Q\}\} \tag{6.4}$$

where [K] is the stiffness matrix, $\{\delta\}$ are displacements, {F} are the applied forces, and $\{\lambda_L\}$ are the Lagrange multipliers. By taking the first variations with respect to the displacements and with respect to the Lagrange multipliers we get:

$$\frac{\partial \Pi_l}{\partial \delta} = 0 \quad , \quad \frac{\partial \Pi_l}{\partial \lambda_L} = 0 \tag{6.5}$$

It leads to the following system of equations:

$$\begin{bmatrix} K & C \\ C & 0 \end{bmatrix} \begin{Bmatrix} \delta \\ \lambda_L \end{Bmatrix} = \begin{Bmatrix} F \\ Q \end{Bmatrix} \tag{6.6}$$

The main disadvantage of the Lagrange multipliers method is obvious in the above. It introduces additional variables in the system which increase the number of columns and rows in the stiffness matrix hence it disturbs the bandedness nature of the stiffness matrix. Besides, introducing zeros on the diagonal may lead to numerical problems.

On the other hand, the Lagrange multipliers have a physical meaning. This is illustrated in the simple example given by Heegaard and Curnier (1993) shown in Fig. 6.1. The constraint is g-δ≥0. This problem may be stated as follows:

$$\Pi_l = \tfrac{1}{2}k\delta^2 - f\delta + \lambda_L\left(g-\delta\right) \tag{6.7}$$

where the variables k, δ, f and g are shown in Fig. 6.1. By taking the first variation we get:

$$\begin{bmatrix} k & -1 \\ -1 & 0 \end{bmatrix}\begin{Bmatrix} \delta \\ \lambda_L \end{Bmatrix} = \begin{Bmatrix} f \\ -g \end{Bmatrix} \tag{6.8}$$

Thus at contact we get:

$$\delta = g \quad , \quad \lambda_L = kg - f \tag{6.9}$$

The Lagrange multiplier is equal to the contact force and it leads to an exact solution.

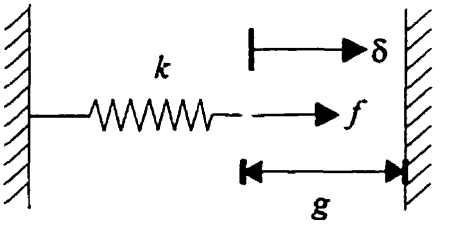

Fig. 6.1 *Simple contact problem from Heegaard and Curnier (1993).*

The penalty method is an alternative method for introducing a constraint in the expression of the potential energy. For a given system subjected to the constraint G, the potential energy could be written as:

$$\Pi_l = \Pi + \tfrac{1}{2}\{G\}^T\alpha_p\{G\} \tag{6.10}$$

where α_p is the penalty factor. Let Π be a structural mechanics system, and let it be subjected to the constraint $\{G\}=[C]\{\delta\}-\{Q\}$:

$$\begin{aligned} \Pi_l &= \tfrac{1}{2}\{\delta\}^T[K]\{\delta\} - \{\delta\}^T[F] \\ &\quad + \tfrac{1}{2}\left([C]\{\delta\}-\{Q\}\right)^T\lceil\alpha_p\rfloor\left([C]\{\delta\}-\{Q\}\right) \\ \Pi_l &= \tfrac{1}{2}\{\delta\}^T[K]\{\delta\} - \{\delta\}^T\{F\} + \tfrac{1}{2}\{\delta\}^T[C]^T\lceil\alpha_p\rfloor[C]\{\delta\} \\ &\quad - \{\delta\}^T[C]^T\lceil\alpha_p\rfloor\{Q\} + \tfrac{1}{2}\{Q\}^T\lceil\alpha_p\rfloor\{Q\} \end{aligned} \tag{6.11}$$

Taking the first variations leads to:

$$\left[[K]+[C]^T\lceil\alpha_p\rfloor[C]\right]\{\delta\} = \{F\}+[C]^T\lceil\alpha_p\rfloor\{Q\} \tag{6.12}$$

The great advantage of the penalty method is that the number of variables is not affected by the constraints. If the penalty method is applied to the simple Heegaard and Curnier (1993) example, the expression for the potential energy becomes:

$$\Pi_l = \tfrac{1}{2}k\delta^2 - f\delta + \tfrac{1}{2}\left[(-1)\delta + g\right]^T\lceil\alpha_p\rfloor\left[(-1)\delta + g\right] \tag{6.13}$$

By setting [C]=[-1] and {Q}={-g}, equation 6.12 then becomes:

$$\begin{aligned}\left[[k]+[-1]^T\lceil\alpha_p\rfloor[-1]\right]\{\delta\} &= \{f\}+[-1]^T\lceil\alpha_p\rfloor\{-g\}\\ (k+\alpha)\,\delta &= f+\alpha_p\, g\\ \left(\frac{k}{\alpha_p}+1\right)\delta &= \frac{f}{\alpha_p}+g\end{aligned} \tag{6.14}$$

The choice of an appropriate penalty factor (α_p) is the difficult task in this method. If the penalty coefficient is too small, the constraint is not satisfied, if it is too high it might lead to numerical problems such as ill-conditioning. The solution obtained from the penalty method is an approximation of the exact solution. The penalty factor may be interpreted as being a stiffness term.

There exists other methods for dealing with contact problems such the flexibility approach (Francavilla and Zienkiewicz, 1975), the direct method, and the boundary element method.

6.2.2 Interface finite element formulation

A finite elements computer program called INTRFACE was developed as part of this study. The code use some of the modules of SAP80 general purpose finite element computer program and the input data follows the SAP80 input data convention. More details on INTRFACE are available in Fronteddu (1997).

The interface finite element adopted herein is the gap-friction element. As demonstrated in Subsection 2.4.3.1, the gap-friction element is the zero-thickness element derived using a lumped interpolation function. The element may be represented schematically as shown in Fig. 6.2 Each gap-friction element represents a certain tributary area A of the interface to be modeled.

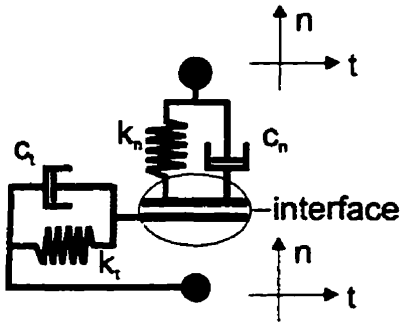

Fig. 6.2 *Gap-friction element*

The three-state constitutive model controls the transfer of forces at the interface. The spring stiffnesses, k_n and k_t, are acting as penalty numbers. The constraints to be enforced are (i) no interpenetration of the joint faces when the interface closes, and (ii) no sliding when the interface "locks" in shear. This type of interface element is the simplest element available. It is also readily available in several commercial finite element computer programs. The element could be oriented along interfaces with arbitrary orientations. In addition, local damping in the normal and tangent direction may be specified. The normal damper will enable dissipation of energy at impact thus acting like a coefficient of restitution. In certain situations, local dampers may stabilize the solution.

In summary, the interface element requires the following input parameters: k_n, k_t, the normal and tangent stiffnesses (N/m/m^2), c_n, c_t, the normal and tangent damper constants (N-s/m/m^2), f_t, tensile strength (N/m^2), τ_i, the initial cohesion (N/m^2), G_f^I, G_f^{II}, the mode I and mode II fracture energies (N/m), λ_d, the dynamic interface factor, χ_i the surface preparation factor, D_{max}, the maximum aggregate size.

The choice of the proper normal and tangent stiffnesses, as explained earlier, has a determinant effect on the answer obtained using these types of elements. The introduction of a plane of weakness or a discontinuity divides the structure in two independent components that interact at the common boundary thus at the discontinuity. The interface elements transmit the boundary conditions from one structure to another. The choice of the normal and tangent stiffnesses is problem dependent. The penalty numbers should be

large compared to the stiffness of the surrounding structure to guaranty that the constraints will be satisfied. However, they should not be too large to avoid ill-conditioning or loss of accuracy.

The criterion for selecting normal and tangent stiffnesses depends on the type of analysis. Under static analysis, the normal and tangent springs should not alter significantly the stress field in the structure compared to a monolithic structure. In addition, for dynamic analysis, the introduction of interface elements should not alter significantly the first few vibration frequencies and mode shapes. A good first trial for the spring stiffnesses per unit area, is to take the modulus of elasticity of the surrounding material multiplied by 10×1/unit of length.

6.3 Nonlinear static analysis

6.3.1 Formulation of the equilibrium equations

The static response of a structural mechanics system may be obtained by solving the first variation of the potential energy, which is written in total form as:

$$[K]\{u\} = \{f\} \tag{6.15}$$

where $\{u\}$ is the displacements vector, and $\{f\}$ is the vector of applied forces. Given the state of load at the interface, the behaviour may become nonlinear: crack opening or sliding. The constraint conditions, which are no interpenetration and stress locking, ought to be released. Several strategies may be adopted for simulating the release of the constraint conditions e.g.: (i) the secant method, (ii) the Newton-Raphson method (tangent method), or (iii) the modified Newton-Raphson method.

As illustrated in Fig. 6.3(a), in the secant method, the global stiffness is updated using the secant stiffness of the elements currently in the nonlinear behaviour. For an interface element, it means that the stiffness (penalty number) is modified to the value that matches actual state of deformation and current strength.

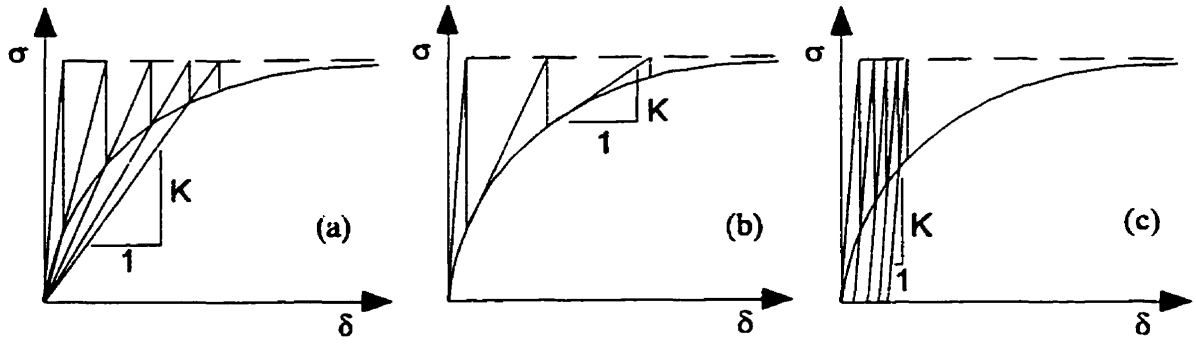

Fig. 6.3 *Stiffness formulation for resolution: (a) secant method, (b) Newton-Raphson, and (c) Modified Newton-Raphson.*

The Newton-Raphson method, also known as the tangent method shown in Fig. 6.3(b), consists of updating the global stiffness matrix using the tangent stiffness of the elements currently in the nonlinear range. For an interface in tension, gap-friction normal stiffness may become negative since the material softens. According to the system being analysed, this may lead to negative values on the diagonal of the global stiffness matrix. For interface sliding using an elastic-perfectly plastic constitutive model, the shear stiffness would be changed to zero thus leading to zero values on the diagonal of the global stiffness matrix henceforth leading to an indeterminate system of equations to be solved. In the modified Newton-Raphson method (Fig. 6.3(c)), the stiffness matrix is kept constant, a system of forces relevant to the elements in the nonlinear range, called unbalanced forces, is applied to the system in order to get the actual strength of the interface for the actual state of deformation. For interface elements it is equivalent to applying concentrated forces at the interface nodes that are equal to the portion of "unbalanced" force in the springs that should not be in the system.

The modified Newton-Raphson method was adopted in this study. Although it is considered as one of the slowest method for achieving convergence, in the context of nonlinear sliding analyses, it is a very stable method. This aspect will be discussed later on. Thus, the equations of equilibrium should be written as:

$$[K]\{u\} = \{f\} + \{\Delta f_{unb}\} \tag{6.16}$$

where $\{\Delta f_{unb}\}$ is the vector of unbalanced forces defined as:

$$\{\Delta f_{unb}\} = \{f\} - \{r\} \tag{6.17}$$

where $\{r\}$ is the vector of restoring forces.

6.3.2 Displacement control algorithm

Two different displacement control algorithms were implemented in the computer program INTRFACE that was developed in this project: (i) the arc length method (Crisfield, 1981) as linearised by Ramm (1987) and adopted by Ghrib and Tinawi (1994), (ii) the indirect displacement method proposed by de Borst (1987) and adopted by Bhattacharjee and Léger (1994).

The arc length method, as described by Ghrib and Tinawi (1994), requires the following elements: (i) the load vector, $\{f\}$, and (ii) the target increment ΔS, which is also called the arc length. The following system of equations is to be solved:

$$[K]\{\Delta u\} = -\left[\{r\} - \lambda\{f\}\right] = R(\{u\},\lambda) \tag{6.18}$$

where λ is the total load factor. For the first increment, the following equation has to be solved:

$$\{\Delta u\}_1 = \Delta\lambda_1 [K]^{-1}\{f\} = \Delta\lambda_1 \{\delta u\}_1 \tag{6.19}$$

thus the increment of the load factor, $\Delta\lambda_1$, is normalised to the target increment as:

$$\Delta\lambda_1 = \frac{\Delta S}{\left\|\{\delta u\}_1\right\|} \tag{6.20}$$

The following increments $\{\delta u\}_i$ are calculated as follows:

$$\begin{aligned} \{\delta u\}_i &= \{\delta u\}_i^R + \Delta\lambda_i \{\delta u\}_i^F \\ &= [K]_{i-1}^{-1}\{R\}_{i-1} + \Delta\lambda_i [K]_{i-1}^{-1}\{f\} \end{aligned} \tag{6.21}$$

The first term on the right hand side of Eq.(6.21), $\{\delta u\}_i^R$, may be considered as the displacement increment due to the load unbalance, while the second term, $\{\delta u\}_i^R$, may be

considered as the displacement increment due to the variation of the load factor which is obtained from:

$$\Delta\lambda_i = -\frac{\{\Delta u\}_1 \{\delta u\}_i^R}{\{\Delta u\}_1 \{\delta u\}_i^F} \tag{6.22}$$

The total displacement, and the total load factor, are calculated as:

$$\begin{aligned} \{u\}_i &= \{u\}_{i-1} + \{\delta u\}_i^R + \Delta\lambda_i \{\delta u\}_i^F \\ \lambda_i &= \lambda_{i-1} + \Delta\lambda_i \end{aligned} \tag{6.23}$$

The arc length method, as described above, is a search for equilibrium after having imposed a certain displacement increment that triggered nonlinearities. The displacement increments that occur after this first "impulse" depend on the unbalanced loads released by all the elements entering or evolving in the nonlinear range. As a matter of fact, the computed response obtained from a method like the arc method is strongly dependent on the initial impulse (i.e. arc length)

The indirect displacement control method proposed by deBorst (1987) is somehow different. There, the target displacement is enforced. Thus, if nonlinearities occur, the total load factor will be decreased to keep the control displacement on the target value. As described by Bhattacharjee and Léger (1994), the method requires the same elements as the arc length method:

$$\begin{aligned} S_i &= S_{i-1} + \Delta S_i \\ \{\Delta f\}_i &= \frac{\Delta S_i}{S_i} \{f\}_{i-1} \\ \{f\}_i &= \{f\}_{i-1} + \{\Delta f\}_i \end{aligned} \tag{6.24}$$

where S_i is the total target displacement, $\{f\}$ is the total load vector, and $\{\Delta f\}$ is the load vector increment. The computed response $\bar{\lambda}_i$ is defined explicitly as:

$$\bar{\lambda}_i^t = u(dof_m) - u(dof_n) \tag{6.25}$$

If the computed response is not within a certain tolerance of the target response, the total load factor is scaled to obtain the target displacement:

$$\{f\}_i^k = \frac{S_i}{\lambda_i^k}\{f\}_i^{k-1} \tag{6.26}$$

When the structure becomes nonlinear behaviour, iterations may be required to reduce the unbalanced forces computed from Eq.(6.17).

6.4 Nonlinear time domain dynamic analysis

6.4.1 Numerical integration of the dynamic equilibrium equations

The dynamic equilibrium equations for a structure subjected to a seismic excitation may be written as:

$$[M]\{\ddot{u}\} + [C]\{\dot{u}\} + \{r\} = -[M]\{\ddot{u}_g\} + \{p\} = \{f\} \tag{6.27}$$

where $[M]$ is the mass matrix, $[C]$ is the damping matrix, $\{r\}$ is the vector of restoring forces, $\{\ddot{u}_g\}$ is the vector of ground accelerations, and $\{p\}$ is the external forces vector.

Time integration methods are required for solving step by step dynamic problems, since first and second displacement derivatives appear in Eq.(6.27). If these derivatives are computed from the displacements, velocities and accelerations of the previous time step, then the time integration method is explicit. Stability is conditional i.e. it is dependent on the time step. The method becomes implicit when the derivatives are part of the equation to be solved. Stability is unconditional, thus not subjected to time step dependency. Many methods have been proposed in the literature: Newmark-β, Wilson-θ, α method, etc.

The α method has been adopted by Bhattacharjee and Léger (1994) and also by Ghrib and Tinawi (1994) for the analysis of crack propagation in concrete dams subjected to seismic excitations. The α method includes Newmark-β and Wilson-θ methods as

special cases thus a single computer program will include three integration methods. Ghrib and Tinawi (1994) observed that dynamic response of concrete dams is dictated by the first modes of vibration. Higher modes occur in the vicinity of the crack faces. These modes are considered to be spurious and ought to be filtered out of the solution by numerical damping. In the α method, numerical damping is controlled by the α parameter. The dynamic equilibrium equation may be written as::

$$\begin{aligned}&[M]\{\ddot{u}\}_i + (1+\alpha)[C]\{\dot{u}\}_i - \alpha[C]\{\dot{u}\}_{i-1} \\ &+(1+\alpha)[K]_i\{u\}_i - \alpha[K]_{i-1}\{u\}_{i-1} = (1+\alpha)\{f_{dy}\}_i - \alpha\{f_{dy}\}_{i-1}\end{aligned} \tag{6.28}$$

The velocities and accelerations are computed according to the Newmark-β method:

$$\begin{aligned}u_i &= \left[u_{i-1} + \Delta t\,\dot{u}_{i-1} + \frac{\Delta t^2}{2}(1-2\beta)\ddot{u}_{i-1}\right] + \Delta t^2\beta\,\ddot{u}_i = \tilde{u}_i + \Delta t^2\beta\,\ddot{u}_i \\ \dot{u}_i &= \left[\dot{u}_{i-1} + (1-\gamma)\Delta t\,\ddot{u}_{i-1}\right] + \Delta t\,\gamma\,\ddot{u}_i = \tilde{v}_i + \Delta t\,\gamma\,\ddot{u}_i\end{aligned} \tag{6.29}$$

where $\tilde{u}_i$ and $\tilde{v}_i$ are the displacements and velocities predictions for time step i computed from the data of the previous time step. Equation (6.29) may be rearranged to express the acceleration and velocities as functions of the displacements:

$$\begin{aligned}\dot{u}_i &= \tilde{v}_i + \frac{\gamma}{\Delta t\,\beta}\left[u_i - \tilde{u}_i\right] \\ \ddot{u}_i &= \frac{1}{\Delta t^2\beta}\left[u_i - \tilde{u}_i\right]\end{aligned} \tag{6.30}$$

The above equations enable to write the dynamic equilibrium as an expression of the displacements (u_i) and the data of the previous time step. Parameters γ and β are functions of the α parameter as:

$$\beta = \tfrac{1}{4}(1-\alpha)^2 \;,\; \gamma = \tfrac{1}{2} - \alpha \;;\; \alpha \in \left[-\tfrac{1}{3}, 0\right] \tag{6.31}$$

Using α=0, the α method reduces to the Newmark-β method.

6.4.2 Damping of interfaces

The classical Rayleigh damping model is adopted. The damping matrix is the sum of a mass proportional and stiffness proportional terms:

$$[C] = a_0[M] + a_1[K] \tag{6.33}$$

where a_0 and a_1 are proportionality factors. Damping plays an important role in the response of a structure, therefore great care should be given to choosing the proportionality factors. In the case of interfaces, damping modelling is even more important since nonlinearities may involve global rigid body type of movements (e.g. sliding, opening). The question is which damping forces should be considered.

The mass proportional term of the damping matrix is equivalent to damping applied to the absolute motion of the mass at a given node. From a practical point of view, that type of damping is equivalent to attach a dashpot from a node to its original position (t=0 position). As a result, interface sliding ought to be overdamped. From a theoretical point of view, mass damping is inversely proportional to the frequency of vibration. Since rigid body motion (sliding) is an extremely low frequency mode f=0$^+$ Hz, sliding will be overdamped. Consequently, in sliding analysis of concrete dams, it is recommended not to use mass proportional damping i.e. a_0=0.

The stiffness proportional term of the damping matrix is equivalent to damping applied to the relative motion of a node to another node. So that type of damping does not counteract rigid body motion (sliding) since these damping forces are in internal equilibrium. However, since the stiffness terms are used to generate the damping matrix, the penalty terms will end up in the damping matrix. That is equivalent to having enormous dashpots connecting each side of the interface. Therefore, the stiffness matrix to be used in Eq.(6.33) should be the elastic stiffness matrix without the penalty terms.

As described in Subsection 6.2.2, local damping in the normal and tangent directions may be specified. The normal damper will enable dissipation of energy at impact thus acting like a coefficient of restitution. The damper is disconnected when the element is in

tension. Numerical simulations on impact problems indicated a better numerical stability when the damper is activated one time step after impact has been detected. The closing of an element results in a numerical shock due to large contact forces. Activating the damper at the same time that the gap stiffness is activated increases the shock on the solution. The superposition of the two effects often results in numerical oscillation.

6.4.3 Energy balance

The energy balance is computed from the integration of the dynamic equilibrium equation (Eq.(6.27)) rearranged as (Uang and Bertero, 1990):

$$[M]\{\ddot{u}_t\} + [C]\{\dot{u}\} + \{r\} = \{p\} \tag{6.34}$$

where $\{\ddot{u}_t\}$ correspond to the total acceleration vector. Integrating the above equation with respect to the relative displacement leads to:

$$\int \{\ddot{u}_t\}^T [M]\{du\} + \int \{\dot{u}\}^T [C]\{du\} + \int \{r\}^T \{du\} = \int \{p\}^T \{du\} \tag{6.35}$$

By substituting the relative displacement term $\{du\}$ by its definition $\{du_t - du_g\}$, the first term on the left hand side of Eq.(6.35) may be rearranged as:

$$\int \{\ddot{u}_t\}^T [M]\{du\} = \int \{\ddot{u}_t\}^T [M]\{du_t\} - \int \{\ddot{u}_t\}^T [M]\{du_g\} \tag{6.36}$$

Substituting the above equation into the expression of the energy balance, Eq.(6.35) results in:

$$\overbrace{\int \{\ddot{u}_t\}^T [M]\{du_t\}}^{E^K} + \overbrace{\int \{\dot{u}\}^T [C]\{du\}}^{E_I^D} + \overbrace{\int \{r\}^T \{du\}}^{E^R} = \underbrace{\int \{p\}^T \{du\}}_{E^P} + \underbrace{\int \{\ddot{u}_t\}^T [M]\{du_g\}}_{E^Q} \tag{6.37}$$

Applying the trapezoidal integration rule to calculate the energy balance at every time step will lead to the following definitions:

The kinetic energy:

$$E_i^K = \frac{1}{2}\{\dot{u}_t\}_i^T [M]\{\dot{u}_t\}_i \tag{6.38}$$

The damping energy:

$$E_i^D = E_{i-1}^D + \frac{1}{2}\left\{\{\dot{u}_t\}_i^T [C]_i + \{\dot{u}_t\}_{i-1}^T [C]_{i-1}\right\}\{u_i - u_{i-1}\} \tag{6.39}$$

The restoring forces energy:

$$E_i^R = E_{i-1}^R + \frac{1}{2}\{r_i + r_{i-1}\}^T \{u_i - u_{i-1}\} \tag{6.40}$$

The work done by the static forces:

$$E_i^P = E_{i-1}^P + \frac{1}{2}\{p\}^T \{u_i - u_{i-1}\} \tag{6.41}$$

The seismic input energy:

$$E_i^Q = E_{i-1}^Q + \frac{1}{2}\{\ddot{u}_{t,i} - \ddot{u}_{t,i-1}\}^T [M]\{u_{g,i} - u_{g,i-1}\} \tag{6.42}$$

Based on the energy balance, an error indicator, the energy error index, *EEI* may be calculated as:

$$EEI_i = \frac{\left(E_i^Q + E_i^P\right) - \left(E_i^K + E_i^D + E_i^R\right)}{\left(E_i^Q + E_i^P\right)} \times 100\% \tag{6.43}$$

The above notation is equivalent to that adopted by Bhattacharjee and Léger (1994). It should be noticed that the energy balance definition is independent of the integration scheme e.g. Newmark-β, Wilson-θ, or α method.

The acceleration at the end of a time step is calculated from the equilibrium equations. Thus part of the error of the iterative process is corrected in the acceleration. As a result, the energy error indicator might not be taken as the only numerical convergence criterion. However, if any errors occurred, they will be amplified in the energy error index.

6.5 Validation

Several validation problems have been analysed to assure that the constitutive models have been implemented correctly in the computer program INTRFACE. Validation problems also enable to determine the limits of application of the numerical methods that were adopted e.g. the constitutive model, the gap-friction interface element, and the control algorithms.

6.5.1 Simple element in tension

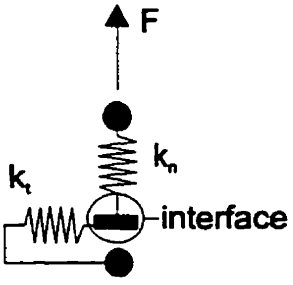

Fig. 6.4 *Gap element in tension.*

The first validation problem is a simple element subjected to tension, as illustrated in Fig. 6.4. This problem controls the adequacy to the fracture energy tensile constitutive model. A single element of unit tributary area ($1m^2$) is subjected to an increasing tensile load. The material parameters are f'_t=2.0MPa, E_c=25000MPa, ν=0.18, and G^I_f=1000.N/m. The gap-friction element parameters used in the analysis are given in Table 6.1.

The resulting stress displacement curve is shown in Fig. 6.5 The peak stress, the displacement at full consumption of fracture energy, and the dissipated fracture energy are in agreement with the constitutive model as described in Chapter 5. The fracture energy is usually considered as being the area enclosed under the softening branch of the response. However, inhere the complete curve, thus the rising branch and the softening branch, enclose the fracture energy.

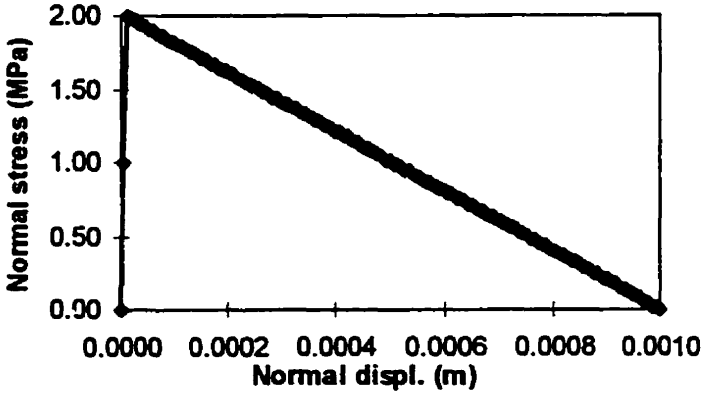

Fig. 6.5 *Axial response of gap element.*

Table 6.1 *Gap-friction element parameters for simple element in tension*

k_n N/m/m^2	k_t N/m/m^2	c_n N-s/m^2	c_t N-s/m^2	f_t N/m^2	τ_i N/m^2	G^I_f N/m	G^{II}_f N/m	μ -	λ_d -	χ_i -
2.0E5	2.0E6	0.0	0.0	2.0E6	50.	1000.	0.	0.5	-	-

Since the crack response is controlled by a penalty parameter, the rising branch does not physically correspond to the elastic response but rather a discrepancy in the condition of no crack opening until crack initiation.

6.5.2 Three-point bending test

The three-point bending test is a typical test in fracture mechanics. A plain concrete beam tested by Bazant and Pfeiffer (1987) was chosen as validation problem (Fig. 6.6(a)). The failure load was reached at 7785 N. The measured material properties were the concrete compressive strength f'_c=33.5 MPa. Bazant and Pfeiffer suggested the following material properties: f'_t=2.886MPa, E_c=27413MPa, ν=0.18, and G^I_f=40.29N/m. The finite element mesh, plane stress elements and gap-elements, used for predicting the response of the beam is shown in Fig. 6.6(b). At the location of the observed experimental crack, an interface was introduced using gap-friction elements. The gap-friction properties are given in Table 6.2.

Table 6.2 *Gap-friction element parameters for three-point beam test.*

k_n N/m/m^2	k_t N/m/m^2	c_n N-s/m^2	c_t N-s/m^2	f_t N/m^2	τ_i N/m^2	G^I_f N/m	G^{II}_f N/m	μ -	λ_d -	χ_i -	D_m
2.7413E14	2.7413E14	0.0	0.0	2.886E6	3.E11	40.29	.	1.E4	-	-	

The two displacement control methods described in Subsection 6.3.2 were used to analyse the beam. The control parameters i.e. target increment, D, and tolerance on unbalanced loads, TL, were varied to converge on the experimentally measured failure load. The normal stiffness, k_n, if taken too soft, leads to rigid body rotation about the center of the assumed crack location and induces overstress of the gap elements in tension resulting in premature failure. The gap elements shear stiffnesses have no effect on the response.

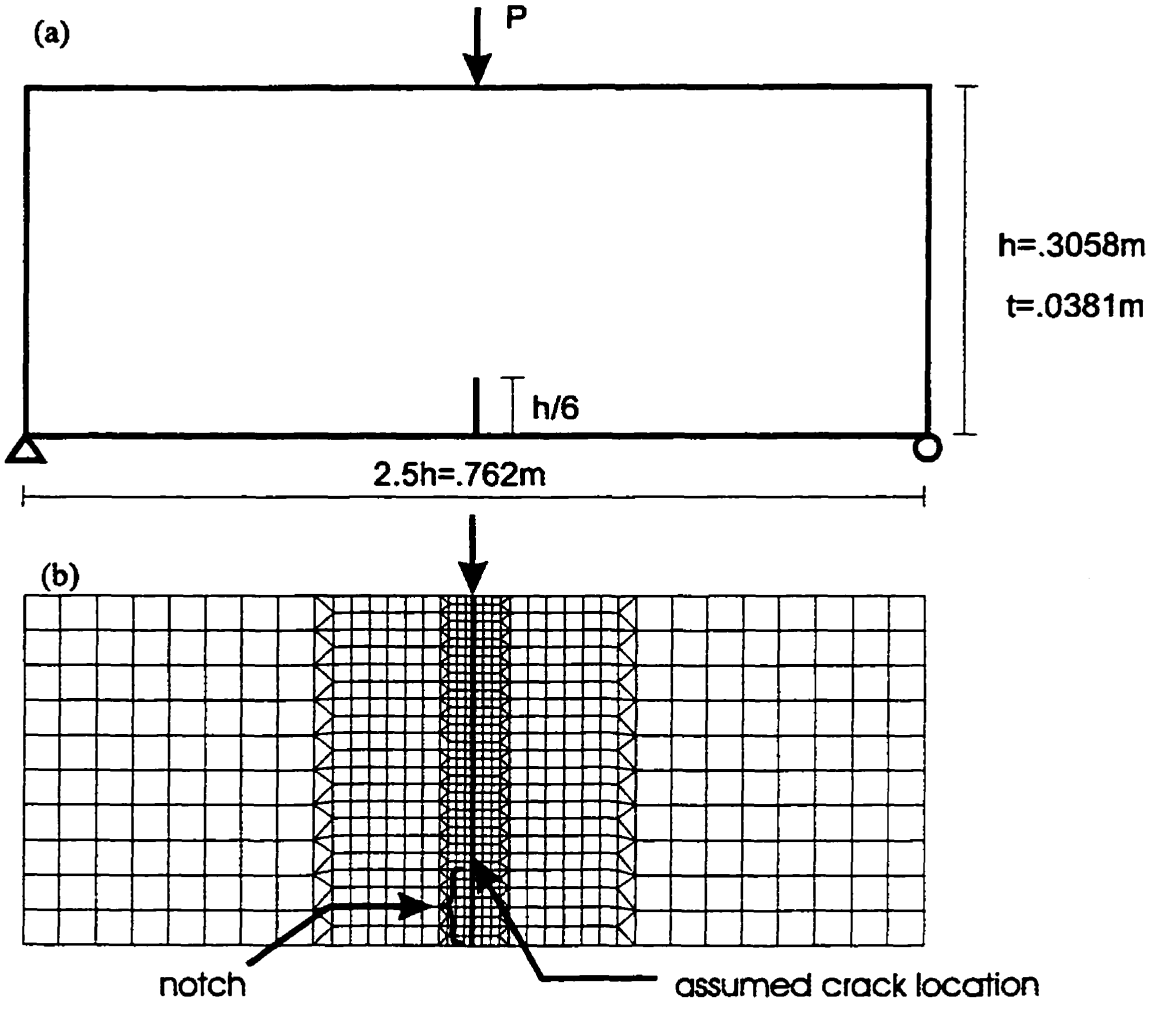

Fig. 6.6 *Three-point beam test and finite element mesh.*

In Fig. 6.7, the computed responses are shown. The arc length method (A.L.) converges from above, while the indirect displacement method of de Borst (dB) converges from below. A striking feature of the load - displacement response is the difference in the computed results between the two control methods. The arc length method converges towards the experimental value (7630 N for $D=1\times10^{-6}$ and $TL=1\times10^{-5}$) while the deBorst method converges to 6550N. This is in agreement with the results obtained by Ghrib and Tinawi (1994) and Bhattacharjee (1993). Thus it appears that deBorst method, in this case underestimates the failure load by 15%.

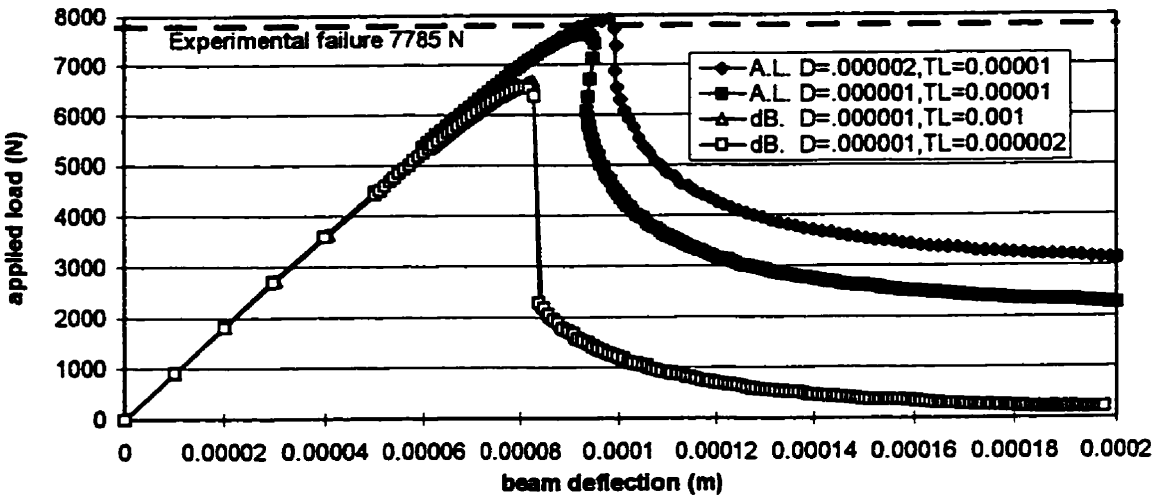

Fig. 6.7 *Computed response of three-point bending test specimen.*

The displacement control analysis on problems with softening of the response involves a numerical iterative procedure for computing the response but also iterations in the choice of the control parameters that will lead the numerical iterative procedure to a solution. For instance, the displacement target increment D mobilizes an applied load that triggers load unbalance which has to be released to reach a new equilibrium point. The amount of load unbalance will dictate the next equilibrium position. The tolerance TL is a measured of the load unbalance that will stay in the solution. In other words, the computed equilibrium position always involves some load unbalance in the gap elements, stringent conditions on the unbalance will always act towards a decrease of the computed applied load.

Hence the choice of the control parameters depends on the material properties, and the nature failure mechanism: ductile i.e. with possibilities of load redistribution or rather very brittle i.e. with very little load redistribution. As a first step, one should perform a load control analysis to get a rough estimate of the failure load and failure deformation. Then, displacement control analyses with a target displacement of about $1/1000^{th}$ of the failure displacement may be undertaken.

6.5.3 Shear beam

A plain concrete notched beam tested by Arrea and Ingraffea (1981) was chosen as validation problem (see Fig. 6.8(a)). The support and loading condition lead to a curved crack profile typical of shear failures. The following material properties were used in the analyses: f_t=2.8MPa, E_c=24800MPa, v=0.18, and G^I_f=100N/m. The gap-friction element parameters are given in Table 6.3.

Table 6.3 *Gap-friction element parameters for shear beam.*

k_n N/m/m^2	k_t N/m/m^2	c_n N-s/m^2	c_t N-s/m^2	f_t N/m^2	τ_i N/m^2	G^I_f N/m	G^{II}_f N/m	μ -	λ_d -	χ_i -	D_m
1.E12	1.E12	0.0	0.0	2.8E6	5.6.E6	100.	-	2.0	-	-	

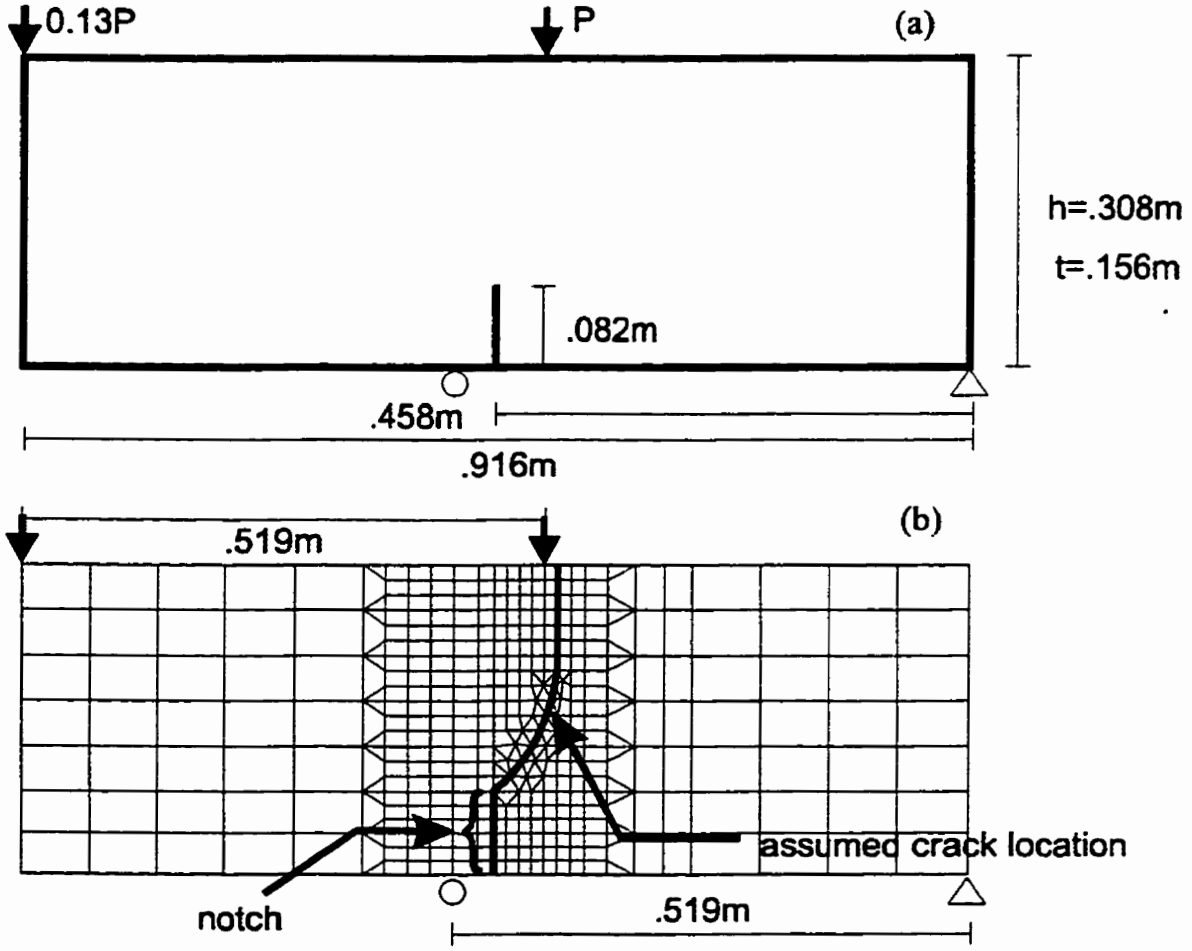

Fig. 6.8 *Single notched shear beam tested by Arrea and Ingraffea (1981).*

The finite element mesh used for predicting the response of the beam is shown in Fig.6.8(b). At the approximate location of the observed curved experimental crack, an interface was introduced using gap-friction elements. Even though the crack indicates a shear failure, mode I failure dominates at the crack. The analysis reached a failure load of 140 kN which is above the measured failure load of 120 kN. This over estimation is related first to the crack profile which is an approximation of the experimental one, and to the material parameters that have not been optimized to reach the measured load.

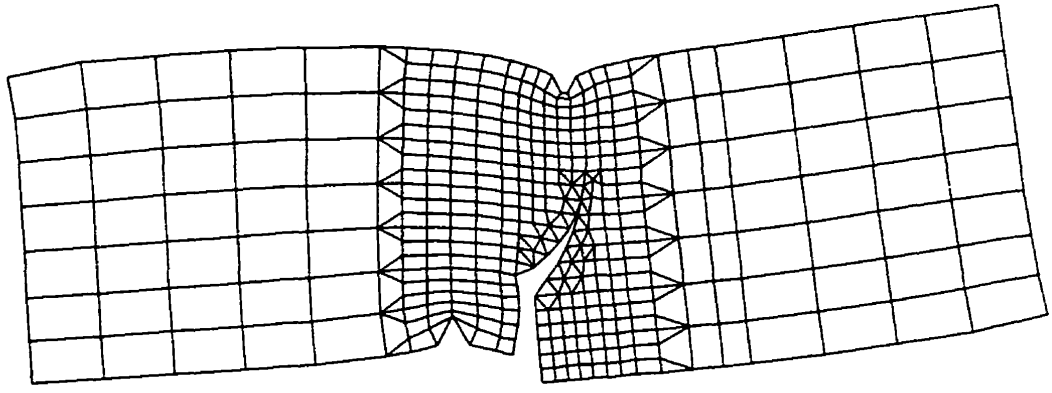

Fig. 6.9 *Deformed shape of the notched shear beam at failure.*

Figure 6.9 illustrates the deformed shaped at failure. It is clear on the picture that the behaviour is mainly mode I along the crack. The distorsions at the supports and at the applied load location indicate how brittle the failure may be since it involves very little displacements

6.5.4 Bazant and Pfeiffer beam

Doubly notched beams were tested by Bazant and Pfeiffer (1986) as illustrated in Fig. 6.10(a). These beams failed in shear with a straight crack running from notch to notch.

Table 6.4 *Gap-friction element parameters for double notched shear beam.*

k_n N/m/m^2	k_t N/m/m^2	c_n N-s/m^2	c_t N-s/m^2	f_t N/m^2	τ_i N/m^2	G^I_f N/m	G^{II}_f N/m	μ -	λ_d -	χ_i -	D_m
1.7125E12	7.136E11	0.0	0.0	3.0E6	6.0E6	43.6	1050	1.0	-	-	

The material parameters measured for these beams were as follows: f'_t=3MPa, E_c=29000MPa, ν=0.2, and G_f=43.6N/m.

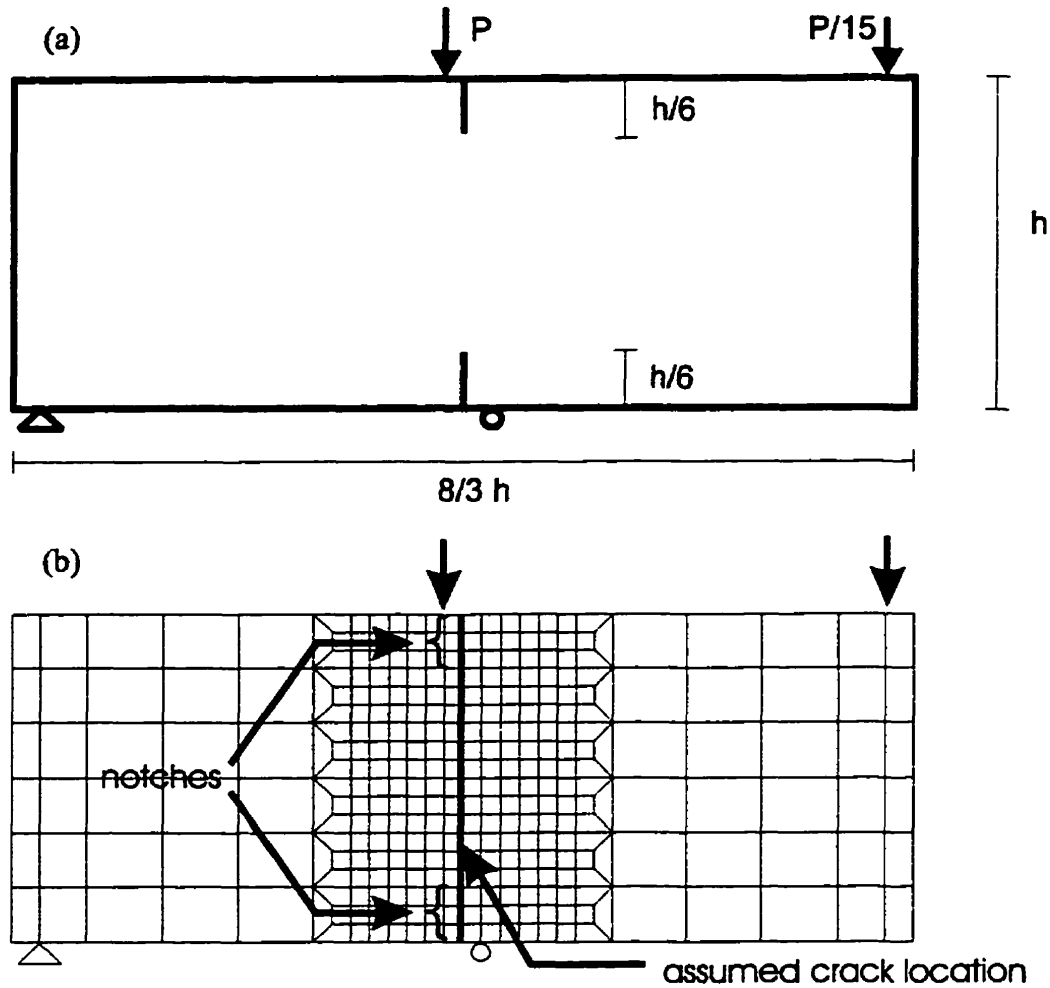

Fig. 6.10 *Double notched shear beam tested by Bazant and Pfeiffer (1986).*

The finite element mesh is shown in Fig. 6.10(b). Gap-friction elements were inserted along the assumed crack location. The gap-friction elements parameters are given in Table 6.4. The experimental failure load for the beam with h=0.3048m and t=0.0381m was 44.5 kN. An elasto-brittle constitutive model in shear never reaches the experimental failure load. There are high concentrations of shear stresses at the crack tips. Once the first element fails, the stress concentration is transferred from element to element as each element fails in shear. As a result, the computed response is controlled by the crack initiation criterion on the crack tip element.

This phenomenon motivated the development of the fracture energy dissipative models in mode II. Bazant and Pfeiffer (1986) introduced the concept of mode II fracture energy, G_f^{II}, in order to capture the failure load. They estimated from numerical studies, the shear fracture energy to be about 25 times the mode I fracture energy. For the beam shown in Fig. 6.10, they suggested the G_f^{II} fracture energy to be 1050 N/m.

A mode II fracture energy model was implemented in the computer program INTRFACE in analogy with the mode I fracture energy model. Using a cohesion equal to 6MPa and G_f^{II}=1050N/m, a failure load of 40.1 kN was attained.

6.5.5 Coulomb friction for dynamic loading

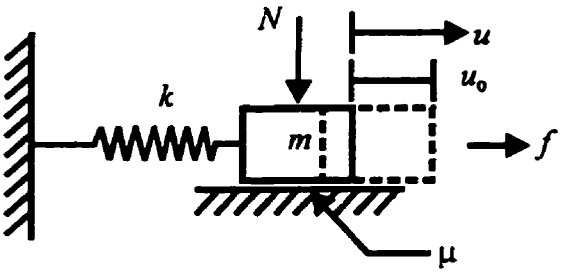

Fig. 6.11 *Coulomb friction problem.*

The Coulomb friction validation problem is to test the implementation of the time integration method, and it also provides a verification of the energy consumption by friction. The test, as illustrated in Fig. 6.11, consists of a prism subjected to a vertical load, N, on the top surface. The prism is attached to a horizontal spring. A horizontal force, f, is applied to move the prism against the spring a certain distance. Then the force is released and the system is left in free vibrations. A friction force equal to the product of the vertical load, N, and fixed coefficient of friction, μ, is developed. After a few cycles the system will come to rest; the energy stored in the spring being dissipated in friction.

Inhere, the problem parameters are as follows: the normal load, N, is equal to 6×10^6N, the mass, m, is equal to 1×10^6 kg, the spring stiffness, k, is equal to 1×10^8 N/m, the coefficient of friction, μ, is set to 0.6, and u_0 is equal to 1.17426 m. The properties assigned to the gap friction element in the analysis are given in Table 6.5.

Table 6.5 *Gap-friction element parameters for Coulomb friction problem.*

k_n N/m/m^2	k_t N/m/m^2	c_n N-s/m^2	c_t N-s/m^2	f_t N/m^2	τ_i N/m^2	G_f^I N/m	G_f^{II} N/m	μ -	λ_d -	χ_i -	D_m
1E8	1E10	0.0	0.0	0.0	0.0	0.0	0.0	0.6	-	-	

There is a theoretical solution to describe the free-vibration motion of the mass in the Coulomb friction problem (Greenwood, 1988). It may be written as follows for the n^{th} half cycle:

$$n^{th}\ \text{½ cycle} \Rightarrow \quad u = (-1)^{n-1}\frac{\mu N}{k} + \left(u_0 - (2n-1)\frac{\mu N}{k}\right)\cos\omega_n t \qquad (6.44)$$

where u is the displacement, u_0 is the initial displacement, μ is the coefficient of friction, N is the applied normal load, k is the spring constant, ω_n is the natural frequency of the spring mass system, and t is the time. The oscillation amplitude decreases by $2\frac{\mu N}{k}$ per half cycle. The comparison between the theoretical solution and the numerical prediction is given in Fig. 6.12. The numerical prediction is in total agreement with the theoretical solution.

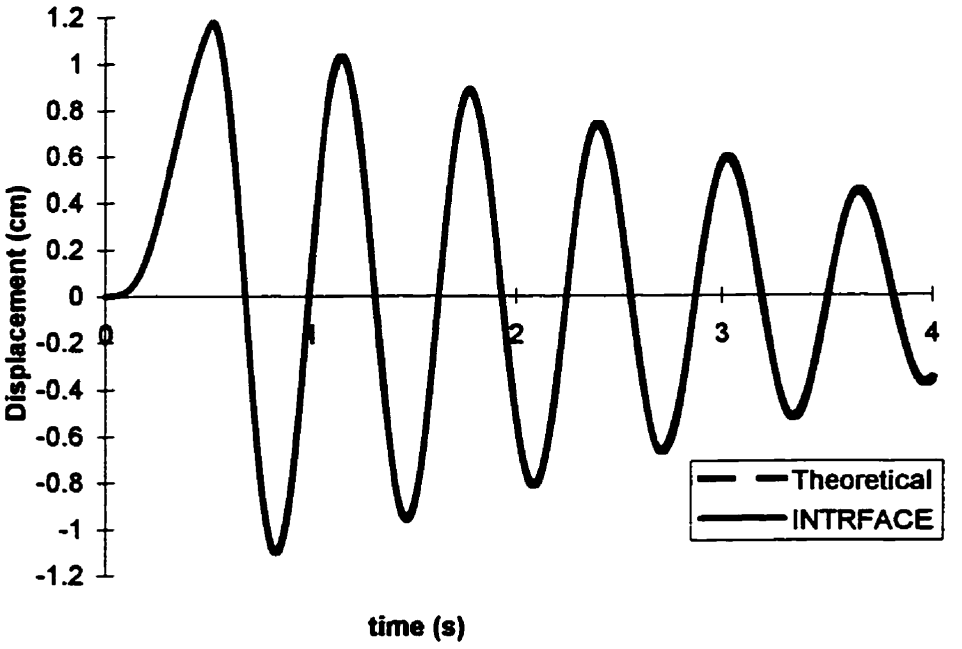

Fig. 6.12 *Coulomb friction theoretical solution vs numerical prediction.*

6.5.6 Coulomb friction on constitutive model

The Coulomb friction problem presented in Subsection 6.5.5 has been computed using the proposed sliding friction constitutive model described in Chapter 5. The four

types of surface preparation tested in this project have been analysed. The sliding friction constitutive parameters are given in Table 6.6.

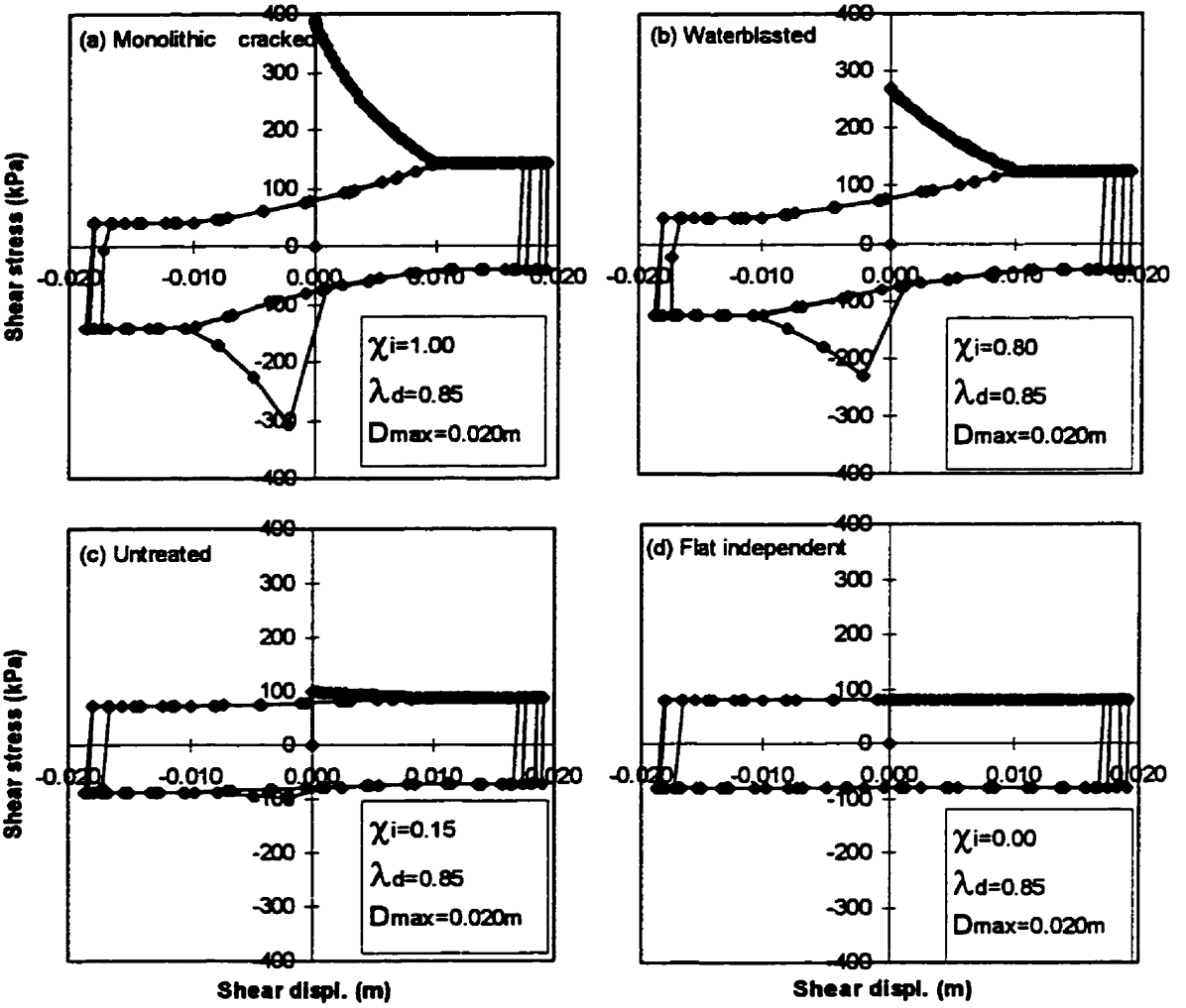

Fig. 6.13 *Coulomb friction problem using the proposed constitutive model.*

Figure 6.13 illustrates the computed shear stress versus shear displacement response of the joint interfaces: monolithic cracked in Fig. 6.13(a), waterblasted in Fig. 6.13(b), untreated in Fig. 6.13(c), and the flat independent surfaces in Fig. 6.13(d).

Table 6.6 *Gap-friction element parameters for Coulomb friction on constitutive model.*

Fig 6.12	k_n N/m/m^2	k_t N/m/m^2	c_n N-s/m^2	c_t N-s/m^2	f_t N/m^2	τ_i N/m^2	G^I_f N/m	G^{II}_f N/m	μ -	λ_d -	χ_i -	D_m
(a)	1E10	1E13	0.0	0.0	0.0	0.0	0.0	0.0	-	0.85	1.00	0.02
(b)	1E10	1E13	0.0	0.0	0.0	0.0	0.0	0.0	-	0.85	0.80	0.02
(c)	1E10	1E13	0.0	0.0	0.0	0.0	0.0	0.0	-	0.85	0.15	0.02
(d)	1E10	1E13	0.0	0.0	0.0	0.0	0.0	0.0	-	0.85	0.00	0.02

The load-displacement responses shown in Fig. 6.13 are typical of the joint behaviour considered in the analyses of concrete dams in Chapter 7.

6.6 Summary and conclusions

This chapter presented the implementation of the nonlinear three-state interface constitutive model in the context of a gap-friction finite element. The solution strategies for the static and dynamic equations of motions were described. Validation problems indicated that these methods enable the prediction of experimentally measured or theoretical responses.

Interestingly, on the three-point bending tests, it was observed that the arc length method converges from above, (Crisfield, 1981), while deBorst (1987) method converges from below. Furthermore the experimentally measured failure load was never attained using deBorst method. The single notched shear beam is similar to the three-point bending since the failure is mainly due to mode I. That problem indicated that a curved layer of gap elements may be used to predict cracking response. The double notched shear beam indicated that a mode II fracture energy model is required in problems where there is crack initiation and propagation in shear, to avoid the "peeling effect".

Finally, the Coulomb friction test shows that the classical friction energy dissipation mechanism due to force displacement is well captured by the constitutive model. Furthermore, it validates key computational aspects.

CHAPTER 7

Seismic response of jointed concrete gravity dams

7.1 Introduction

The constitutive model of Chapter 5 was formulated in the context of a nonlinear gap-friction joint element that was implemented into the finite element program INTRFACE as described in Chapter 6. A typical gravity dam section with lift joints was then analysed. Parametric smeared crack transient seismic analyses on homogeneous concrete dams without lift joints have indicated that the failure mechanism is related to the emergence of two distinct cracks, one at the base of the dam and the other in the upper part of the dam (Léger and Leclerc, 1996). The dam was therefore subjected to seismic loads for two possible situations: Dam I) a single contact joint at the foundation, and Dam II) a foundation contact joint and a lift joint close to the crest.

As a first step, the pseudo-static and pseudo-dynamic analyses were undertaken based on the parameters given in the CDSA guidelines (1995). Then, nonlinear transient dynamic analyses were performed. Comparisons between the standard analyses and the nonlinear finite element analyses (NLFEA) are given. To conclude the chapter, a typical 90m dam profile with 8 lift joints spaced along the height was analysed.

The philosophy behind the CDSA guidelines under a maximum credible earthquake, MCE, is to accept limited damage to the dam as long as there is no loss of the reservoir. However, the sliding safety factors are such that, indeed, no sliding damage is accepted. Hence, an effort is made to establish a rational criterion for sliding that allows some damage to occur.

7.2 System analysed

7.2.1 Description

The system analysed is the typical section of a concrete gravity dam, 90 m in height assuming a rigid foundation condition as shown in Fig.7.1. The following concrete properties are assumed in the sliding response analyses: elastic modulus E=27690MPa, Poisson's ratio v=0.2, mass density=2400 kg/m^3, static tensile strength=2.0 MPa, and dynamic magnification factor tensile strength=1.2 resulting in a dynamic tensile strength=2.4 MPa. In addition to self-weight and hydrostatic pressure, Westergaard added masses are used to represent hydrodynamic interaction forces in seismic analyses. Pore pressures in the dam are assumed to be zero (impervious concrete). Two uplift water pressure conditions were considered for lift joint and dam-foundation interface. A series of analyses without any uplift, and a series of analyses with an initial triangular uplift pressure distribution at the dam-foundation interface and at the lift joint were performed. This initial uplift pressure distribution is assumed to remain constant during the earthquake.

The natural vibration period, T_1, of the 90m dam model with the added mass of the reservoir is 0.27sec. Stiffness proportional viscous damping model, with a value of 5% in the fundamental mode of the dam has been considered to define the damping properties. A time step of 0.001sec and the modified Newton-Raphson method are used to integrate the equations of dynamic equilibrium.

The foundation contact joint and the lift joint have been assigned the same strength properties i.e. no tensile strength, no cohesion and hysteretic model determined from the constitutive model presented in Chapter 5. Two joint surface conditions are assumed: i) water blasted joint surfaces and ii) untreated joint surfaces.

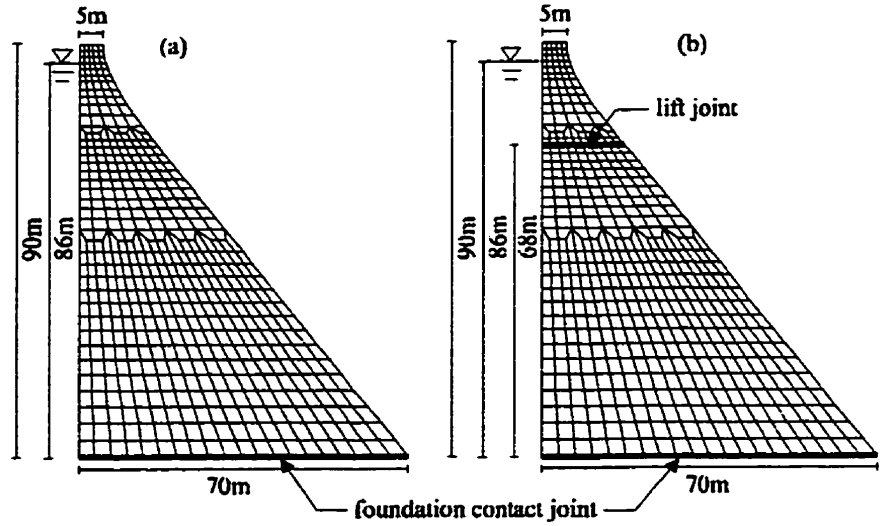

Fig. 7.1 *Dam models: a) contact joint, b) contact and lift joint.*

The reservoir elevation is 86 m. The earthquake input motions were derived from the Saguenay 1988 event to obtain spectrum compatibility with a target design spectra data derived from the Atkinson and Boore (1990) attenuation functions for a Eastern North American magnitude 7 earthquake at 20 km from the site. The peak ground acceleration is 0.36g (see Fig. 7.2).

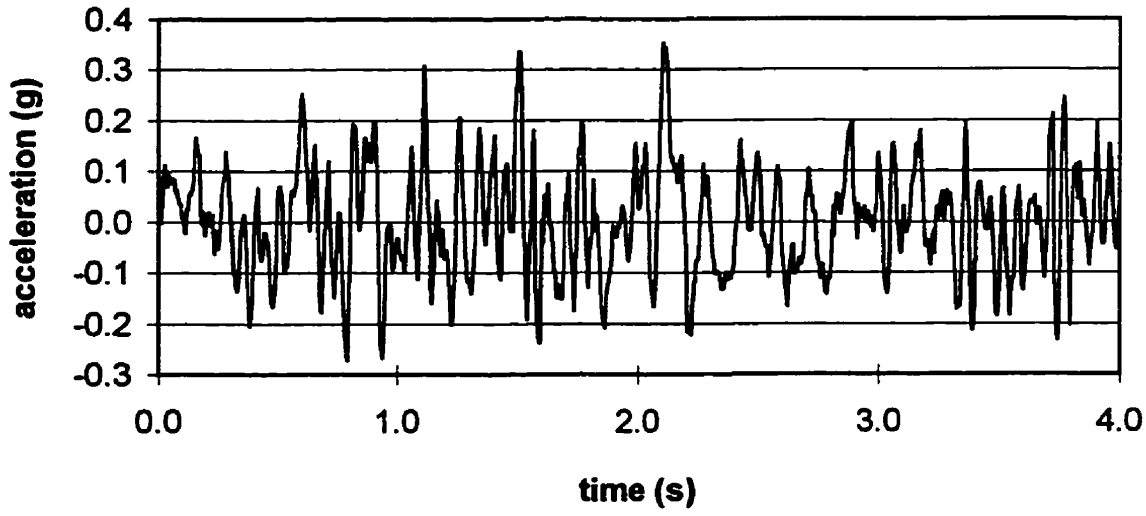

Fig.7.2 *Earthquake record used in the analyses.*

The Saguenay earthquake is quite long therefore to reduce the computing time, the record was truncated to 4 seconds of strong motion. However, this does not affect the conclusions of the study since 90% of the total input energy occurred within these 4 seconds, furthermore the frequency content is the same as the total record. The spectrum of the input accelerogram along with the target design spectrum are illustrated in Fig.7.3.

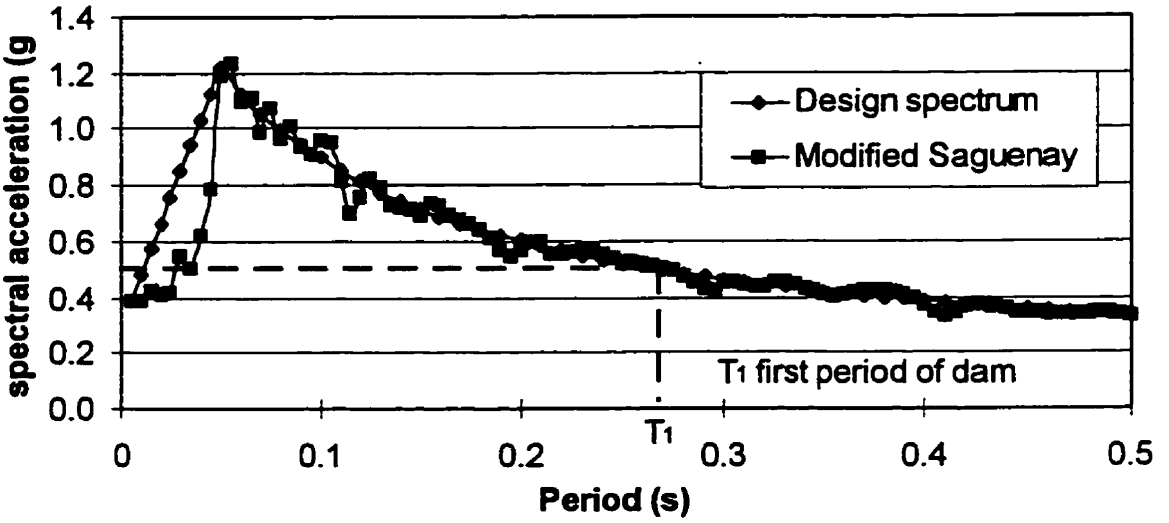

Fig.7.3 *Earthquake spectrum and design spectrum.*

7.2.2 Gap-friction element properties

The gap-friction element response follows the constitutive model described in Chapter 5. Two joint preparation conditions were considered: (a) waterblasted joint surface, and (b) untreated joint surface. The gap-friction element properties are given in Table 7.1. No local damping was considered. The solutions were numerically stable.

Table 7.1 *Gap-friction element parameters for NLFEA.*

	k_n N/m/m^2	k_t N/m/m^2	c_n N-s/m^2	c_t N-s/m^2	f_t N/m^2	τ_i N/m^2	G^I_f N/m	G^{II}_f N/m	μ -	λ_d -	χ_i -	D_m
(a)	2.769E11	2.769E11	0.0	0.0	0.0	0.0	0.0	0.0	-	0.85	0.80	0.02
(b)	2.769E11	2.769E11	0.0	0.0	0.0	0.0	0.0	0.0	-	0.85	0.15	0.02

7.3 Pseudo-static and pseudo-dynamic seismic analyses

CDSA (1995) suggests a first step to verify the seismic stability by using a pseudo-static approach. The design acceleration is selected from a maximum design earthquake. As a second step, according to the type of dam and site conditions, dynamic analyses should be undertaken. These are usually carried out for specialized dam: pseudo-dynamic analysis method (Chopra, 1988), or classical response spectra analyses.

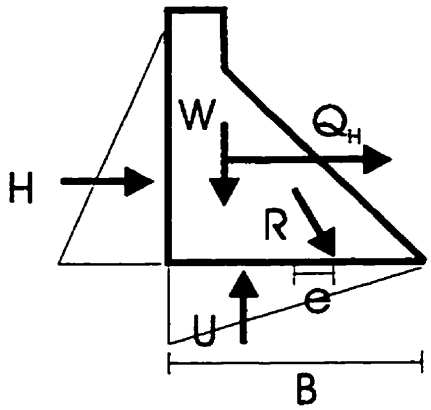

Fig. 7.4 *Dam block resultants.*

The pseudo-static method used seismic coefficients suggested by Dascal et al. (1994). Assuming the dam is in zone II, the seismic coefficient is 0.1. The pseudo-static seismic force is equal to the product of the seismic coefficient by the dead load and added masses of Weestergard. The seismic forces are uniformly distributed on the upstream face. The pseudo-dynamic analysis was performed using only the first vibration mode of the dam yielding a spectral acceleration of 0.5g according to Fig. 7.3. Table 7.2 gives a summary of the applied forces and the various safety factors obtained with the pseudo-static method and with the pseudo-dynamic method without uplift pressures.

As illustrated in Fig. 7.4, **e** is the eccentricity of the applied loads resultant on the base or on the lift joint, **B** is the base width or lift joint width, and **SSF** is the sliding safety factor. For these calculations, a 45° angle (μ=1.0) without cohesion was used to determine the shear strength of the dam-foundation and lift joints.

Under the applied seismic forces, the pseudo-static approach indicates sufficient capacity at the lift joint. The pseudo-dynamic analysis leads to the opposite conclusion. The first mode of vibration, which activates only 47% of the total mass, is enough to induce sliding at the joint.

Table 7.2 *Pseudo-static and pseudo-dynamic analyses without uplift pressures.*

PSEUDO-STATIC SEISMIC COEFFICIENT						PSEUDO-DYNAMIC RESPONSE SPECTRA					
Material properties						Material properties					
AT LIFT JOINT			AT FOUNDATION CONTACT			AT LIFT JOINT			AT FOUNDATION CONTACT		
COHESION	0.00		COHESION	0.00		COHESION	0.00		COHESION	0.00	
FRIC. COEF.	1.00		FRIC. COEF.	1.00		FRIC. COEF.	1.00		FRIC. COEF.	1.00	
RESULTANT FORCES AT LIFT JOINT						RESULTANT FORCES AT LIFT JOINT					
Applied forces in kN			Resistance kN			Applied forces in kN			Resistance kN		
	horizontal	vertical		horizontal	vertical		horizontal	vertical		horizontal	vertical
Seismic	915	0	Dead load	0	5332	Seismic	5681	0	Dead load	0	5332
Hydrostatic P.	1631	0	Shear capacity	5332	0	Hydrostatic P.	1631	0	Shear capacity	5332	0
Uplift	0	0				Uplift	0	0			
Sum	2545	0	SSF	2.09		Sum	7311	0	SSF	0.73	
Overturning moment about centerline of the joint kN-m						Overturning moment about centerline of the joint kN-m					
Seismic	7319		Dead load	14944		Seismic	55997		Dead load	14944	
Hydrostatic P.	9915					Hydrostatic P.	9915				
Uplift	0		% uncracked	100.00		Uplift	0		% uncracked	0.00	
Sum	17234		e/½B	0.05		Sum	65912		e/½B	1.12	
RESULTANT FORCES AT FOUNDATION CONTACT						RESULTANT FORCES AT FOUNDATION CONTACT					
Applied forces in kN			Resistance kN			Applied forces in kN			Resistance kN		
	horizontal	vertical		horizontal	vertical		horizontal	vertical		horizontal	vertical
Seismic	11667	0	Dead load	0	74450	Seismic	11186	0	Dead load	0	74450
Hydrostatic P.	36240	0	Shear capacity	74450	0	Hydrostatic P.	36240	0	Shear capacity	74450	0
Uplift	0	0				Uplift	0	0			
Sum	47907	0	SSF	1.55		Sum	47426	0	SSF	1.57	
Overturning moment about centerline of base in kN-m						Overturning moment about centerline of base in kN-m					
Seismic	370936		Dead load	880171		Seismic	733554		Dead load	880171	
Hydrostatic P.	1038891					Hydrostatic P.	1038891				
Uplift	0		% uncracked	100.00		Uplift	0		% uncracked	98.64	
Sum	1409827		e/½B	0.20		Sum	1772445		e/½B	0.34	

This contradiction is mainly due to the seismic load distribution, as shown in Fig.7.5. Forces based on the seismic coefficient follow the mass distribution, while forces based on a response spectrum correspond to the mode shapes. Since the maximum deflection occurs at the crest in the first mode, the seismic forces derived from the response spectra method are more important in that region. The spectral acceleration required to trigger sliding at the joint is 0.33g instead of the applied value of 0.50g. The resultants all fall within the middle third of the dam except for the lift joint in pseudo-dynamic analysis where the resultant is outside the dam cross-section.

In Table 7.3, the results of the pseudo-static and pseudo-dynamic analyses are given for the case with uplift pressures in the joints. The sliding safety factor (SSF) is above 1.0 for the joint only for the pseudo-static analysis. All other sliding safety factors are below 1.0. The spectral acceleration required to trigger sliding at the joint is 0.19g instead of the applied value of 0.50g. For sliding at the foundation, the pseudo-spectral acceleration to apply is 0.39g.

Table 7.3 *Pseudo-static and pseudo-dynamic analyses with uplift pressures.*

PSEUDO-STATIC SEISMIC COEFFICIENT						PSEUDO-DYNAMIC RESPONSE SPECTRA					
Material properties						Material properties					
AT LIFT JOINT			AT FOUNDATION CONTACT			AT LIFT JOINT			AT FOUNDATION CONTACT		
COHESION	0.00		COHESION	0.00		COHESION	0.00		COHESION	0.00	
FRIC. COEF	1.00		FRIC. COEF.	1.00		FRIC. COEF.	1.00		FRIC. COEF.	1.00	
RESULTANT FORCES AT LIFT JOINT						RESULTANT FORCES AT LIFT JOINT					
Applied forces in kN			Resistance kN			Applied forces in kN			Resistance kN		
	horizontal	vertical		horizontal	vertical		horizontal	vertical		horizontal	vertical
Seismic	915	0	Dead load	0	5332	Seismic	5681	0	Dead load	0	5332
Hydrostatic P.	1631	0	Shear capacity	3808	0	Hydrostatic P.	1631	0	Shear capacity	3808	0
Uplift	0	1523				Uplift	0	1523			
Sum	2545	1523	SSF	1.50		Sum	7311	1523	SSF	0.52	
Overturning moment about centerline of the joint kN-m						Overturning moment about centerline of the joint kN-m					
Seismic	7319		Dead load	14944		Seismic	55997		Dead load	14944	
Hydrostatic P.	9915					Hydrostatic P.	9915				
Uplift	4323		% uncracked	100.00		Uplift	4323		% uncracked	0.00	
Sum	21557		e/½B	0.20		Sum	70235		e/½B	1.71	
RESULTANT FORCES AT FOUNDATION CONTACT						RESULTANT FORCES AT FOUNDATION CONTACT					
Applied forces in kN			Resistance kN			Applied forces in kN			Resistance kN		
	horizontal	vertical		horizontal	vertical		horizontal	vertical		horizontal	vertical
Seismic	11667	0	Dead load	0	74450	Seismic	11186	0	Dead load	0	74450
Hydrostatic P.	36240	0	Shear capacity	44922	0	Hydrostatic P.	36240	0	Shear capacity	44922	0
Uplift	0	29528				Uplift	0	29528			
Sum	47907	29528	SSF	0.94		Sum	47426	29528	SSF	0.96	
Overturning moment about centerline of base in kN-m						Overturning moment about centerline of base in kN-m					
Seismic	370936		Dead load	880171		Seismic	733554		Dead load	880171	
Hydrostatic P.	1038891					Hydrostatic P.	1038891				
Uplift	344495		% uncracked	66.60		Uplift	344495		% uncracked	32.01	
Sum	1754322		e/½B	0.66		Sum	2116940		e/½B	0.79	

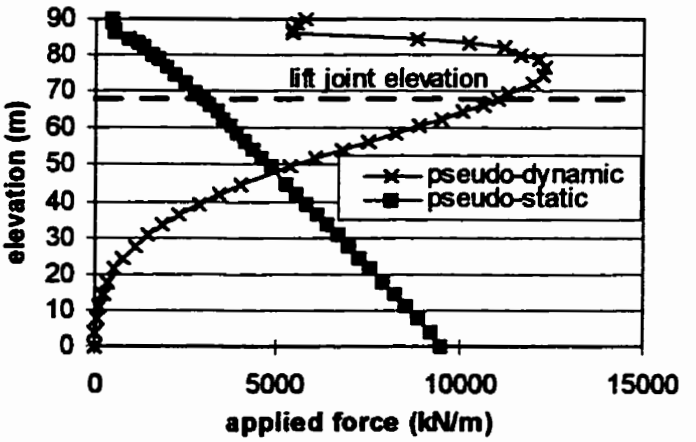

Fig.7.5 *Seismic forces distribution along dam height.*

The assumed strength at the foundation contact is not adequate for the intensity of applied seismic forces. Sliding safety factors (SSF) are just below the CDSA criterion of 1.0. The resultants do not fall in the middle third of the base since some cracking is expected to occur at the heel. The dam-foundation contact would be able to resist an

earthquake load equivalent to a seismic coefficient of 0.074 i.e. zone I or a spectral acceleration of 0.39g.

7.4 Nonlinear finite element analyses NLFEA

The dam models shown in Fig.7.1 were analysed using the finite element computer program INTRFACE. A series of nonlinear time history analyses were performed incrementing the intensity of the input accelerogram until dynamic instability was triggered. The earthquake record (Fig.7.2) was normalized to a given peak ground acceleration intensity (PGA) starting at 0.05g and ending at 1.0g with increments of 0.05g.

The computed residual joint sliding displacement is considered as the average of the results of gap-friction elements located at the upstream face, at midspan, and at the downstream face. The opening is taken at the upstream face and at the downstream face. The computed accelerations are evaluated at the center of gravity (C.G.) of the dam as a whole, at the C.G. of the lower and upper blocks for the dam with a lift joint, and finally at the crest. The lower block in Dam II is delimited by the base contact joint and the lift joint, while the upper block is delimited by the lift joint and the crest.

Figure 7.6 shows the computed responses for Dam I, with an untreated joint at the base and no uplift pressure. Base sliding started at a PGA=0.20g with 2.3 mm. The energy response ratios (Fig. 7.6(c)) indicate that friction becomes the primary energy dissipative mechanism at 0.25g compared to the other energies which are kinetic, elastic, and damping. The tensile capacity was reached in mass concrete elements for a PGA of 0.55g at elevation 67m.

Figure 7.7 shows the computed responses for Dam I, with a waterblasted base joint, and no uplift pressure. Base sliding started at a PGA=0.30g with 1.6 mm. Between PGA=0.05g and PGA=0.30g, the upstream base opening is larger than base sliding because the dam is basically rotating about the toe. The energy response ratios

(Fig. 7.7(c)) indicate that friction becomes the primary energy dissipative mechanism at 0.70g.

Figure 7.8 shows the computed responses for Dam I, with a waterblasted base joint, and triangular uplift pressures. Base sliding started at PGA=0.10g with 1.8 mm. The energy response ratios (Fig. 7.8(c)) indicate that friction is the primary energy dissipative mechanism regardless of the PGA. Tensile capacity was reached at 67m at PGA=0.55g. It should be noticed that when the base uplift pressures are considered, the dam is very close to instability. For untreated base joint with uplift pressures, instability occurred under the applied static loads. Therefore that situation was not analysed. However, the uplift pressures diagram is very conservative since dams 90m high usually have a drainage system to release the uplift pressures.

The sliding displacements and base openings according to the joint surface preparation are compared in Fig.7.9. Uplift pressure has a significant effect on the residual sliding displacements. Waterblasting treatment shifts the behaviour at PGA below 0.40g, from a dominating sliding mode to opening mode . The downstream opening starts at 0.45g. Comparing the computed accelerations in Fig. 7.6(b), Fig. 7.7(b), and Fig. 7.8(b), between PGA=0.45g and PGA=0.70g, crest accelerations are about the same for the various models. Then, interestingly, for the model with a waterblasted base joint with uplift pressures, the crest accelerations flatten out for PGA greater than 0.70g (Fig. 7.8(c)). The joint under the applied normal load acts as a base isolator.

The energy response ratios indicate energy dissipation in friction prior to global joint sliding displacement. Even if the joint does not slide as a whole, there is local joint sliding along the upstream portion of the joint which is sufficient to dissipate a noticeable amount of energy.

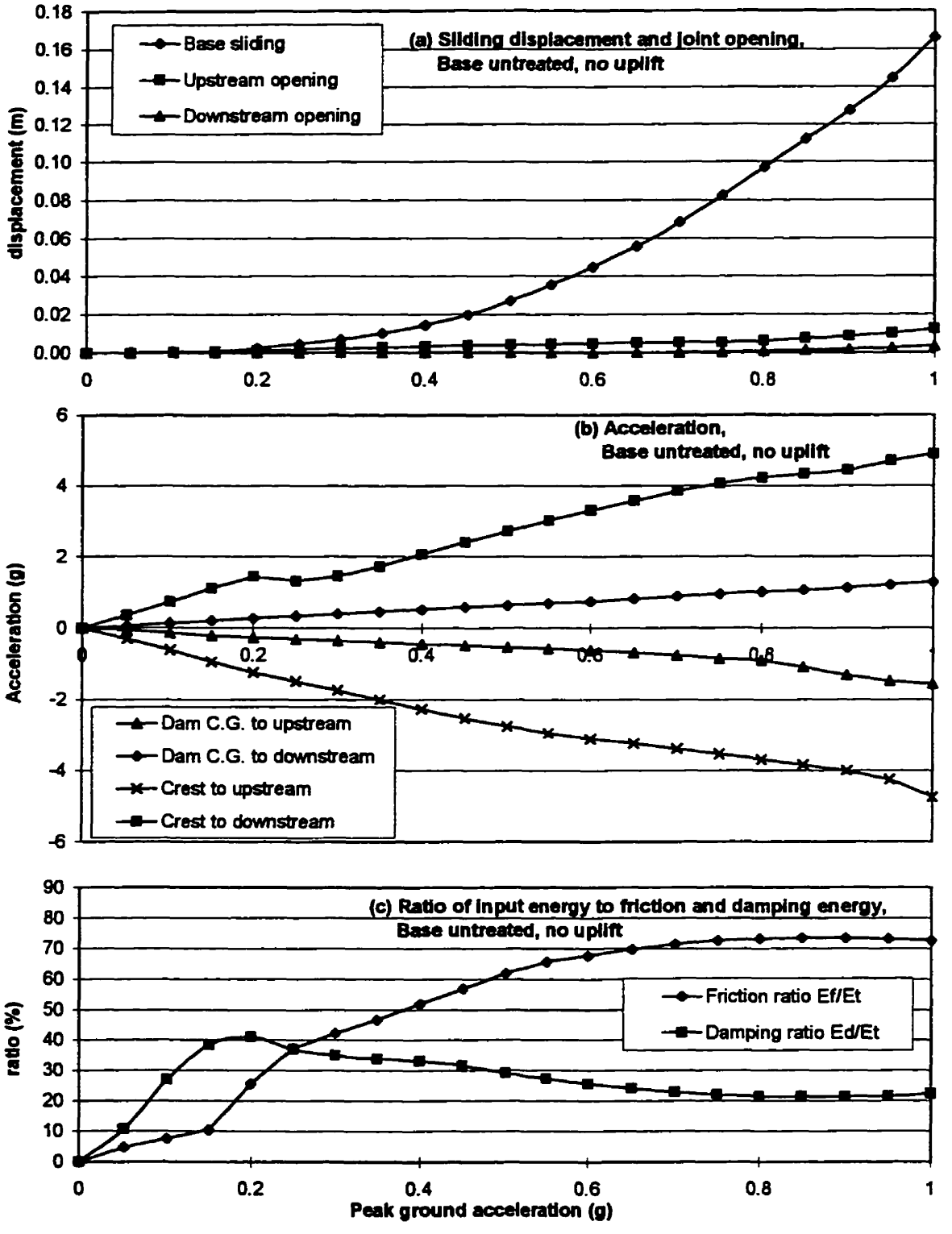

Fig. 7.6 *Dam I, untreated joint at the base without uplift computed response.*

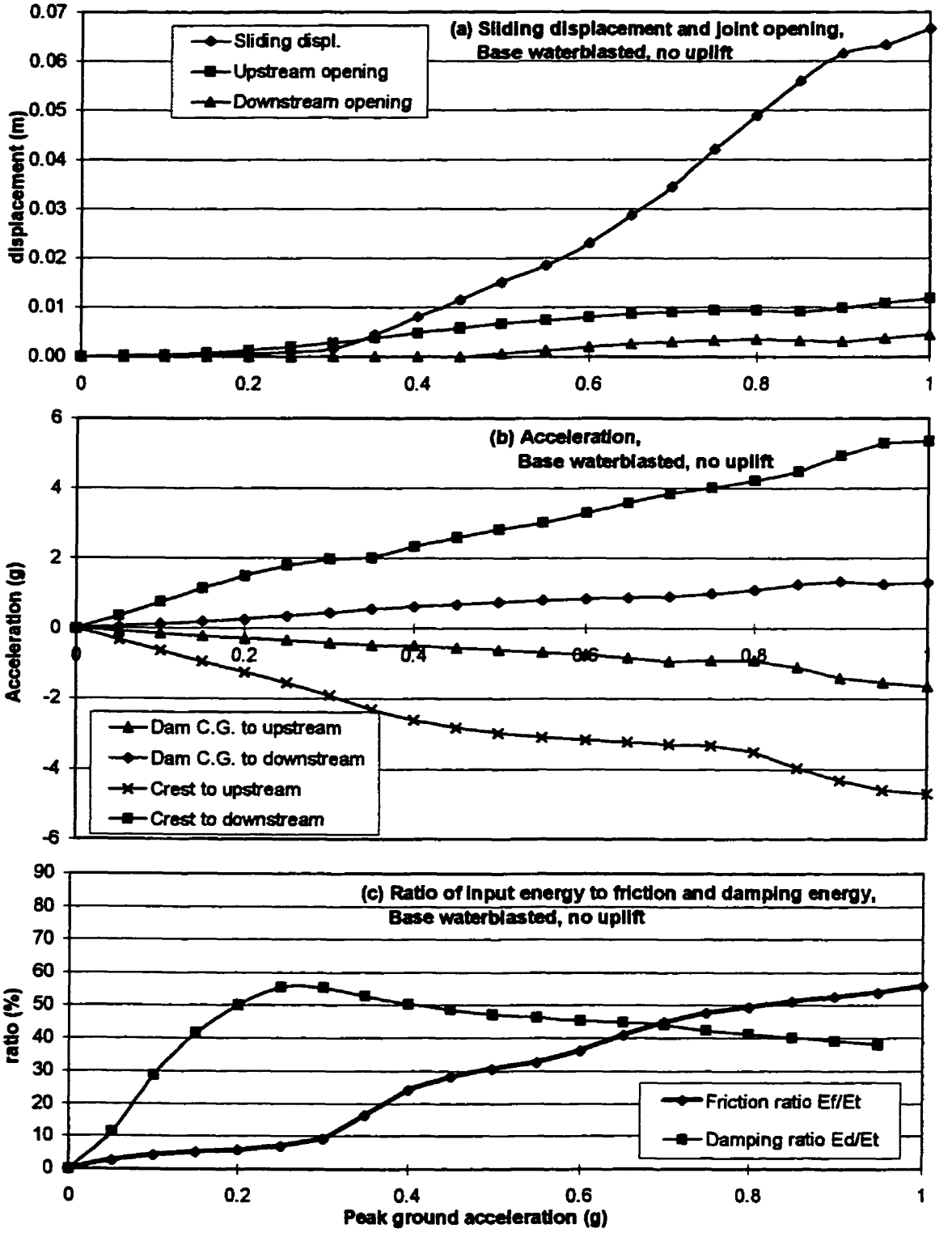

Fig. 7.7 *Dam I, waterblasted joint at the base without uplift, computed response.*

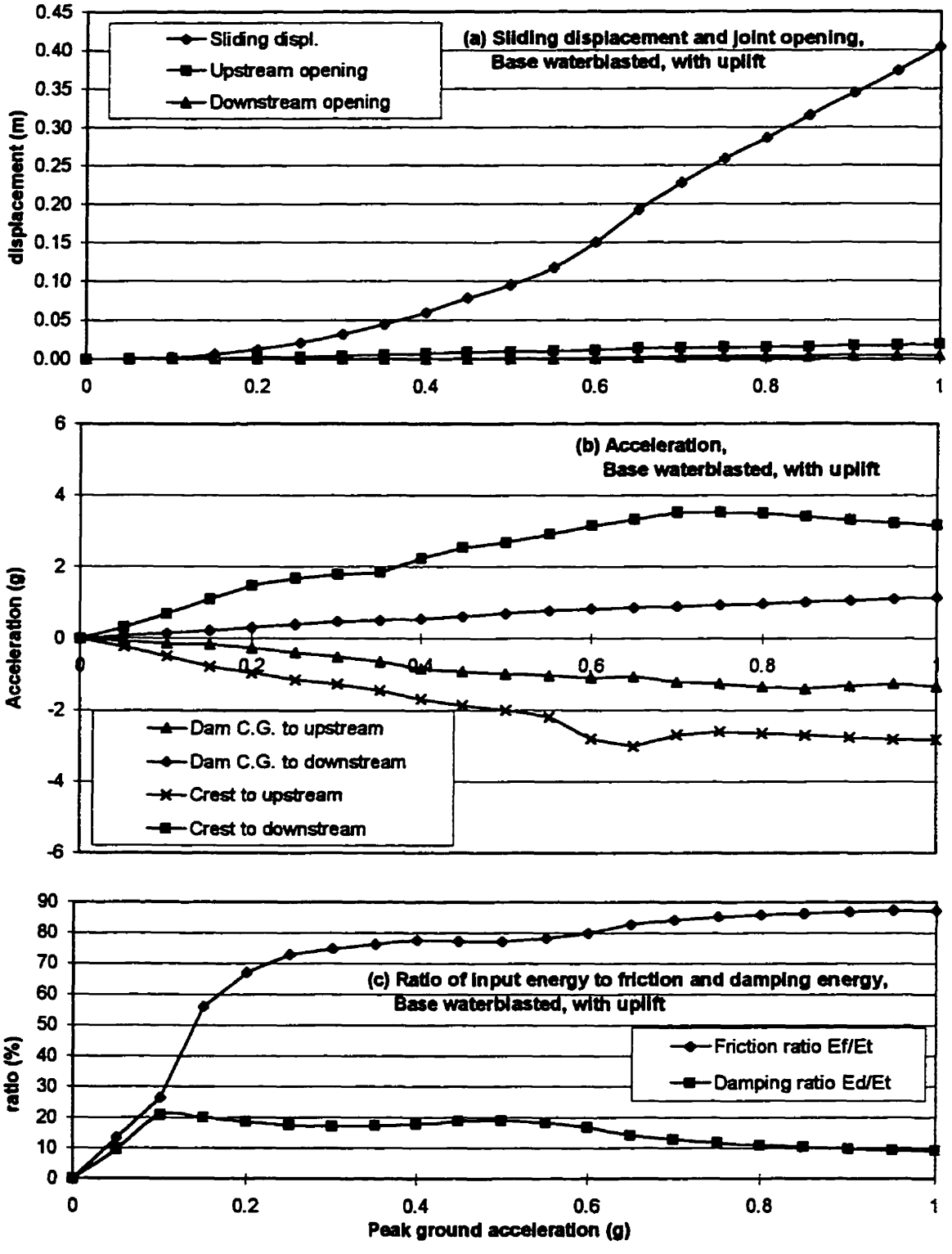

Fig. 7.8 *Dam I, waterblasted joint at the base with uplift, computed response.*

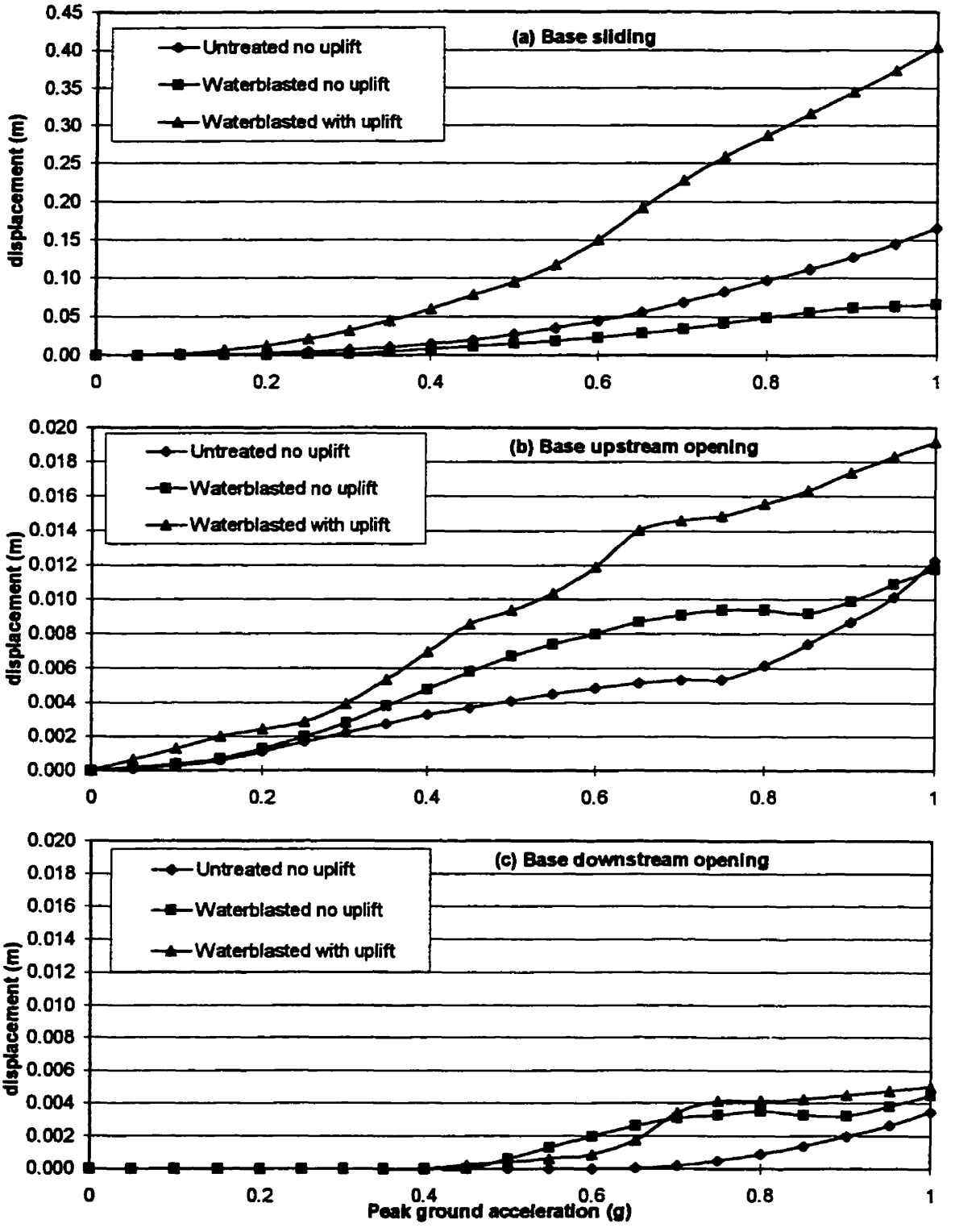

Fig. 7.9 *Dam I, displacements comparisons according to joint faces treatment.*

Figure 7.10 shows the computed responses for Dam II, base and lift joints untreated without uplift pressure. Base sliding started at a PGA=0.25g with 1.4 mm, while upper joint sliding started at PGA=0.10g. The energy response ratios (Fig. 7.10(c)) indicate that friction becomes the primary energy dissipative mechanism at 0.25g when the base begins sliding. The tensile capacity was reached for a PGA of 0.60g in the mass concrete elements in the vicinity of the lift joint.

Figure 7.11 shows the computed responses for Dam II, with waterblasted base and lift joints without uplift pressure. Base sliding started at PGA=0.45g with 2.0 mm, while joint sliding occurred at 0.15g with 2.6 mm. Between PGA=0.05g and PGA=0.40g, upstream base opening is larger than base sliding because the dam is basically rotating about the toe. At PGA=0.40g, the opening reached 1.2 mm. The energy response ratios (Fig. 7.11(c)) indicate that friction becomes the primary energy dissipative mechanism at 0.70g. The tensile capacity was reached for PGA=0.40g in the vicinity of the lift joint.

Figure 7.12 shows the computed responses for Dam II, with waterblasted base and lift joints and with uplift pressures. Base sliding started at PGA=0.15g with 3.4 mm while lift joint sliding began at PGA=0.10g with 1.0mm. From PGA=0.60g, base and lift joints sliding are about the same. The energy response ratios (Fig. 7.12(c)) indicate that friction is the primary energy dissipative mechanism starting at PGA=0.10g. The tensile capacity was reached for PGA=0.45g in the vicinity of the lift joint. It should be noticed that under the applied uplift pressure, the dam is very close to instability. Again, the untreated base joint with uplift pressures produced instability under the applied static loads. Therefore that situation was not analysed.

The computed sliding displacements and joint openings as a function of joint surface preparation are compared in Fig.7.13. Uplift pressure has a significant effect on the base sliding displacements but it does not affect the upper joint sliding displacement since upper block with waterblasted joint surfaces responded in a rocking mode.

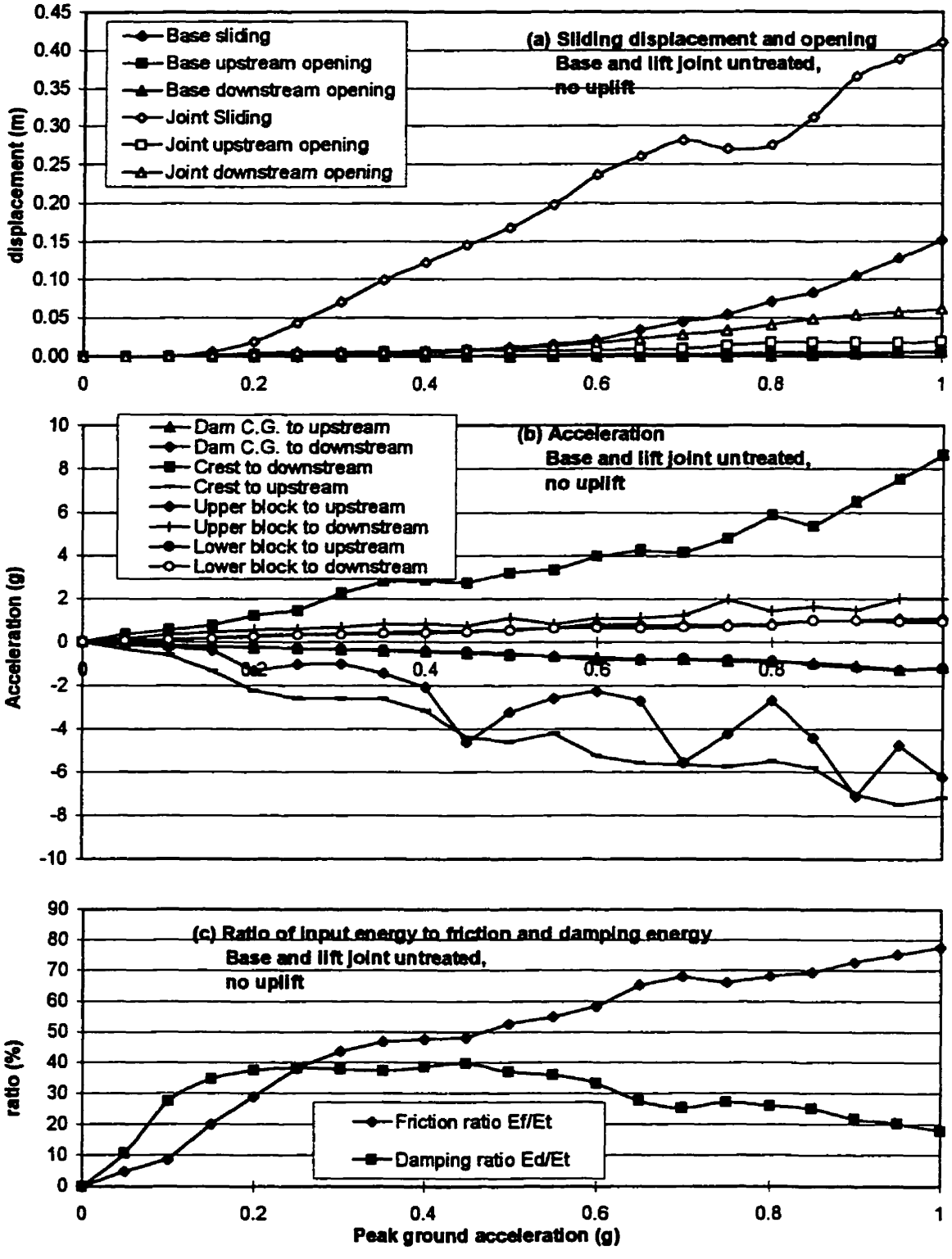

Fig. 7.10 *Dam II, untreated base and upper joint, no uplift.*

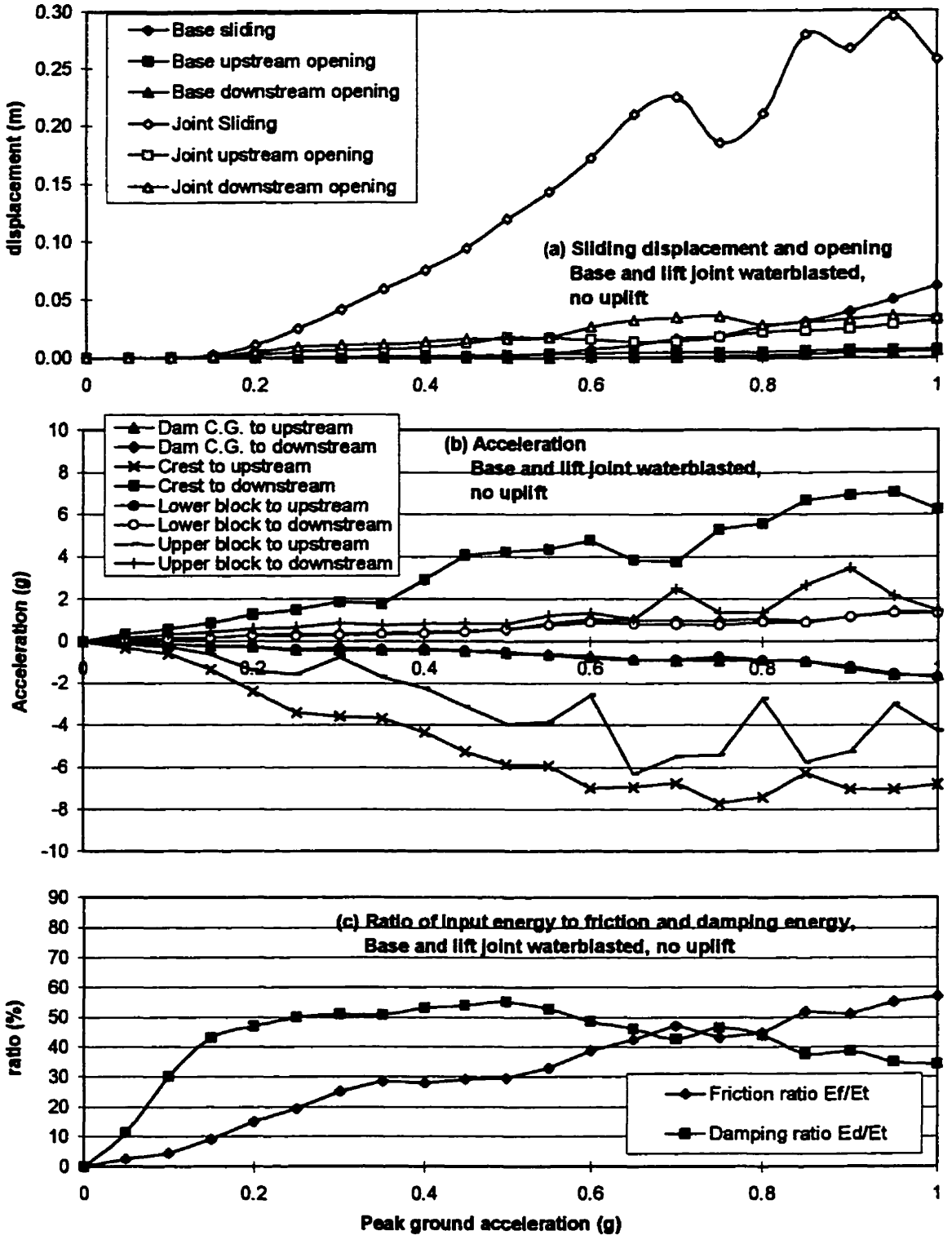

Fig. 7.11 *Dam II, waterblasted base and upper joint, no uplift.*

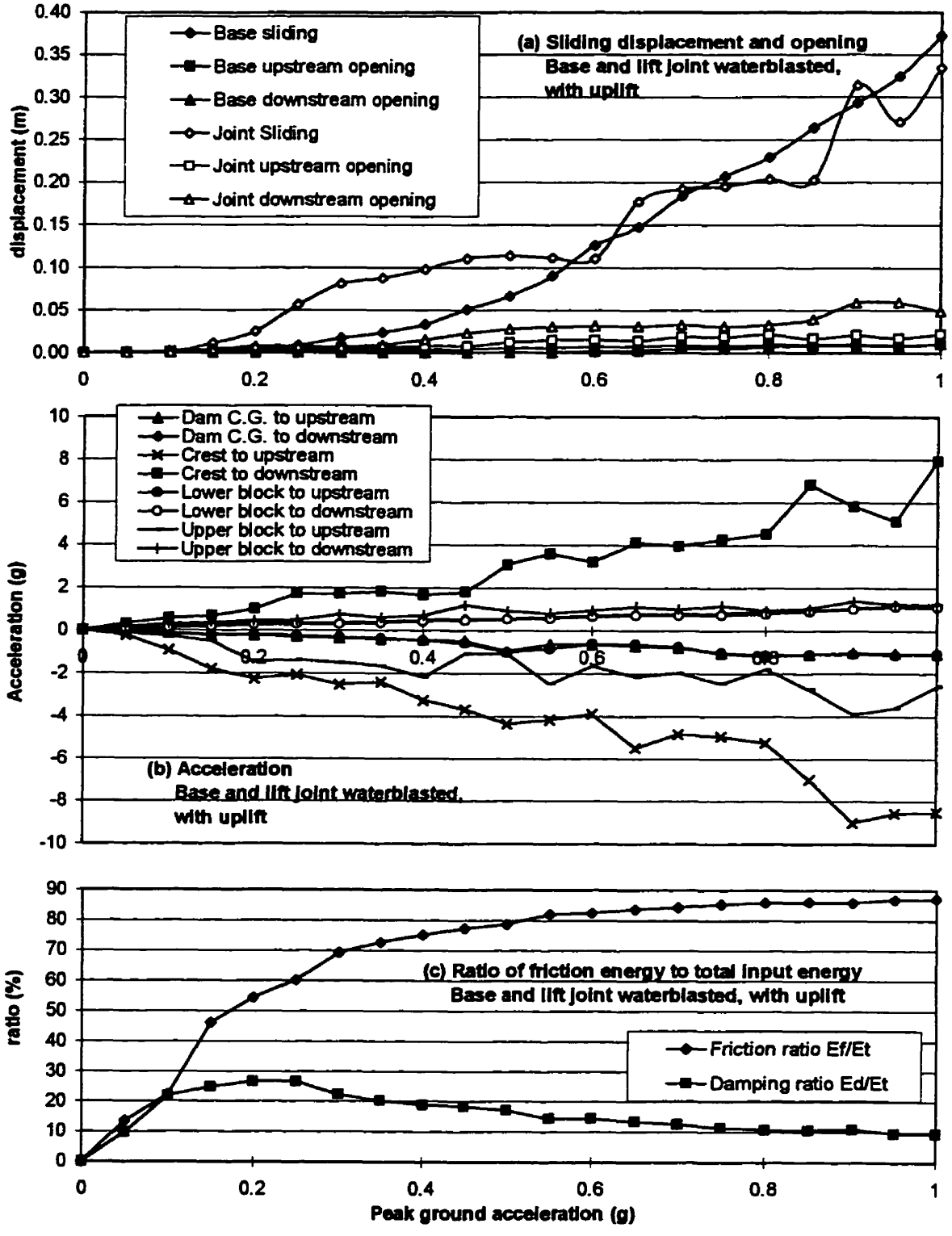

Fig. 7.12 *Dam II, waterblasted base and upper joint, with uplift.*

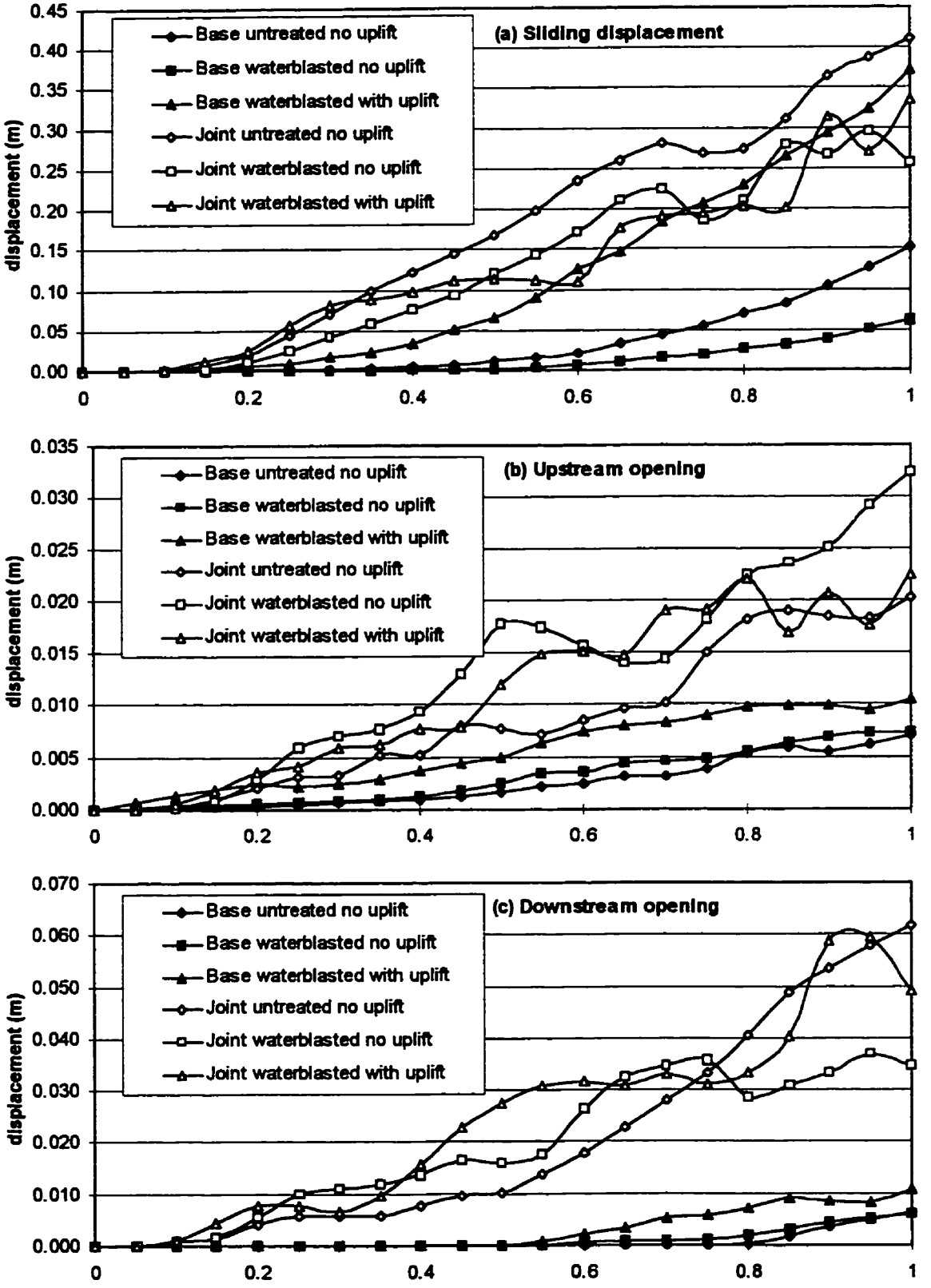

Fig. 7.13 *Dam II, displacements comparisons according to joint faces treatment.*

The presence of a weak lift joint at the top (Dam II) reduces the applied shear forces at the base since all joint conditions models exhibited sliding displacements larger for Dam I than for Dam II. However, the opposite effect occurs at the crest where the computed acceleration increased with the introduction of the lift joint for the various joint surfaces conditions.

The PGA required to reach the tensile strength in the concrete mass was given in the above for the various dam models and joint surface preparations. For the dam with a single joint at the base (Dam I), the tensile strength was reached at the elevation of the lift joint (Dam II). Thus a question arises: would the crack be confined to the joint or would the crack rather dive in the concrete mass at some point? In the case of a very weak lift joint, as modelled inhere, with no tensile strength, limited secondary cracking would occur after reaching a certain level of acceleration. However, this cracking involves very few elements near the joint in the vicinity of the upstream and downstream faces. This type of cracking would pull out a small wedge of concrete at the end of the joint, thus it may be interpreted as additional damage in the surroundings of the joint; probably caused by impact as the joint open and close and not as generalized structural cracking of the concrete mass.

7.5 Comparisons between pseudo-static, pseudo-dynamic and NLFE analyses

The conclusions drawn from the pseudo-dynamic approach or the NLFEA are similar. Sliding at the foundation contact joint would occur at a level of acceleration of 0.10g. However, the NLFEA gives an additional information which is the amount of residual sliding displacements. At a PGA of 0.10g, the residual sliding displacement is negligible. Thus, based on this knowledge, the maximum level of acceleration could be raised depending on the allowable residual sliding displacement. For example, if 5 cm is considered as an acceptable maximum displacement, Dam I would be considered to be able to sustain 0.60g for untreated base joint with no uplift, 0.80g for waterblasted joint

with no uplift, 0.35g for waterblasted joint with uplift, while Dam II would resist 0.25g for untreated joint with no uplift, 0.30g for waterblasted no uplift, 0.20g for waterblasted with uplift. The key results of the various analyses are summarized in Table 7.4.

Table 7.4 *Summary of PGA at initial sliding for the various models.*

	Dam I		Dam II			
Joint condition	PGA at initial sliding	related residual sliding	PGA at initial base sliding	related base residual sliding	PGA at initial lift joint sliding	related residual sliding
Untreated no uplift	0.20g	2.3mm	0.25g	1.4mm	0.10g	0.3mm
Waterblasted no uplift	0.30g	1.6mm	0.45g	2.0mm	0.15g	2.6mm
Waterblasted with uplift	0.10g	1.8mm	0.15g	3.4mm	0.10g	1.0mm

7.6 Analysis of a dam with several joints

A series of analyses, using the same input data that was used in Section 7.4, has been undertaken on a 90m dam with 8 joints evenly distributed along the height. The objective here was twofold: first to evaluate the capabilities of the computer program INTRFACE to deal with multiple joints, and secondly to determine if the response of a dam with several joints is whether controlled by a few joints, or rather by all joints.

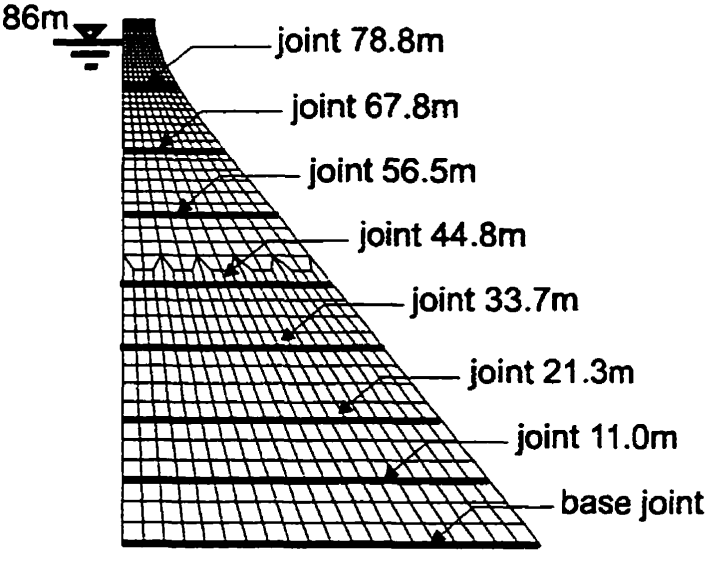

Fig. 7.14 *Jointed dam finite element model.*

The finite element model of the dam is shown in Fig. 7.14. The joints were all considered to be waterblasted, with no tensile strength, and no cohesion. The reservoir level is set at 86m, no uplift pressures were considered. The input ground acceleration record is the modified Saguenay earthquake scaled at incremental levels of peak ground acceleration. Viscous damping at 5% critical, on the stiffness only was applied. The gap-friction elements properties corresponding to waterblasted joints are given in Table 7.5.

Table 7.5 *Gap-friction element parameters for multi-joints analyses.*

k_n N/m/m^2	k_t N/m/m^2	c_n N-s/m^2	c_t N-s/m^2	f_t N/m^2	τ_i N/m^2	G^I_f N/m	G^{II}_f N/m	μ -	λ_d -	χ_i -	D_m
2.769E11	2.769E11	0.0	0.0	0.0	0.0	0.0	0.0	-	0.85	0.80	0.02

The following figures describe the characteristic results of the analyses. Figure 7.15 shows the maximum average sliding displacement per joint at every level of peak ground acceleration. The complete set of results is given in Fig. 7.15(a) and a zoom of the same results between 0.000m and 0.020m sliding displacements are given in Fig. 7.15(b). There are really two joints that dominate the sliding response: the joint at 67.8m (joint modelled in Dam II) and the joint at 78.8m. The peak ground accelerations to initiate sliding per joint are as follows: PGA=0.55g for base joint, PGA=0.50g for joint 11.0m, PGA=0.45g for joint 21.3m, PGA=0.40g for joint 33.7m, PGA=0.35g for joint 44.8m, PGA=0.35g for joint 56.5m, PGA=0.20g for joint 67.8m, and PGA=0.15g for joint 78.8m.

Base joint average sliding dominates the response of the lower joints (up to 44.8m in height over the dam) up to PGA=0.45g. The hydrostatic trust induces significant shear displacement along the upstream half of the base joint.

Figure 7.11(a) shows the sliding displacements of the joint 67.8m in Dam II. Comparing Fig. 7.11(a) with Fig. 7.15(a) shows that the introduction of several lift joints reduced, by a factor of 2, the computed maximum sliding displacement at joint 67.8m. The base joint maximum sliding displacement also decreased significantly, from 0.0187m in Dam II, it dropped to 0.0048m for the dam with several lift joints thus showing a reduction of 75% .

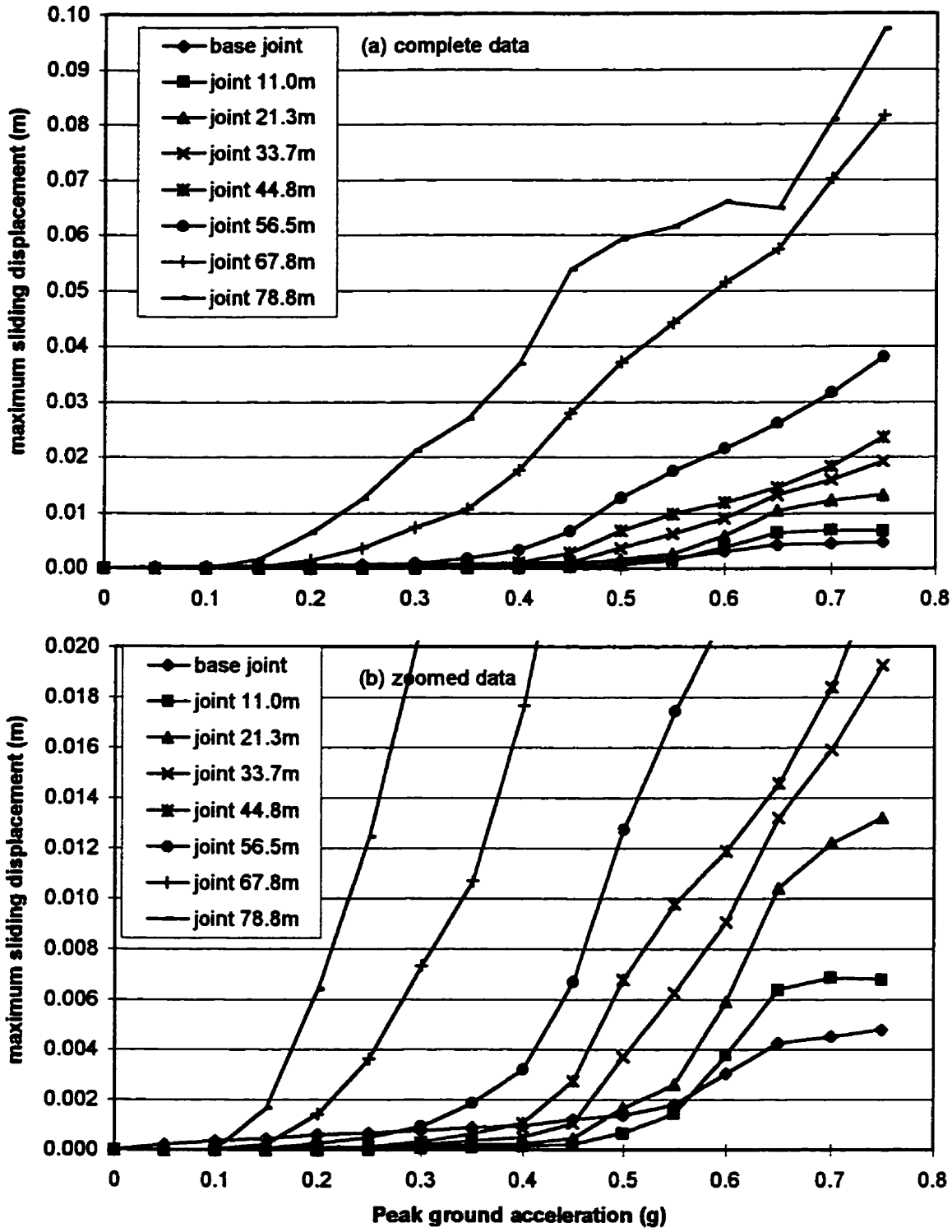

Fig. 7.15 *Multi-joints dam, maximum sliding displacements.*

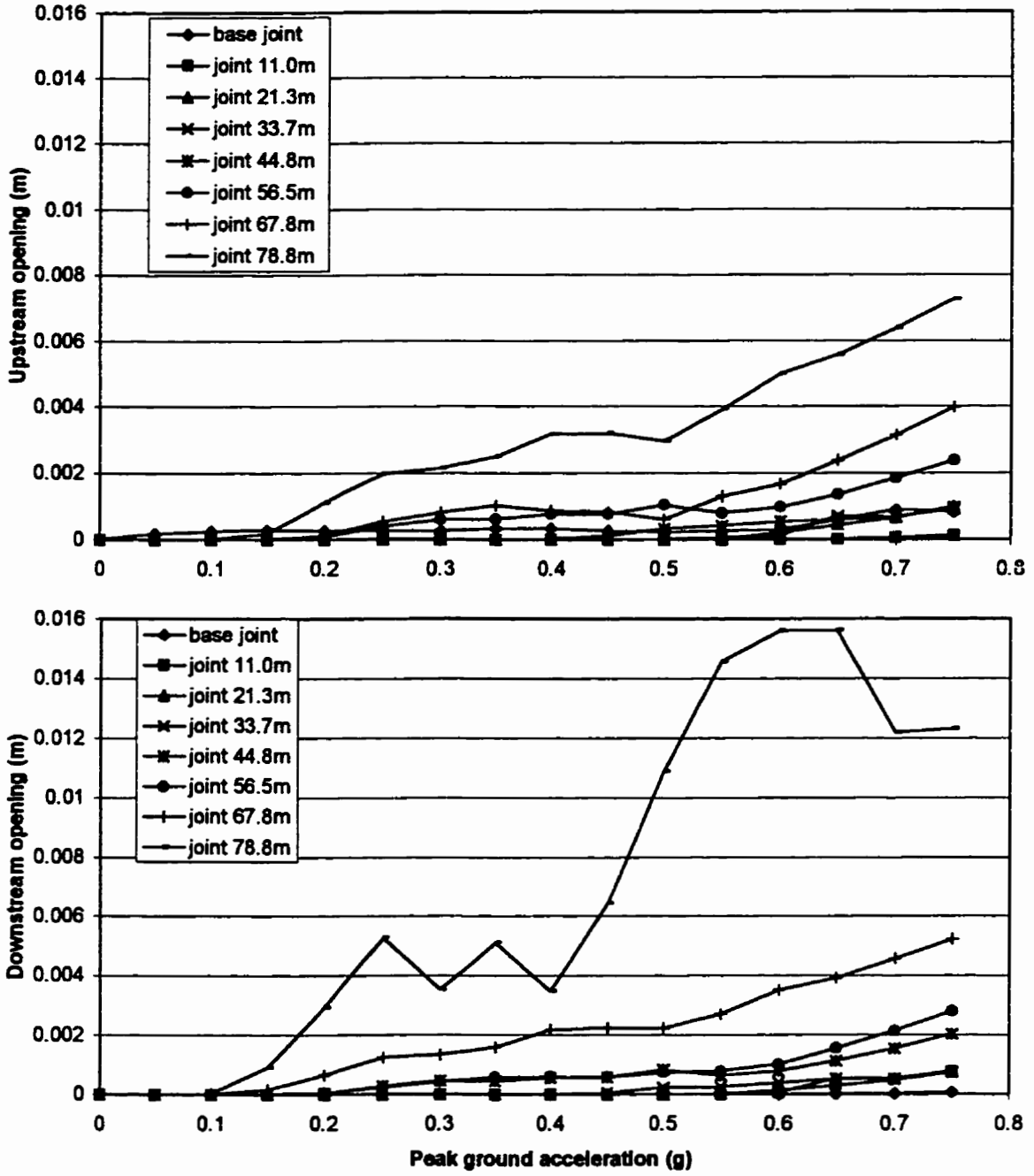

Fig. 7.16 *Upstream and downstream maximum joint opening.*

The maximum upstream and downstream joint openings are presented in Fig. 7.16. The upstream joint opening dominates the response of the base joints, for all the other joints, the maximum downstream opening is greater than maximum upstream joint

opening. A comparison between the results of Dam II given in Fig. 7.11(b) and the results in Fig. 7.16 for the dam with several joints shows that the opening was reduced by the introduction of several lift joints. The upstream maximum opening at the base joint was reduced from 4.78mm to 0.82mm, while the downstream maximum opening was reduced from 1.06mm to 0.07mm. The upstream maximum opening at the joint 67.8m was reduced from 18.16mm to 3.98mm, while the downstream maximum opening was reduced from 35.95mm to 5.24mm.

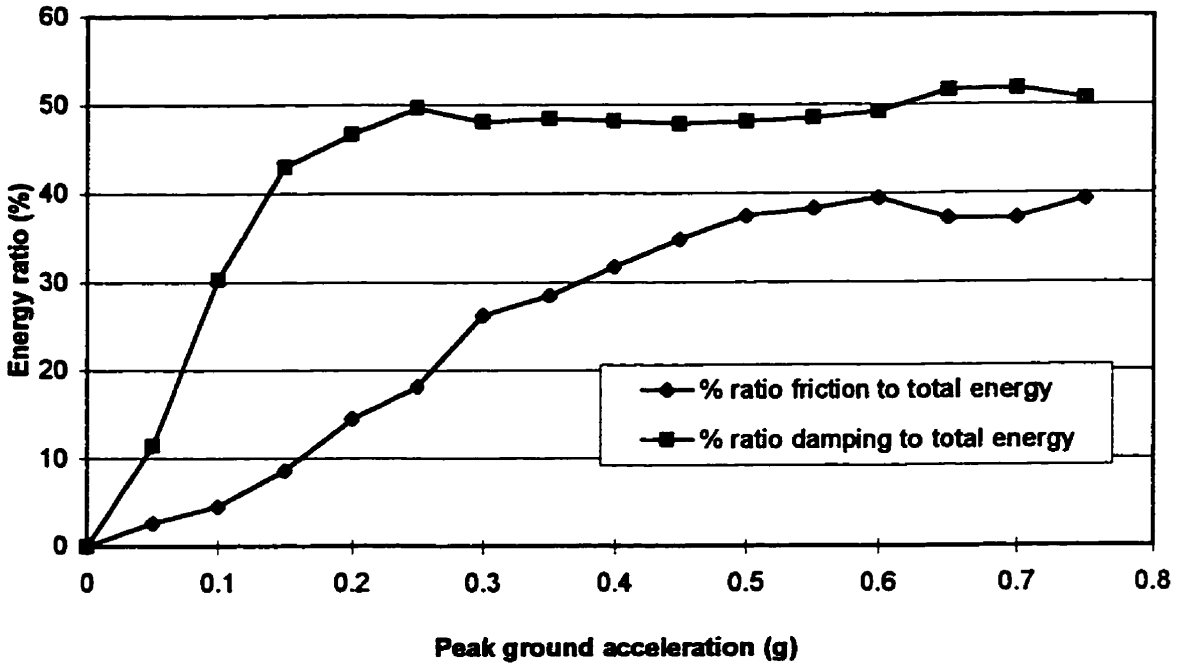

Fig. 7.17 *Friction energy and damping energy to total energy ratios.*

Figure 7.17 shows the diagram of the friction and damping energy to total energy ratios as a function of the peak ground acceleration. Even though there are numerous joints in the dam, viscous damping is the primary energy dissipation mechanism. Figure 7.17 may be compared to Fig. 7.11(c). The curves are very similar. Comparing the absolute values of the energies at 0.75g, Dam II computed frictional dissipated energy was 1.52×10^6N-m, while the multi-jointed dam computed frictional dissipated energy was 1.60×10^6 N-m. These values show that increasing the number of joints did not increase

the total amount of energy dissipated by friction. Furthermore, the reduction of the sliding displacements and the constant value of the absolute value of the friction energy dissipated indicates that introduction of additional joints just redistributes along the height the energy to be dissipated by friction.

Figures 7.18 and 7.19 illustrate the type of information that may be obtained from NLFEA on jointed dams. The deformed shape of the dam is a visual indicator of the relative sliding and opening between the joints. Figure 7.18(a) illustrates the deformed shape of the multi-jointed dam at a peak ground acceleration of 0.30g at time 3sec. The relative displacement values along the joint length, opening and sliding displacement are shown in Fig. 7.18(b) and (d). The stress distributions along the lift joint are given in Fig. 7.18(c) and (e). These figures indicate the dominant response mechanisms.

Figure 7.19 presents the state of the gap-elements per joint layer for the complete time history. From that figure, an evaluation of the extent of joint opening along the dam section and time is obtained. Joints may be compared one to another. For instance, in this particular case, it is obvious that all the nonlinearities occur in the four upper joints (joint 44.8m, joint 56.5m, joint 67.8m, and joint 78.8m).

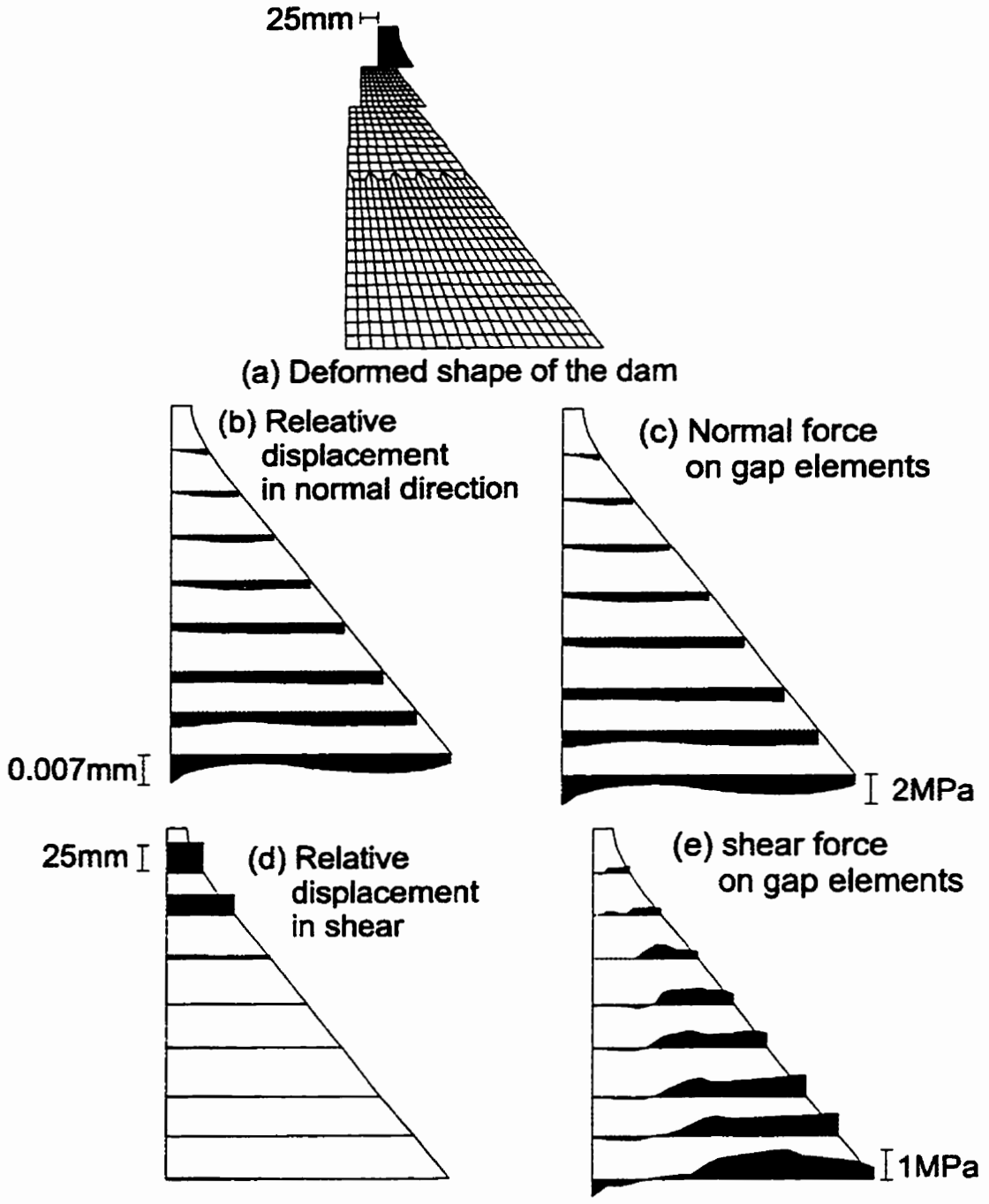

Fig. 7.18 *Results of multi-jointed dam analysis at PGA=0.30g and t=3.00sec.*

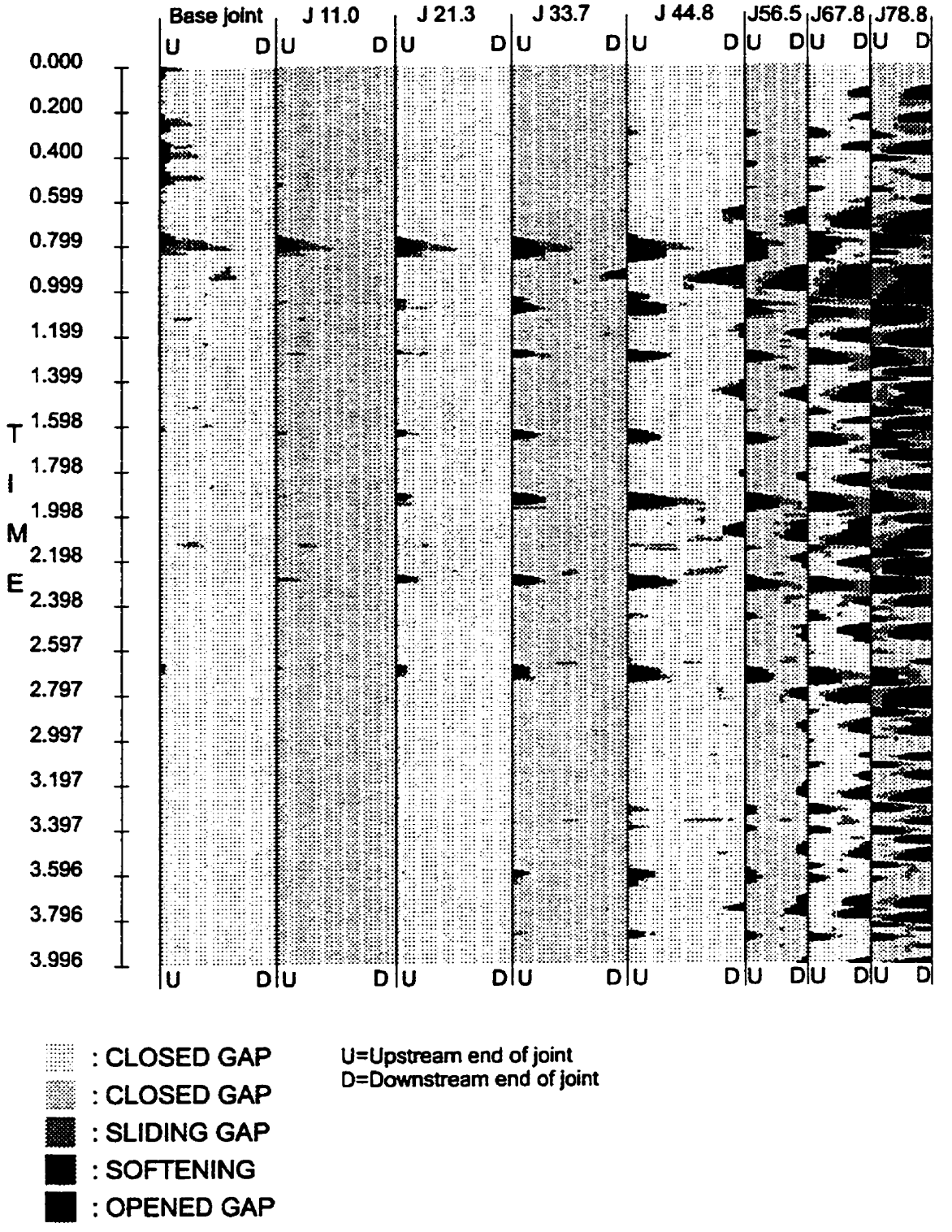

Fig. 7.19 *Gap elements state per joint for the whole analysis.*

7.7 Summary and conclusions

The significance of lift joints on seismic dam safety was assessed by investigating the critical peak ground acceleration to induce significant residual displacements. A comparison between pseudo-static, pseudo-dynamic, and the nonlinear transient dynamic analyses (NLFEA) results in about the same intensity of applied ground acceleration for sliding to be initiated.

Analyses with a simple joint at the base indicated important residual sliding. They also indicated that secondary cracking would occur close to the crest. The introduction of a lift joint close to the crest reduces the displacements at the base. The total input seismic energy is smaller at low intensity earthquakes for a dam with the introduction of a lift joint. The overall effect of surface preparation, waterblasted surface as compared to a untreated surface, is to decrease the sliding displacement. However, joint opening is greater for waterblasted joints. Thus surface preparation imposes a gradual shift in the behaviour from pure sliding to combined sliding and rocking.

Finally, the introduction of several joints along the dam height indicated that only the two upper joints dominate the response. The energy dissipation mechanism and distribution of energy between friction and viscous damping has not been affected by the introduction of several joints. The residual displacements decreased when several lift joints were considered in the finite element model as compared to the dam with a joint at the base and a lift joint close to the crest.

However, NLFEA at larger intensity of peak ground acceleration indicates the maximum residual sliding displacements that could be adopted as a basis for assessing the potential damage and acceptability of a very severe earthquake.

CHAPTER 8
Conclusions

8.1 Summary of the thesis

Lift joints in dams are planes of weakness in an otherwise monolithic structure. Cracking and failure along a lift joint involve frictional strength characteristics which, under transient cyclic loadings such as earthquakes, may lead to energy dissipation by friction sliding. Seismic dam stability assessment requires to develop structural analysis tools that enable a rational modelling of potential failure mechanisms along joints recognizing cyclic load-displacement responses. In addition, the cyclic load-displacement behaviour of lift joints ought to be characterized experimentally since little may be found in the literature.

The thesis presented a comprehensive review of the available literature on concrete lift joints covering the experimental joints material data together with the values suggested in dam safety guidelines. Various constitutive models applicable to joints were presented. The implementation of joint models into a finite element analysis was discussed. Past investigations and case studies of static and seismic safety assessment of "jointed" gravity dams were reviewed.

An experimental programme on concrete lift joints has been devised in this project. The first objective was to provide experimental results to validate the numerical modelling of concrete-concrete lift joints dynamic sliding. The second objective was to establish a relationship between dynamic shear strength response and static shear strength tests. The third objective was to study the effect of the frequency content on the dynamic sliding properties.

Eighteen specimens with an interface area of 500mm×250mm were subjected to friction tests. Static shear strength results, and bending test results that served to generate crack profiles for the sliding friction tests were presented. In the bulk of this experimental

programme, i.e. the sliding friction tests, the effect of surface preparation on joint response, and the determinant effect of the surface roughness on the load-displacement response, could be observed. The accumulated effect of cycles of displacement on the frictional response was inquired.

Based on the experimental results, a hysteretic concrete-concrete lift joint interface constitutive model was developed. Crack initiation and propagation at the interface was reproduced using a fracture energy based model. The initial linear elastic response of the interface, the crack initiation and propagation, and the fully cracked sliding friction response, were combined in a constitutive model called the three-state lift joint constitutive model. Water pressure inside the joints was also simulated. It was treated as an external load that varies according to damage state of the joint.

The three-state constitutive model was implemented into the newly developed finite element program INTRFACE. The nonlinear gap-friction interface element was selected as the numerical support to the three-state constitutive model. Indirect displacement control solution strategies were adopted for the static equilibrium equations. The α solution method of dynamic equations of motions was selected for the transient time history analysis of jointed dams. Validation problems indicated the limitations of the various solution strategies.

A typical 90 m concrete gravity dam section with lift joints was analysed. The dam was subjected to seismic loads for three possible situations: (i) a single contact joint at the foundation, (ii) a foundation contact joint and a lift joint close to the crest, and (iii) eight lift joints evenly distributed along the dam height. As a first step, pseudo-static and pseudo-dynamic analyses were undertaken based on joint material parameters given in the CDSA guidelines (1995). Then, nonlinear transient dynamic analyses were performed with incremental levels of peak ground acceleration. Maximum displacements, residual joint sliding displacements, maximum accelerations, energy dissipation by friction and viscous damping were computed. The standard analyses and the nonlinear finite element

analysis, NLFEA, were compared. Residual sliding displacement was used as safety index.

8.2 Conclusions

8.2.1 Review of literature

The review of the available literature on lift joints revealed that the Mohr-Coulomb failure criterion is generally adopted for representing joint behaviour. Furthermore, Coulomb frictional parameters (τ, ϕ) measured for existing dams have been widely reported in the literature. However, dam safety factors based on allowable stresses with Mohr-Coulomb failure criterion are not really adapted to the oscillatory sliding problem in earthquakes.

The use of simple static shear test results in dynamic studies is debatable. Intuitively, friction properties could be thought of being affected by the frequency content, the acceleration, the velocity, or any joint degradation due to loading cycles. The experimental programme performed in this project helped to answer some of these questions

8.2.2 Experimental programme

The coefficient of friction is found to decrease with increasing applied normal stress. The specimen behaviour in sliding friction depends on joint surface preparation. Cracks induced along waterblasted joint surfaces are rough, while cracks induced along unprepared joint surfaces are flat. As a result, waterblasted joints behave like cracked monolithic concrete. Unprepared joint surfaces behave like flat independent concrete surfaces.

Hysteresis loops are very stable; there is no significant degradation in response. The frequency content of the imposed sliding displacements has no effect on the measured

response. The coefficient of friction is somehow dependent on sliding velocity. There is no relation between the coefficient of friction and the acceleration.

An original empirical concrete-concrete joint sliding friction constitutive model was proposed. The friction angle characterizing the shear strength may be calculated as the sum of a basic angle and a roughness angle. The concept of peak and residual friction coefficients are adequate to describe the joint frictional behaviour. The roughness of waterblasted joints is equal to 80% of the roughness of monolithic cracked specimens, while the roughness of untreated joints is equal to 15% of the roughness of monolithic cracked concrete. The dynamic sliding hysteresis loops are enhanced by reducing the basic friction coefficient to 85% of the static value.

8.2.3 Implementation and validation of lift joint constitutive model

A three-state constitutive model using the gap-friction element as the numerical support, was found to be adequate for the simulation of concrete-concrete lift joints behaviour. Solution strategies for the static equilibrium equations indicated an important dependency on the control parameters i.e. initial displacement step and tolerance on the unbalanced load. The solution of the dynamic equations of motions showed no particular problem except in situations that involve extensive opening and closing of the interface or impact at the interface. Impact waves tend to produce numerical shocks in the mass structure thus some viscous damping is required to attenuate this secondary effect that may amplify and lead to numerical instability. Validation problems indicated that the developed static and dynamic algorithms enable the prediction of experimentally measured or theoretical responses.

Interestingly, on the three point bending tests, it was proven that the arc length method converges from the top while deBorst (1987) method converges from below. Furthermore the experimentally measured failure load was never attained using deBorst method. The single notched shear beam is similar to the three point bending since the failure is mainly due to tensile mode I response. This problem indicated that a curved

layer of gap elements may be used to predict the cracking response. The double notched shear beam indicated that a mode II fracture energy model is required to avoid the "peeling effect". Finally, the Coulomb friction test showed that the friction energy dissipation mechanism is well captured by the constitutive model. Even more, it validates the implementation of the dynamic response numerical algorithm.

8.2.4 Seismic safety evaluation of gravity dams considering lift joints

The significance of lift joints on seismic dam safety was assessed by investigating the critical peak ground acceleration for dynamic instability. A comparison between pseudo-static, pseudo-dynamic, and nonlinear transient dynamic analyses (NLFEA) results in about the same intensity of applied ground acceleration for sliding to be initiated. However, NLFEA at larger intensity of peak ground acceleration indicates the amount of energy dissipated by friction, and the maximum residual sliding displacements that could be adopted as a basis for assessing the potential damage and acceptability of a very severe earthquake. Analyses with a simple joint at the base indicated important residual sliding. They also indicated that secondary cracking would occur close to the crest. The introduction of a lift joint close to the crest reduces the displacements at the base. The total input seismic energy is smaller at low intensity earthquakes for a dam with the introduction of a lift joint. The overall effect of surface preparation, waterblasted surface as compared to a untreated surface, is to decrease the sliding displacement. However, joint opening is greater for waterblasted joints. Thus surface preparation imposes a gradual shift in the behaviour from pure sliding to combined sliding and rocking.

Finally, the introduction of several joints along the dam height indicated that only the two upper joints dominate the response. The energy dissipation mechanism and distribution of energy between friction and viscous damping has not been affected by the introduction of several joints. The residual displacements decreased when several lift joints were considered in the finite element model as compared to the dam with a joint at the base and a lift joint close to the crest.

The joint constitutive model modified the response as compared to a simple fixed coefficient of friction Mohr-Coulomb model. First, the introduction of a peak friction coefficient delays and reduces the amount of sliding displacement. The decrease of the coefficient of friction with increasing normal stress level brought the untreated joint model into instability under the static loads. In the multijointed dam, this decrease of the coefficient of friction will result in a redistribution of the sliding displacements from the crest joints to the base joint.

For fully cracked joints, it is found that secondary cracking would be likely to occur in the vicinity of the joint. However, this secondary cracking would lead to a wedge crack at the joint ends; not to a major crack running from joint to joint in the concrete mass. For fully cracked joints, the effect of uplift pressure is determinant. For untreated joints, uplift pressure triggered global instability under static loads. For waterblasted joints it increased the residual sliding but decreased the crack opening thus inducing a shift from combined rocking and sliding to rather dominant sliding response.

The finite element method is based on small displacements theory. Sliding displacements result in a change of geometry of the structure similar to the P-Δ effect. At some point the assumption of small displacements does not hold true anymore and global numerical instability occurs. Inhere, the analyses stayed below that instability point since the sliding displacement and openings were relatively small compared to the size of the structure. However, a numerical instability criterion has to be determined for accepting the numerical results. The change in slope of the residual sliding as a function of the peak ground acceleration is a good indicator. The first change in slope indicated the mobilization of the sliding friction mechanism then an exponential increase followed by erratic increase indicates numerical instability.

8.3 Recommendations

The engineer who is called on the seismic safety assessment of an existing dam should in the first place, gather all the existing measurements made at the site. A thorough site

inspection of the dam should be undertaken. Concrete samples and joint samples should taken from the dam and frictional tests performed using the Lo et al. (1991) method where the dilatancy or joint opening during the direct shear tests is recorded. The engineer should also study the available information gathered at the time of construction: the instructions given to the contractors, the notes from the site engineer, the drawings, the photographs, etc. At this point, the joints of the dam should be characterized as a whole e.g. are the joints very good, good, bad, or very bad.

Then a progressive analysis methodology should be undertaken as proposed by Ghrib et al. (1997). First the simple rigid bloc stability analysis is performed. Then pseudo-dynamic analyses and linear finite element analyses are advisable. Cracking analysis and sliding failure analysis may follow. This type of analysis should explicitly recognize the presence of weak lift joints as presented in thesis.

8.4 Future research and developments

8.4.1 Experimental research on joints

It is suggested to increase the number of variables in the testing programme. The aggregate size should be varied in order to assess its effect on roughness. The concrete strength should also be varied in order to study its effect on the response. Wet joints should be tested. Although the effect of water pressure is very well known and is captured using the effective stress concept. However the effect of water on the frictional properties i.e. basic friction coefficient is not known. The effect of velocity could be inquired by varying the imposed displacement frequencies. The testing sequence could also be varied: (i)) by doing complete displacement cycles in both directions, (ii) by subjecting the specimens to dynamic displacement cycles after static tests for a given normal stress level before having increased the normal stress level.

The specimen size is also a variable that should be varied to assess the significance of roughness on joint behaviour when it comes to extrapolate the results obtained from joint

samples to the actual structure. Some experimental work ought to be performed on the rehabilitation techniques of bad lift joints for improving the seismic resistance of dams. The frictional response of grouting materials, the efficiency of post-tensioning could be investigated.

8.4.2 Numerical analysis of jointed dams

The numerical aspects of the analysis of jointed dams may be enhanced in many ways. In the constitutive model, the sliding displacement is considered without any dilatation. Dilatation does occur and its effects on crack propagation are to be determined. The finite element itself may be modified since inhere only frictional gap-elements have been adopted. The zero thickness element could also be used. The state determination could be refined by adopting a layer by layer update approach.

The uplift pressures have a determinant effect on the response of jointed dams. Attention could be devoted to the modelling of the uplift pressure diagram. In addition, the evolution of the uplift pressure during the earthquake, dynamic effects due to opening and closing of the crack could be taken in consideration.

The question of the crack trajectory in the case of bonded lift joints, whether the crack will be confined or not confined to the lift joint, requires special tracking of the stress state in the concrete mass. The smeared crack approach, proved to be effective in the context of earthquake analysis of gravity dams, could be coupled to interface joint elements for a thorough analysis of crack propagation in jointed gravity dams.

8.4.3 Seismic safety analysis of jointed dams

Three dimensional effects play an important role in the seismic resistance of a massive structure such as a dam. Beneficial effects such as friction along contraction joints or detrimental effects such as geometrical irregularities, important stiffness changes (e.g. from concrete gravity dam to the penstock or the powerhouse) or weak abutments require three dimensional modelling for a thorough assessment of stability

The definition of a sliding displacement safety index, thus the determination of actual allowable sliding displacement values for existing dams, would involve serious dialog with dam owners. At first, a survey of the various elements in a dam being affected by global sliding is mandatory i.e. drainage systems, important equipment, foundations, environmental issues. Indices could be determined from a classification system based on the location, the size, and the importance of the dam, coupled with the position along the dam profile where sliding would be considered. As this is currently the practice in the nuclear industry in the context of earthquake analysis, numerical tools (e.g. some commercial or in house computer programs) should be identified by dam safety authorities as the official computer programs for performing seismic sliding safety analyses of concrete dams, after a thorough validation process done by a group of dam safety experts.

REFERENCES

AHMADI, M.T., AND KHOSHRANG, G.H., 1992. "Sefidrud Dam's dynamic response to the large near-field earthquake of June 1990", *Dam Engineering*, Vol III, No 2, pp.85-115.

AHMADI, M.T., KHOSHRANG, G.H., MOKHTARZADEH, A., AND JALALZADEH, A., 1992. "Behavior of a large concrete dam due to an actual maximum credible earthquake", Proceedings of the Tenth World Conference on Earthquake Engineering, Madrid, Vol.7, pp.3995-4000.

AMERICAN CONCRETE INSTITUTE, COMMITTEE 207, (ACI 207), 1980. Mass Concrete for Dams and other Massive Structures, ACI 207.1R-70.

AMERICAN CONCRETE INSTITUTE, 1990. Building Code Requirements for Reinforced Concrete, ACI 318-89, Detroit, Michigan, USA.

ARREA, M., AND INGRAFFEA, A.R., 1981. "Mixed-mode crack propagation in mortar and concrete", Department of Structural Engineering Report 81-13, Cornell University.

ATKINSON, G.M., AND BOORE, D.M., 1990. "Recent trends in ground motion and spectral response relations for North America", *Earthquake Spectra*, Vol 6, No 1, pp.15-35.

AUSTRALIAN NATIONAL COMMITTEE ON LARGE DAMS (ANCOLD), 1991. Guidelines on Design Criteria for Concrete Gravity Dams, Australia, 34pp.

AYARI, M.L., AND SAOUMA, V.E., 1990. "A fracture mechanics based seismic analyses of concrete gravity dams using discrete cracks", *Engineering Fracture Mechanics*, Vol. 35, No. 1/2/3, pp.587-598.

BANDIS, S.C., 1990. "Mechanical properties of rock joints", *Proc. Int. Symp. Rock Joints*, Loen, Norway, Barton, N. and Stephansson, O., Eds., pp.125-140.

BANDIS, S.C., LUMSDEN, A.C. and BARTON, N.R., 1981. "Experimental studies of scale effects on the shear behaviour of rock joints", *Int. J. Rock Mech. Min. Sci. & Geomech.*, Vol.20, No.6, pp.249-268.

BANDIS, S.C., LUMSDEN, A.C. and BARTON, N.R., 1983. "Fundamentals of rock joint deformation", *Int. J. Rock Mech. Min. Sci. & Geomech.*, Vol.20, No.6, pp.249-268.

BARTON, N.R., BANDIS, S.C. and BAKHTAR, K., 1985. "Strength, deformation and conductivity coupling of rock joints", *Int. J. Rock Mech. Min. Sci. & Geomech.*, Vol.22, No.3, pp.121-140.

BATHE, K.-J. and CHAUDHARY, A., 1985. "A solution method for planar and axisymmetric contact problems", *International Journal for Numerical Methods in Engineering*, Vol.21, pp.65-88.

BAZANT, Z.P., 1990. "A critical appraisal of no-tension dam design: a fracture mechanics viewpoint", Dam Engineering, Vol I, No 4, pp.237-247.

BAZANT, Z.P. and GAMBAROVA, P.G., 1980. "Rough cracks in reinforced concrete", ASCE, *Journal of Structural Engineering*, Vol.106, No.4, April, pp.819-842.

BAZANT, Z.P. and OH, B.H., 1983. "Crack band theory for fracture of concrete", *Materials and Structures*, (RILEM, Paris), Vol.16, pp.155-177.

BAZANT, Z.P. and PFEIFFER, P.A., 1986. "Shear fracture tests of concrete " *Materials and Structures*, V. 19, No.110, pp. 111-121.

BAZANT, Z.P. and PFEIFFER, P.A., 1987. "Detremination of fracture energy from size effect and brittleness number". *ACI Material Journal*, Vol. 84, , pp. 464-480.

BHATTACHARJEE, S.S., 1993. "Smeared fracture analysis of concrete gravity dams for static and seismic loads", *Ph.D. Thesis*, Dept. of Civil Eng., McGill University, Montréal, Canada, February, 183pp.

BHATTACHARJEE, S.S. and LÉGER, P., 1992. "Concrete constitutive models for nonlinear seismic analysis of gravity dams - state-of-the-art", *Canadian Journal of Civil Engineering*, Vol. 19, pp.492-509.

BHATTACHARJEE, S.S. and LÉGER, P., 1994. "Application of NLFM models to predict cracking in concrete gravity dams ", ASCE, *Journal of Structural Engineering*, Vol.120, No.4, pp.1255-1271.

BHATTI, A., TENG, S. and ASHTON, W.D., 1994. "Simplified finite element analysis of a cracked concrete arch dam", *Concrete International*, January, pp.53-57.

BÖHM, J., 1987. "A comparaison of different contact algorithms with applications", *Computers and Structures*, Vol.26, No.1/2, pp.207-221.

BRO, A., 1992. "Failure of stepped joints: an analysis and comparison with a measured failure geometry", *Int. J. Rock Mech. Min. Sci. & Geomech.*, Vol.29, No.2, pp.179-186.

BRÜHWILER, E. and WITTMANN, F.H., 1990. "Failure of dam concrete subjected to seismic loading condition", *Engineering Fracture Mechanics*, Vol. 35, No. 1/2/3, pp.565-571.

CAMPOS, L.T., ODEN, J.T. and KIKUCHI, N., 1982. "Numerical analysis of a class of contact problems with friction in elastostatics", *Comp. Methods Appl. Mech. Eng.*, Vol.34, pp.821-845.

CANADIAN DAM SAFETY ASSOCIATION (CDSA), 1995. Dam Safety Guidelines, Edmonton, Alberta, pp.9-1 - 9-14.

CANADIAN ELECTRICAL ASSOCIATION, Research and Development, (CEA), 1990. Safety Assessment of Existing Dams for Earthquake Conditions, Seismic Analysis of Concrete Dams, CEA Report No. 420 G 547, Background Volume C-4, Montreal, Quebec.

CANADIAN STANDARDS ASSOCIATION (CSA), 1990. Concrete Materials and Methods of Concrete Construction, CAN/CSA A23.1-M90.

CAROL, I. and ALONSO, E., 1983. "A new joint element of the analysis of fracture rock", Int. Congress on Rock Mechanics, Melbourne, Australia, pp.147-151.

CHAVARRI, G., DEFRIES, A., SHIEH, W.Y. and YEH, C.H., 1979. "Raising Guri Gravity Dam, stability and stress investigations", Commission des Grands Barrages, Treizième Congrès des Grands Barrages, New Delhi, India, Q.48 R.3, pp.45-56.

CHEN, E.Y.-T. and SCHNOBRICH, W.C., 1981. "Models for the post-cracking behavior of plain concrete under short term monotonic loading", *Computers and Structures*, Vol.13, pp.213-221.

CHEN, W.-H. and TSAI, P., 1986. "Finite element analysis of elastodynamic sliding contact problems with friction", *Computers and Structures*, Vol.22, No.6, pp.925-938.

CHOPRA, A.K., 1988. "Earthquake response analysis of concrete dams. Advanced dam engineering for design, construction and rehabilitation", Edited by R.B. Jansen, Van Nostrand Reinhold., pp.416-465.

COOK, R.D., MALKUS, D.S. and PLESHA, M.E., 1989. Concepts and Application of Finite Element Analysis, John Wiley & Sons, NewYork, U.S.A., 630pp.

CRISFIELD, M.A., 1981. "A fast incremental/iterative procedure that handles snap through", *Computers & Structures.*, Vol.13, pp.55-62.

DAHLBLOM, O. and OTTOSEN, N.S., 1990. "Smeared crack analysis using generalized fictitious crack model", ASCE, *Journal of Engineering Mechanics*, Vol.116, 1, pp.55-76.

DASCAL, O., LECONTE, P., NGUYEN, D. and LAROCQUE, G.-S., 1994. "Paramètres de mouvements sismiques pour l'évaluation de la stabilité parasismique des barrages", CDSA-CANCOLD Joint Conference, Winnipeg, Manitoba, pp.329-339.

DE BORST, R., 1987. "Computation of post-bufurcation and post-failure behaviour of strain-softening solids", *Computers & Structures.*, Vol.25, No.2, pp.211-224.

DIVAKAR, M.P. and FAFITIS, A., 1992. "Micromechanics-based constitutive model for interface shear", ASCE, *Journal of Structural Engineering*, Vol.118, No.7, pp.1317-1337.

DIVAKAR, M.P., FAFITIS, A. and SHAH, S.P., 1987. "Constitutive model for shear transfer in cracked concrete", ASCE, *Journal of Engineering Mechanics*, Vol.113, No.5, May, pp.1046-1062.

DOWLING, M.J. and HALL, J.F., 1989. "Nonlinear seismic analyses of arch dams", ASCE, *Journal of Engineering Mechanics*, Vol.115, No.4, April, pp.768-789.

DUFRESNE, P., LOVIN, M. and JOBIN, H., 1992. "Réfection de la partie amont de piliers d'évacuateurs avec impact minimal sur l'environnement. Aménagement hydro-électrique d'Isle-Maligne, Alma, Québec", Canadian Dam Safety Conference, Quebec City, pp.213-227.

DUVAUT, G. and LIONS, J.L., 1972. *Les inéquations en mécanique et en physique*, Dunod, Paris, 387pp.

EL-AIDI, B. and HALL, J.F., 1989a. "Non-linear earthquake response of concrete gravity dams part I: modelling", *Earthquake Engineering and Structural Dynamics*, Vol.18, pp.837-851.

EL-AIDI, B. and HALL, J.F., 1989b. "Non-linear earthquake response of concrete gravity dams part II: behaviour", *Earthquake Engineering and Structural Dynamics*, Vol.18, pp.853-865.

ELECTRICAL POWER RESEARCH INSTITUTE (EPRI), 1992. "Uplift pressures, shear strengths and tensile strengths for stability analysis of concrete gravity dams", Vol.1, Denver Colorado, August.

FAN, B.H. and SLED, J.J., 1992. "Seismic evaluation of gravity dams - practical aspects", Proceedings of the Tenth World Conference on Earthquake Engineering, Madrid, pp.4645-4650.

FARDIS, M.N. and BUYUKOZTURK, O., 1979. "Shear transfer model for reinforced concrete", ASCE, *Journal of Engineering Mechanics*, Vol.105, 2, pp.255-275.

FEENSTRA, P.H., DE BORST, R. and ROTS, J.G., 1991a. "Numerical study on crack dilatancy. I: models and stability analysis", ASCE, *Journal of Engineering Mechanics*, Vol.117, No.4, pp.733-753.

FEENSTRA, P.H., DE BORST, R. and ROTS, J.G., 1991b. "Numerical study on crack dilatancy. Ii: applications", ASCE, *Journal of Engineering Mechanics*, Vol.117, No.4, pp.754-769.

FELTRIN, B., WEPF, D. and BACHMANN, H., 1990. "Seismic cracking of concrete gravity dams", *Dam Engineering*, Vol I, No 4, pp.279-289.

FENWICK, R.C. and PAULAY, T., 1968. "Mechanisms of shear resistance of concrete," ASCE, *Journal of Structural Engineering*, Vol.94, No.10, pp.2325-2350.

FERGUSON, S.N., SMITH, N.J. and SCHELLENBERG, G., 1994. "Seven Sisters generating station stability evaluation and anchoring program", Canadian Dam Safety Conference, Winnipeg, pp.71-94.

FRANCAVILLA, A. and ZIENKIEWICZ, O.C., 1975. "A note on numerical computation of elastic contact problems", *International Journal for Numerical Methods in Engineering*, Vol.9, pp.913-924.

FRONTEDDU, L., 1994. "Weak planes in dams, a literature review", Technical Report, École Polytechnique de Montréal, No EPM/GCS-1994-18, 225pp.

FRONTEDDU, L., 1997. "INTRFACE Finite element program, User's manual", Technical Report, École Polytechnique de Montréal, in preparation.

GAJER, G. and DUX, P.F., 1990. "Crack band based model for FEM analysis of concrete structures", ASCE, *Journal of Structural Engineering*, Vol.116, 6, pp.1696-1714.

GAJER, G. and DUX, P.F., 1991. "Simplified nonorthogonal crack model for concrete", ASCE, *Journal of Structural Engineering*, Vol.117, 1, pp.149-164.

GAMBAROVA, P.G. and KARACOC, C., 1983, "A new approach to the analysis of the confinement role in regularly cracked concrete elements," *Trans. 7th Struct. Mech. in Reactor Tech (SMiRT) Conf.*, Vol. H, pp. 251-261.

GAMBAROVA, P.G. and VALENTE, G., 1990. "Smeared crack analysis for fracture and aggregate interlock of concrete", *Engineering Fracture Mechanics*, Vol. 35, No. 4/5, pp.651-663.

GARKUN, L.M., MARKIN, L.I. and VEDENEEV, B.E., 1989. "Cracking in massive concrete lifts of large dams in Siberia", Int. Symp. on Analytical Evaluation of Dam Related Safety Problems, Copenhagen, pp.226-234.

GERRARD, C., 1986. "Shear failure of rock joints: appropriate constraints for empirical relations", *Int. J. Rock Mech. Min. Sci. & Geomech.*, Vol.23, No.6, pp.421-429.

GERSTLE, W.H. and XIE, M., 1992. "FEM modeling of fictitious crack propagation in concrete", ASCE, *Journal of Engineering Mechanics*, Vol.118, 2, pp.416-434.

GHABOUSSIS, J., WILSON, E.L. and ISENBERG, J., 1973. "Finite element for rock joints and interfaces", ASCE, *Journal of Soils Mechanics and Foundation Division*, Vol.99, SM10, October, pp.833-848.

GHRIB, F. and TINAWI, R., 1994. "Sur l'analyse de la fissuration des barrages en béton par la mécanique de l'endommagement continu - Comportement statique et dynamque", École Polytechnique de Montréal, Report No EPM/GCS-1994-12, 283pp.

GHRIB, F., LÉGER, P., TINAWI, R., LUPIEN, R. and VEILLEUX, M., 1997. "Seismic safety evaluation of gravity dams", Hydropower & Dams, No.2, pp.126-138.

GOODMAN, R.E., 1974. "The mechanical properties of joints", *Proc. 3rd Congr. ISRM*, Denver, Vol.1A, pp.127-140.

GOODMAN, R.E., 1976. Methods of Geological Engineering in Discontinuous Rocks, West Publishing Co., Berkeley.

GOODMAN, R.E. and DUBOIS, J., 1972. "Duplication of dilatancy in analysis of jointed rock", ASCE, *Journal of Soils Mechanics and Foundation Division*, Vol.98, SM4, April, pp.399-422.

GOODMAN, R.E., TAYLOR, R.L. and BREKKE, T.L., 1968. "A model for the mechanics of jointed rock", ASCE, *Journal of Soils Mechanics and Foundation Division*, Vol.94, SM3, pp.637-659.

GORE, I.W. and BICKLEY, J.A., 1987. "Big Eddy Dam, investigation and rehabilitation of a severely deteriorated gravity structure", *Concrete International*, June, pp.32-38.

GREENWOOD, D.T., 1988. *Principles of Dynamics*. 2nd edition, Prentice-Hall, Englewoods Cliffs, New Jersey.

HANDANYAN, J.M., DANEK, E.R., D'ANDREA, R.A. and SAGE, J.D., 1990. "The role of tension in failure of jointed rock", *Proc. Int. Symp. Rock Joints*, Loen, Norway, Barton, N. and Stephansson, O., Eds., pp.195-202.

HEEGAARD, J.-H. and CURNIER, A., 1993. "An augmented lagrangian method for discrete large-slip contact problems", *International Journal for Numerical Methods in Engineering*, Vol.36, pp.569-593.

HOHBERG, J.-M., 1992. "A joint element for the nonlinear dynamic analysis of arch dams", *Ph.D. dissertation*, Swiss Federal Institute of Technology, Zurich, January 284pp.

HOLLINGWORTH, F. and DRUYTS, F.H.W.M., 1979. "The raising and strengthening of concrete gravity dams", International Commission on Large Dams, Thirteenth Congress, New Delhi, India, Q.48 R.17, pp.295-310.

HORSWILL, P., SNOWDEN, H.N. and WEEKS, R.C., 1994. "Val de la Mare Dam, Jersey: instrumentation, monitoring and stability analysis of an asr damaged dam," *Proc. of the Eigth Conference of the British Dam Society held at the University of Exeter*, pp. 161-172.

HOUDE, J. and MIRZA, M.S., 1974. "Finite element analysis of shear strenght of reinforced concrete beams," *Special Publication SP42*, ACI, pp. 103-128.

HUANG, T.H. and DOONG, Y.S., 1990. "Anisotropic shear strength of rock joints", *Proc. Int. Symp. Rock Joints*, Loen, Norway, Barton, N. and Stephansson, O., Eds., pp.211-218.

IBRAHIMBEGOVIC, A. and WILSON, E., 1989. "Dynamic analysis of large linear structure-foundation systems with local nonlinearities", *Report No. UCB/SEMM 89/14*,, U. of California, Berkeley, 166pp.

INDERMAUR, W., BRENNER, R.P. and ARASTEH, T., 1991. "The effects of the 1990 Manjil Earthquake on Sefid Rud Buttress Dam", *Dam Engineering*, Vol II, No 4, pp.275-305.

INTERNATIONAL COMMISSION ON LARGE DAMS (ICOLD), 1986. "Materials for joints in concrete dams", *Bulletin*, 57, Paris, France, 45pp.

INTERNATIONAL COMMISSION ON LARGE DAMS (ICOLD), 1990. "Manual of Dam Construction", *Bulletin*, 59, Paris, France, 45pp.

JAEGER, J.C. and COOK, N.G.W., 1979. Fundamentals of Rock Mechanics, 3rd Edn, Chapman & Hall, London.

KATANI, M., NISHI, K. and NOGAMI, T., 1997. "Earthquake response of submerged gravity foundation on soft rock", *Soil Dynamics and Earthquake Engineering*, Vol.16, pp.125-139.

KHRAPKOV, A.A., LAWKIN, M.S., TSYBIN, A.M., VOVKUSHEVSKY, A.V., 1989. "Strength analysis of concrete gravity and buttress dams taking account of joint opening and consequences of construction", Int. Symp. on Analytical Evaluation of Dam Related Safety Problems, Copenhagen, pp.141-150.

KULHAWAY, F.H., 1975. "Stress-deformation properties of rock and rock discontinuities", *Engng Geol.*, Vol.8, pp.327-350.

LADANYI, B. and ARCHAMBAULT, G., 1969. "Simulation of shear behaviour of a jointed rock mass", *Rock Mechanics - Theory and Practice: Proc. 11th Symp. Rock Mech.* , W.H. Somerton Ed., Am. Inst. Min. Metall. Petr. Eng., Berkeley, Calif., pp.105-125.

LAIBLE, J.P., WHITE, R.N. and GERGELY, P., 1977. "Experimental investigation of shear transfer across cracks in concrete nuclear containment vessels," *Special Publication SP53*, ACI, pp. 203-226.

LEE, S.H., 1993. "Rudimentary considerations for adaptative gap/friction element based on the penalty method", *Computers and Structures*, Vol.47, No.6, pp.1043-1056.

LÉGER, P. and KATSOULI, M., 1989. "Seismic stability of concrete gravity dams", *Earthquake Engineering and Structural Dynamics*, Vol.18, pp.889-902.

LÉGER, P. and LECLERC, M., 1996. "Evaluation of earthquake ground motions to predict cracking response of gravity dams", Engineering Structures, Vol.18, No.3, pp.227-239.

LINK, H., 1969. "The sliding stability of dams", *Water Power*, March, April, May, pp.99-103, 135-139, 172-179.

LINSBAUER, H.N., 1985. "Fracture mechanics models for characterizing crack behaviour in concrete gravity dams", Commission des Grands Barrages, Quinzième Congrès des Grands Barrages, Lauzanne, Suisse, Q.57 R.16, pp.279-291.

LO, K.Y., LUKAJIC, B., WANG, S., OGAWA, T. and TSUI, K.K., 1990. "Evaluation of strength parameters of concrete-rock interface for dam safety assessment", Canadian Dam Safety Conference, Toronto, pp.71-94.

LO, K.Y., OGAWA, T., LUKAJIC, B., SMITH, G.F. and TANG, J.H.K., 1991a. "The evaluation of stability of existing concrete dams on rock foundations and remedial

measures", International Commission on Large Dams, Seventeenth Congress, Vienna, Austria, pp.963-990.

LO, K.Y., OGAWA, T., LUKAJIC, B., SMITH, G.F. and DUPAC, D.D., 1991b. "Measurements of strength parameters of concrete-rock contact at the dam foundation interface", *Geotechnical Testing Journal*, Vol.14, No.4, December, pp.383-394.

LOTFI, H.R. and SHING, P.B., 1994. "Interface model applied to fracture of masonry structures", ASCE, *Journal of Structural Engineering*, Vol.120, No.1, January, pp.63-80.

MATTOCK, A.H., 1974. "Shear transfer in concrete having reinforcement at an angle to the shear plane," *Special Publication SP42*, ACI, pp. 17-42.

MCLEAN, F.G. and PIERCE, J.S., 1988. "Comparison of joint shear strengths for conventional and roller compacted concrete", Roller Compacted Concrete II, *Proc. Conf. sponsored by Const, Geotech. Eng., Mat. Eng. Divisions of ASCE*, San Diego, Eds K.D.Hansen and L.K.Guice, pp.151-169.

NATIONAL RESEARCH COUNCIL (NRC), 1990. *Earthquake Engineering for Concrete Dams; Design, Performance and Research Needs*. National Academy Press, Washington, D.C., USA, 143pp.

ODEN, J.-T. and MARTINS, J.A.C., 1985. "Models and computational methods for dynamic friction phenomena", *Comp. Methods Appl. Mech. Eng.*, Vol.52, pp.527-634.

ODEN, J.-T. and PIRES, E.B., 1983. "Nonlocal and nonlinear friction laws and variational principles for contact problems in elasticity", *ASME J. Appl. Mech.*, Vol.50, pp.67-76.

OLIVER, J., ONATE, E. and HERRERO, E., 1988. "A case study of a gravity dam subjected to severe internal actions: description and numerical simulation", International Commission on Large Dams, Sixteenth Congress, San Francisco, États-Unis, C.29, pp.1387-1409.

OREKHOV, V.G., BARANOV, A.E., SHIMEL'MITS, G.I. and ZAKHAROV, V.F., 1986. "Model investigation of the powerhouse section of a concrete gravity dam", *Gidrotekhnicheskoe Stroitel'stvo (Hydrotechnical Construction)*, Vol.20, No.4, pp.209-212.

OREKHOV, V.G., SHIMELMITS, G.I., ZAKHAROV, V.F., ZERTSALOV, M.G. and TOLSTIKOV, V.V., 1989. "Study of bearing capacity of concrete dams by numerical methods", Int. Symp. on Analytical Evaluation of Dam Related Safety Problems, Copenhagen, pp.162-172.

PACELLI, W.A., ANDRIOLO, F.R. and SARKARIA, G.S., 1993. "Treatment and performance of construction joints in concrete dams", *International Water Power and Dam Construction*, Vol.45, No.11, pp.26-31.

PANDE, G.N. and SHARMA, K.G., 1979. "On joint/interface elements and associated problems of numerical ill-conditioning", *International Journal of Numerical and Analytical Methods in Geomechanics*, Vol.3, pp.293-300.

PANDE, G.N., ZIENKIEWICZ, O.C. and BICANIC, N., 1979. "Influence of interface non-linearity on the behaviour of dams strengthened by buttresses", International Commission on Large Dams, Thirteenth Congress, New Delhi, India, Q.48 R.36, pp.661-674.

PAULAY, T. and LOEBER, P.J., 1974. "Shear transfer by aggregate interlock," *Special Publication SP42*, ACI, pp. 1-15.

PLESHA, M.E., 1987. "Constitutive models for rock discontinuities with dilatancy surface degradation", *International Journal for Numerical and Analytical Methods in Geomechanics*, Vol.11, pp.345-362.

PRUIJSSERS, A.F., 1988. "Aggregate interlock and dowel action under monotonic and cyclic loading", *Ph.D. Dissertation*, Delft University of Technology, 165pp.

RAMM, E., 1987. "Strategies for tracing the nonlinear response near limit points", In *Nonlinear finite element analysis in structural dynamics*, Wunderlich, W., Stein, E. and Bathe, K.J., editors, Berlin, pp.63-83.

RAPHAëL, J.M., 1984, "Tensile strength of concrete" ACI Journal, *Proceedings*, V. 81, No. 2, pp. 158-165.

REICH, R.W., 1993. "On the marriage of fracture mechanics and mixed finite element methods: an application to concrete dams", *Ph.D. Thesis*, University of Colorado, Boulder, 336pp.

REINHARDT, H.W. and WALRAVEN, J.C., 1982. "Cracks in concrete subject to shear", ASCE, *Journal of Structural Engineering*, Vol.108, No.1, January, pp.207-224.

REINHARDT, HANS W., CORNELISSEN, HANS A.V. and HORDIJK, Dirk A., 1986, "Tensile tests and failure analysis of concrete," *Journal of Structural Eng.*, ASCE, Vol. 112, No. 11, November, pp.2462-2477.

RIGGS, H.R. and POWELL, G.H., 1986. "Rough crack model for analysis of concrete", ASCE, *Journal of Engineering Mechanics*, Vol.112, No.5, May, pp.448-464.

ROSENBAUM, D.B., 1991. "Structure is wired together", *Engineering News Record*, Vol.226, April 8, pp.19-20.

ROTS, J.G. and DE BORST, R., 1987. "Analysis of mixed-mode fracture in concrete", ASCE, *Journal of Engineering Mechanics*, Vol.113, No.11, pp.1739-1758.

SAEB, S. and AMADEI, B., 1992. "Modelling rock joints under shear and normal loading", *Int. J. Rock Mech. Min. Sci. & Geomech.*, Vol.29, No.3, pp.267-278.

SAOUMA, V.E., BROZ, J.J., BRUHWILER, E. and BOGGS, H.L, 1991a. "Effect of aggregate and specimen size on fracture properties of dam concrete", ASCE, *Journal of Materials in Civil Engineering*, Vol.3, No.3, August, pp.204-218.

SAOUMA, V.E., BROZ, J.J. and BOGGS, H.L, 1991b. "In situ field testing for fracture properties of dam concrete", ASCE, *Journal of Materials in Civil Engineering*, Vol.3, No.3, August, pp.219-234.

SEBJ, 1992. Private communication.

SHARMA, K.G. and DESAI, C.S., 1992. "Analysis and implementation of thin-layer element for interfaces and joints", ASCE, *Journal of Engineering Mechanics*, Vol.118, No.12, December, pp.2442-2462.

SINGHAL, A.C. and NUSS, L.K., 1991. "Cable anchoring of deteriorated arch dams", ASCE, *Journal of Performance of Construction Facilities*, Vol.5, No.1, pp.19-36.

SKRIKERUD, P.E. and BACHMANN, H., 1986. "Discrete crack modelling for dynamically loaded unreinforced concrete structures", *Earthquake Engineering and Structural Dynamics*, Vol.14, pp.297-315.

SUIDAN, M. and SCHNOBRICH, W.C., 1973, "Finite element analysis of reinforced concrete," *Journal of Structural Eng.*, ASCE, Vol 99, No. 10, pp.2109-2122.

SUN, Z., GERRARD, C. and STEPHANSSON, O., 1985. "Rock joint compliance tests for compression and shear loads", *Int. J. Rock Mech. Min. Sci. & Geomech.*, Vol.23, No.4, pp.197-213.

SUPRENANT, B., 1988. "Construction joints for multistory structures", *Concrete Construction*, Vol.33, June, pp.577-578.

TASDEMIR, M.A., MAJI, A.K. and SHAH, S.P., 1990. "Crack propagation in concrete under compression", ASCE, *Journal of Engineering Mechanics*, Vol.116, 5, pp.1058-1076.

TASSIOS, T.P. and VINTZÈLEOU, E.N., 1987. "Concrete-to-concrete friction", ASCE, *Journal of Structural Engineering*, Vol.113, No.4, pp.832-849.

TAYLOR, H.P.J., 1974. "The fundamental behaviour of reinforced concrete beams in bending and shear," *Special Publication SP42*, ACI, pp. 43-77.

TOLSTOI, D.M., 1967. "Significance of the normal degree of freedom and natural normal vibrations in contact friction", *Wear*, Vol.10, pp.199-213.

TSCHEGG, E.K., TAN, D.M., KIRCHNER, H.O.K. and STANZI, S.E., 1993. "Interfacial and subinterfacial fracture in concrete", *Acta Metallurgica Mater.*, Vol.41, No.2, pp.569-576.

TURCOTTE, L., SAVARD, B., LOMBARDI, G. and JOBIN, H., 1994. "The use of grout and G.I.N. technique in grouting for dam rehabilitation", Canadian Dam Safety Conference, Winnipeg, pp.137-162.

UANG, C.M. and BERTERO, V.V., 1990. "Evaluation of seismic energy in structures", *Earthquake Engineering and Structural Dynamics*, Vol.19, pp.77-90.

UCHIDA, T. and HIGASHIGAWA, T., 1979. "A study on interface of new and old concrete, with particular reference to the raising of a gravity dam", International Commission on Large Dams, Thirteenth Congress, New Delhi, India, Q.48 R.25, pp.431-457.

U. S. BUREAU OF RECLAMATION, Design of Gravity Dams, Denver Colorado, 1976.

VOLPE, R.L., AHLGREN, C.S. and GOODMAN, R.E., 1991. "Selection of engineering properties for geologically variable foundations", International Commission on Large Dams, Seventeenth Congress,, Vienna, Austria, pp.1087-1101.

WALRAVEN, J.C., 1981. "Fundamental analysis of aggregate interlock", ASCE, *Journal of Structural Engineering*, Vol.107, No.11, November, pp.2245-2270.

WALRAVEN, J.C., 1994. "Rough cracks subjected to earthquake loading", ASCE, *Journal of Structural Engineering*, Vol.120, No.5, pp.1510-1524.

XIA, S.-Y., FU, Z.-X., ZHANG, C.-F., SHU, S.-W. and SHENG, T.-L., 1979. "Effect of longitudinal joint on behaviour of concrete gravity dams", International Commission on Large Dams, Thirteenth Congress, New Delhi, India, Q.48 R.60, pp.1073-1090.

XIURUN, G., 1981. "Non-linear Analysis of a joint element and its application in rock engineering", *International Journal for Numerical and Analytical Methods in Geomechanics*, Vol.5, pp.229-245.

YOSHIKAWA, H., WU, Z. and TANABE, T., 1989. "Analytical model for shear slip of cracked concrete", ASCE, *Journal of Structural Engineering*, Vol.115, No.4, pp.771-788.

ZHONG, Z.-H. and MACKERLE, J., 1992. "Static contact problems - A review", *Engineering Computations*, Vol.9, No.1, pp.3-37.

IMAGE EVALUATION
TEST TARGET (QA-3)

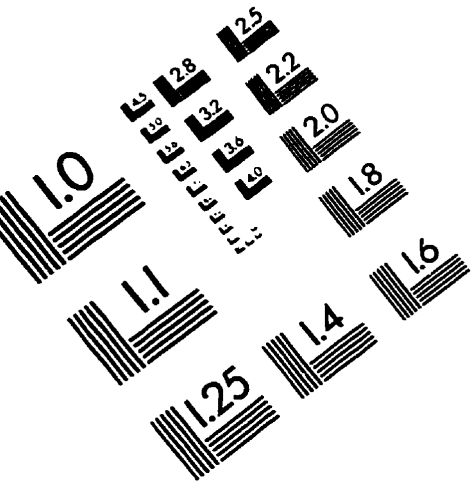

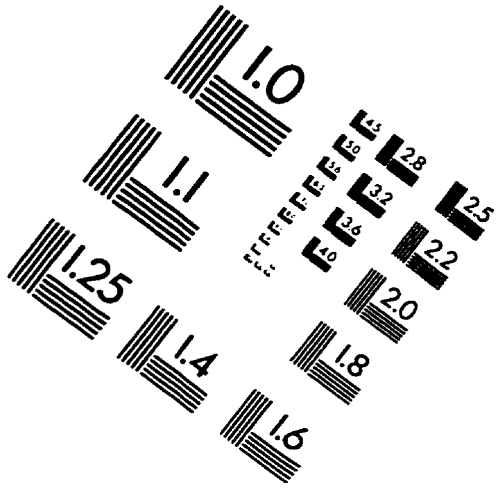

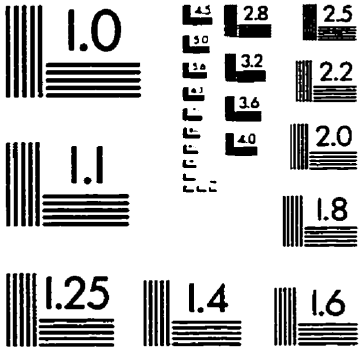

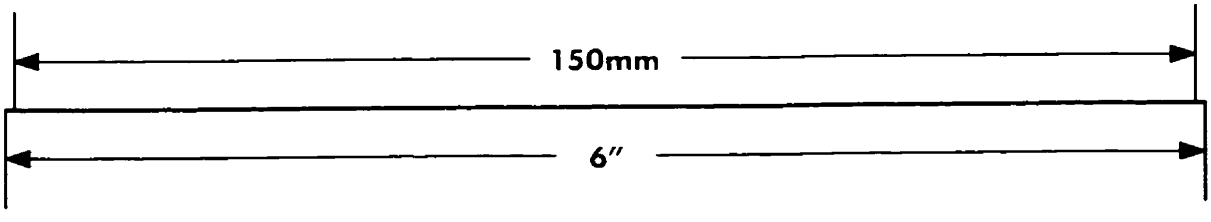

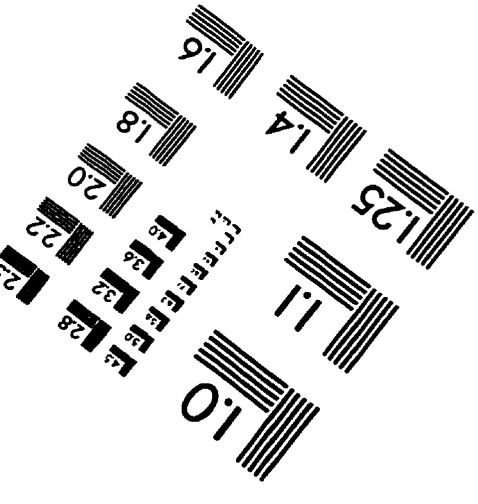

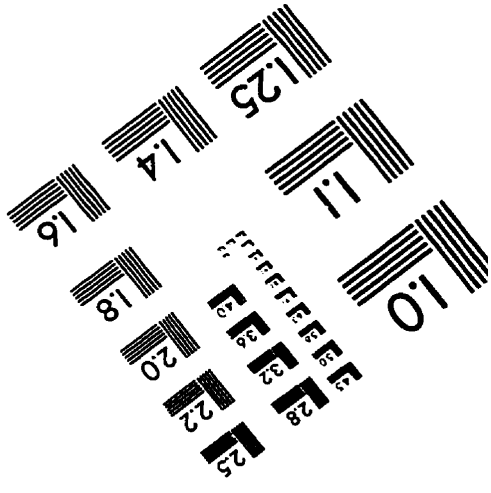

APPLIED IMAGE, Inc
1653 East Main Street
Rochester, NY 14609 USA
Phone: 716/482-0300
Fax: 716/288-5989